GEOLOGICAL AND GEOPHYSICAL STUDIES OF THE ATACAMA FAULT ZONE IN NORTHERN CHILE

Thesis by

Walter Joseph Arabasz, Jr.

In Partial Fulfillment of the Requirements

For the Degree of

Doctor of Philosophy

California Institute of Technology

Pasadena, California

1971

(Submitted July 10, 1970)

ACKNOWLEDGMENTS

Field work in Chile and completion of the varied aspects of this investigation would have been impossible without the help and cooperation of numerous individuals and organizations. Foremost in facilitating the study was the cooperative support of the California Institute of Technology and the Instituto de Investigaciones Geológicas (I.I.G.) of Chile.

I am especially indebted to Clarence R. Allen, under whose supervision this study was formulated and carried out. His excellent judgment and motivation added much to this endeavor and are greatly appreciated. I also would especially like to thank Carlos Ruiz F. and José Corvalán D. of the I.I.G. for extending the gracious support of that institute, and for their own enthusiastic cooperation. Their assistance, as well as that of many other geologists and personnel of the I.I.G., was indispensable and is gratefully acknowledged. I.I.G. Geologists F. Ortiz, A. Moraga, G. Chong, and H. Conn were particularly helpful.

The oceanographic investigations were made possible by the generous support of the Scripps Institution of Oceanography through H. W. Menard. The officers, crew, and members of the scientific party -- particularly Tanya Atwater -- of the R/V Thomas Washington are thanked for their assistance in gathering the offshore data. I also appreciate the cooperation of the Instituto Hidrográfico de la Armada, R. Herrera, Director. W. R. Normark and E. A. Silver of Scripps

were of great help in guiding the construction of line drawings of the reflection records. The writer benefited from discussion with D. W. Scholl and R. von Huene of the United States Geological Survey.

Special thanks are due E. Kausel, A. Cisternas, and other members of the Departamento de Geofísica y Geodesía of the University of Chile for helpful discussion and cooperation in aspects of the geophysical work, particularly the undertaking of gravity and magnetic surveying. J. Parra of that department completed the gravity and magnetic readings. I also thank N. Rojas of the I.I.G. for assistance in surveying the geophysical profile lines.

J. N. Brune introduced the writer to micro-earthquake research and encouraged the seismic survey. His advice and helpful comments are gratefully acknowledged. Ruth Talovich, J. van der Woude, and L. Lenches kindly assisted with the illustrations.

It is a special pleasure to acknowledge and thank L. Villalobos, L. Gomez, and J. Alfaro of the I.I.G. for logistical help in the field. Appreciation is expressed to E. Solis and family for their generous hospitality in Taltal.

Financial and logistical support came from the California Institute of Technology, the Instituto de Investigaciones Geológicas of Chile, the National Science Foundation grant GA-931, and C. R. Allen's G. K. Gilbert Award in Seismic Geology. Scripps ship time is supported by block funds from the National Science Foundation and the Office of Naval Research.

ABSTRACT

The Atacama fault, a suggested regional strike-slip fracture parallel to the coastline of northern Chile, is a major structural break that has undergone a complicated history of movement since Mesozoic time. Abundant Quaternary scarps attest to continuing activity; however, the Atacama fault does not appear to be an active strike-slip fault -- at least not along its central segment between 24°S. and 26°S.

In the map area, the Coast Ranges are underlain predominantly by crystalline rocks that have been intensely broken by high-angle faults of the Atacama fault system. A eugeosynclinal section, chiefly comprising Jurassic-Cretaceous andesites, overlies Paleozoic metamorphic and plutonic rocks and has been intimately intruded by batholithic rocks of Late Jurassic to Tertiary (?) age. An older more voluminous suite of rocks ranging from gabbro to adamellite, with abundant diorite and pyroxene granodiorite, is discordantly cut by stocks of more homogeneous hornblende-and-biotite granodiorite, adamellite, and tonalite.

In the Taltal area, the Atacama fault zone was obliquely cut and left-laterally offset 10 km by the northwest-trending Taltal fault during mid- to late Tertiary time. Lateral motion on the Taltal fault appears to have ceased before the Pliocene epoch. A structural "knot" presently constrains lateral motion along truncated branches of the Atacama fault. A northwest-curving branch that escapes truncation by

the Taltal fault has been more recently active both onshore and offshore, with recent motion predominantly vertical.

Strike-slip displacement occurred during the early history of the Atacama fault. Subsequent to its segmentation, individual sectors have been reactivated independently and have accommodated vertical block motions in their recent history. No convincing evidence was found for any recent lateral displacement. Aspects of the origin of alluvial scarps displaying an anomalous ridge-trench-ridge morphology remain enigmatic, but the features are not necessarily indicative of strike-slip movement as had earlier been considered.

Offshore studies near the map area indicate major faulting on the upper continental slope, beginning within 10 to 20 km of the coastline, that has resulted in the tilting and down-dropping of blocks toward the trench axis. Late Cenozoic tectonics in the Coast Ranges appear to be directly related to the development of the Peru-Chile trench.

A reconnaissance micro-earthquake survey along the Atacama fault shows virtually no activity, or at most very little, in the immediate vicinity of the fault. Abundant micro-aftershock activity from an offshore aftershock zone related to the magnitude 7.5 Taltal earthquake (Dec. 28, 1966) was detected. Gravity and magnetic profiles across the Atacama fault zone reveal no distinctive anomalies that would allow correlation of major branches over large distances. No large-scale gravity anomalies occur across the fault zone.

Schemes of consistent lateral offset along the Atacama fault and its branches have not emerged from systematic regional mapping. Large vertical separation along the faults is a chief control of the regional distribution of rocks. No need is seen to hypothesize strike-slip displacements of hundreds of kilometers along the Atacama fault zone, but suggestive lines of evidence call for a component of lateral displacement measured at least in tens of kilometers. The vertical component of total displacement probably amounts to several kilometers of uplift of the east side. Taking into account map relations which appear to constrain the amount of allowable lateral displacement, it is judged that total strike-slip displacement may be moderate, amounting only to a few tens of kilometers of right-lateral slip.

Photographic materials on pp. 11, 13, 15, 72, 73, 78, 79, 129, 144, 162, 177 are essential and will not reproduce clearly on Xerox copies. Photographic copies should be ordered.

TABLE OF CONTENTS

TABLE OF CONTENTS (continued)

TABLE OF CONTENTS (continued)

TABLE OF CONTENTS (continued)

TABLE OF ILLUSTRATIONS

TABLE OF ILLUSTRATIONS

I. INTRODUCTION

THE PROBLEM

The Atacama fault of northern Chile has been recognized as a major structural feature of the circum-Pacific tectonic region and has been considered to be analogous to regional transcurrent faults such as the San Andreas fault of California and the Alpine fault of New Zealand (St. Amand and Allen, 1960; Allen: 1962, 1965). Detailed information on the Atacama fault, however, is scanty and no thorough study has been documented to elaborate convincingly the nature and history of the fault. St. Amand and Allen (1960) were the first to identify the great extent of the structure (Fig. 1), but they relied primarily on indirect evidence such as linearity, length, "rift topography", moletrack scarps, and horizontal slickensides to suggest that the fault had an overall history of dextral strike-slip (see Allen, 1965). The clearest evidence for Recent lateral motion was found in the Camarones area, where northeast-trending faults with good stream offsets were judged to be conjugate to the north-trending Atacama fault zone (St. Amand and Allen, 1960).

While other workers have recognized parts of the fault zone traced by St. Amand and Allen (see Part VI), no documentation of large-scale lateral offsets along the Atacama fault has been put forth, and the predominance of strike slip has not been fully demonstrated. Even the continuity of two major segments of the fault extending north and south of Taltal was open to question, inasmuch as Bowes et al.

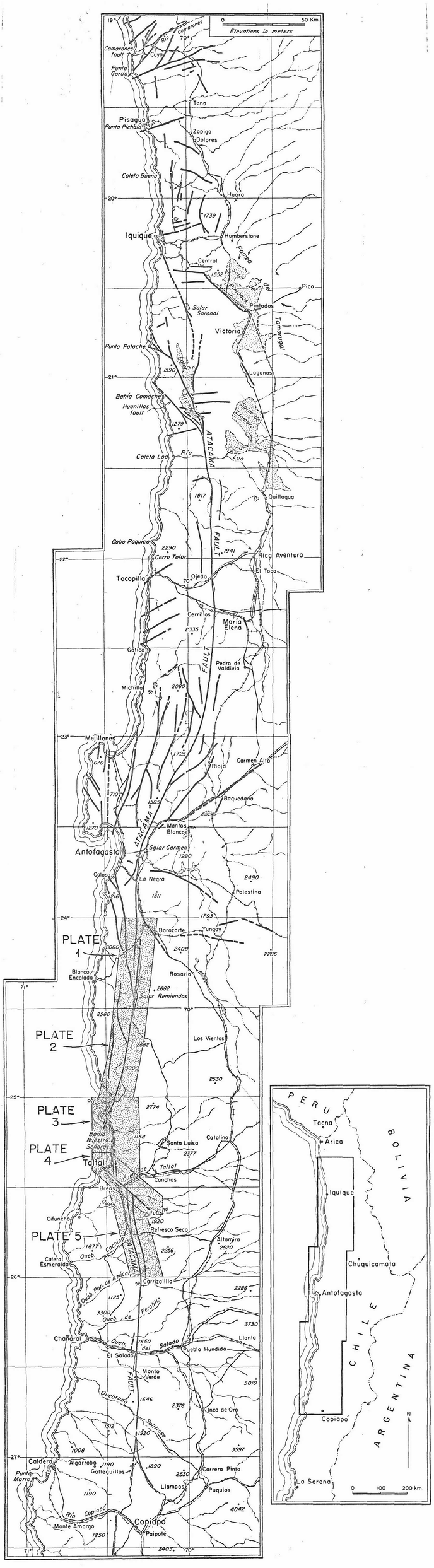

Fig. 1. Index map of the Atacama fault zone (unpublished map of St. Amand and Allen). Shaded area between 24°S. and 26°S. corresponds to area of geologic mapping completed in this study (Pls. 1 to 5).

(1961) differed with St. Amand and Allen's interpretation of the continuity of a single fault zone through the Taltal area (see Arabasz, 1968, p. 837; also, Fig. 1).

The inherent incompleteness of St. Amand and Allen's reconnaissance study, the absence of detailed geologic mapping along much of the fault zone, and the problem of the continuity of the Atacama fault zone through the Taltal area prompted this supplementary field study which was aimed at the following specific problems: (1) Nature of the fault zone: definitive documentation of the Atacama fault zone as a structural break and delineation of major rock units adjacent to the faults; (2) Sense of displacement: evidence for the presence or absence of significant lateral offsets; (3) Continuity: relationship between St. Amand and Allen's El Salado sector (south of Taltal) and Salar del Carmen sector (north of Taltal); (4) Age: time of origin of the structure and its past history; (5) Degree of current activity: relative age of alluvial materials cut by branches of the Atacama fault system and relationship between the Atacama fault zone and the high seismicity of northern Chile; (6) Tectonic significance: relation of the Atacama fault zone to other large features of western South America, particularly the Peru-Chile trench. Discussion of the approaches used to investigate these problems and the interpretation of new information -- considered in light of recent developments in plate tectonics and sea floor spreading -- constitute the main purpose of this paper.

OUTLINE OF METHODS OF STUDY

Both geological and geophysical techniques were used in the field study. Regional geologic mapping was completed on 1 : 60, 000 aerial photographs and compiled at a scale of 1 : 100, 000 (Pls. 1-5). The extent of the Atacama fault did not allow a study of its entirety so field work was focused on a central segment between latitudes 24° S. and 26° S. (Fig. 1), where mapping was carried out along the major fault branches. More detailed studies were made in critical areas. Simultaneously with mapping, a reconnaissance seismic survey was carried out with a single, portable, high-gain seismograph to investigate the level of micro-earthquake activity in the vicinity of the Atacama fault zone.

With the help of the Scripps Institution of Oceanography, records of sub-bottom reflection profiling (air gun), magnetometry, and continuous bathymetry were taken to evaluate the continuity of offshore branches of the Atacama fault system and to trace other offshore structures which might shed light on a relationship between the Atacama fault and the Peru-Chile trench.

As part of the regional mapping, plutonic rocks were extensively sampled to allow petrographic differentiation of major rock units across the larger faults (see Appendix Pls. A, B, C, D). Finally, gravity-magnetic profiles were established across the Atacama fault zone in four localities.

GENERAL PROCEDURE OF THE PROJECT

Six weeks were spent in Chile during August and September of 1966 for the purpose of outlining this study and in initial work in the Taltal area. Two subsequent trips were made between late June and early December of 1967, and between early July, 1968 and mid-April, 1969. During these three trips approximately 280 days were spent in the field completing the geologic mapping and geophysical field work.

Micro-earthquake surveying was carried out intermittently between late July, 1968, and late February, 1969. Oceanographic work was completed in early January, 1969, during the Piquero II expedition of R/V Thomas Washington. The gravity-magnetic profiles were surveyed and staked in early December, 1968; readings were made in early October, 1969.

GEOGRAPHY

Principal Physiographic Features

Three nearly parallel morphological units characterize the physiography of northern Chile north of latitude 27° S. -- the Coast Ranges, the Longitudinal Depression and the Andes. The Coast Ranges vary in width from 50 to 75 km and have moderate elevations, generally between 1000 and 2500 m. They show an arid-cycle, old-age topography which has been disturbed by faulting and incised near the coastline, where descent to sea level is abrupt. To the east the coastal mountains gradually disappear beneath the nitrate pampas

(flat-floored basins) of the Longitudinal Depression, which intervenes between the Coast Ranges and the Andean foothills. This longitudinal trough is continuous as the Pampa del Tamarugal north of 23°15' S.; however, southward it is less well defined and consists of a series of separated basins and non-aligned mountains.

Oblique aerial photographs illustrating numerous features of these physiographic units are included in the geographic discussions of Rich (1941, 1942) and Light and Light (1946); Bowman's (1924) classic geographic treatise includes additional photography. Graphic panoramas of northern Chile are also contained in recent Apollo 7 photographs that are here included as Figures 2, 3, and 4. Figure 3 is particularly illustrative of the physiography described above, showing the faulted Coast Ranges and the irregular aspect of the Longitudinal Depression south of the Pampa del Tamarugal.

The various mapped sectors of this study are included in the domain of the Coast Ranges. Elevations range from sea level to +2664 m. Faulting exerts a profound topographic control throughout, as is well expressed in Figures 3 and 4. Comparison with Figure 1 shows that the shadowed lineaments cutting the Coast Ranges do indeed correspond to fault traces.

South of the latitude of Taltal (Pl. 5), the Atacama fault zone is several kilometers wide, including numerous interlacing branches that occupy both central and marginal positions in an alluviated "fault rift" (Sharp, 1954). This north-northwest-trending zone cuts across large east-west seaward-heading drainages, branches of which have alluviated

the fault rift. The average elevation of this sector approximates 1000 m; however, elevations locally reach 1774 m at Cerro del Pingo.

North of the Taltal airport the rift is truncated by northwest-trending faults which have provided a structural control for stream erosion. Headward erosion of lower Quebrada de Taltal has resulted in the capture and diversion of inland drainage northwestward to the sea. Inland topography is typified by the southeastern third of Plate 4 which includes part of the mature drainage basin of Quebrada de la Peineta, a broad valley with low-relief hills and coalescing aggraded surfaces but with sharp remnant divides.

The topography near the coast, in contrast, is much more youthful. Between Taltal and Paposo (Pl. 3) a narrow coastal platform borders the sea, but peaks higher than 1000 m stand less than 3 km from the coastline, and topographic gradients exceeding 30° are common along the coastal escarpment. East-west antecedent drainage lines incise this uplifted block. Their upper reaches are still aggraded but completely out of equilibrium with their lower segments, which have carved a rugged topography. While not a simple fault scarp in itself, the steep coastal escarpment attests to fault-related motion.

North of 25° S. (Pl. 1 and 2) major branches of the Atacama fault zone bound tilted and uplifted blocks that display classic features of young block faulting, which dominates the physiography. Linear fault-angle valleys (Cotton, 1950) of north-trending faults disrupt east-west drainage. To the east, the Sierra Vicuña Mackenna diverts drainage from the Andes northwestward to Antofagasta and

southwestward to Cifuncho (see Fig. 4) so that no large inland drainage reaches the sea between 24° and 25° S. The upper surfaces of large fault blocks in this region illustrate the subdued old-age landscape with moderate to steep local relief that is characteristic of the Coast Ranges. Elevations exceeding 2000 m are common within 8 km of the sea.

Climate and Vegetation

The area of this study lies wholly within the Atacama Desert of northern Chile, the driest coastal desert in the world in terms of precipitation (Meigs, 1966, p. 110) and a unique regime for the preservation of certain geomorphic features -- in particular, those related to faulting. Climatic data is pertinent in considering the age of such features.

According to Meigs (1966, Table 8E), annual precipitation at Iquique averages 0.04 in. (30 years recording) and at Antofagasta, 0.32 in. (30 years rec.); the annual average at Taltal is slightly higher -- 0.98 in. (21 years rec.), which partially reflects maritime conditions on the coastal platform that contrast with the aridity at short distances inland.

Together with the extreme aridity, one other climatic anomaly is notable -- brief periods of torrential rainfall which may occur at intervals of several years (Rudolph, 1953; Trewartha, 1961). Rudolph (1953, p. 565) notes the occurrence of heavy rains and floods

in northern Chile in 1925 and 1953, the latter "...considered by the oldest dwellers of Chile's Antofagasta Province to be the heaviest in their lifetime". Bowman (1924, p. 40-41) discusses other periods of exceptional rains and floods, especially 1911, but the extent of flooding in a given year of heavy rainfall is difficult to determine.

Vegetation ranges from nonexistent in the arid inland desert to small gardens and groves of trees in irrigated places such as in and near Taltal. Also nonpluvial moisture in the form of fog and dew supports abundant cacti, scrub, and woody shrubs on the seaward facing slopes of the coastal scarp.

Fig. 2. (following page) Apollo 7 photograph of coastal northern Chile showing the extensive trace of the Atacama fault zone (D, E, F). The distance between B and C is approximately 200 km. The Mejillones Peninsula (A) in the foreground provides convenient reference for comparison with Figure 1. Note South arrow.

A. Mejillones Peninsula

B. Antofagasta

C. Taltal

D. Main trace of the Atacama fault northeast of Antofagasta

E. Linear segment of the Salar del Carmen sector of the Atacama fault zone

F. El Salado sector of the Atacama fault zone south of Taltal

G. Salar de Punta Negra

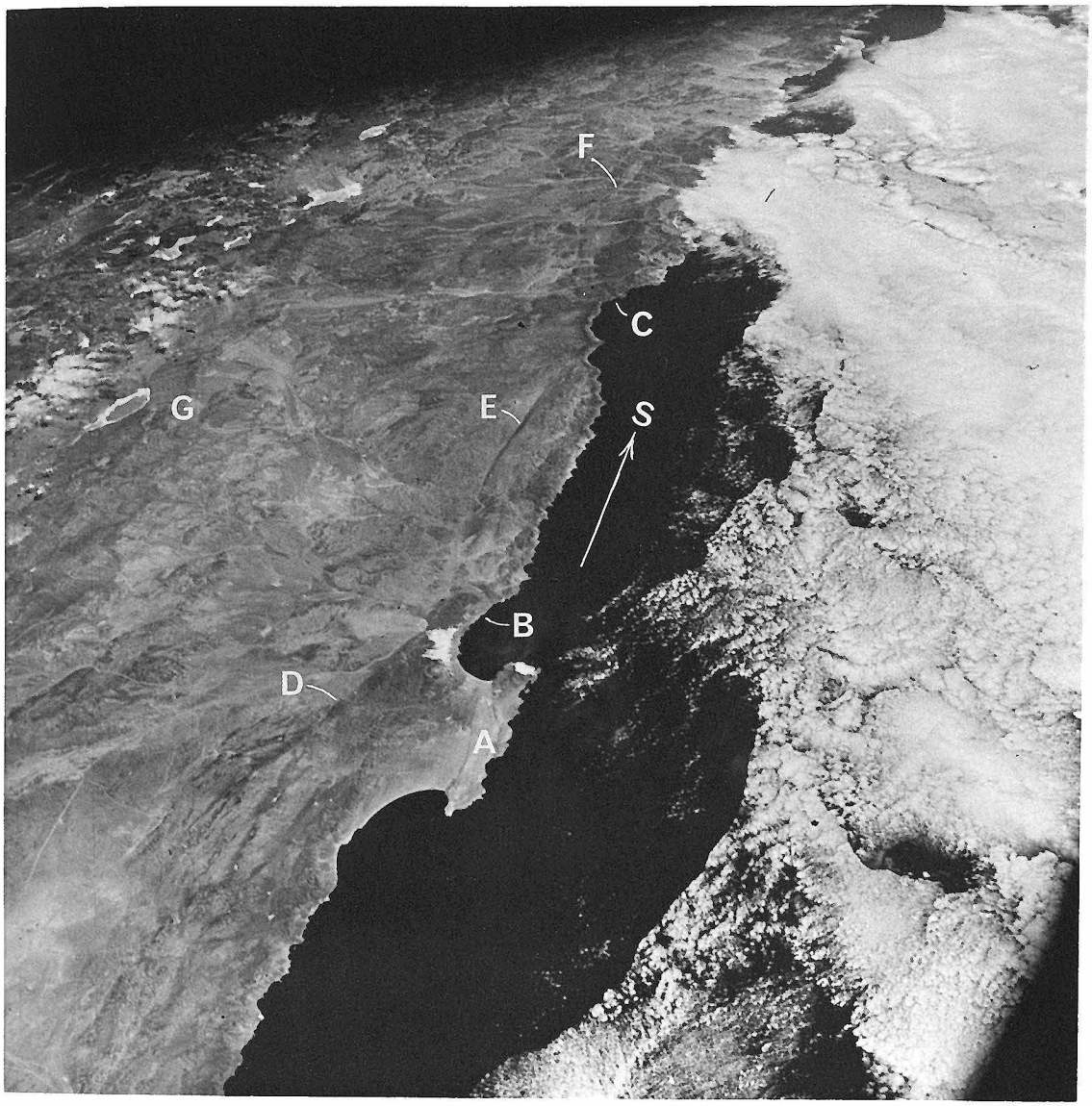

Figure 2

Fig. 3. (following page) Apollo 7 photograph of northern Chile showing fault-controlled topography in the Coast Ranges (foreground) north and south of Antofagasta (C). Compare with Figure 1. The relation of the Coast Ranges to the larger morphological features of northern Chile is also illustrated. View is to the southeast.

A. East-facing scarp of Morro Mejillones, a horst block on Mejillones Peninsula

B. Main trace of Atacama fault northeast of Antofagasta

C. Antofagasta

D. East-facing scarp of the Salar del Carmen (Atacama) fault

E. Sierra Vicuña Mackenna

F. Pampa del Tamarugal (Longitudinal Depression)

G. Salar de Atacama

H. Salar de Punta Negra

Figure 3

Fig. 4. (following page) Apollo 7 photograph of coastal northern Chile showing major features of faulting in the Antofagasta-Taltal area. Most of the area mapped in this study is included. The distance between B and H is approximately 200 km. Low clouds abut against the steep coastal escarpment between F and H.

A. Morro Moreno, at southern end of Mejillones Peninsula

B. Antofagasta

C. Northeast-facing scarp of the Caleta Coloso fault

D. Sierra Vicuña Mackenna

E. Linear east-facing scarp of the Salar del Carmen (Atacama) fault

F. Quebrada de Remiendos

G. East-facing scarp of the Izcuña fault

H. Taltal

I. Curving trace of the Aguada Chépica fault

Figure 4

II. REGIONAL SETTING

The general geology of Chile has been summarized by Brüggen (1950), Muñoz Cristi (1956), Zeil (1964), and Ruiz (1965); Harrington (1961) and García (1964) limit discussion to northern Chile. In addition, the revised Geologic Map of Chile (Instituto de Investigaciones Geológicas, 1968) represents a recent compilation of regional geologic mapping at a scale of 1 : 1, 000, 000. Emphasis in the following outline is placed on the setting of the Coast Ranges in the vicinity of this study.

Two relations are exceedingly important in considering the tectonic environment of the Coast Ranges: (1) their spatial relation to the site of the great Mesozoic Andean geosyncline; and (2) their present setting between, and parallel to, the Peru-Chile trench and the Andean cordillera. The site of the Coast Ranges marked the western marginal area of the Andean geosyncline (Ruiz, 1965, p. 42), where extensive andesitic volcanism dominated the eugeosynclinal infilling in Jurassic and Cretaceous time. An underlying continental basement of Paleozoic metamorphic and granitic rocks had foundered beneath the geosynclinal trough and was later intimately intruded, together with the geosynclinal fill, by a suite of Late Mesozoic to Tertiary batholithic rocks. Intense high-angle faulting and moderate folding has affected the entire sequence. At the latitudes of this study, all the above-mentioned crystalline rocks are exposed, together with fragmentary or less extensive outcrops of key sedimentary rocks which allow refinement of the stratigraphy and history (see Part III).

The manifestations of current tectonic activity in northern Chile are well known -- the active volcanism in the Chilean Andes (Casertano, 1963), the high seismicity of northern Chile (Willis, 1929; Gutenberg and Richter, 1954; Lomnitz, 1964; Barazangi and Dorman, 1969), the steepness of the east-west gravity gradient (Lomnitz, 1962), and the steep topographic gradient from the heights of the Andes to the depths of the Peru-Chile trench, as emphasized by Lomnitz (1962). Continuing tectonic deformation of the Coast Ranges is specifically indicated by abundant Quaternary scarps along the Atacama fault and its branches. Clearly, faulting in the coastal mountains must bear some relation to the larger scale tectonics of the South American continental margin. Moreover, the fact that the Atacama fault, as a proposed regional transcurrent fault, is in a tectonic environment quite distinct from that of the San Andreas and Alpine faults (Allen, 1965, p. 85-87) warrants some introductory remarks about the framework of the continental margin in northern Chile.

Crustal cross sections based on geophysical data for the latitude of Antofagasta near 23°S. (Fig. 5) provide a useful starting point for discussion. The axis of the Peru-Chile trench parallels the coastline at a distance of 80-95 km, while the Andes are more than twice that distance inland. The rapid eastward crustal thickening beneath the continental margin and the steep gradient of the continental slope are striking. Both gravity data (Fig. 5b) and seismic refraction data (Fig. 5a) imply a crustal thickness exceeding 25 km beneath the Coast Ranges, and a crustal thickness beneath the trench axis that is significantly greater than that west of the trench -- 10.5 km versus 6 km, according

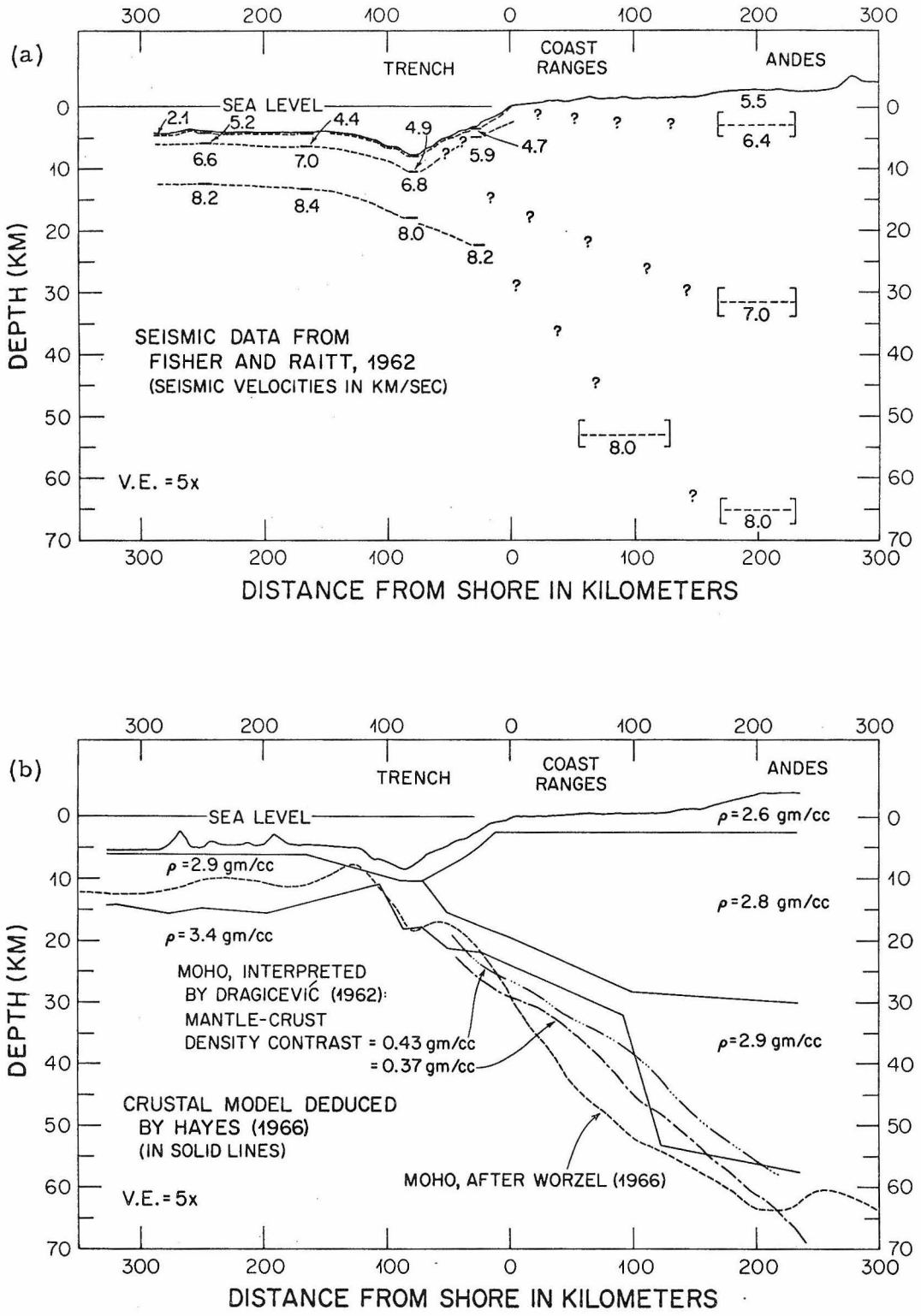

Fig. 5. Geophysical crustal sections of western South America at the latitude of Antofagasta (23.7°S.), based on seismic refraction data (a) and gravity (b).

to Woolard (1960, p.110).

The spatial distribution of earthquakes had allowed earlier interpretation of the transverse deep structure of the continental margin. Profiles of earthquake foci suggested the delineation of zones that were interpreted by Benioff (1949, 1954) as representing a great fault dipping under the South American continent. Shallow seismicity predominates near the coast, while earthquake depths increase progressively eastward to a depth of about 650 km, with a curious absence of shocks between 300 km and 550 km.

The above facts lead to some comments on the setting of the Coast Ranges. First, the proximity of the Atacama fault to the trench adds importance to understanding the history of the fault and the coastal structure, particularly in view of the need to further understand the trench (Scholl et al., 1968; Scholl et al., in press). Second, if the trench represents a large down-faulted structure as envisioned in models of Worzel (1966, p. 369), then the Coast Ranges are located near a critical zone of extension, despite the seemingly large distance to the axis of the trench. Third, because numerous shallow earthquakes that are associated with the Benioff zone occur beneath the coastal area, it is difficult to distinguish crustal macroseismicity that can be linked to energy release along the Atacama fault zone; a large depth uncertainty that is common in the location of hypocenters in this area effectively blurs the association of seismicity with surficial faults. In addition, observations of fault displacements accompanying historical earthquakes in northern Chile are absent, and to the writer's knowledge, no

compilation of reliable locations has demonstrated a close relation between shallow earthquakes and the Atacama fault zone. This background lent some importance to undertaking a micro-earthquake survey along the fault (Part VII).

The type of geophysical perspective contained in Figure 5 is valuable, but the need to take a new look at continental margins in terms of sea floor spreading and plate tectonics is recognized. A detailed discussion is deferred to Part IX to include the results of this study.

How would an up-to-date view of the continental margin change the perspective of Figure 5? According to the concepts of the new global tectonics (Isacks et al., 1968), a slab of lithosphere about 100 km thick (composed of oceanic crust and the rigid upper mantle above the low velocity zone) is spreading eastward from the East Pacific rise and plunges beneath the western margin of South America, where it is bounded on the upper surface by a seismic zone.

To compare the hypothetical structure section of Isacks et al. (1968, p. 5869) with the continental margin of northern Chile (Fig. 5), and to locate the upper surface of the down-going slab, requires either defining the zone of shallow seismicity or imaginatively following a bend of oceanic crust beneath the continental margin. A sharp boundary is not defined by the shallow earthquakes in northern Chile, but the following observations can be considered: (1) Refined locations indicate events generally shallower than 80 km beneath the coastline (Olea, 1967). (2) Earthquakes are generally restricted to the landward side of the trench axis (see Barazangi and Dorman, 1969). (3) Benioff (1954)

indicated that the layer defined by shallow earthquake sequences intersects the continental slope and dips 23° landward in Chile. (4) A regional fault, or zone of faulting, is interpreted by Plafker and Savage (1970) in connection with the 1960 earthquake sequence of southern Chile as intersecting the continental slope and dipping 35.5° landward; they judge that movement on the fault was compatible with active underthrusting of the lithosphere.

Significant problems have arisen in attempting to apply the concepts of the new global tectonics to the Chilean margin -- the most notable being difficulties with the postulation of plate convergence at the trench (Scholl et al., 1968; Scholl and von Huene, 1970; Scholl et al., in press). Also, "The occurrence of large active strike-slip faults that trend along the arc structure, such as...the Atacama fault in Chile, offers some difficulties." (Isacks et al., 1968, p. 5892.)

The geologic studies of the Atacama fault will now be considered in detail but, as noted, the implications of sea floor spreading and plate tectonics will be returned to in Part IX. Tectonism of the Coast Ranges must at some point be framed in this broader structural view in which the offshore trench, coastal faulting, and uplift and volcanism in the Andes are related.

III. ROCK UNITS

INTRODUCTORY STATEMENT

The rock units that were mapped have been grouped into four categories that facilitate an overview of the general geologic history of the Coast Ranges: (1) Paleozoic metamorphic and granitic rocks, (2) Mesozoic geosynclinal rocks, (3) Mesozoic-Tertiary plutonic rocks, and (4) Tertiary-Quaternary sediments. Subdivision of the lithologic units was aimed at providing a workable scheme for documenting, as accurately as possible, the relationships of major rock types across the Atacama fault and within numerous fault blocks and slices. The following discussion outlines the important rock types that were mapped and follows the geologic history that is related to the rocks. Unfortunately, major problems persist with regard to stratigraphy and to the dating of plutonic rocks in the area, as discussed below, so that understanding of the geologic history is generalized.

Some new stratigraphic observations are reported, but most of the stratigraphy is based on the work of other investigators in northern Chile. Study of the plutonic rocks was more detailed than that of earlier work in the area; the mapping provides a valuable view of the regional distribution of plutonic rock types. Their general characteristics are described in this part, while descriptions of individual bodies that relate to fault displacement are elaborated in Part VI.

The reader is referred to Appendix Plates A, B, C, and D for the location of cited rock samples. Sample numbers prefixed by "PA" correspond to Plate A, by "S" to Plate B, by "T" to Place C, and by

"CE" to Plate D. In addition, underlining of a sample number indicates that its mode is contained in Appendix Tables 1 to 10.

PALEOZOIC METAMORPHIC AND GRANITIC ROCKS

General Statement

The oldest known rocks that were mapped are pre-Triassic metasedimentary rocks that crop out in two general areas: (1) near and north of Paposo in the block bounded by the Salar del Carmen and Izcuña faults (Pls. 2 and 3), and (2) east of the Atacama fault zone between the southern map limit and Paposo (Pls. 3, 4, and 5). Quartzites, phyllites, argillites, and mica schists predominate. Identical rocks occur more extensively to the west of the map area in the coastal belt between Taltal and Chañaral (Bowes et al., 1961). No fossil determination has been made in the Taltal area; however, comparison with similar rocks of the El Toco formation exposed near Tocopilla (see Harrington, 1961) leads to a Late Paleozoic age assignment (Ortiz et al., 1960; Zeil, 1960). Wetzel (1927) dated the El Toco formation as Permo-Carboniferous on the basis of plant remains.

Other evidence supports the Paleozoic age assignment. Stocks and small bodies of light-colored, quartzose granites and adamellites intrude the metasedimentary rocks. Key stratigraphic relationships in the Cifuncho-Posada de los Hidalgos area, some 30 to 40 km south-southwest of Taltal, imply that both the host rocks and the above-mentioned intrusives are unconformably overlain by a conglomerate-rhyolite section of probable Triassic age, and that all these rocks are

unconformably overlain by Hettangian (Early Jurassic) marine rocks (Ruiz et al., 1961, p. 1552; Bowes et al., 1961). Moreover, a lead-alpha radiometric age determination of an adamellite from that same area -- assumed to be Paleozoic from field relations -- indicates an age of 340 ± 40 million years (Levi et al., 1963, p. 16).

El Toco-Type Metasedimentary Rocks

The most commonly encountered Paleozoic metasedimentary rocks are pale brownish gray, fine- to medium-grained, indurated quartzites, and grayish green, chloritic phyllites. Other lithologies that are abundant locally include: (1) pale to dark greenish gray mica schists, (2) gray to black, laminated and indurated argillites and argillaceous sandstones -- grading to graywacke, (3) dark greenish gray slates, (4) micaceous sandstones of various grain sizes and colors, and (5) purplish brown fissile shales. Some of the lithologies are described in sedimentary rather than metamorphic terms, but virtually all show evidence of low-grade regional metamorphism.

An alternation of arenites and lutites was either observed or interpreted in most locales. Two common sequences are: (1) thick-bedded, massive, indurated quartzites, up to a few meters thick, with thin intercalations of broken and often highly contorted phyllites; and (2) rhythmic sequences comprising sharply defined beds 10-30 cm thick of alternating thin-bedded, fine-grained, shaly sandstones and shales, and thick-bedded, massive, fine-grained quartzites.

The Paleozoic metasedimentary rocks within the map area occur primarily as septa and roof pendants within younger batholithic rocks, so that estimating their thickness is difficult. Cecioni reportedly measured a 3,430-m thickness of the El Toco formation where neither base nor roof was exposed (García, 1964, p. 23). Exposures are generally poor. Hills mantled with broken fragments of quartzite and phyllite are commonly the only outcrops available. One notable exception is the area north of the Taltal fault where young dissection near the coast provides better exposure; the best was observed in a foot traverse along Quebrada Cortaderas (Pl. 4).

The degree of deformation shown by the Paleozoic metasedimentary rocks is noteworthy because Mesozoic rocks in the Coast Ranges show no strong regional folding, but rather are either tilted or very gently folded. Despite intense local deformation, the metasedimentary rocks tend to display original bedding more commonly than cleavage, as noted by Bowes et al. (1961), and they show open folding on a scale of tens of meters. Recrystallization of quartz along fractures is common. More intense modification has resulted near the Atacama fault zone, where the rocks have been affected by both cataclasis and migmatization (see discussion of gneissic and migmatitic rocks), or where the rocks occur in narrow septa between batholithic rocks. Contact metamorphic effects are seen along the northwestern boundary of the swath of metasedimentary rocks cropping out west of the Salar del Carmen fault, where a band of spotted slates approximately 1 km wide parallels the intrusive contact of Jurassic-Cretaceous dioritic rocks (Pl. 2).

Ruiz (1965, p. 19) discusses the distribution of Paleozoic rocks in Chile, linking them with one or more ancient geosynclinal troughs that extended to Bolivian and Argentine territory. The character and lithological alternation of the metasedimentary rocks are consistent with such a relation, for they constitute a flysch-like sequence deposited in a marine environment of considerable depth (see Dżułynski and Walton, 1965, p. 3).

Because their internal structure and stratigraphy could not be readily mapped, the Paleozoic metasedimentary rocks were grouped as a single unit. Their contacts are exclusively fault or intrusive contacts. Being the oldest rocks in the area, they have been affected by at least three cycles of plutonic activity, as well as numerous pulses of dike intrusions. The most common dike swarms are andesite feeder dikes related to extrusive activity during the Jurassic and Cretaceous Periods.

Paleozoic Granitic Rocks

Where they constitute mappable bodies, Paleozoic granitic rocks have been separated from the metasedimentary rocks. Designation of a Paleozoic age is based mainly on spatial association with Paleozoic metasedimentary rocks and petrographic criteria outlined in the following discussion.

The distinctive character of Paleozoic granitic rocks, as compared to those of Mesozoic and Cenozoic age, has been generally recognized in Chile. Petrographic comparison is summarized by Levi et al. (1963), showing that, in general, the Paleozoic granitic rocks tend

to be coarser grained, lighter colored, more leucocratic, more potassic, more silicic, and more highly tectonized. Mineralogically, biotite predominates as the major ferromagnesian mineral; microperthite or microcline-perthite is the most common potassium feldspar; modal quartz greater than 40% is not uncommon (Levi et al., 1963).

The generalizations outlined above apply to the granitic rocks that were assigned a Paleozoic age in this mapping. Rock types that were distinguished include: (1) medium- to coarse-grained leucogranite, (2) medium- to coarse-grained equigranular biotite adamellite, (3) fine- to coarse-grained, inequigranular to porphyritic, biotite adamellite, and (4) fine- to medium-grained granophyric leucogranite. (See Appendix Table 1.)

Both the biotite adamellites and leucogranites are silicic, containing 25-50% quartz, generally more than 35%. The leucogranites, in addition, contain 40-65% microperthite, 5-10% oligoclase, and less than 2% biotite; the biotite adamellites, in addition to quartz, contain 20-35% calcic oligoclase to sodic andesine, 15-40% microperthite, and 3-10% biotite. In hand specimen the most distinctive features of both classes are their light color (pale gray, whitish gray, yellowish gray, pale grayish orange), friable coherence (because of coarse grain size and pervasive cleavage), and quartzose texture. Gray quartz occurs either in regularly spaced anhedral patches up to 1 cm in diameter, or in granophyric intergrowths with K-feldspar. Where biotite increases in abundance in the coarser-grained adamellites, it tends to be distinctively euhedral.

Bodies of Paleozoic granitic rocks occur: (1) within a fault-bounded block in the Sierra del Carmen area (Pl. 5), (2) near Estación Central (Pl. 4), (3) in the Sierra Finca (Pl. 3), and (4) west of the Salar del Carmen fault in the Cerro Yumbes area (Pl. 2). On aerial photographs, these light-colored intrusives generally display a distinctively high albedo, which contrasts sharply with black dikes intrusive into them.

The extensive occurrence of Paleozoic granitic rocks in Chile (Ruiz, 1965, p. 30), particularly in the Taltal-Chañaral area (Bowes et al., 1961), indicates that Paleozoic intrusions were of batholithic proportions -- a fact that must be kept in mind when considering the relations of isolated outcrops. Ruiz et al. (1961) consider that the batholithic intrusion can be related to a late phase of Hercynian orogeny. Both the geosynclinal metasedimentary rocks and the granitic rocks of Late Paleozoic age imply that the site of the Coast Ranges was characterized by crustal mobility prior to development of the Andean geosyncline during the Mesozoic.

MESOZOIC GEOSYNCLINAL ROCKS

General Statement

The development and stratigraphy of the Mesozoic Andean geosyncline has been summarized by Muñoz Cristi (1956) and is more extensively discussed by Ruiz (1965). The setting of the Coast Ranges in relation to the geosyncline was emphasized earlier (Part II), where it was noted that their site occupies the western eugeosynclinal area.

Information from the map area is insufficient for detailing the Mesozoic stratigraphy because post-Paleozoic sedimentary rocks are not abundant; moreover, although stratified volcanic rocks of Jurassic and Cretaceous age are abundant, their stratigraphy is poorly deciphered. Consequently, information from other areas is critical. Ruiz (1965), García (1964), and Harrington (1961) all include pertinent stratigraphic discussions. Other important references are cited below. This discussion outlines the stratified rocks that were mapped and treats their relation to the general stratigraphy of northern Chile.

Triassic Rocks

Although no rocks of known Triassic age crop out within the map area, the Cifuncho formation, assigned to that period, crops out nearby in a band between Quebrada Cifuncho and Quebrada Pan de Azucar, 30 to 75 km south of Taltal. Arkosic sandstones, arkosic pebble and cobble conglomerates (with fragments of Paleozoic granite and metasedimentary rocks), devitrified acidic tuffs, keratophyres, and rhyolite or soda-trachyte flows, are irregularly exposed and lie unconformably upon Paleozoic rocks similar to the El Toco formation (Ruiz et al., 1961; Bowes et al., 1961; García, 1964). The character of these rocks provides an important clue to interpreting the earliest history of the Andean geosyncline.

Corvalán (in Ruiz, 1965, p. 34-40), in synthesizing the distribution and character of Triassic rocks in Chile, interprets the former existence of a continental platform -- the result of consolidation of a Paleozoic geosyncline -- which at various times during the Triassic

was subject to cycles of erosion and sedimentation, epeirogenic sinking and marine transgression, and cycles of silicic volcanic activity of enormous extent. The Triassic clastic-volcanic sequence described briefly above indicates that, in the Taltal area, as in other areas of northern Chile, the Andean geosyncline developed upon a platform that was continental in character. Moreover, the initial Mesozoic extrusive cycle was predominantly acidic.

Liassic Marine Rocks

The oldest Mesozoic rocks that were mapped are Liassic marine rocks that crop out in two general areas: (1) near and north of Paposo in the block bounded by the Salar del Carmen and Izcuña faults (Pls. 2 and 3), and (2) at Cerro Blanco, a few kilometers west of Taltal (Pl. 4). Rocks of this group had earlier been recognized in reconnaissance by Burnol and Bournat (1966) 10 km north of Paposo at the edge of the coastal escarpment. The latter authors describe "...une série schisto-calcaire formée d'une alternance de bancs calcaires de vingt a cinquante centimetres de puissance et de schistes gris-verdatres de puissance variable." Included in the section are "...des conglomérats en bancs de un a trois metres de puissance séparés par des schistes lie de vin. Ces conglomérats sont formés d'éléments arrondis, polygéniques (quartz, grés, schistes, roches granitiques) d'une taille variant de un a cinq centimetres, englobés dans un ciment gréseux" (Burnol and Bournat, 1966).

Burnol and Bournat indicated that the above-described rocks extended 2 km in a north-northeast direction in a band about 800 m wide.

Mapping in the area, however, shows that they are more extensive (Pl. 2). Southwest of Cerro Yumbes above the coastal scarp, rocks similar to those observed by Burnol and Bournat constitute a band 1.5 - 3 km wide that extends approximately 11 km. A detailed study of the stratigraphy was not made; because outcrops are not continuous throughout the band, particularly to the north and west, the structure and character of the sedimentary rocks are generalized.

Included in the section are calcareous shaly sandstones and fissile shales, alternating with thick beds of fine-grained calcareous sandstones and limestones. Olive, greenish gray, drab, and purplish colors are common. Light to dark gray and bluish gray, laminated to thin-bedded, cherty shales and siltstones were also observed at several localities southwest of Cerro Yumbes at what would be interpreted as intermediate and higher levels of the sedimentary section. The entire section dips westward with local strikes varying between northeast and northwest. To the east an intrusive rhyolite massif separates the sedimentary sequence from Paleozoic metasedimentary rocks. Fragmentary outcrops of the Liassic marine rocks along the eastern contact of the rhyolite massif allow the interpretation of original unconformable deposition of the Liassic rocks upon the Paleozoic rocks. To the west, the Liassic rocks are bounded by a swath of andesitic rocks that, in part, are clearly intrusive. Field and map relations, although not definitive, suggest that the sedimentary rocks are capped by westward-dipping extrusive andesite flows before abutting against the Izcuña fault. Andesite dikes and sills intrude all levels of the sequence. To the north

and south, the section is intruded by Jurassic-Cretaceous granitic rocks.

C. Klohn reportedly had sampled sedimentary rocks from this area by helicopter and labeled them as Jurassic (Burnol and Bournat, 1966). Molluscan remains collected by this writer near sample locality S-310 (Appendix Pl. B) at a point high in the exposed section, have been identified and assigned a Sinemurian (Early Liassic) age (J. Corvalán, 1970, written communication). These fossils include the pelecypods Gryphaea sp. and Weyla alata (Buch), and arietitid ammonites of the genus Arnioceras. To the north of sample locality S-310, the sedimentary rocks are excellently exposed and can be seen as a westward-dipping homoclinal sequence with numerous bedding-plane slopes developed on resistant beds of calcareous sandstone. A thickness of sedimentary section of the order of 1700 m to 2000 m is estimated to be exposed between the rhyolite massif and the Izcuña fault.

Observation of laminated cherty shales and siltstones within the section above the coastal scarp is important in understanding outcrops of similar rocks in three other localities which had not earlier been recognized. Near the point where the Izcuña fault crosses the beach at Rada Paposo (Pl. 2), cherty shales and siltstones are exposed to the east of the fault and are intruded by andesite porphyry. Outcrops are fragmentary because of burial by clastic debris sweeping down from the coastal scarp.

At another locality a few kilometers south of Paposo, a large alluvial fan is built at the mouth of Quebrada Paposo, burying rocks on

the coastal platform (Pl. 3). Where the fan has been cut back by wave attack at the beach, however, a homoclinal sedimentary sequence striking northwest and dipping southwest is uncovered. A section approximately 950 m thick includes rhythmically bedded cherty shales and siltstones, very coarse pebble gravels, and silicified calcareous sandstones. The bulk of the section consists of light gray, greenish gray, bluish gray, pink, and black, indurated, cherty shales and siltstones that are both finely laminated and very thin-bedded, with beds generally less than a few centimeters thick. The regularity of rhythmic bedding is striking. Microscopic observation shows that the rocks are predominantly detrital, but they have interbedded chert and apparently are pervasively silicified.

To the northeast these rocks unconformably overlie slates, quartzites, and other metasedimentary rocks of the Paleozoic type which are markedly deformed in contrast to the regularly bedded overlying rocks. In an interval approximately 350 to 450 m above the base of the post-Paleozoic section, coarse to very coarse pebble conglomerates are found. These consist of gray to greenish gray, indurated, massive conglomerates, with subangular to subrounded clasts of quartz, quartzite, and what appear to be resistant facies of the Paleozoic metasedimentary rocks, in a silicified, argillaceous to sandy matrix. A few small granitic pebbles (Paleozoic ?) were found in minor abundance. The conglomerate beds vary in thickness from less than 1 m to more than 3 m, and are separated by massive, indurated, siltstones and sandstones with gradational boundaries.

Rhythmically bedded cherty shales similar to those lower in the section succeed the conglomeratic interval, and in the upper 150 m of the exposed section are interbedded with thin beds of gray, olive-gray, and greenish gray, fine-grained calcareous sandstones. Pelecypod and ammonite remains were collected from this upper interval, near sample locality T-134 (Appendix Pl. C), by this writer and geologists of the Instituto de Investigaciones Geológicas. Identification of impressions of a large, coarsely ribbed pelecypod valve of the genus Weyla, and impressions of the flank of whorl fragments of an arietitid ammonite that probably belongs to the genus Coroniceras, leads to assignment of a Sinemurian (Early Liassic) age (J. Corvalán, 1970, written communication).

The precise relation between Liassic marine rocks at the top of the 950-m section just described, and stratified andesite flows exposed continuously on the southwest to Punta Grande, is confused both by a small intrusive body of andesite, and a zone of andesite dikes which intervene between the two stratified sequences. (Massive andesite dikes up to several meters wide intrude all the Liassic and older rocks.) However, there is a general conformity in attitude between the two sequences; the andesite flows are clearly younger and do not appear to lie with great angular discordance upon the Liassic marine rocks.

The third locality in which banded cherty beds crop out is 2.5 km southeast of Paposo in a fault slice bounded by the Salar del Carmen fault and a converging fault 0.5 km to the west (Pl. 3). Exposures are incomplete, and sills of pinkish gray to dark olive-gray dacite porphyry,

as well as andesite dikes, intrude the section. Rhythmically bedded cherty siltstones, silicified calcareous mudstone, and indurated coarse pebble conglomerates were identified and related, because of similar -- though not identical -- character, to the sequence cropping out along the beach to the west.

This fault-bounded section is intruded on the north by granodiorite; a contact with andesitic rocks is inferred to the south. A thickness of at least several hundred meters must be included in the fault slice, although exposure is poor away from Quebrada Paposo. The distinctive section of Liassic rocks maintains map continuity to the Salar del Carmen fault and constitutes a potentially important marker unit. At sample locality T-94 (Appendix Pl. C), for example, distinctive rocks in contact with the fault include olive-yellow, indurated, medium to coarse pebble conglomerates, with subrounded fragments of quartz, siltstone, and quartzite in a silicified argillaceous matrix.

The regional stratigraphy helps to understand the significance of the marine sedimentary rocks near and north of Paposo. Important unpublished work of Ortiz, summarized by Ruiz (1965, p. 45) and García (1964, p. 40), has shown that between Taltal and Chañaral, 1700 m of Early to Middle Jurassic fossiliferous marine rocks, including calcareous shales, limestones, sandstones, and andesitic breccias, unconformably overlie both the Triassic (?) Cifuncho formation and Paleozoic rocks. The base of the section is Hettangian (Liassic); andesitic volcanic rocks of the La Negra formation, labeled Dogger by García, are superposed with angular discordance on the earlier Jurassic

marine strata (García, 1964, p. 31).

Pale green and pale drab calcareous sandstones, shales, mudstones, and limestones occurring in the fault-bounded outcrop at Cerro Blanco, near Taltal, are assumed to be Liassic and lie along a projected line of the Liassic outcrops occurring south of Taltal.

It is likely that the marine rocks exposed near and north of Paposo are correlative with those south of Taltal, although some lithologic differences are apparent. All the marine rocks discussed are judged to be Jurassic in age and are interpreted to have been deposited unconformably upon Paleozoic rocks inasmuch as Triassic-like rocks were not recognized. No formational name is applied; in this report the strata are simply termed Liassic marine rocks and mapped as a single unit, although there is some lateral variation between the rocks above the coastal scarp and those southwest of Paposo.

Thus, the continental platform developed during the Triassic had foundered by Liassic time. Marine rocks of true geosynclinal character represent early infilling of the trough, but by the Middle Jurassic, outpouring of andesites completely predominated the geosynclinal filling at the site of the Coast Ranges, as discussed next.

Jurassic-Cretaceous Volcanic-Clastic Rocks

General statement. -- The most extensive stratified rocks in the map area belong to a volcanic-clastic sequence of great thickness that is directly related to volcanic activity in the Andean geosyncline.

Beginning in early to mid-Jurassic and continuing intermittently through early Cretaceous time, the products of andesitic volcanism dominated the infilling of the western eugeosynclinal area and were widespread in northern Chile (Muñoz Cristi, 1956; Ruiz, 1965). Formerly, extrusive Mesozoic andesites were collectively grouped into the "Porphyritic formation" -- "Formación porfirítica" (see Brüggen, 1950, p. 15) -- because of their petrographic similarity and similar tectonic environment. Stratigraphic refinement became possible where intercalation or interfingering with fossiliferous marine rocks was observed. Nevertheless, in many areas such as the Taltal area, stratigraphic problems persist. The absence of marker horizons, displacement or consumption by batholithic rocks, alteration and mineralization, and intense faulting pose serious difficulties to using a refined stratigraphy.

In this study, the mapping of andesitic rocks in various fault blocks and roof pendants presented problems, because an arbitrary age assignment to either the Jurassic or Cretaceous could imply the relation or dissociation of andesites across a fault. Also, similarly appearing, altered andesitic rocks occur as stratified flows, as complexes of flows, sills, and dikes, as larger hypabyssal intrusive bodies, and as metavolcanic complexes of undetermined structure. Systematic distinction of these units was not possible everywhere in the regional mapping. For these reasons, all andesitic rocks were grouped into a composite map unit; subdivisions, indicated in the map explanation, were applied where an understanding of the rocks justified them. In a few areas the character of the rocks suggested close similarity to rocks determined to be

Jurassic or Cretaceous elsewhere (discussed below); despite the use of different symbols of Period, the same map color is retained because location of the Jurassic-Cretaceous boundary is unknown.

The portion of the volcanic-clastic section belonging mainly to the Jurassic System (La Negra formation) will be distinguished from that belonging mainly to the Cretaceous (Bandurrias and Caleta Coloso formations) for the sake of relating to the regional stratigraphy as determined outside the map area.

La Negra formation. -- The term, La Negra formation, was used by García (1964, p. 53-56) to include a thick sequence of andesite flows and breccias with intercalations of red continental clastic beds that is extensively exposed in the Coast Ranges from south of Taltal to south of Iquique. A thickness greater than 10, 000 m was estimated by García to be exposed at the type area in Quebrada La Negra, 6 km south of Antofagasta. Stratigraphic relations bearing on the age of the La Negra formation are summarized by Tobar (1966), who refines the Dogger age applied by García (1964); the base of the La Negra formation is clearly post-middle Liassic in the Posada Los Tres Hidalgos area, but elsewhere appears to have a range between middle Liassic and Kimmeridgian (late Malm).

Andesitic rocks almost certainly belonging to the La Negra formation crop out west of the Atacama fault and southwest of the Taltal fault in the areas of Plates 4 and 5. Andesites exposed between Paposo and Punta Grande west of the Salar del Carmen fault (Pl. 3) likewise are probably correlative with the La Negra formation because of their

apparent superposition upon Liassic marine rocks. Elsewhere, evidence for labeling other andesite outcrops as pre-Cretaceous is not conclusive.

The Jv map unit (La Negra formation) as well as most of the JKv unit (undifferentiated Jurassic and/or Cretaceous volcanic-clastic rocks) comprises mainly dark-colored, massive, andesite flows, flow breccias, agglomerates, and tuffs, with intercalations of reddish brown, terrestrial sandstones, shaly sandstones, and conglomeratic lenses -- almost exclusively of andesitic detritus. Individual lava flows are typically several meters to a few tens of meters thick, while flow breccias attain greater thicknesses.

Dikes, sills, and intrusive bodies of andesite intrude the stratified rocks, contributing greatly to their volume as well as complicating their internal structure. Succeeding flows are often fed by dikes that crosscut the previously consolidated flow, so that cross-cutting networks result.

The regular succession of massive andesite flows characteristic of the La Negra formation at its type locality can best be seen west of the Aguada Chépica fault, as seen in the northern half of Plate 5. In most other areas, the structural attitude of the andesites was much more difficult to interpret because of alteration, intense fracturing, poorer exposures, and intrusive complications. Confidence in mapping structural attitudes was gained when sedimentary intercalations could be found.

Although no chemical analyses are available for volcanic rocks of this area, petrographic study suggests that they are predominantly andesitic. Gradation to basaltic andesite or basalt may occur. Several studied samples that are representative of andesites encountered in the mapping include: dark violet-gray, micro-porphyritic andesine andesite (T-2); dark olive-gray, amygdaloidal andesine andesite (T-21); dark grayish olive, porphyritic labradorite andesite (CE-29); maroon to reddish brown, porphyritic augite-labradorite andesite (CE-40); maroon to purple, porphyritic andesine andesite (CE-45); dark olive-gray, finely prophyritic andesine andesite (S-73); greenish gray, porphyritic meta-andesite (S-78E); dark greenish gray to black, porphyritic clinopyroxene-andesine andesite (PA-107); and greenish black, coarsely porphyritic labradorite andesite (S-116D).

Texturally, nearly all the andesites are porphyritic -- micro-porphyritic (phenocryst size = 0.2-1.0 mm) to coarsely prophyritic (phenocryst size from 5 mm up to a few centimeters) -- with phenocrysts of andesine-to-labradorite plagioclase and clinopyroxene. The size and proportion of plagioclase phenocrysts, as well as the degree of development of vesicles, or more commonly amygdules, provides a basis for hand-specimen classification. Textural variations and differences in extent of alteration within individual lava flows, in addition to those from flow to flow, preclude regional mapping on the basis of texture or degree of alteration, unless detailed studies are made (see, for example, Levi, 1969).

Modal percentages of phenocrysts determined in the petrography of some of the andesites are: (1) T-2: 8-10% andesine (An_{35-37}) + 2-3% clinopyroxene; (2) T-21: 2-3% andesine (An_{34}) + 3-4% zeolite-filled amygdules; (3) CE-29: 50-55% labradorite (An_{62-68}); (4) CE-40: 30-35% labradorite (An_{50-67}) + 3-5% augite; (5) CE-45: 30-35% labradorite (An_{56-69}) + 1-2% epidote and chlorite after clinopyroxene; (6) S-73: 35-40% andesine (An_{30-38}) + 5-7% chlorite after a ferromagnesian mineral; (7) PA-107: 23-27% andesine (An_{47-49}) + 6-8% altered clinopyroxene; and (8) S-116D: 33-37% labradorite (An_{56-66}).

The groundmass of the andesites is most commonly hyalopilitic, intersertal, or intergranular, and typically comprises plagioclase laths and microlites with interstitial opaque granules, epidote, chlorite, devitrified glass, and carbonate.

Meta-volcanic equivalents of the andesites preserve original volcanic textures, but are massive and very dark colored, showing recrystallization of the groundmass to actinolite-chlorite-epidote aggregates and altered, more sodic plagioclase.

Alteration of the andesites was not studied in detail, but other workers have indicated that volcanic rocks of the Andean geosyncline display evidence of burial metamorphism (Levi and Corvalán, 1964; Levi, 1969). Levi (1969) reports greenschist facies and prehnite-pumpellyite facies metamorphism of a Mesozoic andesite pile in the Coastal Range west of Santiago.

A concise interpretation of the character of the volcanic activity represented by stratified volcanic rocks, such as the La Negra

formation, in the western part of the Andean geosyncline was offered by Howell Williams (reported by Ruiz, 1965, p. 68). The great regularity and extent of the lava flows, the absence of preserved structures of volcanoes, the numerous andesitic dikes cutting the Mesozoic series, and the absence of air-transported pyroclastic tuffs, led Williams to suggest: (1) characterization of the eugeosynclinal part of the Andean geosyncline as a flat-bottomed graben; (2) volcanic extrusion through linear fissures in a relatively tranquil form; and (3) gentle sinking of the trough simultaneous to its infilling, such that great depths below sea level did not result.

Caleta Coloso and Bandurrias formations. -- In the Quebrada Way, 20 km south of Antofagasta, terrestrial conglomerates, sandstones, and shales of the Caleta Coloso formation are separated by a marked unconformity from the underlying La Negra formation (García, 1964; Harrington, 1961; Alarcón and Vergara, 1964). These rocks are of Tithonian-Berriasian age (Malm-Neocomian) and are concordantly overlain by the marine, middle to late Neocomian, El Way formation (see Ruiz et al., 1961; Tobar, 1966). In the region to the north of Copiapó, Segerstrom (1960a) named a sequence of interfingering clastic-volcanic rocks and marine beds, concordantly overlain by clastic-volcanic rocks, the Bandurrias formation, which in part has lithologic similarities to the La Negra formation, but whose base is middle Neocomian. The problem is this: definition of the top of the La Negra formation could not be made in this mapping, but yet it is clear that rocks similar to the Caleta Coloso and Bandurrias formations, i.e.

post-La Negra, do crop out within the map area. An attempt was made to distinguish such rocks from the composite Jurassic-Cretaceous volcanic-clastic sequence that was mapped, in order to facilitate future studies.

At the northern end of Plate 1, to the west of the Salar del Carmen fault, reddish brown pebble breccias, pebble conglomerates, and fine- to coarse-grained arkosic sandstones, were found in association with dark olive-gray and chocolate-brown, porphyritic andesites. Burnol and Bournat (1966) described a single outcrop of conglomeratic rocks in that area, and reported finding both granitic and andesitic clasts. Ruiz et al. (1961, p. 1554) describe granitic clasts within the Caleta Coloso formation at its type locality. Petrography of a sandy pebble breccia (PA 106) shows the predominance of volcanic detritus in an arenaceous matrix cemented by a ferruginous material. A few subrounded pebbles of granophyric leucogranite are included.

A. Moraga (personal communication) judges that the clastic rocks found to the west of the Salar del Carmen fault are clearly part of the Caleta Coloso formation. Because of poor exposure -- mainly due to deep weathering of the soft sedimentary rocks -- the relation between the clastic rocks and porphyritic andesites could not be determined. Outcrops where clastic rocks with characteristics similar to those of the Caleta Coloso formation were observed, are indicated by a special map symbol (see map explanation).

In the vicinity of Taltal airport (Pl. 5), clastic sedimentary rocks and andesites with intercalations of marine limestone are very likely

equivalents of the Bandurrias formation. Conspicuous fault slices of limestones occurring in the central part of the Atacama fault zone between Taltal airport and Quebrada de la Cachina (see Fig. 31) are thought to be Neocomian by Chilean geologists; the only available fossils, however, are pelecypod remains of Exogyra, sp., which do not allow a precise age determination because their range includes both the Jurassic and Cretaceous Periods (J. Corvalán, personal communication). Cropping out to the west of these limestone fault slices and east of the Aguada Chépica fault are isolated small hills with exposures of reddish brown shales, siltstones, sandstones and conglomerates, with brownish drab to purplish brown porphyritic andesites. Field inspection by J. Corvalán led him to believe that all these rocks bear much greater similarity to the Bandurrias rather than the La Negra formation (J. Corvalán, personal communication).

In Quebrada Carrizalillo, to the east of the Atacama fault zone (near southern limit of Pl. 5), eastward-dipping marine limestones are intercalated within a series of andesite flows; the only fossils found were fragments of calcareous worm tubes, Serpula, of undeterminable age (J. Corvalán, 1970, written communication). If the limestones are of Neocomian age, stratified andesites in that general area may correlate with the Bandurrias formation. Outcrops more clearly assignable to the Bandurrias formation are indicated in the maps.

Another area in which andesitic rocks may likely be Cretaceous is in Quebrada de la Peineta, within and to the north of the Taltal fault zone. Violet-gray and maroon, fine-grained, arkosic sandstones

unconformably overlie Paleozoic quartzites and phyllites at a locality 4 km north-northeast of the Mackenna mine (Pl. 4). Included in the section are maroon to olive-gray breccias with an argillaceous to sandy matrix containing distinctly heterogeneous clasts -- angular to subangular and generally less than 10 mm long, but up to 22 mm long. The fragments include quartzite, argillite, angular clasts of a chert-like rock, and numerous coarse pebbles and cobbles of heterogeneous granitic rocks identical to facies which are judged to belong to an older group of Mesozoic granitic rocks (see Mesozoic-Tertiary plutonic rocks) rather than the Paleozoic. Although displaying an appearance less typically Bandurrias-like, these clastic rocks and overlying andesites are probably Cretaceous in age.

MESOZOIC-TERTIARY PLUTONIC ROCKS

General Statement

Major batholithic intrusions in northern Chile have been dated as late Paleozoic, Late Jurassic, and middle Cretaceous (Ruiz et al., 1961; Levi et al., 1963); also, plutonic activity in the Tertiary has been recognized (Levi et al., 1963; Ruiz, 1965, p. 66). No less than two-thirds of the area mapped in this study is underlain by post-Paleozoic plutonic rocks, but no samples from this area have been radiometrically dated, and stratigraphic bracketing is poor. Consequently, age designations are necessarily generalized.

Subdivision of the plutonic rocks was clearly a necessity for fault studies, and was a major task for the large area and numerous

fault blocks involved. Nevertheless, during the course of the mapping and after widespread sampling (Appendix Pls. A-D), sufficient information was gathered to demonstrate the occurrence of post-Paleozoic plutonic rocks representing at least two distinct periods of intrusion: an older, more voluminous suite of rocks that is markedly variable -- both texturally and compositionally (gabbro to adamellite) -- and a younger suite of more homogeneous granodiorites, adamellites, and tonalites that occur mainly in large discordant stocks. On a regional scale identical facies of the older suite recurrently appear on both sides of the Atacama fault and frequently exhibit such local spatial variations that subunits could not be completely mapped at a scale of 1 : 100, 000. As a result, the older post-Paleozoic suite is mapped as a composite map unit -- designated Jurassic and/or Cretaceous in age; specific lithologic names are assigned where the rocks were observed and studied. The unit is herein referred to as the JK suite for convenience.

The younger suite demonstrably crosscuts the various facies of the older group, including the more felsic phases, and is considerably less tectonized. Characteristically, the younger bodies are homogeneous, uniformly xenolithic, and marked by the absence of andesitic dikes, in contrast to the older granitic rocks. The younger suite is designated as Cretaceous and/or Tertiary in age, and is herein referred to as the KT suite.

Brief petrologic observations in the Taltal area were made by Bowes et al. (1961). Burnol and Bournat (1966) include more

systematic hand-specimen descriptions of granitic rocks that they encountered in reconnaissance in the coastal area between Paposo and Antofagasta.

Because rocks of similar composition occur, in some cases, in both suites of rocks, the following discussion is outlined on the basis of composition. Modal quartz $\geqq$10% separates tonalites (quartz diorites) from diorites, adamellites (quartz monzonites) from monzonites, and so forth. Rocks having substantial modal quartz <10% are termed quartz-bearing. Standard K-feldspar/total feldspar ratios of 1/10, 1/3, and 2/3 demarcate tonalite, granodiorite, adamellite, and so forth. Approximate modes for representative samples of the important rock units are presented in the Appendix Tables.

Dioritic Rocks

Dioritic rocks, predominantly of medium to coarse grain size, but not uncommonly finer-grained, are a major constituent of the JK suite in the map area. These include diorite, melanodiorite to gabbro, and complexes of mixed diorite, meta-andesite, and gabbro.

Medium- to coarse-grained equigranular diorite.-- Medium- to coarse-grained equigranular diorites are ubiquitous throughout the map area, although they are most abundant west of the Salar del Carmen fault between 24°S. and 25°S. (Pls. 1 and 2). These rocks are variable in color index (15-45), quartz content (0-9%), and K-feldspar content (0-20%), as well as in the relative proportion of the mafic minerals (see Appendix Table 3). Pyroxene and green-brown hornblende are the

most important mafic minerals. Secondary amphibole predominates in the altered samples. Plagioclase (50-75%) is generally calcic andesine, occasionally sodic labradorite. The various facies may be distinguished as pyroxene diorite, hornblende diorite, quartz-bearing pyroxene or hornblende diorite, and perhaps monzodiorite where K-feldspar becomes relatively abundant. Hand specimen recognition of these distinctions is often difficult.

All the facies appear to be gradational among themselves. Gradation between medium- to coarse-grained pyroxene diorite and pyroxene granodiorite is interpreted from field relations and from striking textural similarities between the two. Both, for example, typically display coarse multiform grains of tabular or equant plagioclase that is commonly cloudy or greenish gray, with green to greenish black prismatic pyroxene and hornblende. A finer matrix of quartz and K-feldspar distinguishes the granodiorite.

Fine- to medium-grained diorite.-- Fine- to medium-grained diorite, gradational to quartz-bearing diorite and tonalite, was observed as a locally abundant phase of the JK suite. Samples from an area south of Cerro Parañave (Pl. 2) illustrate the variability of quartz (Appendix Table 3: S-120, S-121A, S-121B). Color indices of 30-40 help distinguish them from similar textured altered granodiorites of the JK suite. Alteration of the mafic minerals and saussuritization of plagioclase gives the rocks a greenish gray color, which together with a slightly inequigranular texture allows hand-specimen distinction from the fine- to medium-grained tonalites occurring as facies of the KT

suite. Other differences in the former include the presence of actinolite and calcic andesine to labradorite; the tonalites of the KT suite (Appendix Table 9: S-80A, S-82) have a more sodic andesine and fresher biotite and hornblende.

Melanodiorite to gabbro. -- Rocks termed gabbro by Burnol and Bournat (1966) were recognized by them near Cerro Mulato (23°59'S., west of Pl. 1), and along the road to Blanco Encalada that passes 11 km south of Cerro Cristales (Pl. 1). Study of similar rocks in those areas (Appendix Table 2: PA-103(2), PA-111) shows that despite a black color, they have color indices only between 35 and 50 and are not necessarily pyroxenic; use of the term gabbro should perhaps be qualified. In this report, rocks having a very dark "melanocratic" aspect, little or no quartz, and a plagioclase in the labradorite range, are termed gabbros, while similar rocks with a less calcic plagioclase are perhaps more properly termed melanodiorites (see Appendix Table 2).

Greenish black to black melanodiorite to gabbro was observed as local phases of large diorite bodies west of the Salar del Carmen fault between 24°S. and 25°S., as a part of complexes of mixed dioritic rocks and meta-andesite that occur both to the east and west of the Salar del Carmen fault, and as a border phase of a diorite stock north of Estación Central (Pl. 4).

Granodioritic Rocks

General statement.-- Rocks of granodioritic composition occur in great abundance in the map area and have been separated petrographically into two groups: (1) pyroxene granodiorites, and (2) biotite and hornblende granodiorites. The first group is restricted to the JK suite, while the second group includes rocks of both the JK and KT suites.

Pyroxene granodiorite.-- Rocks within the compositional range of granodiorite that have a significant modal percentage of pyroxene are termed pyroxene granodiorites in this report. Such rocks are lithologically important within the JK suite and have been subdivided into three map units on the basis of grain size and texture. A fourth unit is characterized by the distinctive accompaniment of biotite.

The pyroxene granodiorites commonly exhibit a greenish greasy luster because of alteration of the pyroxene and calcic plagioclase. A high degree of tectonization, intrusion by andesitic dikes, and crosscutting by rocks of the KT suite added confidence in associating them with the older granitic rocks. Also, Levi et al. (1963) have pointed out that pyroxene is characteristic of granitic rocks of Jurassic age in Chile.

Medium- to coarse-grained, porphyritic pyroxene granodiorites that are gradational to diorite and adamellite represent older rocks of this group as evidenced by the degree of their tectonization and injection by finer grained compositionally equivalent rocks. The predominance

of pyroxene is distinctive in some samples (Appendix Table 5) but may not be general; the occurrence of large grains of unusually calcic plagioclase -- often labradorite -- together with andesine or oligoclase-andesine is common. Best exposed in the Matancilla area east of Paposo (Pl. 3), these rocks are distinctive in hand specimen. Phenocrysts of clear to milky gray plagioclase, both tabular and equant, up to 1 cm in size constitute a variable fraction of the rock -- up to one-half. Together with altered prismatic mafic minerals, the plagioclase phenocrysts are set in a pink quartzofeldspathic matrix, giving the rock a pink and greenish gray color. Reduction in the phenocryst to groundmass ratio moves the rock toward an adamellitic composition. Remarkably similar rocks are described by Tilling (1962) in the Copiapó area under the name adamellite porphyry. In the Matancilla area, fine- to medium-grained inequigranular adamellite to granodiorite with scattered phenocrysts of large plagioclase grains injects the coarser grained pyroxene granodiorite as dikes and apophyses, but the two rock types appear to be genetically related. Both are crosscut by andesitic dikes and aphanitic basic dikes.

The pyroxene granodiorites, particularly the medium- to coarse-grained type, are ubiquitous in outcrops of the JK suite on both sides of the Atacama fault. They have been observed in great abundance (1) east of the Atacama fault between Taltal and Quebrada de Yumbes (Pls. 2, 3, 4), and (2) west of the Salar del Carmen fault in the Cerro La Chira-Quebrada Remiendos area (Pls. 1 and 2).

Biotite and hornblende granodiorites of the KT suite. -- The most abundant rocks of the KT suite are medium-grained equigranular granodiorites characterized by biotite and hornblende -- most commonly in near-equal abundance. These rocks occur throughout the map area in discordant stocks of various size, including the following, from north to south: (1) a small stock of biotite leucogranodiorite (X-5) three kilometers west of the Salar del Carmen fault at the northern map limit (Pl. 1), (2) large bodies of hornblende-biotite granodiorite (PA-104b) bounded by the Caleta Coloso fault between Cerro Cristales and Quebrada de Remiendos, (3) a large pluton of granodiorite to adamellite bounded on the west by the Salar del Carmen fault in the Pampa de Remiendos (Pl. 1), (4) a pluton of biotite-hornblende granodiorite (S-86, S-90) bounded on the west by the Salar del Carmen fault in the central to northern area of Plate 2, (5) small coalescing stocks of granodiorite in the western Quebrada San Ramon area (Pls. 3 and 4), (6) a pluton of hornblende-biotite granodiorite (CE-8, CE-31) bounded on the west by the Atacama fault zone in the Sierra del Pingo area (Pls. 4 and 5), and (8) a granodiorite stock in the Pampa Barreal Seco area (southeastern part of Pl. 5).

Color indices for these hornblende and biotite granodiorites are generally in the range of 10-25. Leucocratic phases such as that represented by X-5 (Appendix Table 7) are an exception. The mineralogy of typical samples of the biotite and hornblende granodiorites (Appendix Table 4) consists of 10-25% brown biotite and green hornblende, 45-60% normally zoned oligoclase-andesine, 15-30% quartz, and 10-15% K-feldspar.

In hand specimen these rocks are whitish gray, gray, or pinkish gray in color, generally with a fresh appearance. Dark biotite flakes and prismatic hornblende can be readily distinguished, along with clear quartz, clear to whitish gray tabular plagioclase, and white to pink K-feldspar.

Fine-grained mafic xenoliths, or inclusions, within the granodiorites and other rocks of the KT suite are variable in size, shape and texture. A detailed study was not made. Their mineralogy is similar to that of the host rock, but with a greater abundance of mafic minerals. Hornblende exceeds biotite and K-feldspar is absent. Commonly the inclusions are spheroidal in shape with flattening more common near the margins of the bodies.

Biotite and hornblende granodiorites of the JK suite. -- Fine- to medium-grained granodiorites that contain no recognizable pyroxene were encountered as phases of the JK suite. Other samples from the same body may contain a minor amount of pyroxene. The rocks are typically inequigranular and have color indices greater than 15. They occasionally bear a close resemblance to rocks of the KT suite, but field relations showed that they are associated with characteristic phases of the JK suite, and together with those rocks, they are cut by andesite dikes and rocks of the KT suite.

Petrographically, these granodiorites are sometimes difficult to distinguish from granodiorites of the KT suite. (See T-93, T-47, S-84B, S-88 for representative modes.) An inequigranular texture due

to a seriate size distribution of plagioclase is common, and mafic minerals tend to be more altered. Some of these bodies are locally xenolithic, so that care must be used in applying the latter criterion for distinguishing rocks of the two suites.

Granodiorites with hematized mafic minerals. -- To the east of the Atacama fault between Taltal and Paposo, stocks of medium-grained equigranular rocks with hematized mafic minerals discordantly cut pyroxene granodiorites and other highly tectonized rocks of the JK suite. The rocks are pink to reddish gray in color and are in the compositional range of granodiorite to adamellite with color indices of about 15. Texturally they are most similar to medium-grained equigranular rocks of the KT suite. In addition, they are typically xenolithic with hematized xenoliths. Distinctive lithologies of the JK suite were observed to be locally hematized, but the rocks described above appear to form homogeneous bodies. Mapping of most of their contacts is based heavily on photogeologic interpretation because of problems of accessibility. These rocks are tentatively assigned to the KT suite on the basis of texture and discordant crosscutting of rocks of the JK suite.

Adamellitic Rocks

General statement. -- Together with diorite and granodiorite, adamellite constitutes a rock type of major abundance in the map area, occurring as gradational and late phases of the JK suite, and as homogeneous stocks of the KT suite. In terms of volume, adamellites are

perhaps more important in the older JK suite; granodiorite constitutes the greatest proportion of the younger granitic rocks.

Small outcrops of adamellitic rocks were occasionally difficult to work with in terms of deciding whether the rocks were late phases of the older batholithic suite, or related to younger adamellite stocks of the KT suite. Basis for distinction was not everywhere available, so that some adamellitic rocks assigned to the older batholithic suite may actually be younger. A distinction between felsic rocks of two plutonic episodes is believed to be valid. Clear cases were seen where felsic adamellites are crosscut by rocks of the KT suite that are more mafic. In addition, the regional intrusion of andesite dikes provided a time marker. An illustrative example is the following. At sample locality PA-212 (Appendix Pl. A), a pink, medium-grained, leucocratic biotite adamellite was observed to be xenolith-free and crosscut by porphyritic andesite dikes. Both dikes and host rock are discordantly cut by a light gray, medium-grained, xenolithic biotite-hornblende granodiorite that is not cut by andesite, just as all rocks of the KT suite are not.

On the basis of grain size and texture, several types of adamellite have been distinguished, some of which are confidently assigned to either the JK or KT suites.

Fine- to medium-grained, inequigranular to porphyritic adamellite. -- One of the most important rock types of the JK suite is a fine- to medium-grained, inequigranular adamellite that was found intimately related with diorites, pyroxene granodiorites, and other

rocks of the JK suite in virtually every area where they were mapped. It is demonstrably younger than the coarser-grained rocks, commonly intruding them as dikes or as larger bodies that locally contain xenoliths of the coarser-grained rocks. On the other hand, it is crosscut -- together with the other facies of the JK suite -- by discordant stocks of the KT suite.

In hand specimen the adamellite is gray to pinkish gray in color, with a distinctly inequigranular to porphyritic texture. Large grains of milky gray or greenish gray plagioclase, either equant or tabular, occasionally exceed 5 mm. Mafic minerals appear as dark clots (2-5 mm wide) of fine grains, as irregular prismatic grains, and as individual tiny grains finely peppered throughout a fine-grained quartzofeldspathic matrix. In altered samples the matrix is commonly orange-colored, while plagioclase phenocrysts become greenish gray, and the mafics become green, all combining to give a characteristic green and orange appearance.

Microscopic study of several samples of the inequigranular to porphyritic adamellite (CE-7, S-142, S-199A, CE-314A, PA-397A, S-126) indicates a compositional gradation to granodiorite.

Brown biotite and green hornblende are the predominant mafic minerals occurring as ragged anhedral grains, commonly in nests. Bleached cores and reaction rims associated with larger hornblende grains suggest original pyroxene. Normally zoned oligoclase-andesine is typical. Larger plagioclase grains exhibit cores of calcic andesine.

Adamellites of the KT suite. -- Relatively homogeneous bodies of adamellite of the KT suite occur (1) in the Quebrada de Yumbes area (Pl. 2) as a small stock of medium-grained, hornblende-biotite adamellite (S-131), inferred to be bounded on the west by the Salar del Carmen fault; (2) west of the Izcuña fault in the northern half of the area of Plate 2, as both medium-grained equigranular and medium- to coarse-grained prophyritic adamellites; (3) west of the Salar del Carmen fault in the Quebrada de Remiendos area (Pl. 1) as a body of medium- to coarse-grained, porphyritic hornblende-biotite adamellite; and (4) in the Sierra el Jote area (Pl. 3) between the Salar del Carmen and Sierra el Jote faults, as a small stock of medium-grained adamellite.

Adamellites of the KT suite do not exhibit great textural similarity from body to body, as is shown by granodiorites of that suite over an extensive area. Field relations such as the absence of andesite dikes, crosscutting of rocks of the JK suite, and the uniform presence of xenoliths had to be depended on to assign certain adamellites to the KT suite. One quite distinctive texture of the latter suite is that of the medium- to coarse-grained prophyritic adamellites that have coarse phenocrysts of pink orthoclase up to a few centimeters long in a medium-grained equigranular matrix. Such rocks were sampled at localities PA-220 (Appendix Pl. A) and S-191A (Appendix Pl. B).

Other adamellites. -- Rocks of adamellitic composition occur as local gradational phases of granodiorites of the JK suite that are difficult to distinguish on the basis of color index or texture. This is true in the

Quebrada de Remiendos area (PA-109). Generally, though, the late phase adamellites tend to be fine- to medium-grained leucocratic rocks that are easily recognizable as adamellite because of abundant pink or flesh-colored K-feldspar intergrown with quartz. No felsic rocks within the true compositional range of granite were recognized. Fine- to medium-grained equigranular adamellites intrude mafic phases of the JK suite as small irregular bodies in the Cerro Paranal area (Pl. 2) and other areas of minor importance. Where such rocks are not xenolithic, or where field criteria were not found to help distinguish them, their assignment to one of the suites is uncertain. They have been assumed to be late phases of the older suite, just as the inequigranular to porphyritic adamellites, where they occur within a broad terrain of rocks of the JK suite with no proximity to a recognized adamellitic body of the KT suite. Such is the case in the Cerro Paranal area (S-92).

Tonalitic Rocks

General statement. -- In the map area, tonalites occur as phases of both the JK and KT suites. In the older suite they occur as (1) minor local variants of diorite plutons, and (2) as mappable geographically restricted bodies. Tonalites in the younger suite occur as (1) minor border phases of some granodiorite and adamellite stocks, and (2) as a single small stock.

Tonalites of the JK suite. -- The common occurrence of quartz-bearing diorites within the JK suite has already been noted. Variations

certainly include tonalite.

In the area of Cerro Yumbes and Cerro Paraña̲ve (Pl. 2), fine- to medium-grained diorites with color indices of 35-40 become quartz-bearing and occasionally tonalitic (Appendix Table 3: S-120, S-121A, S-121B). Likewise, quartz-bearing diorites of fine to medium grain size with hornblende as their principal mafic mineral recurrently crop out over a broad area on both sides of the Atacama fault at the latitude of Cerro Cristales (Pl. 1) and are gradational to tonalite.

As part of the JK suite, tonalite occurs (1) as medium-grained hornblende tonalite (S-72) east of Cerro Yumbes (Pl. 2) in a fault block bounded by the Salar del Carmen fault and a parallel fault 1-2 km to the west; and (2) as medium-grained biotite-hornblende tonalite (PA-110B) in the Cerro Cristales area (Pl. 1), in a fault slice bounded on the east by the Caleta Coloso fault. The medium-grained hornblende tonalite in the first area has a color index of only 15, a distinctly high percentage of quartz, and only hornblende as a principal mafic mineral. The tonalite in the second locality is characterized by the development of stubby euhedral prisms of greenish-black hornblende (1-3 mm long) in a whitish gray matrix of plagioclase and quartz.

Tonalites of the KT suite.-- The only mappable body of tonalite belonging to the KT suite that was encountered occurs in the Quebrada de Yumbes area (Pl. 2) on the east side of the Salar del Carmen fault. The body is a small stock of fine- to medium-grained hornblende-biotite tonalite (S-80A, S-82). Its relation to an adjacent body of adamellite

of the same suite is obscured by alluvium. Like other bodies of the KT suite, the stock of tonalite is homogeneous, xenolithic, and notably free of andesite dikes. This makes a sharp contrast across the Salar del Carmen fault because the medium-grained hornblende tonalite on the opposite side of the fault is injected by numerous andesitic dikes (compare Fig. 6 with Pl. 2).

The fine- to medium-grained tonalites of the KT suite consist of 60-65% oscillatory zoned andesine, 10-15% quartz, 0-3% interstitial K-feldspar, 7-15% green hornblende, and 6-13% brown biotite. In hand specimen, they are gray equigranular rocks. Clear gray tabular plagioclase, clear quartz, black biotite, and prismatic black hornblende can be recognized.

Migmatitic and Gneissic Rocks

Migmatitic and gneissic rocks occur on the east side of the Salar del Carmen fault near Paposo (Pls. 2 and 3), and also along the eastern margin of the Quebrada del Hueso segment of the Atacama fault (Pl. 4). The rocks constitute a complex of finely laminated to gneissic metasedimentary rocks, orthogneissic rocks and migmatites.

Near Paposo such rocks can be traced on the east side of the Salar del Carmen fault in a band nearly 1 km wide and about 12 km long. In Quebrada Paposo, García (1964) noted the occurrence of granitized metasedimentary rocks at a locality within this band. Foliation does not parallel the trace of the Salar del Carmen fault (N 10°-15° E), but instead trends N 30°-50° E. South of Quebrada Paposo the gneissic rocks

are in fault contact with fine- to medium-grained biotite-hornblende granodiorite of the JK suite; in Quebrada Paposo and to the north, there appears to be a gradational contact with tectonized pyroxene granodiorite and adamellite, also of the JK suite.

Gneissic rocks near Quebrada del Hueso along the eastern margin of the Atacama fault zone (Pl. 4) make up a narrow, highly irregular band, whose eastern margin is gradational and approximately traced. Migmatitic rocks are common. Mixing of granodioritic rocks of the JK suite and Paleozoic metasedimentary rocks is interpreted. These rocks are similar in appearance to those near Paposo, and northeast-trending foliation is general.

Elsewhere along the Atacama fault zone foliation of granitic rocks is common, but the zones of gneissic rocks near Paposo and Quebrada del Hueso are distinctive. Granitic rocks of both the JK and KT suites are foliated near the trace of the Salar del Carmen fault to the north (Pl. 2), and along the easternmost branch of the Atacama fault zone in the area of Pl. 5.

Minor Intrusive Rocks

Dikes crosscutting rocks of the JK batholithic suite include andesite, diabase, lamprophyre, microdiorite, and rhyolite. Very fine-grained to aphanitic microdiorite, microgranodiorite and lamprophyre cut younger rocks of the KT suite. Hypabyssal dacite porphyry intrudes the Liassic marine rocks near Paposo. Hypabyssal intrusives of fluidal rhyolite were mapped in three areas: (1) In the

Cerro Yumbes area (Pl. 2) an elongate massif nearly 11 km long intrudes Paleozoic metasedimentary rocks, Liassic marine rocks, and dioritic rocks of the JK suite. Rhyolite dikes are common within the block between the Izcuña and Salar del Carmen faults in this area. The rhyolite massif is itself crosscut by massive andesite dikes. (2) Fragmentary outcrops of similar rhyolite occur west of the Salar del Carmen fault southeast of Cerro Paranal (Pl. 2). (3) Within the Quebrada del Hueso segment of the Atacama fault zone east of Taltal, a small elongate body of rhyolite intrudes andesitic rocks and is laterally displaced by the Taltal fault (Pl. 4).

TERTIARY-QUATERNARY SEDIMENTS

A wide variety of unconsolidated to poorly consolidated clastic material occurs in the map area in such different environments as the arid inland desert and the maritime coastal platform. These include: aggradational deposits accumulated on old erosion surfaces, on pediments, and in tectonic depressions; stream deposits in transverse canyons and valleys; and marine gravels and a coverhead of clastic debris on the coastal platform. Marine terrace deposits are indurated.

Recognition of numerous types of alluvial material is possible, both photogeologically and in field observation, but mapping them all is impossible at a scale of 1 : 100, 000. Four basic subdivisions were made: (1) Tertiary-Quaternary alluvium: primarily basin deposits, pediment gravels, older alluvium, and coalescing colluvium and younger

alluvium that occurs in inland basins and on older erosion surfaces. Locally this includes a thin blanket of aeolian sand. Notation of subunits is made where feasible on the map. Geomorphological studies completed in the Copiapó area (see Part IV) indicate that some basin deposits, pediment gravels, and older alluvium that mantle the old-age topography of northern Chile are Tertiary in age and that in some locales, the landscape has been modified very little since the Late Miocene (Clark et al., 1967a). For this reason the deposits are indicated as possibly being Tertiary, in part. Differentiation of the sediments would require more detailed geomorphological study. (2) Quaternary stream channel deposits: stream gravel and sand occurring in narrow youthful seaward-draining canyons or ravines. Because of the narrowness of the alluvial channels at the map scale, it was generally impossible to separate older terraced alluvium and Recent alluvium that is being actively transported or deposited. This is done, however, in lower Quebrada de Taltal (Pl. 4). (3) Quaternary nonmarine coverhead: accumulation of clastic debris, consisting of alluvial fans, talus cones, colluvium, landslide material, and debris-flow material that has been spread over the coastal platform both during and after marine terracing. (4) Quaternary marine terrace deposits.

IV. GEOMORPHOLOGY

INTRODUCTION

Only those aspects of the geomorphology that are relevant to bracketing the time of movement along the major faults and to interpreting their current activity are discussed here. These include reference to processes and land forms in the inland desert and to major features of the coastal geomorphology. Also, observations on alluvial fault scarps that display an enigmatic ridge-trench-ridge form are reported. Such scarps are abundant in the Atacama fault trough south of Taltal airport (Pl. 5, Fig. 31), but occur along numerous faults throughout the map area and appear to reflect unusual environmental factors in the Atacama Desert.

OLDER EROSION SURFACES

An old-age topography that is displaced by faulting in the Coast Ranges is characterized by deeply weathered rocks, veneered pediments, and low-relief surfaces that are interrupted by residual hills of sharp relief. In the area of this study, this is best displayed inland from the coastal scarp in the area of Plates 1 and 2. Fault scarps such as that of the Salar del Carmen, Izcuña, and Caleta Coloso faults dominate the present physiography, but the upper surfaces of individual blocks exhibit deeply weathered rocks and remnants of low-relief surfaces. This is well accentuated on aerial photographs that show the receding coastal scarp intersecting the old-age topography along a well-defined line resulting in sharp contrast. For example, note the truncation of

the southwest flank of Cerro Carnero in Figure 6. (See also Rich, 1942, photo. 230.)

Gentle aggradation surfaces typically surmount the high-standing blocks of the Coast Range, except near the coastline, where they have been incised by youthful drainage. Piedmont gravels blanket the linear depressions formed by block faulting. Between Taltal and Paposo (Pl. 3), the old-age topography is conserved 10-20 km inland from the coast.

Topography illustrated in Plate 5 also displays a mature aspect; deeply weathered rocks and pediments are common both within and beyond the broad trough of the Atacama fault zone. Elevations, however, are several hundred to a thousand meters lower than in the inland area north of Paposo.

Formation of vast surfaces of low relief by extensive denudation in the Atacama Desert during the early to middle Tertiary has been discussed by various workers (Bowman, 1924; Willis, 1929; Brüggen, 1950; Segerstrom, 1963; Galli-Olivier, 1967). Correlation of the old-age landscape north of Paposo, however, with the Oligocene-Miocene pre-Andean "Choja Pediplain" of Galli-Olivier (1967) or the mid-Tertiary "matureland" of Segerstrom (1963) is not warranted. Study of the topographic evolution of the Atacama Desert between the Río Huasco (28°40'S.) and the Río Salado (26°25'S.) has shown that landform development was multicyclic, involving at least three periods of pediplain formation (Clark et al.: 1967a, 1967b; Sillitoe et al., 1968).

Although detailed studies of the regional geomorphology have not been carried out within the map area, the results of Clark et al. (1967a, 1967b) and Sillitoe et al. (1968) must be generally applicable because of the proximity and extent of their area of study. These workers have developed a chronology of landform evolution for the southern Atacama Desert based on interrelationships of pediplanation, ignimbrite eruption, and supergene mineral alteration that is summarized here. Important aspects of their chronology include:

(1) Formation, during a prolonged period of erosion, of an old topography of probable subdued relief -- the "Summit Surface" -- onto which a series of acidic pyroclastic flows were extruded. Potassium-argon dating of the volcanic rocks indicates a Lower Eocene minimum age for the erosion surface.

(2) Block faulting causing disturbance of the continuity of the Summit Surface.

(3) Regional uplift and development of a second extensive surface, the 'Intermediate Surface", by pediplanation during the Eocene to Miocene epochs (age uncertain).

(4) Tectonic activity, uplift, and formation of a third regional planation surface, the "Atacama Pediplain". Potassium-argon dating of ignimbrites intercalated with aggradational gravels implies active pediplanation 12.5 ± 0.5 m.y. BP, but near cessation of pediplanation by 11.6 ± 0.5 m.y. BP. One of the youngest pediplains was cut before 9.15 ± 0.25 m.y. BP.

(5) Incision of the Atacama Pediplain commencing in the Pliocene epoch; canyon cutting along the Río Huasco, Río Copiapó, and Río Salado during a period of marine regression.

(6) Aggradation in valleys and along the coast during a period of marine transgression.

(7) Intense weathering of the alluvial deposits of stage (6) in local areas.

(8) Marine regression, during which aggradation deposits were dissected, and canyons produced in stage (5) were modified. New canyon rock walls developed locally. Formation of fluvial and marine terraces.

Applying this chronology to the area of this study must obviously be done with care, but it is judged that the sequence provides a valuable framework for bracketing some of the structural events in the map area (Part VI), and the stage numbers are referred to subsequently. It is concluded here that the old-age surface or surfaces that surmount the high-standing fault blocks between 24°S. and 25°S. (Pls. 1 and 2) are not younger than late Miocene, but they may be older -- Eocene to Miocene. Surfaces of low relief between 25°S. and 26°S. (Pls. 4 and 5) are related, in part, to the development of large transverse quebradas (discussed next).

DRAINAGE PATTERNS

The regional drainage pattern between 24°S. and 25°S. differs from that between 25°S. and 26°S. In the first interval, east-west drainage is not continuous because the Sierra Vicuña Mackenna and the Salar del Carmen fault scarp form topographic barriers (see Figs. 3 and 4). Drainage from the Andes is diverted to the north of 24°S. and the south of 25°S. West of the Salar del Carmen fault, subsequent canyons have developed by headward erosion from the coastline. Topographic trends suggest that an antecedent Quebrada de Remiendos (Pl. 1) may have been disrupted by uplift along the Salar del Carmen fault (see Fig. 4).

Closed basins with interior drainage have developed along the Salar del Carmen fault (Pls. 1 and 2). Consequent drainage of the fault scarp (Fig. 6, point D) produces coalescing alluvial fans that infill the western part of these basins. The southernmost basin has been captured by headward erosion of drainages in the Paposo area (Pls. 2 and 3, Fig. 6), and the northernmost, immediately north of Pampa de Remiendos (Pl. 1), drains northward into a drainage system that breaches the Coast Ranges in the vicinity of Antofagasta (see Fig. 3). Younger inland topography in the northern half of Plate 1 reflects lower elevations and the consequences of exterior drainage.

Between Taltal and Paposo (Pl. 3) drainage lines are continuous from east to west, but the near-coastal segments of the quebradas are out of equilibrium with their upper reaches. Exceptionally steep

gradients and dry waterfalls near the coastline indicate drastic tectonic or sea-level movements subsequent to the original cutting of the quebradas. Their upper reaches inland are aggraded, while their lower reaches are marked by young downcutting. A major knick point in the stream profiles occurs between 250 m and 500 m above sea level.

The interval between 25.5°S. and 26°S. has a regional drainage pattern that is more typical of that of the southern Atacama Desert. Broad aggraded quebradas trending west-southwest are generally continuous from the Andean foothills to the sea, except for the interval between Taltal airport and Quebrada de la Cachina where uplift along the western branch of the Atacama fault zone has caused aggradation of the fault trough (see Fig. 31). Headward erosion along lower Quebrada de Taltal has captured inland drainage north of Taltal airport so that upper Quebrada de Taltal presently drains seaward through that channel (see Fig. 33). Aggradation within Quebrada de Taltal preceded its capture.

It is most likely that the large west-southwest-trending quebradas, including Quebrada de Taltal, Quebrada de la Cachina, and Quebrada Pan de Azucar, along with their tributaries (see Fig. 1), were cut during the same period as the canyon of the Río Salado -- located only about 40 km south of the southern limit of Plate 5. These large quebradas parallel the trend of the canyon of the Río Salado, are just as long, and have similar relief. On this basis, their incision commenced in Pliocene time (Sillitoe et al., 1968, p. B168), and

aggradational deposits in their channels would appear to be Plio-Pleistocene in age (stage 6). This age assignment is emphasized because it has an important bearing on the dating of faulting in the Taltal area.

COASTAL GEOMORPHOLOGY

The coastal platform in the map area (Pls. 2, 3, and 4) varies in width from a few meters at Paso Malo to about 2 km near Punta Grande. Features displayed by the platform correspond to the late-youth stage of a marine cycle of erosion for a steeply dipping shoreline of emergence (Putnam, 1937; Davis, 1933). An emerged rock-cut platform of marine abrasion, locally veneered with indurated marine gravels, is covered by alluvial fans and other clastic debris. Wave cutting has truncated the coverhead of detritus (see Fig. 6), resulting in the development of composite cliffs (Figs. 7 and 8), which are characteristic of the coastline from south of Taltal to north of Paposo.

Crystalline rocks are exposed at the base of the composite cliffs. The veneer of marine gravels is not ubiquitous; locally it exceeds 3 m in thickness and becomes conglomeratic, with large boulders in a sandy to pebbly matrix that includes marine shell material. Bedded alluvial gravels (Fig. 6, point G), or talus and colluvial debris (Fig. 6, point H), comprise the bulk of the coverhead. Landslides, debris flows, and mud flows along the steep coastal escarpment provide a contrast with arrested erosive processes in the inland desert. At the mouths of quebradas, ephemeral stream channels that have been

Fig. 6. (following page) Salar del Carmen fault and coastal platform near Paposo. Vertical aerial photograph showing the linear trace of the Salar del Carmen (Atacama) fault (A, B) and features of the coastal morphology.

A. One of small ravines in which cataclastic rocks of the Salar del Carmen fault are exposed

B. Trace of Salar del Carmen fault

C. Massive andesite dikes intrusive into Jurassic-Cretaceous tonalite

D. Consequent drainage typical of Salar del Carmen fault scarp along its trace

E. Mature topography

F. Emerged platform of crystalline rocks

G. Coverhead comprising alluvial gravels

H. Coverhead comprising colluvial detritus

I. Clouds abutting against coastal escarpment

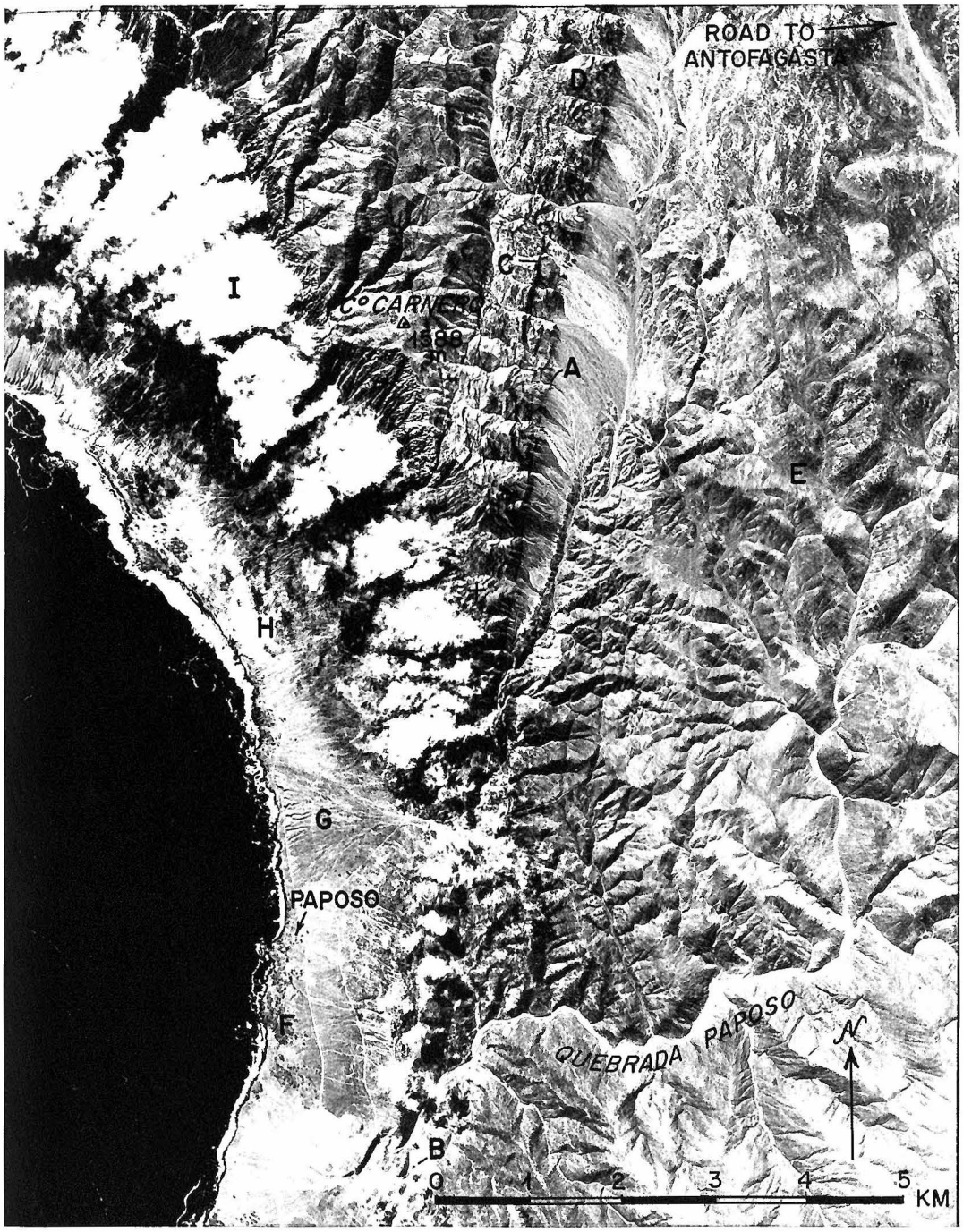
ROAD TO
ANTOFAGASTA
D
C
I
Co CARRETO
1580
A
E
H
G
PAPOSO
F
QUEBRADA PAPOSO
B
0 1 2 3 4 5
KM

Figure 6

Fig. 7. Composite cliff of alluvial coverhead and wave-cut crystalline rocks, southeast of Punta Bandurrias (Pl. 3). Compare with Figure 8. Cliff in the left middle distance is approximately 50 m high. View is to the southeast.

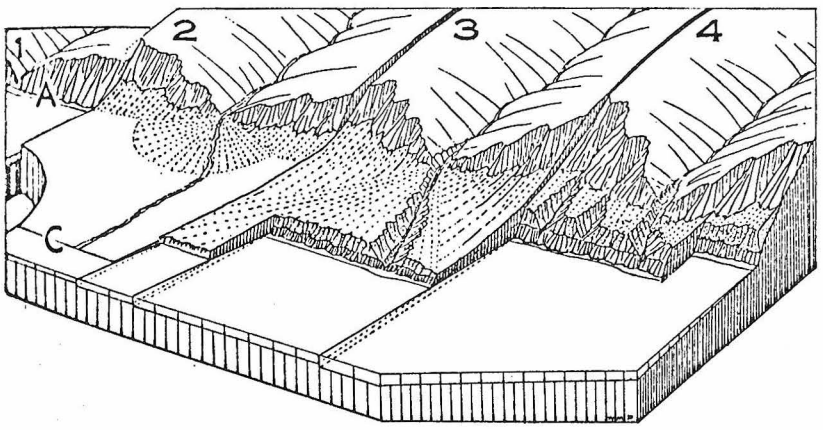

(a) Development and abrasion of a detrital cover on an emerged platform.

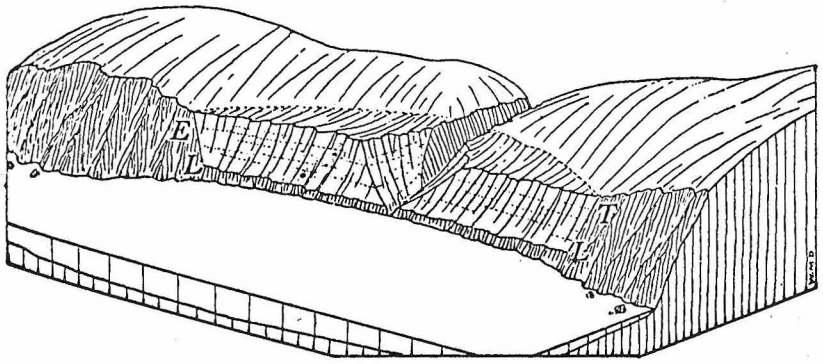

(b) Composite cliff in a bight between the simple cliffs of two headlands

Fig. 8. Features of an emergent coastline. Figures and captions from Davis (1933).

lowered to sea level incise the terraced coastal platform. Characteristically, the emerged rock-cut platform of crystalline rocks is monticulate, or knobby, rather than a smoothly beveled surface (see Fig. 7; see also Brüggen, 1950, p. 174-176).

These observations along the shoreline are presented to complement information gathered on the continental shelf (Part V), and to outline a general chronology of coastal events. Data on shoreline levels elsewhere along the coast of northern Chile (Fuenzalida et al., 1965), indicate that the following relative changes in sea level were important: (a) a marine regression from a high Pliocene level (250-500 m above sea level) to below sea level; (b) a major transgression to a level 80-137 m above sea level, and long stillstand, culminating with the formation of well developed abrasion platforms or aggradation surfaces; and (c) a fall of sea level to its present height. The phase (a) regression is compatible with stage 5, the phase (b) regression and long stillstand is compatible with stages 6 and 7, and the phase (c) regression is compatible with stage 8.

In the Taltal coastal area, it is difficult to separate the effects of eustatic changes in sea level from the tectonic components of emergence on the basis of available observations. Nevertheless, the original "cliff-base shoreline" (Davis, 1933, p. 1051) of the emerged platform between Taltal and Paposo occurs at elevations between approximately 100 m and 150 m above sea level, and cutting of the platform probably occurred during the marine transgression of phase (b). Deposition of a veneer of marine gravel accompanied the

transgression, after which emergence of the platform resulted in blanketing by a terrestrial cover and progressive cliff cutting of the shore. No data are available for the accurate timing of the phase (b) transgression. Indurated marine gravels that veneer the emerged platform and which underlie terraced alluvium and colluvium are assumed to be Pleistocene.

The knick points at elevations of 250-500 m in stream profiles between Taltal and Paposo may be related to a large relative change in sea level during phase (a).

RIDGE-TRENCH-RIDGE ALLUVIAL FAULT SCARPS

Introduction

Abundant alluvial fault scarps occurring within the Atacama fault trough south of the Taltal fault (Fig. 31), as well as at numerous other localities, display an anomalous morphology in which a narrow trench marking the trace of the fault is bordered by ridges of uplifted alluvium that stand higher than the undisturbed alluvial surface (Figs. 9, 10, 11). Tensional fault trenches are not uncommon fault forms, and neither are compressive ridges such as moletrack scarps. The ridge-trench-ridge forms, however, seemed to present conflicting evidence for both tension and compression. C. R. Allen (personal communication) had at one time considered them to be suggestive evidence of strike-slip displacement because there appeared to be no vertical offset across many of them. More detailed studies were undertaken to decide what bearing the ridge-trench-ridge fault

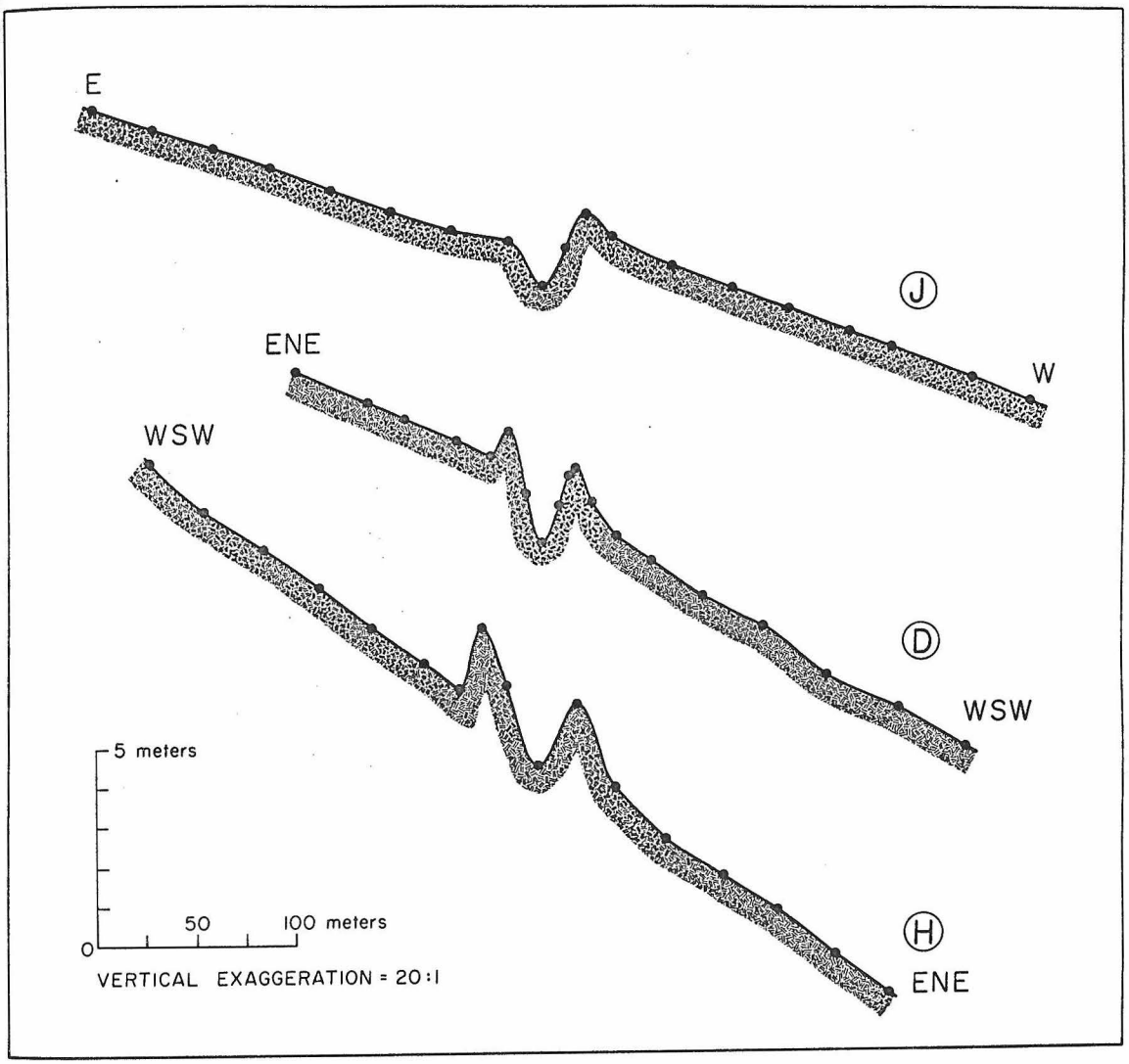

Fig. 9. Plane-table profiles of ridge-trench-ridge alluvial fault scarps. Locations of the profiles are shown in Figure 31.

Fig. 10. Ridge-trench-ridge alluvial fault scarp. Parallel dark-colored ridges mantled with coarse debris, and an intervening trench characterize the trace of the fault cutting the alluvial fan in the foreground. Locality: 0.4 km south of 24°S., 2 km west of Panamerican highway. View is to the south.

Fig. 11. View of ridge-trench-ridge alluvial scarp within the Atacama fault zone south of Taltal airport (point F, Fig. 31). Men in the middle distance stand astride the line of profile D (Fig. 9). Downfan direction is to right. The ridge to the right is well developed, but the one on the left does not persist laterally.

features could have on arguments for recent strike-slip displacement. Their general characteristics are discussed, including observations based on plane-table and penetration profiles, along with ideas on their origin.

General Characteristics

Topographic form. -- In order to document the relief of the ridges and trenches, and to determine whether alluvial surfaces cut by the faults were vertically displaced, plane-table profiles about 400 m long were measured with an alidade across twelve such fault scarps. Data for ten of the profiles are summarized in Table 1; plots for three profiles, whose locations are shown in Figure 31, are arranged in Figure 9.

Some important results of the measurements are the following: (1) In every case the trench bottom is lower than the undisturbed alluvial surface on either side; the ridges are higher than the surface on the same side of the trench -- usually higher than the surface on either side. (2) Distance from ridge top to ridge top ranges from 14 to 68 m, averaging approximately 40 m. (3) Relief between the trench bottom and the top of the higher ridge is of the order of a few meters. (4) The inner trench is characterized by gentle smooth flanks rather than steep walls (slopes not exceeding 15°). (5) The height of the ridges above the undisturbed alluvial surface varies along strike. Ridges are not everywhere well developed and occasionally have significant height on only one side of the trench. (6) In at least three cases, where

Table 1. Summary of data on plane-table profiles of ridge-trench-ridge alluvial fault scarps.

Profile	Site*	Length of profile (m)	Trend of Profile	Max. Relief--Trench bottom to ridge top (m)	Ridge-to-ridge distance (m)	Height of higher ridge above alluvial surface (m)	Estimate of vertical offset across fault (m)
A	1	448	N 70° E	5.1	68	2.6	1.3 to 1.7 (W side up)
D	2	391	N 77° E	2.9	34	1.2	<1 (E side up)
E	2	257	N 73° E	1.7	33	0.7	0.3 (E side up)
F	2	466	N 90° W	3.4	63	1.4	(no smooth surface)
G	3	468	N 65° E	4.2	58	1.6	0
H	4	370	N 75° E	3.5	48	2.0	0
I	4	424	N 90° E	2.4	24	1.2	~1 (E side up)
J	5	461	N 89° W	1.8	40	0.5	1.0 to 1.3 (W side up)
K	6	390	N 52° W	2.1	43	1.2	0
L	6	168	N 61° W	0.7	14	0.2	0.1 to 0.2 (W side up)

*1: Trace of Caleta Coloso fault east of Cerro Cristales (Pl. 1).

2: Branches of Atacama fault zone cutting across mouth of Quebrada del Pingo (Pl. 5).

3: Trace of fault passing west of Cerro Concha (Pl. 5).

4: Trace of Aguada Chépica fault southwest of Taltal airport (Pl. 5).

5: Prominent alluvial scarp east of Taltal airport (Pl. 4).

6: North-trending fault southeast of Estación Central (Pl. 4).

relief of trench bottom to ridge top is 2.1 m, 3.5 m, and 4.2 m, no vertical displacement of the alluvial surface was measured. The alluvial surface whose ridge-trench-ridge scarp had maximum relief (5.1 m) and maximum ridge height (2.6 m) had a measurable vertical displacement of 1.3-1.7 m across the fault. Relief clearly exceeds the amount of any vertical offset.

Nature of the undisturbed alluvial surfaces.-- The plane-table profiles were made across a variety of alluvial surfaces, but most of the surfaces were characterized either by a smooth pavement of granules and pebbles, or very low rills, ridges, and channels. Cobbles and small boulders generally cover less than 10% of the surface area, occasionally up to 30%. A thin veneer 1-3 cm thick of loose granule and pebble gravels without fines, overlying a compact surface of sand and silt, was most typical. Excavations were not made, but the character of the alluvial surfaces suggests substantial weathering and transformation. The sand and silt occurring a few centimeters below the surface probably represents a weathering horizon (see Denny, 1965, Fig. 11).

Nature of the ridges.-- (1) The ridges have the darkest tonality associated with the fault scarps (well illustrated in Fig. 10), which is due to a greater surficial accumulation of coarser debris. (2) They are not entirely made up of coarse clasts. Abundant fines are visible beneath a surficial veneer of pebbles and granules. This veneer is thickest on the ridges, but generally measures only several centimeters or less. A maximum thickness of 20 cm of loose medium to coarse

pebbles was measured. (3) Quite commonly the ridges do not have a greater concentration of cobble-size clasts than the undisturbed alluvium, but rather a distinctly higher concentration of coarse pebbles.

Nature of the trench bottoms. -- (1) The trench bottom is usually notable for the conspicuous absence of coarse material, compared to the ridges and undisturbed alluvium, except where the updrainage ridge does not persist laterally as a topographic barrier (Fig. 11). (2) Fine material in the trench comprises compact sand and silt thinly veneered by 0-3 cm of coarse sand to pebble material. This is not simply due to post-trench infilling of fines. The compact sand and silt is stratigraphically continuous beneath the ridges. In profile K (Table 1), 30 cm of well stratified, very coarse sand was excavated before a compact clay pan was encountered. A shallow trench dug across the floor-flank boundary showed no change in material and stratification paralleling the ground surface. (3) The trench bottom and inner flank typically display either a hummocky relief or a polygonal patterning due to warping of a finer sand and silt substratum into mounds. Relief of the mounds reaches 13 cm, but usually is less than 5 cm. On the inner flanks of the trench, migration of pebbles and cobbles to margins of the mounds results in the polygonal accentuation. The polygons are slightly elongate with a greatest dimension ranging from 0.5 m to 2.0 m. Data on the orientation of polygon borders are insufficient; a tendency to parallel the trench axis is common but not consistent.

Relation to bedrock faults.-- Field observations support the fact that the ridge-trench-ridge features occur along fault lines. In most cases they can be traced to mapped basement faults. The features were seen at various localities throughout the map area (see Table 1), and they are developed along faults of different azimuth, not only along the north-trending faults of the Atacama fault zone. For example, the features characterize at least 4 km of the trace of a fault, trending about N.45° E., on the southeast flank of the Sierra Vetada (west of Pl. 5, lower Quebrada de Cifuncho). In the Pampa de Remiendos area (Pl. 1), well developed ridge-trench-ridge forms even cut across the heads of some alluvial fans along the fault line at the base of the Salar del Carmen fault scarp, where recurrent vertical uplift is interpreted. A good example occurs near sample locality PA-102 (Appendix Pl. A).

Age of faulted alluvium.-- The ridge-trench-ridge fault scarps transect alluvium of a variety of ages, including young modern wash material. Despite the extreme aridity, climatic data (Part I) supports the occurrence of periodic heavy rainfall and flooding in the Atacama Desert during this century, so that it is reasonable to suspect that the age of the youngest disturbed alluvium in the modern washes may be up to a few hundred, rather than many thousands, of years old. Characteristics such as desert varnish, lichen-covered boulders, desert pavement, the absence of rills and channels, and so forth, imply the older age of material where the ridges are best developed. A maximum age for the alluvium in the Atacama fault trough south of Taltal airport is considered to be Plio-Pleistocene (stage 6) for reasons discussed earlier.

Sequential development. -- There appears to be a progressive growth of the features with time -- both in ridge height and ridge-to-ridge distance. Along the same fault, where material of different ages is transected, the relief in the younger material is subdued, but measurement shows ridge-trench-ridge morphology completely analogous to the larger scale development in the older alluvium (Table 1, profile L).

Thickness of alluvium. -- Thickness of alluvium does not appear to have a direct bearing on the development or absence of the fault features. They occur in broadly alluviated areas, such as the Atacama fault trough south of Taltal airport, where alluvium is estimated to attain a thickness of 50-100 m, as well as in small washes, where alluvium cannot be more than several meters thick.

Penetration Tests

Penetration tests were made across seven of the ridge-trench-ridge scarps to provide a rough comparison of the material at depth. A pointed steel rod, 1.5 m long and 3 cm in diameter, was driven with a 14-lb sledge hammer from the rear platform of an open truck. Penetration was measured after every 10 blows and plotted (Fig. 12). The rod was driven in the trench bottom, on top of each ridge, and in the undisturbed alluvial surface on both sides of the fault. The technique is basically a shear test and is standardized in engineering practice by the use of a standard weight falling from a standard height. As used in this study it provides some qualitative information: (1) In virtually every profile, the trench bottom was the least penetrable.

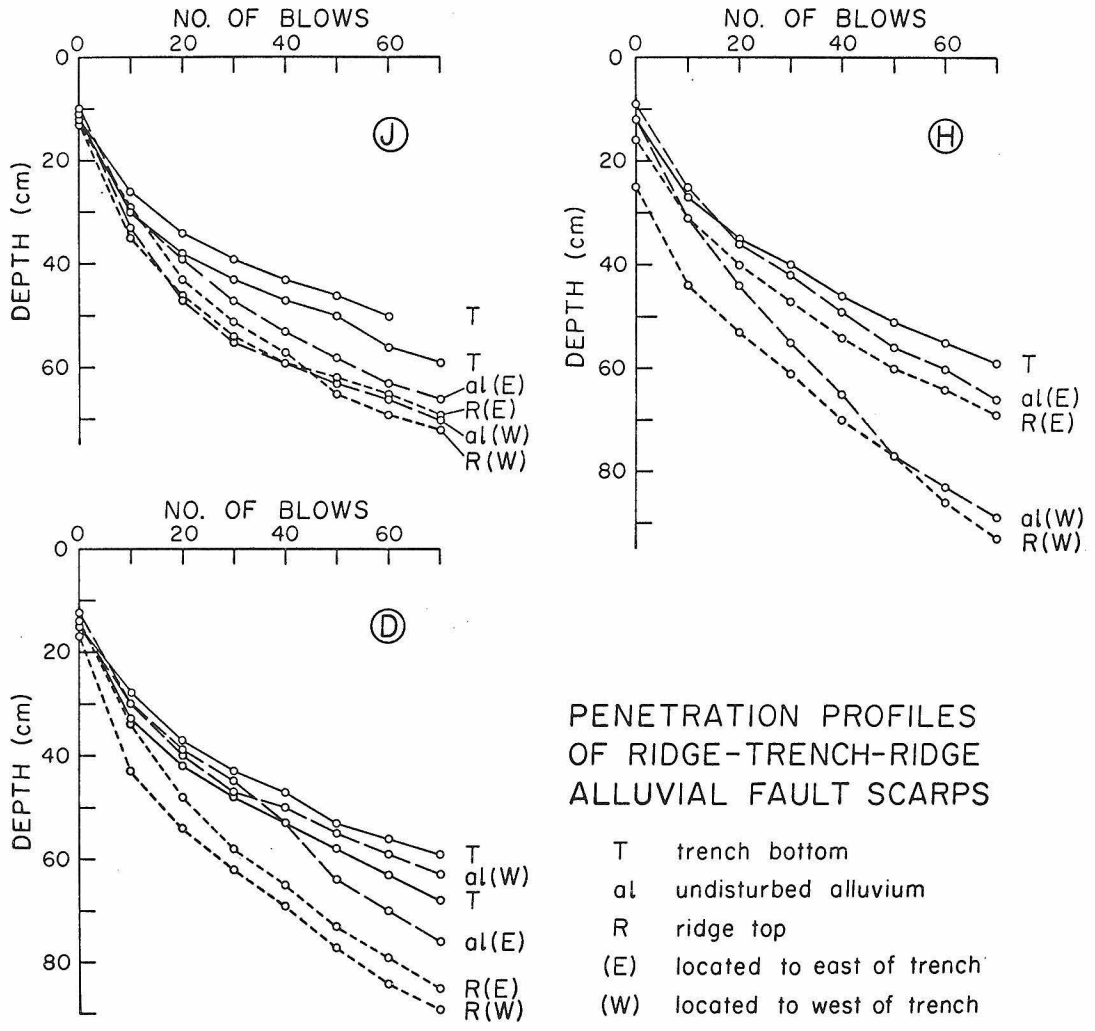

Fig. 12. Summary of penetration data for points along the three profiles shown in Figure 9. (See text for discussion.) The steel rod was driven by hand into the alluvium in the same manner at each point before beginning the count of blows. Differences in the initial depth reflect near-surface penetrability.

(2) In all profiles the greatest penetration was reached on top of a well developed ridge. (3) Nearly all the penetration curves are concave upward indicating an increasing shear strength with depth. (4) The ridges were generally more penetrable than the undisturbed alluvium, but not in all cases. In some profiles the curves for the ridges and undisturbed alluvium are closely spaced, while in others there is a similarity between undisturbed alluvium and the ridge on that side of the fault. (5) Despite the fact that the ridges are relatively more penetrable, compactness is indicated less than 1 m below the surface, and the material frequently appears to be similar to that beneath the undisturbed alluvium.

Discussion of Origin

One of the main reasons for studying the ridge-trench-ridge fault scarps was to determine whether they were indicative of strike-slip movement, particularly in view of the absence of vertical offset across many of them. Or can the features be developed along fault lines over a long period of time by non-tectonic means? Expansive fine soils are reportedly common in arid regions; such soils shrink and are compacted during arid weather and can produce heaving or uplift pressures of considerable intensity with an increase of moisture content (Lambe and Whitman, 1969, p. 6-7; Leonards, 1962, p. 1022-1023). Concentration of ground water may occur along fault lines where alluvium has been broken, so that it is not inconceivable to have uplift of the ridges by expansive soils. In a speculative manner crudely analogous to ice-wedging (Lachenbruch, 1962, Fig. 1), an

expansive wedge of soil beneath a trench could give rise to ridges and a central trough. Another factor that may be important is the high salinity of soil in the Atacama Desert. At any rate, the operation of non-tectonic processes on the ridge-trench-ridge scarps has to be considered seriously.

The origin of patterned ground within the trenches is uncertain. Numerous hypotheses have been advanced to explain similar patterned ground in other areas (see Washburn, 1956, for a review), some involving water circulation or cycles of expansion and compaction over a period of time. Patterned soil structures have most commonly been reported for high latitudes where frost action and solifluction are important agents; agents that may be operative in a desert environment include desiccation and local differential heaving on the scale of the polygons. The concentration of coarse debris on top of the ridges may be explained by long-term weathering processes that produce a lag of gravels. A dynamic upheaval does not have to be invoked.

Sampling and testing the soils for expansivity and excavating across a ridge-trench-ridge form could advance an understanding of the origin of the fault features. However the scarps are explained, alluvium is definitely faulted along their traces and a tectonic contribution to their relief cannot be disregarded. This is clear in profile J (Figs. 9 and 31), where uplift of the western side of the fault is important, and in other profiles where definite vertical offsets across the faults have been measured, with control over a large horizontal distance (Table 1).

In this writer's opinion, the ridge-trench-ridge forms are not necessarily indicative of strike-slip movement. A non-tectonic agent, such as expansive soil, could conceivably cause the development of such features in faulted alluvium. Episodic fault motion does not have to be invoked to explain every increment of their growth. It would appear hazardous, then, to attribute their origin or development to strike-slip movement simply because of the frequent absence of vertical offset across them, or because of the seeming necessity to explain the ridges by tectonic compression.

Antithetic faulting and reverse drag (Hamblin, 1965) have been considered to explain the ridge-trench-ridge morphology, but appear inadequate. If ground displacement along a fault should accompany an earthquake in northern Chile, field studies will be extremely important and investigators should note observations that may have a bearing on these anomalous fault features. They may indeed reflect lateral motion, although this writer believes that vertical faulting is presently more important in the area.

V. OCEANOGRAPHIC STUDIES

INTRODUCTION

Inspecting the map of the Atacama fault system in Figure 1 reveals that some branches have sub-sea traces and that interpretation of the offshore structure can be complicated, as in the Bahía Nuestra Señora near Taltal. The bathymetry and aspects of the structure of the Peru-Chile trench have been studied (Zeigler et al., 1957; Fisher and Raitt, 1962; Hayes, 1966; Scholl et al., 1968), but little concentrated offshore work had been done near the map area of this study. Therefore, a proposal for oceanographic studies was submitted to the Scripps Institution of Oceanography in March of 1968 with the following specific problems in mind:

(1) The correlation and continuity of branches of the Atacama fault zone beneath Bahía Nuestra Señora were open to question. A 10 km left-lateral offset of the Atacama fault zone by the Taltal fault had been documented (Arabasz, 1966), leading to various interpretations of sub-sea fault configurations for major faults that project seaward into the bay. If one assumes the former continuity of the El Salado and Salar del Carmen sectors of the Atacama fault (see Fig. 1; Pls. 2, 3, 4), then their traces can be connected by bowing or a series of step offsets that might be expected to have resulted from the disruption of the fault zone. The inference that the two faults are correlative is based on their similar continuity, trend, and general make-up. Alternatively, the slight northwest trend of the El Salado sector suggested that it might project offshore west of Paposo, instead of connecting with the Salar

del Carmen sector. Another possibility is to project the Salar del Carmen sector offshore to the southwest, west of Taltal. Such a configuration could result from: (i) disruption of a continuous fault zone by the Taltal fault, causing subsequent prolongation of the Salar del Carmen sector as an adjustment response, or (ii) complete independence of the Salar del Carmen and El Salado sectors. Also, a large offshore fault, or faults, could be postulated immediately west of the Bahía Nuestra Señora controlling the upper continental slope, but perhaps independent of the onshore fault system because of different age. Both the steep coastal topography of northern Chile and the Peru-Chile trench seemed to call for offshore normal faulting of this continental margin.

(2) Sub-sea fault configurations were also in question in Bahía Moreno or the Bay of Antofagasta (see Fig. 1). The problem of fault configuration can be seen in Figures 2, 3, and 4. Faults bounding the uplifted block of the Mejillones Peninsula on the east can either be projected southeast across the Bay of Antofagasta to connect with a diverging branch of the Atacama fault system -- the Caleta Coloso fault, or the faults can be projected due south as an independent, offshore, coastal fault zone.

(3) With the axis of the Peru-Chile trench lying about 100 km distant from the Atacama fault, it was of interest to determine whether the latter fault was a "master fault" of the continental border, or only one of a series of similar north-trending major faults parallel to the oceanic trench. Added interest was given to the offshore structure near

Taltal because of the occurrence of a major earthquake ($M \cong 7.5$) on December 28, 1966 and aftershock activity in an offshore zone paralleling the coast (Pitt and Ellis, 1968; Fig. 36).

Ship-time was graciously arranged by H. W. Menard of Scripps, and these oceanographic studies were carried out in early January, 1969 during the Piquero II expedition of R/V Thomas Washington. The purpose, then, was to extend knowledge of the structure of mapped onshore faults, and to achieve some understanding of structure on the continental slope -- and hence some relation between the Atacama fault and the Peru-Chile trench.

AREAS OF STUDY AND METHODS

A program of continuous reflection profiling using a pneumatic sound source (air gun) was outlined by this writer and conducted with the help of Tanya Atwater and the scientific party of R/V Thomas Washington (Piquero II) off the coast of northern Chile. Records of continuous bathymetry and magnetometry (not included here) were taken along the entire ship's track plotted in Figure 13; seismic reflection profiling was completed for all segments of the track indicated by a solid line.

The plan was to concentrate nearshore profiling in the Bay of Antofagasta and the Bahía Nuestra Señora areas, to carry out longer profiles between the latitudes of Antofagasta and Taltal to study the upper continental slope, and finally to crisscross the trench axis en route south to Valparaíso. The locations of nearshore seismic profiles

are indicated in Figures 14 and 15. Because instrumental difficulties interrupted the seismic profiling on the upper slope between Antofagasta and Taltal (Fig. 13), bathymetric data are included for all the long east-west profiles so that topography can be compared sequentially from profile to profile (Fig. 27). Bathymetric profiles for the trench crossings are shown in Figure 28.

The air-gun system used consisted of a single Bolt air gun (20 in^3) supplied with compressed air at 1750 psi by a Rix compressor and firing at 5-second intervals. Simultaneous recording was made with: (1) a Gifft recorder (GDR-19) with a Bolt amplifier and Krohn-Hite filter; and (2) a Mark XV recorder with a Prototype Huckaby filter-amplifier. Both systems allowed a bandpass of approximately 30 to 120 Hz.

Radar was primarily relied on for nearshore navigation, generally allowing an accuracy to within 1 km for locations within 20 km of the coast, and an accuracy to within 2 km for larger distances up to 60 km from the coast. These accuracies apply to all the profiles except the trench crossings.

SEISMIC AND BATHYMETRIC PROFILES

Presentation of Data

The line drawings shown in Figures 16 through 26 represent tracings of all the east-west seismic profiles except the long trench crossings. Bottom, sub-bottom, and internal multiples have been

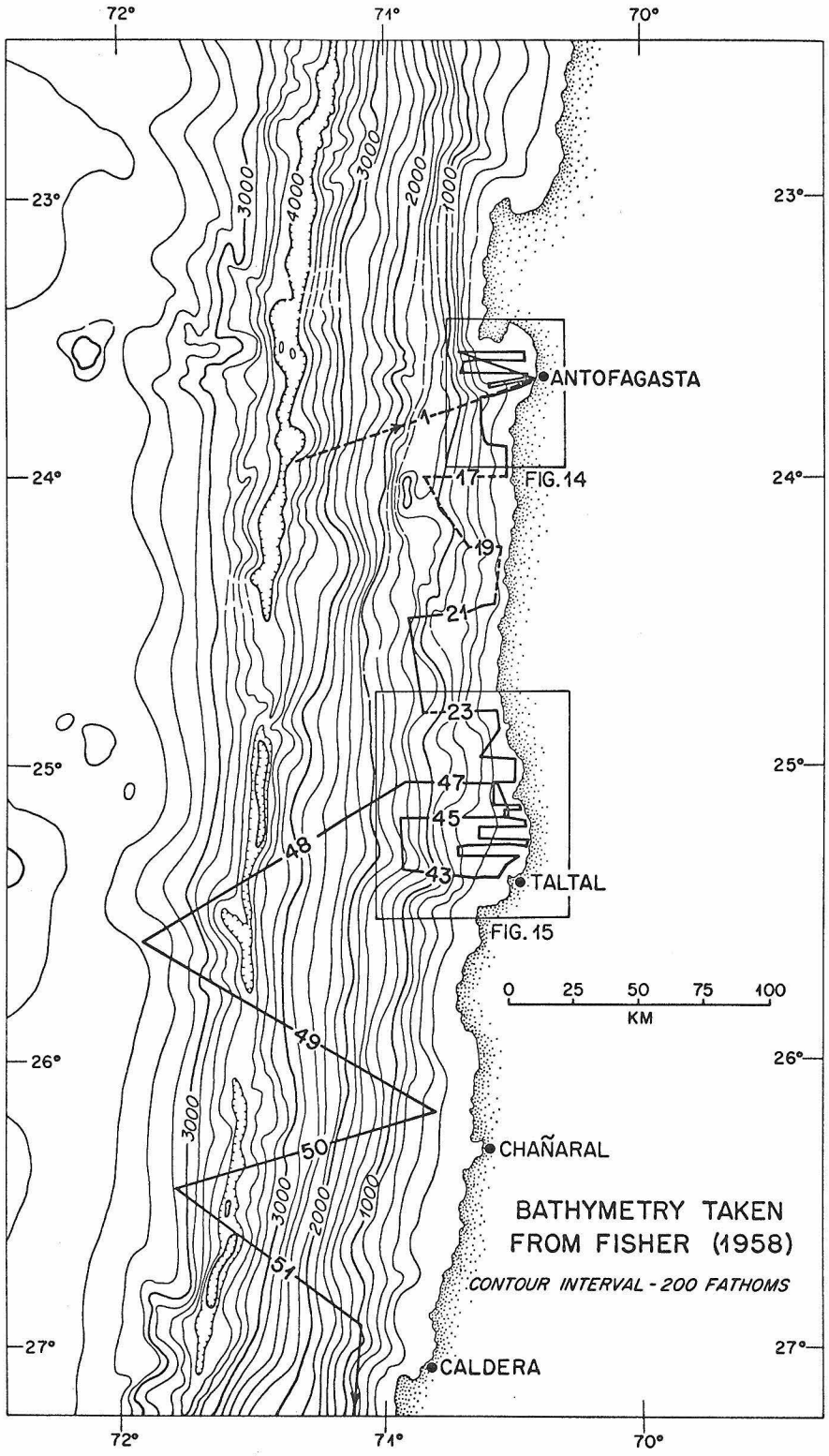

Fig. 13. Ship's track for seismic reflection and bathymetric profiles reported in this study.

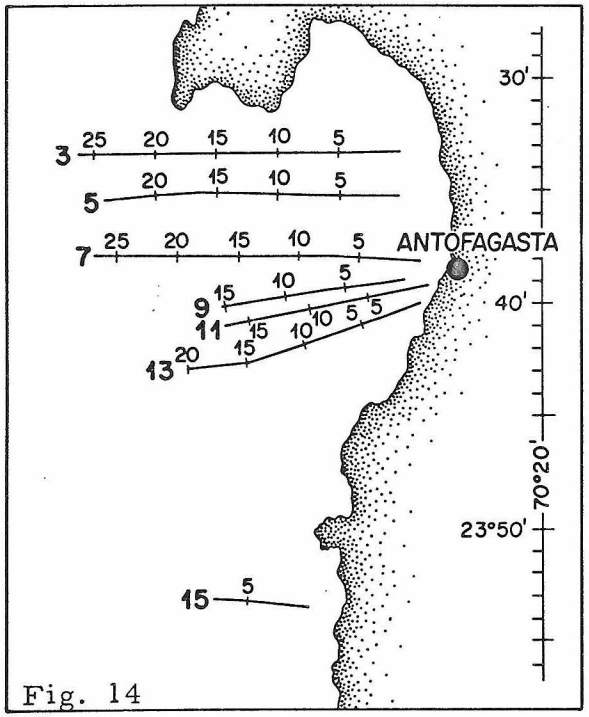

Fig. 14

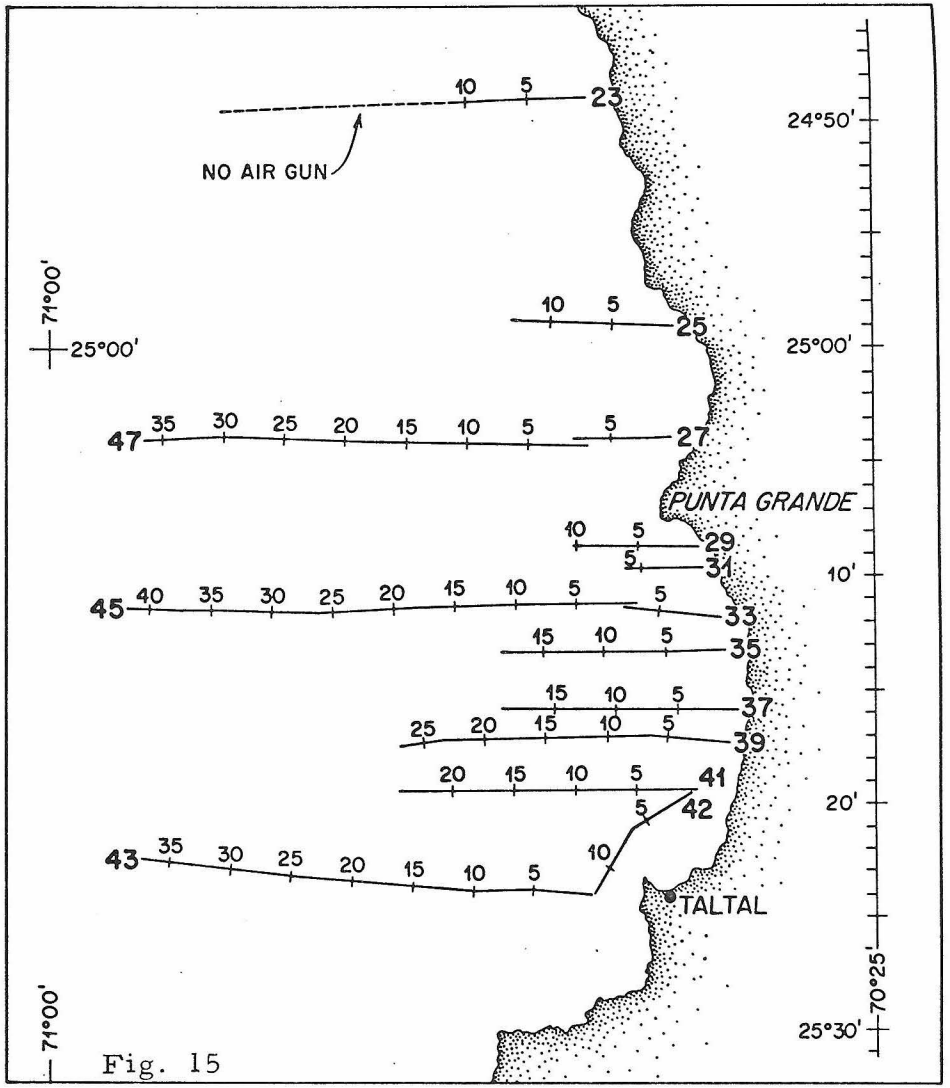

Fig. 15

Figs. 14 and 15. Location of seismic reflection profiles. Kilometer marks are keyed with the line drawings (Figs. 16 to 26). Rectangles are located in Figure 13.

removed -- both for reflector to sea-surface multiple reflections and also for reflections caused by a delayed "bubble pulse", so that only real reflectors have been traced. A horizontal scale in kilometers corresponds to the keyed track lines in Figures 14 and 15, according to which the profiles are arranged with the landward side of the section to the right. For all the profiles, the vertical scale in seconds represents round-trip travel time; a sound velocity in sea water equal to 1500 m/sec was assumed in labeling the depth axes in meters. With ship speed averaging 8 to 10 knots, a sizeable vertical exaggeration results in the line drawings -- roughly a factor of 20 to 30, as noted. For the bathymetric profiles which are based on echo soundings on a conventional Precision Depth Recorder (Figs. 27, 28), the vertical exaggeration has been reduced to 5 : 1 and profiles are corrected for changes in ship speed.

Profiles 3 through 25 were traced from recordings that were not half-wave rectified (see Hersey, 1963, p. 54), as were those subsequent to Profile 25. The latter display enhanced clarity because of phase correlation, while the former display an envelope correlation that was more difficult to interpret. As a result, line drawings for the earlier profiles are less detailed.

Two basic units have been distinguished in the line drawings: (1) acoustically penetrable sedimentary deposits with internal reflectors, and (2) acoustically reflective basement, or simply acoustic basement. As is common in reflection profiling, strong reflections are recorded from the sea floor and from the surface of bedrock that underlies softer

sediments, so that these two surfaces are the easiest to identify. Usage of the term acoustic basement follows Scholl et al. (1966) in not strictly implying a "basement" of crystalline rocks; nevertheless, the acoustic basement underlying the shelf deposits is traceable to outcrops of granitic, volcanic, and metamorphic rocks of Mesozoic and Paleozoic age that are exposed at the shoreline, thus implying that acoustic basement in the included line drawings is equivalent to crystalline basement -- at least beneath the shelf, and almost certainly on the upper slope.

Acoustic basement is shaded in the line drawings where its upper surface is clearly recognizable. No effort was made to trace the complicated and indistinct reflectors that are typical of basement rocks beneath the highly reflective upper surface.

With regard to structure, where a fault is interpreted, its presence is indicated by a heavy line that in nearly all cases is plotted as vertical because of the exaggeration. Offset of both acoustic basement and overlying stratified sediment provides the strongest evidence for the interpretation of a fault while topographic evidence, although suggestive in many cases, is admittedly not definitive. Uncertain structures are queried.

Description and Interpretation

Profiles 3 through 13 (Figs. 16, 17, 18) in the Bay of Antofagasta reveal similar features: an outer-shelf basement ridge, a sedimentary wedge with internal reflectors that is ponded or faulted on the landward

side of the ridge, and a tapering wedge of sediment at the shelf break that overlaps onto the continental slope. A wave-cut platform of basement rock emerges near the shore in profiles 11 and 13.

Gentle sea-floor gradients of less than 1° contrast with slopes of 7°-10° beyond the shelf break, which occurs at depths of about 150 m in profiles 9, 11, and 13, but at depths between 200 and 250 m in profiles 3, 5, and 7. Disruption of both sediments and basement by faulting is best illustrated in profiles 9, 11, and 13. The sea floor itself is disrupted (also observable on the echo-sounding records), implying that faulting has been recent enough to affect the uppermost layers of sediment. Taken as a group, profiles 3 through 13 suggest uplift and perhaps westward tilting of the basement blocks forming the outer-shelf ridge. Sedimentation, in part contemporaneous with faulting, is suggested by the distribution of sediments on the landward side of the ridges. Assuming a sound velocity in sediment (hereafter referred to as V_s) of 2.0 km/sec implies a thickness of sediment of up to 300 m in profile 5; the same assumption implies apparent basement offsets of the order of 50 m in profiles 9 and 13.

A topographic basement high that appears on the upper slope in profile 5 has no expression in the adjacent profiles (profiles 3 and 7), precluding continuity in a north-south direction.

In map view (Fig. 29), the shelf is seen to be about 20 km wide in the Bay of Antofagasta. Two segments of the outer-shelf ridge have different trends that may intersect or connect in profile 7. The ambiguity, unfortunately, could not be resolved by the data. Further

interpretation is discussed below.

Between the Antofagasta and Taltal areas, nearshore profiles (Fig. 19, profiles 15, 23) show sediment draped on the upper continental slope that is continuous with shelf deposits (profile 23). The shelf width, however, is much smaller than near Antofagasta, measuring only 3-5 km.

Profiles 25 through 42 (Figs. 19, 20, 21, 22) show the nearshore structure just to the north of, and in, the Bahía Nuestra Señora near Taltal. A sharp shelf break is observed, with sediments in all cases progradational onto the upper slope, where they are apparently affected by slumping in some cases (profiles 25, 27, 33) and definitely affected by faulting in some others (profiles 41, 42). Deformation of the sediment blanket in profile 25 cannot be definitely associated with a fault, although a step in the basement is suggestive. Topographic irregularity in the upper surface of the slope sediments (profiles 25, 27, 35) could be due to channeling. The depth of the shelf break is constant at approximately 160-170 m in nearly all these profiles, except profile 25 (190 m) and profile 27 (140 m); shelf width measures 3-8 km (Fig. 30).

The clarity of the records for profiles 25 through 42 allowed tracing near the shelf break of oblique stratification -- consistently seen in most of the profiles -- that is interpreted as foreset bedding in the upper shelf deposits, and is suggestive of a discordance in the shelf sequence.

The lowermost strong reflector is unquestionably the sediment-basement contact. Acoustic basement that emerges at the feather edge of the wedge of shelf deposits correlates with outcrops of crystalline basement at the shoreline (see Pls. 2, 3, 4). Both the shelf and slope deposits attain thicknesses generally exceeding 100 m and approaching 200 m (assuming V_s = 2.0 km/sec).

The clearest evidence for faulting is observed not on the shelf, but on the continental slope. Profiles 37, 39, and 41 strongly suggest block faulting rather close to the shelf break. Clear basement offset across the fault at Km 7.4 in profile 41 measures 50-60 m with the west side up; the fault at Km 6.8 in profile 42 has an offset of 20-25 m, also with the west side up. The map view (Fig. 30) suggests that these faults are the same and correlative with the inferred faults at Km 14 in profile 39 and at Km 15.8 in profile 37 -- both of which also have their west side up.

The case for block faulting on the upper continental slope is strengthened by profiles 21, 43, 45, and 47 (Figs. 23 to 26). Profile 47 (Fig. 26) shows a large horst-like block and two perched basins, of which the higher one is interpreted to be definitely fault-bounded. Faulting, perhaps contemporaneous with sedimentation in the higher basin, is suggested by the attitude of sediments along its western margin. The maximum sediment thickness in the higher basin (assuming V_s = 2.0 km/sec) is about 470 m, and in the lower basin is about 210 m. A reflection profile similar to profile 47, and located a short distance to the north, has been published by Scholl and von Huene

(1970, p. 489, profile D-8). Their profile transects a considerably greater thickness of sediment in the lower basin, and comparison with profile 47 suggests some caution in correlating the layered reflectors on top of the horst-like block in the latter profile because of a lack of close three-dimensional control. The sediments on top of the block should not be inferred to be simply correlative with the beds in the lower basin to the landward side. Faulting on the seaward side of the high-standing block is indicated by a slope with segments exceeding 24°--one of the steepest gradients encountered on the upper continental slope in this survey.

Block faulting is also suggested in profiles 21 (Fig. 23) and 45 (Fig. 25), but the evidence is mainly topographic. The distribution of sediment and the highly irregular topography on the upper slope in profile 45 is interpreted as indicative of faulting. Topographic expression of the acoustic basement in both profiles 45 and 21, where little sediment blankets the slope, intimates both seaward-facing and landward-facing fault scarps.

Faulted acoustic basement and sediment is also seen in profile 43 (Fig. 24), where faulting and sedimentation again appear to have been in part contemporaneous. The occurrence of sediment on a plateau at about Km 17 facilitates the interpretation of a fault at the base of a steeper slope. Similar abrupt changes of slope in profiles 21 and 45 also probably represent the presence of faults, but the absence of recognizable deformed sediment makes interpretation more speculative.

The bathymetry for the four longer east-west profiles just discussed is plotted in Figure 27, together with the bathymetry for other profiles for which seismic reflection was not completed (Fig. 13). The profiles are arranged according to latitude from north to south and are aligned with respect to longitude with the landward side of each profile to the right. The important feature illustrated by the combined profiles is the absence of cylindrical symmetry along the continental slope. Instead, a disordered topography is seen that is judged to be the result of ragged block faulting, roughly parallel to the strike of the continental slope on a regional scale -- as suggested by the bathymetric map in Figure 13 -- but quite irregular locally. Construction of a structural map for the upper continental slope is impossible without more closely spaced track lines.

Bathymetric profiles for the longest lines that extend to, or cross, the trench axis (Fig. 28) are presented to consider the entire landward flank of the trench near the area of study, in light of the structure that has been investigated on the upper slope. Comparison can be made with other published profiles across the trench (Zeigler et al., 1957; Fisher and Raitt, 1962; Hayes, 1966; Scholl et al., 1968; Scholl and von Huene, 1970).

Although seismic reflection profiling was completed for the trench crossings (Fig. 13), line drawings were not constructed because very little sediment is recognizable on the landward flank. The profiles confirm that slope deposits are restricted to the upper slope and that only acoustic basement can be interpreted on most of the landward

flank of the trench (see Scholl and von Huene, 1970, profiles D-8 and D-17).

Areas where slope deposits are recognizable in the reflection profiles that are not included are the following. Slope deposits reaching a thickness of about 150 m occur on the uppermost slope in profiles 49 and 50 as a body of sediment that is similar in form to that at Km 10 in profile 41 (Fig. 22). The deposits quickly taper out downslope and are down-faulted to the east, forming a landward-facing scarp that is shown in Figure 28 at about 450 m depth in profiles 49 and 50. The seismic reflection profile corresponding to profile 49 shows that buried acoustic basement is uplifted at least 40 m to the west by that fault. The faulting is more complicated in profile 50, but the structure appears to be northeast-trending. Accurate projection of the fault is made difficult because it is located close to a turning point in the ship's track. A tentative estimate is that the projection of the fault intersects the coastline at approximately 26°00' S.

An indistinct pocket of sediment, perhaps approaching 100 m in thickness, occurs at the base of the relatively steep (15°), seaward-facing scarp above 3000 m in profile 51. Elsewhere, the only slope deposits discerned in the profiles occur more or less above 5000 m as thin, very local deposits at the immediate base of oversteepened slopes. No entrapment basins comparable to those in profile 47 (Fig. 26) appear in profiles 48 through 51 on the landward flank of the trench.

The trench crossings are oblique to the strike of the continental slope and have not been projected, but they indicate a reasonably

accurate view of the topography of the landward flank of the trench. Measured slope values are thus approximate. The main feature displayed by the profiles is segmentation of the slopes into long segments of more or less uniform gradient -- typically 5°-7° -- that are separated by shorter segments of either greater or lesser angle. Seaward-facing scarps with slopes of 15°-20° or greater are seen in profile 1 at depths of 1000 m and 2000 m, in profile 49 at 3500 m, and in profile 51 at 2500 m. The landward continuation of profile 48 (profile 47) also shows a similar steep, seaward-facing scarp mentioned earlier. Faulting and down-dropping of the seaward block is suggested in each case.

Westward tilting of some blocks is suggested by the pattern of offset of slope segments, such as in profiles 50 and 51, in which the upslope projection of lower segments of the profile is higher than the next upslope segment. Faulting has already been indicated with the west side up at 450 m depth in profile 50; downslope, another landward-facing scarp at about 1800 m depth is compatible with westward tilting of the block between those two points.

The data are not sufficient to demonstrate the structure of the entire body of the landward flank, particularly in view of differing ideas concerning the material making up the lower slope (Scholl and von Huene, 1970; Seyfert, 1969). Nevertheless, evidence for block faluting on the upper slope is good. The landward flank in the area of this study is interpreted to be segmented into large blocks 25-35 km wide -- although smaller and more irregular on the uppermost slope -- that are down-dropped and tilted toward the trench axis.

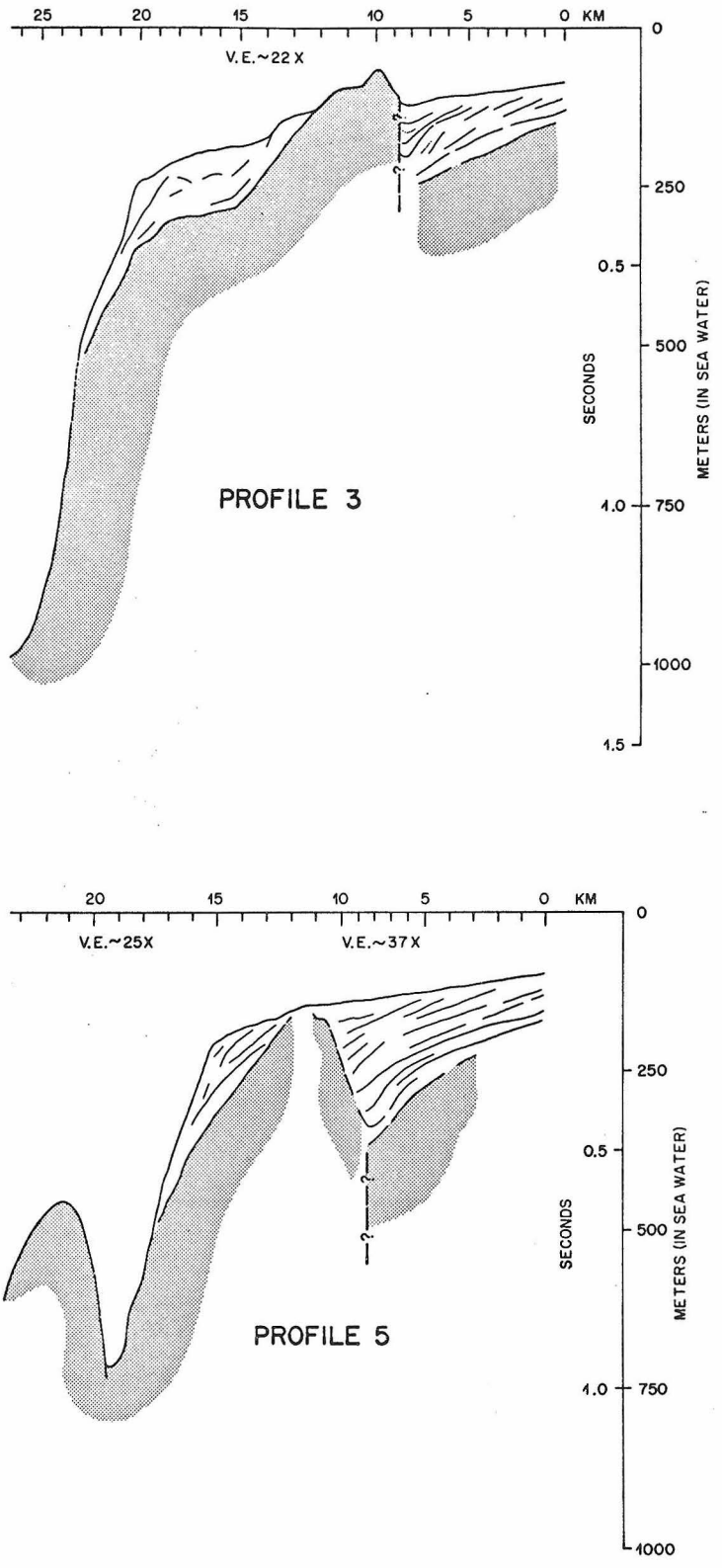

Fig. 16. Line drawings of seismic reflection profiles keyed to Figure 14.

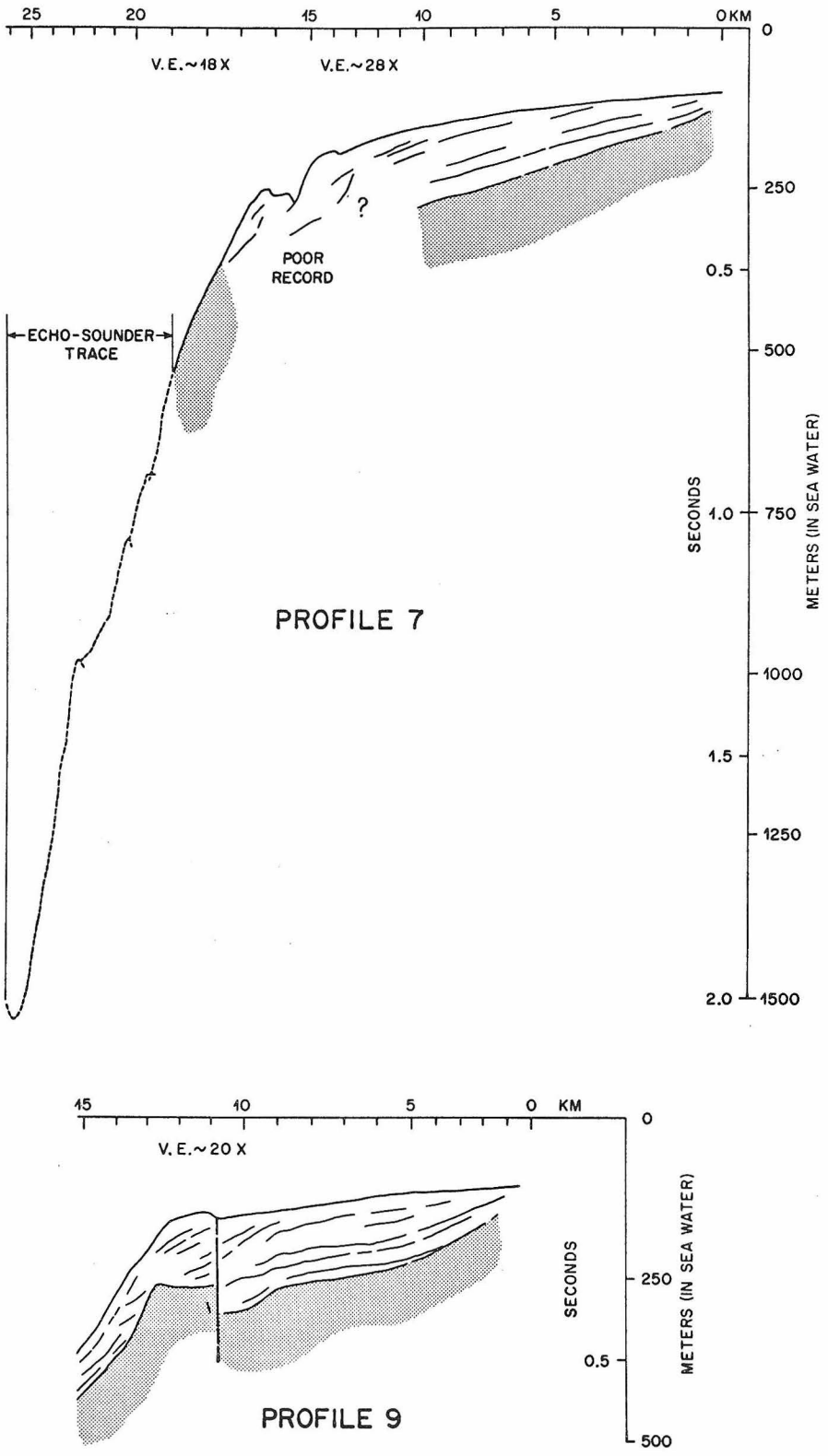

Fig. 17. Line drawings of seismic reflection profiles keyed to Figure 14.

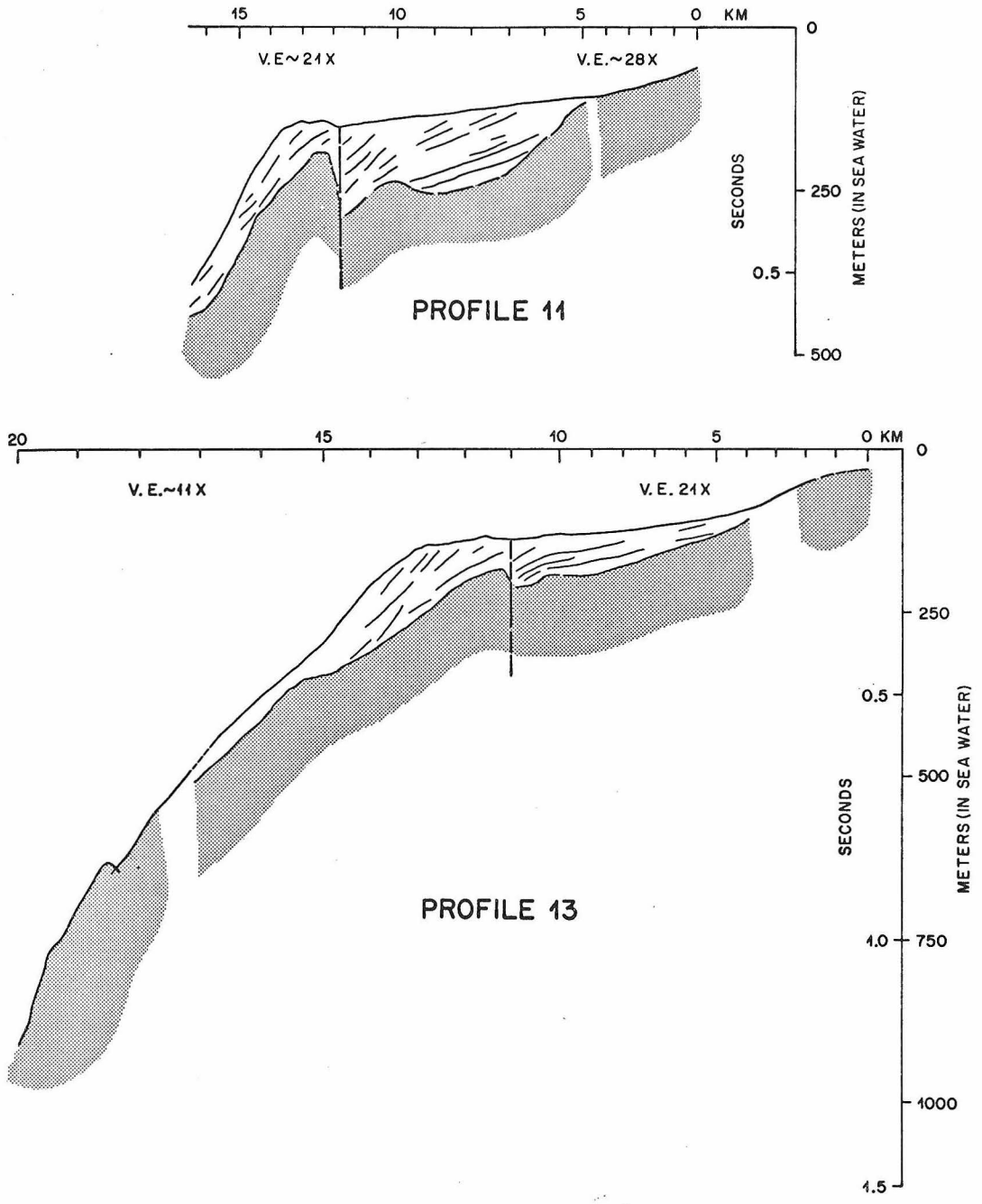

Fig. 18. Line drawings of seismic reflection profiles keyed to Figure 14.

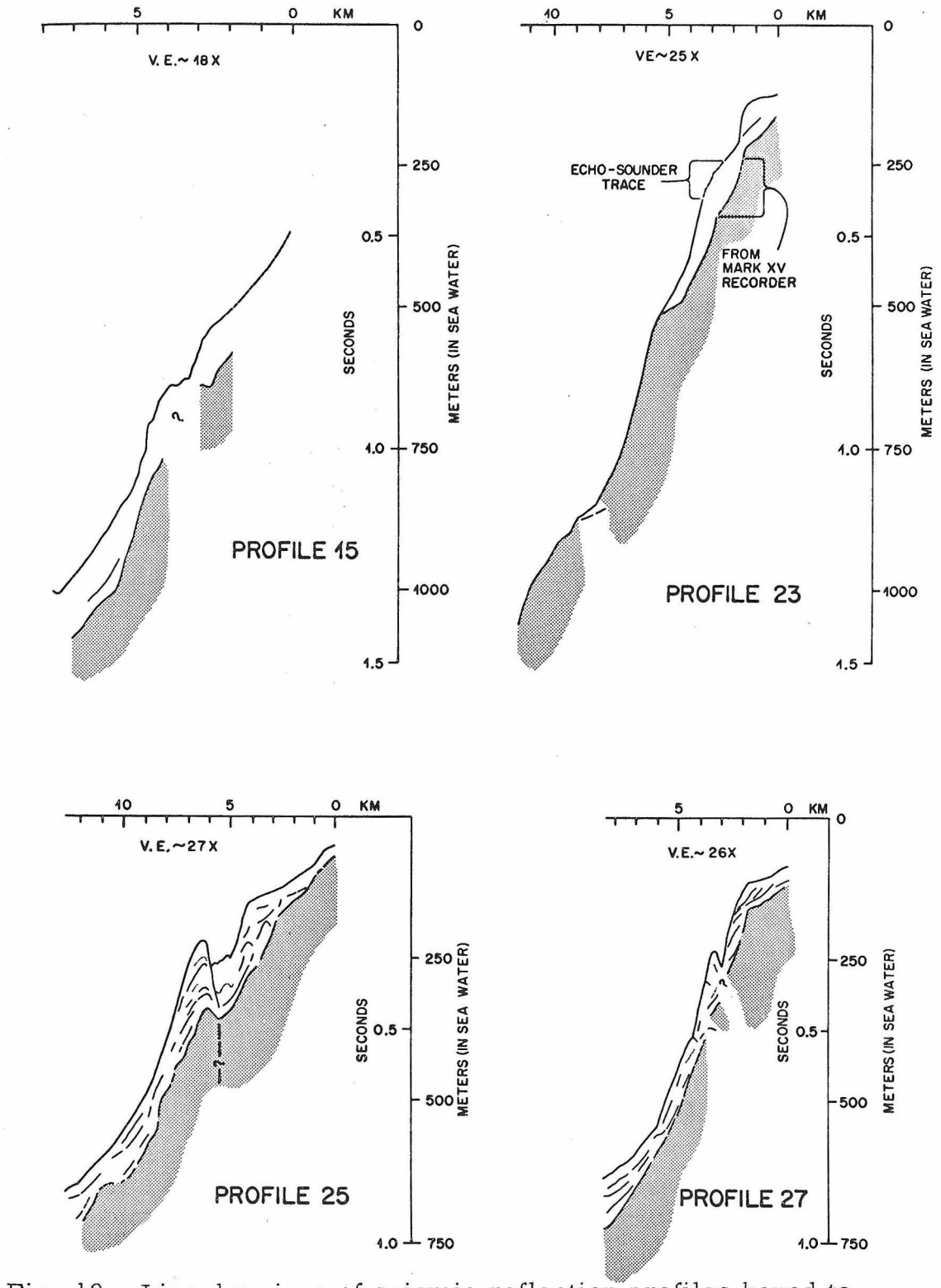

Fig. 19. Line drawings of seismic reflection profiles keyed to Figures 14 and 15.

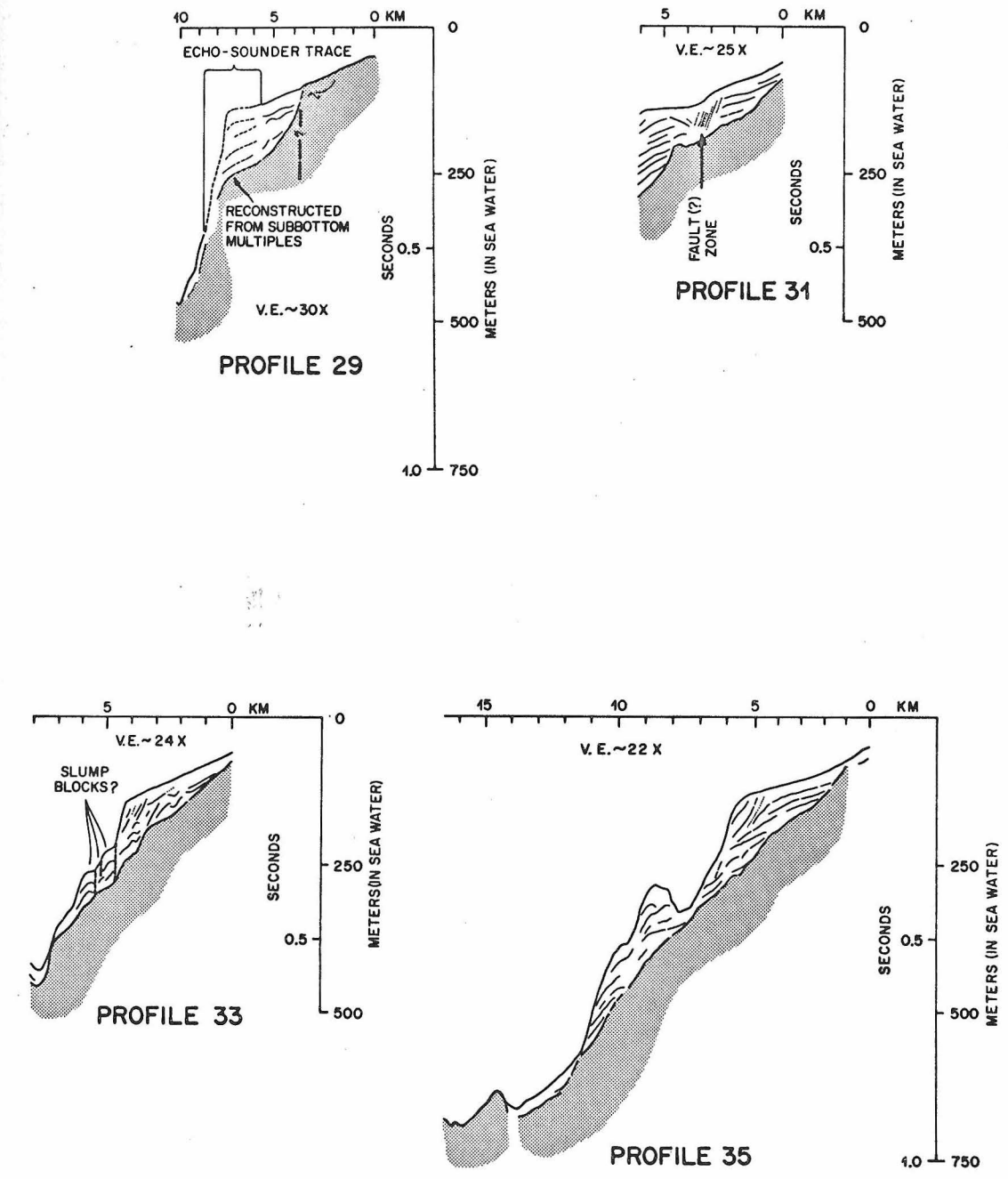

Fig. 20. Line drawings of seismic reflection profiles keyed to Figure 15.

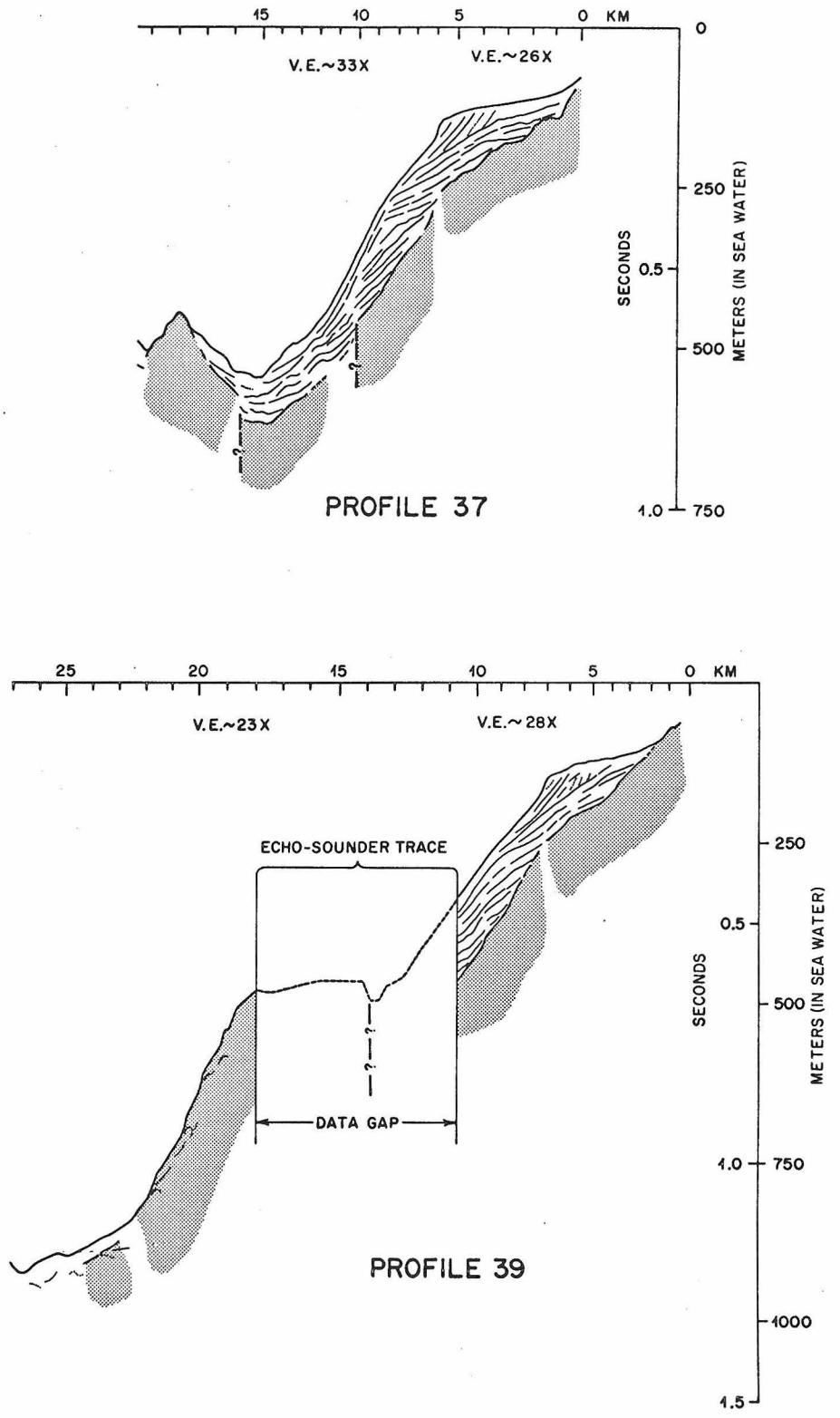

Fig. 21. Line drawings of seismic reflection profiles keyed to Figure 15.

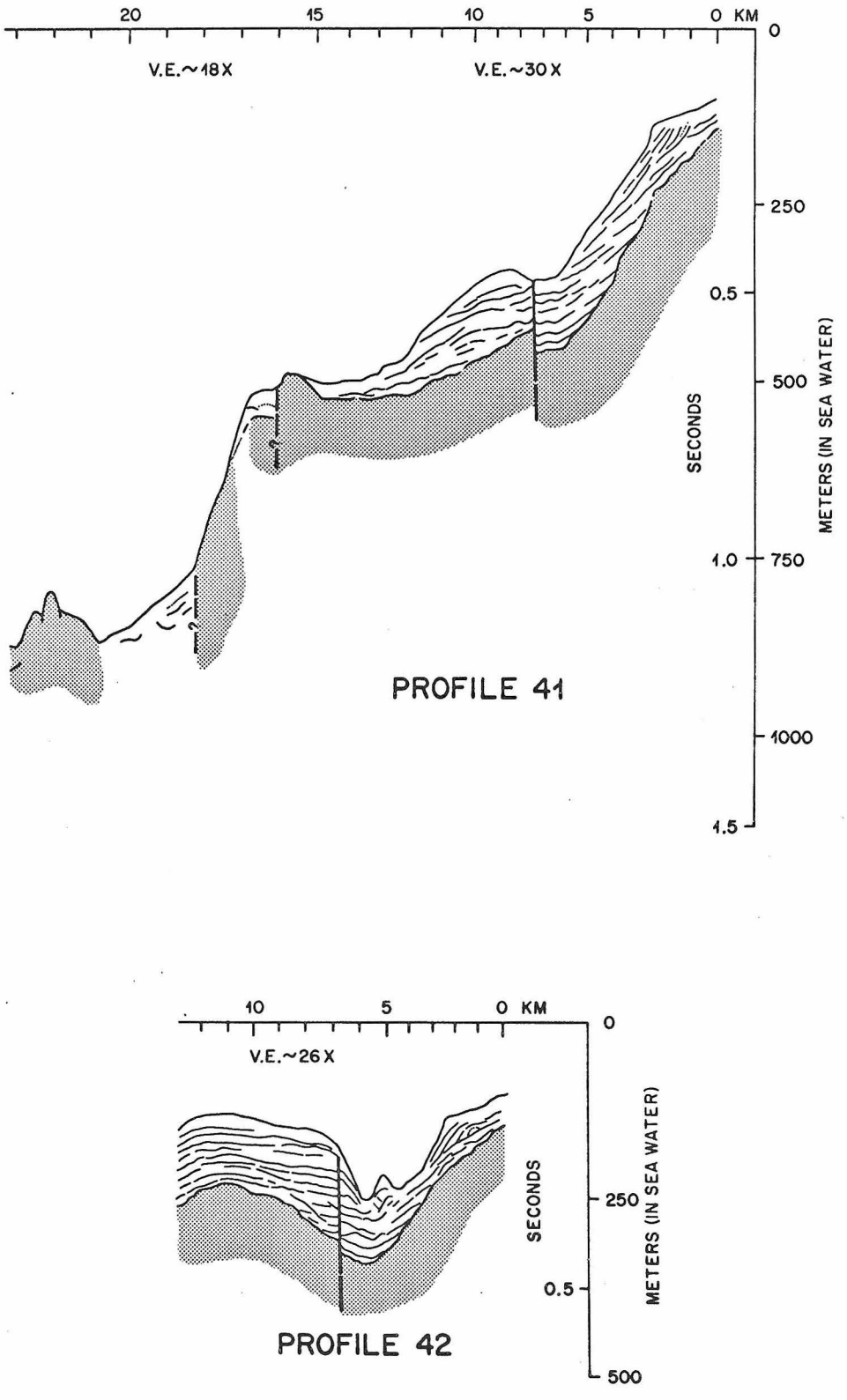

Fig. 22. Line drawings of seismic reflection profiles keyed to Figure 15.

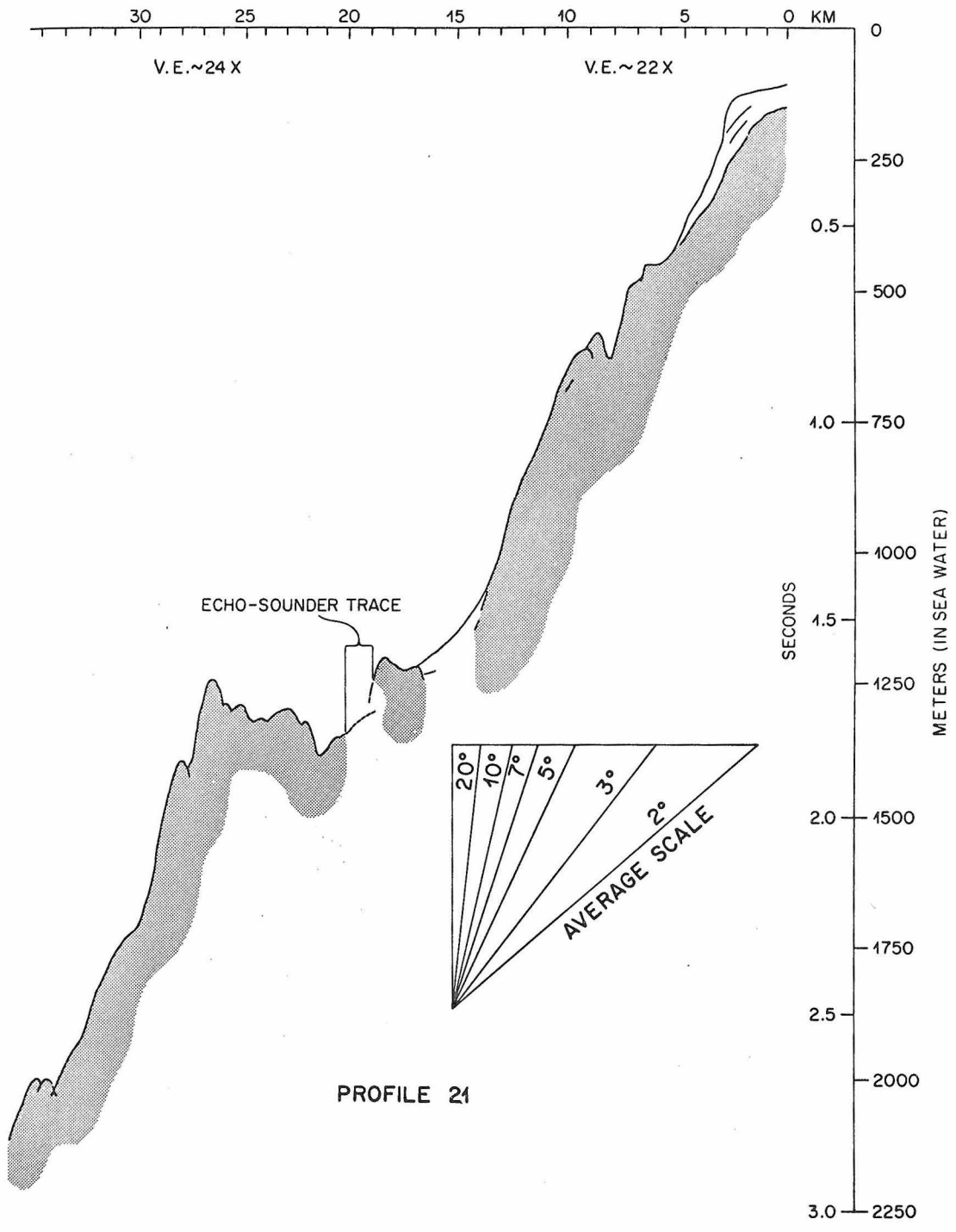

Fig. 23. Line drawing of seismic reflection profile keyed to Figure 15.

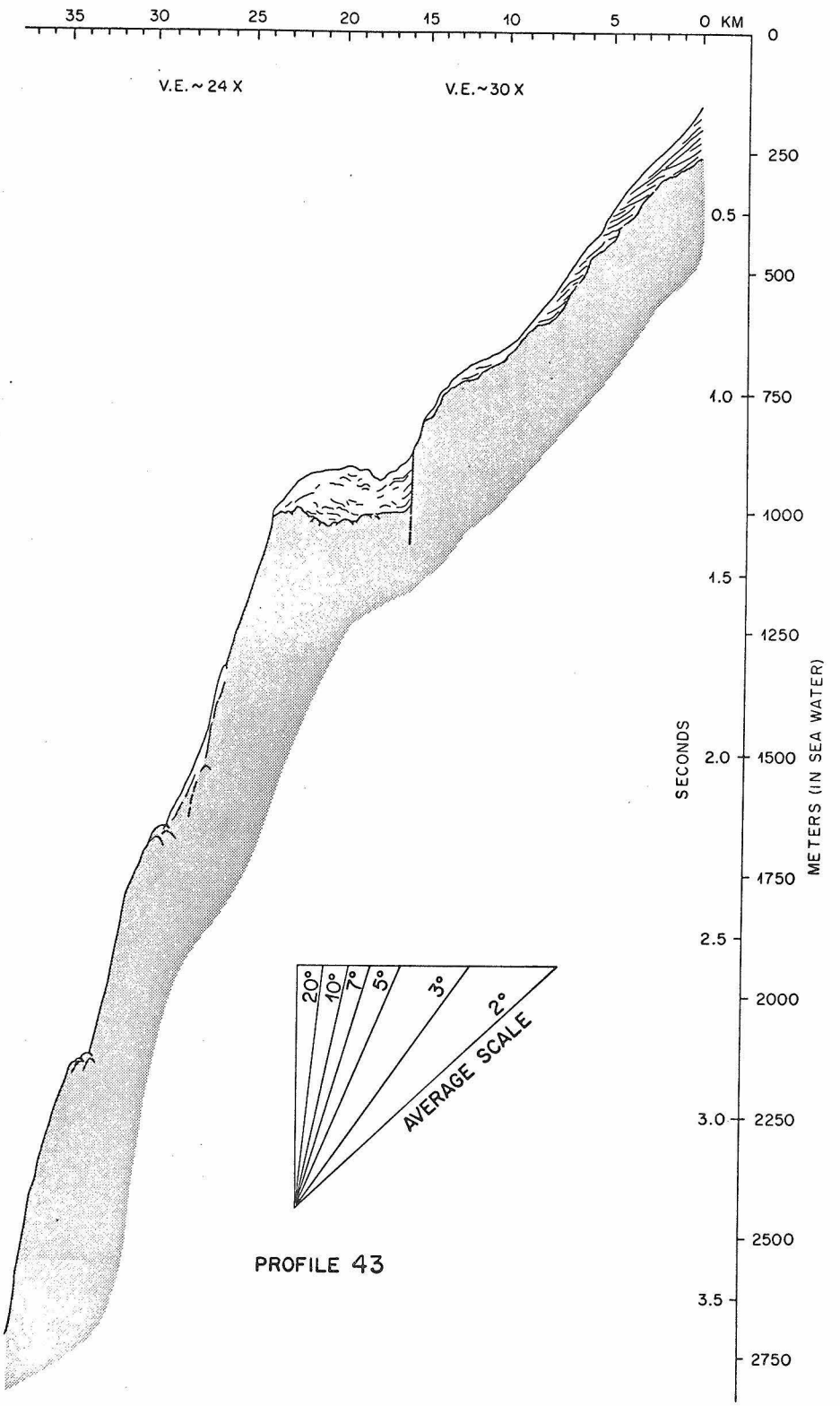

Fig. 24. Line drawing of seismic reflection profile keyed to Figure 15.

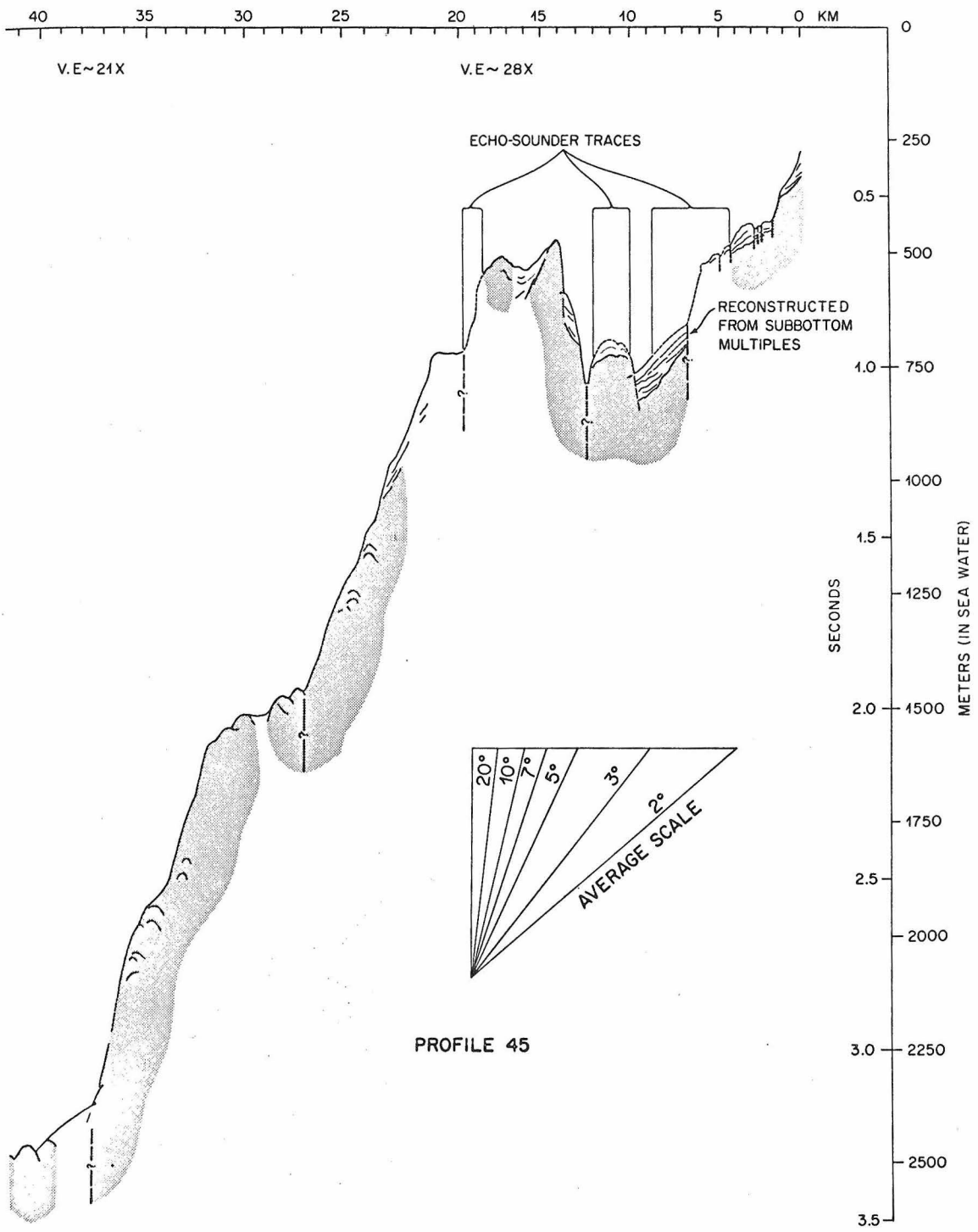

Fig. 25. Line drawing of seismic reflection profile keyed to Figure 15.

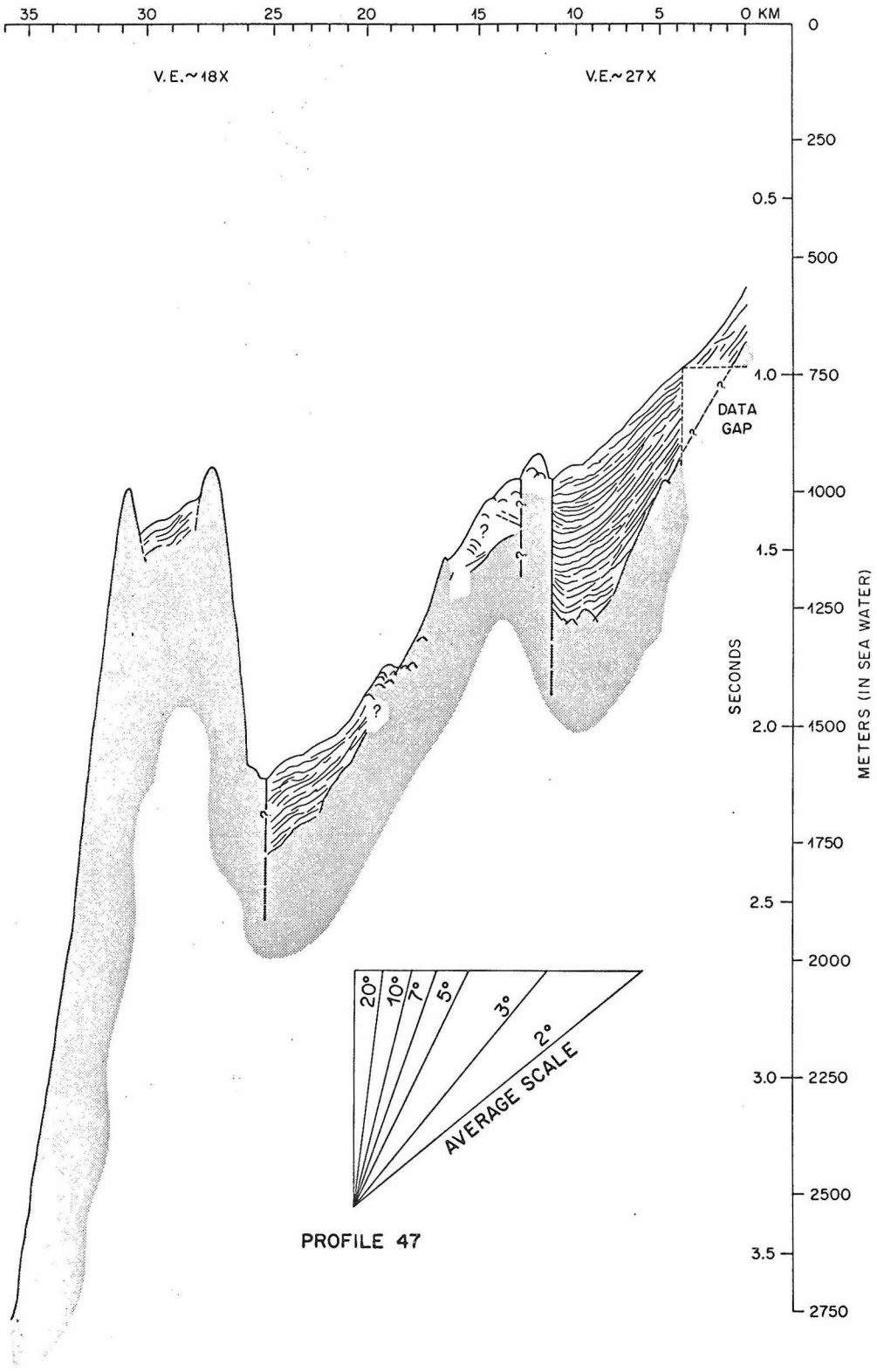

Fig. 26. Line drawing of seismic reflection profile keyed to Figure 15.

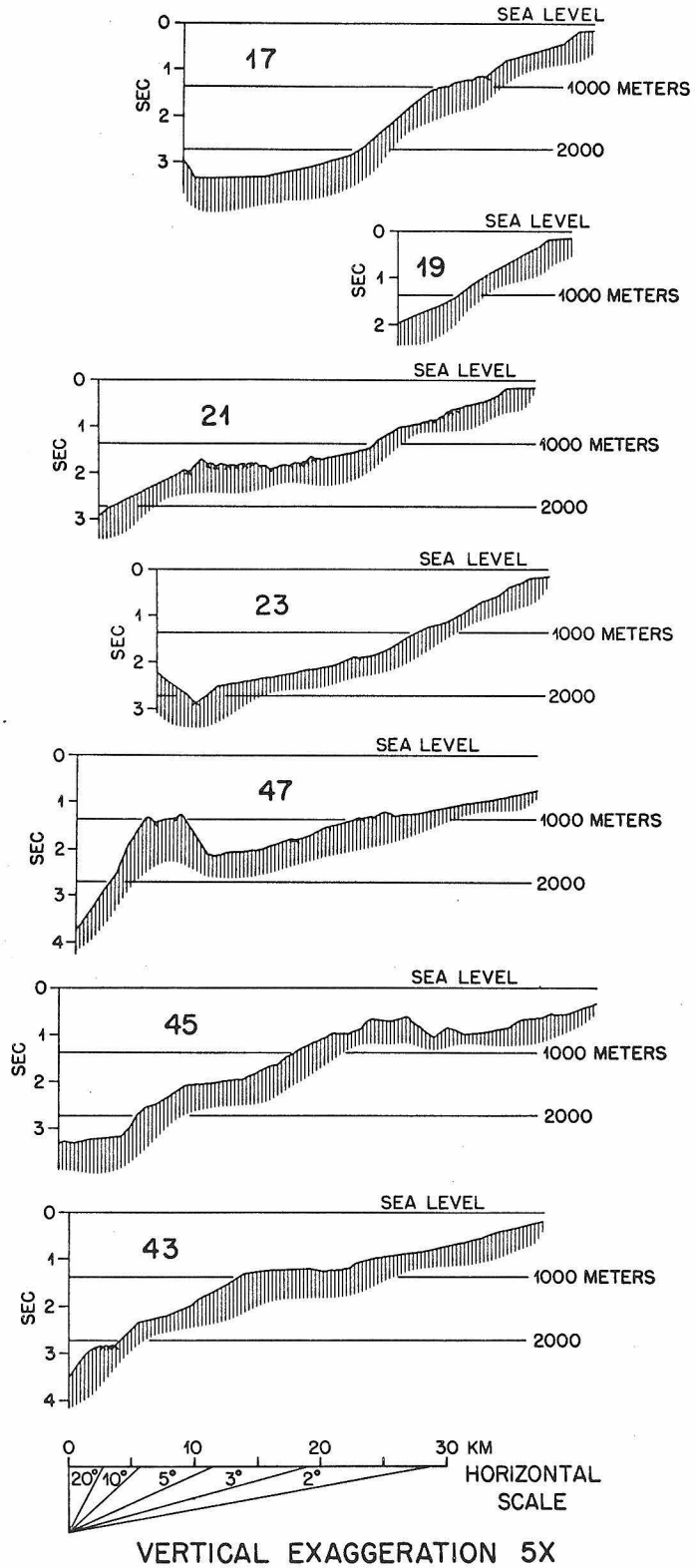

Fig. 27. Bathymetric profiles of the upper continental slope between Antofagasta and Taltal. Locations shown in Figure 13. Profiles aligned with respect to longitude.

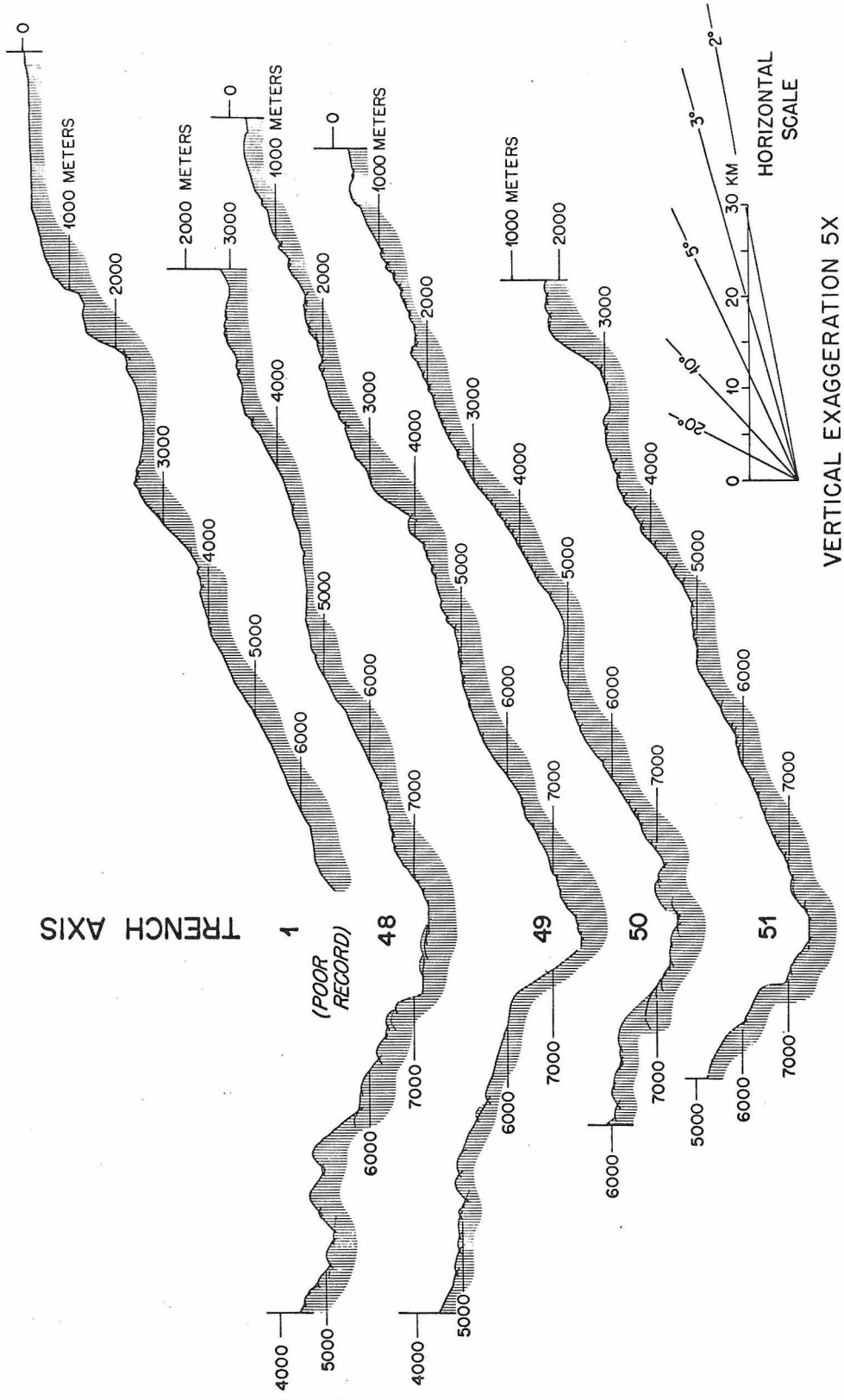

Fig. 28. Bathymetric profiles of the landward flank of the Peru-Chile trench. Locations shown in Figure 13.

DISCUSSION

Emphasis in this treatment of the offshore data is placed on the structural geology, leaving some important problems unexplored. Scholl et al. (in press) elaborate on aspects of sedimentation and age relationships in the development of the Peru-Chile trench, and the reader is referred to that paper for a more complete discussion. Their observations on shelf and slope deposits off the coast of northern Chile are particularly relevant, however, and merit brief mention. First, a two-layer shelf sequence is distinguished that comprises an upper, mostly undeformed layer -- only a few meters or tens of meters thick -- overlying a slightly- to moderately-deformed lower layer that blankets acoustic basement, and is presumed to be chiefly Tertiary in age. Second, slope deposits off the coast of northern Chile are noted to be restricted to the upper part of the slope and to be "...traceable to the Tertiary beds that make up the bulk of the shelf sequence" (Scholl et al., in press). Thus, the sedimentary deposits that have been distinguished in the line drawings (Figs. 16-26) are complex, and in some cases would appear to represent a considerable expanse of time; structural interpretations based on assumptions of their age must be made with care.

One of the main problems motivating the oceanographic work was the configuration of faulting beneath the Bahía Nuestra Señora.

The data show that some of the major fault traces have no marked topographic or sub-bottom expression that was resolvable by the methods of the survey, as they cross the shelf. Nevertheless, some key information was gathered regarding the geometry and sequence of faulting.

Both profiles 29 and 31 cross the Salar del Carmen fault as it projects southwest into the Bahía Nuestra Señora (see Fig. 30). Neither profile shows convincing evidence for the location of the fault trace. In profile 29, a small discontinuity in the gradient of the sea floor is the only suggestive feature, but it occurs at the feather edge of the shelf deposits and is located to the west of the fault projection. Profile 31 shows a zone where sediment reflectors are interrupted and where weak oblique reflectors may indicate either fault disturbance or complicated three-dimensional geometry in the sediment structure. These points are plotted as question marks in Figure 30. Slumping on the upper slope appears to align with a southwestward projection of the Salar del Carmen fault in profiles 33 and 35, but other profiles to the north show similar suggestive evidence of slumping, implying that slumping may be common just below the shelf break at most points along its sinuous trace. Thus, the location of the sub-sea trace of the Salar del Carmen fault could not be documented because of the absence of the fault's expression.

Profiles 37 and 39 cross the projection of the north-trending, offset segment of the Atacama fault zone near Quebrada del Hueso (Fig. 30), but, again, no expression of the fault zone was detected on the shelf.

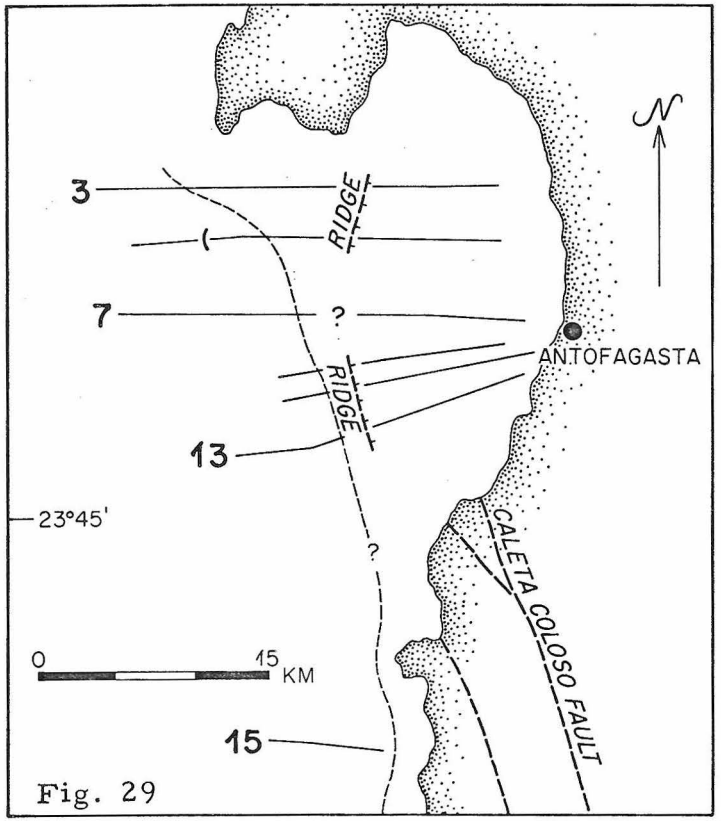

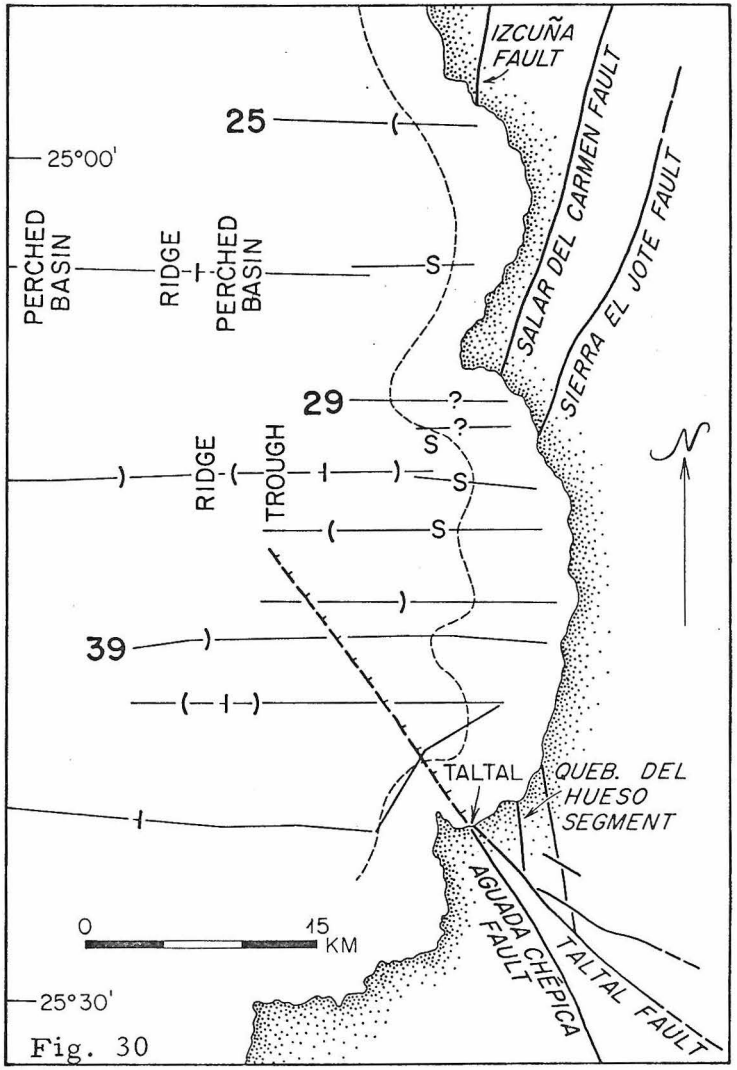

EXPLANATION FOR OFFSHORE STRUCTURE

NORMAL FAULT; HACHURES ON DOWNTHROWN SIDE

) PROBABLE OR POSSIBLE FAULT, CONCAVE TOWARD DOWNTHROWN SIDE

S PROBABLE SLUMPING

SHELF BREAK

Figs. 29 and 30. Offshore structural information near Antofagasta (Fig. 29) and Taltal (Fig. 30).

Neither is there any evidence for northwestward projection of this fault segment to the west of Punta Grande.

Strongest evidence for sub-sea faulting in the Bahía Nuestra Señora occurs along the trace of a fault trending N. 30°- 35° W. that aligns with the projection of the Aguada Chépica fault mapped onshore (Part VI; Pls. 4 and 5). No other onshore fault projecting into the bay has such clear expression. Both acoustic basement and sediments are faulted with the west side uplifted, consistent with the sense of offset observed onshore along the Aguada Chépica fault. The Taltal fault projects seaward trending N. 45°- 50° W., implying that it is cut offshore by the extended Aguada Chépica fault. The latter fault, thus, appears to have been more recently active than the Taltal fault, just as it does onshore (Part VI).

In the Bay of Antofagasta, the data were not sufficient to elucidate a sub-sea pattern of faulting that is simply correlative with the traces of known onshore faults. It was anticipated that the trace of the Caleta Coloso fault (Fig. 29) would be detected, but it was not. Also it was expected that a zone of faulting bounding the uplifted blocks of the Mejillones Peninsula on the east (see Fig. 1) would either be traceable to the Caleta Coloso fault or would linearly project offshore. The detectable fault pattern is not so simple.

The fault interpreted in profiles 3 and 5 (Fig. 29) may be the same as an important fault that bounds the east side of Morro Moreno at the southern end of the Mejillones Peninsula (Brüggen, 1950, p. 182-187). The correlation may not be exact, however, in view of the

irregularity of uplifted horsts that make up the peninsula (see Figs. 2, 3, 4; also Brüggen, 1950, p. 183). Nevertheless, the fault in profiles 3 and 5 is located within the extension of a zone of north-trending faults with east-facing scarps that control the eastern relief of the peninsula. Scholl and von Huene (personal communication) have data showing that this zone of faulting continues into the bay north of the peninsula (see Figs. 2 and 3).

A fault detected in profiles 9, 11, and 13 has a distinct northwest trend and cannot connect with the main branch of the Caleta Coloso fault (Fig. 29). It does appear to project landward rather than continuing parallel to the coastline, and may connect with a fault located west of the Caleta Coloso fault. There is not sufficient evidence to interpret a single continuous fault break curving beneath the Bay of Antofagasta. Continuity is confused by the poor record of profile 7. Curiously, though, if there were a single curving fault as suggested in Figure 29, its curvature would parallel a major bend in the main trace of the Atacama fault zone east of Antofagasta (see Figs. 1, 2, 3, 4). On the other hand, if one imagines a seismic reflection survey across the Mejillones Peninsula, assuming that it were submerged, irregularity of fault blocks would be the rule, and the orientation of the outer-shelf basement blocks (Fig. 29) might not be surprising.

The complexity of onshore faulting in the vicinity of the coastline of northern Chile has been noted and is well expressed in the Apollo 7 photos (Figs. 2, 3, 4). Offshore data prove that faulting is not restricted to a narrow localized zone along the Atacama fault system. The

expression of faulting on the upper continental slope, beginning within 10-20 km of the coastline, is fully as impressive as that of major fault branches onshore. The very narrow shelf, faulting of sediment aprons on the shelf and upper slope, perched basins, and irregular faulting resulting in the tilting and down-dropping of blocks toward the trench axis reflect the great tectonic instability of the offshore zone. The oceanographic profiles are judged to support interpretation of a tensional down-dropping of the Peru-Chile trench that has been suggested by various workers (Worzel, 1966; Hayes, 1966; Scholl, 1968; Isacks et al., 1968; von Huene et al., 1968; Scholl and von Huene: 1969, 1970; Malahoff, 1970; Scholl et al., in press). The observation of extensional faulting on the upper slope is not original. Fisher and Raitt (1962, p. 426), for example, noted that on the landward flank of the trench south of 26° "...steep upper slopes may be related to recent faulting and uplift in the area". The profiles of this study contributed to the documentation of faulting on the upper slope and provide a view of major blocks and faults that are associated with the down-dropping of the trench.

It is significant that this "collapse" begins along faults very close to the present coastline, and it is difficult to imagine that roughly parallel onshore faults -- including the Atacama fault -- are dissociated from this vertical tectonics.

The aftershock zone of the 1966 Taltal earthquake (see Part VII) shows no correlation with any single offshore fault, but does correlate with a zone of irregular, major vertical faulting on the upper continental slope between depths of 500 m and about 2000 m.

VI. STRUCTURE

INTRODUCTION

The Coast Ranges are characterized by intense faulting, particularly so in the area of this study. Faulting exerts a profound topographic control. Onshore faulting is dominated by north-northwest to north-northeast-trending branches of the Atacama fault zone which display a complicated map geometry in the Taltal area. It was earlier noted that major regional folding has only affected rocks of pre-Triassic age; Mesozoic stratified rocks in the Coast Ranges are either tilted or gently folded. Concern in this report is primarily focused on fault-related problems.

Before beginning a systematic review of the major faults, introductory remarks on nomenclature are warranted. The term, Atacama fault, was applied by St. Amand and Allen (1960) to an extensive fault zone, some segments of which had been recognized earlier and termed differently. The segment south of Taltal (Fig. 1) extends some 200 km to the Copiapó region and has been called the El Salado, Manto Atacama, or Manto Verde fault (Ruiz, 1943; Segerstrom et al., 1960; Bowes et al., 1961; Segerstrom and Ruiz, 1962). This segment was referred to by St. Amand and Allen as the El Salado sector of the Atacama fault and was shown to be truncated and left-laterally offset by the northwest-trending Taltal fault at its northern end (Arabasz, 1968). North of Bahía Nuestra Señora (Fig. 1), another segment, which reportedly can be traced northward approximately 450 km until it branches out to sea south of Iquique (St. Amand

and Allen, 1960), was earlier termed the Salar del Carmen fault by Knowles et al.(1959), and has been known locally as the La Negra fault. Brüggen (1950, p. 97, 311) briefly discussed this fault as it appears east of Antofagasta and referred to it simply as a "falla reciente", i.e., a recent fault. The segment between Bahía Nuestra Señora and Ojeda is designated the Salar del Carmen sector of the Atacama fault by St. Amand and Allen, who then termed the segment between Ojeda and Iquique the Salar Grande sector (see Fig. 1).

In this report, St. Amand and Allen (1960) are followed in referring to the entire fault zone paralleling the coast as the Atacama fault. For discussion it will be convenient to refer to the Salar del Carmen fault as synonymous with the main branch of the Atacama fault north of Bahía Nuestra Señora. South of the Taltal fault, the Atacama fault zone will also be referred to as the El Salado sector; its displaced equivalent on the north side of the Taltal fault in the Quebrada del Hueso area (Pl. 4) is called the Quebrada del Hueso segment of the Atacama fault zone. Names are applied to other important fault branches, as discussed below, for the sake of reference herein.

EL SALADO SECTOR OF THE ATACAMA FAULT ZONE

Previous Work

Segments of what is termed the El Salado sector of the Atacama fault zone have been recognized for some time south of the map area because of fault control of important mineralization along its trace north of Copiapó (Ruiz, 1943). After 1955, serial aerial photos of

northern Chile became available and were invaluable in the recognition of the extent of faulting. The fault map of St. Amand and Allen (Fig. 1) is believed to be the first to show the northward continuity of the El Salado sector and its truncation by an oblique fault near Taltal. In 1960 a reconnaissance map of the Chañaral-Taltal area (1 : 250, 000) was compiled by Bowes et al. (1961) incorporating extensive photogeology. North of 26°45'S., the map traces the "Atacama fault zone" -- restricted by Bowes et al. to indicate the El Salado sector of this report -- as "...not a single break but...a series of strands which converge, emerge, and diverge from and within a continuously defined zone" (Bowes et al., 1961). Field work by the latter workers was limited to a two-week period and was focused on reconnaissance for uranium. Geologic mapping in the present report constitutes the first systematic study of the major faults included in the map area.

Features of the Fault Trace

General statement. -- South of the Taltal fault (Pls. 4 and 5), the Atacama fault zone occupies a broad, low-relief trough several kilometers wide that includes numerous interlacing branches with various fault forms, and that might be termed a fault rift (Sharp, 1954). Allen (1965, Fig. 6) includes a photo of somewhat similar rift topography along the same fault zone near El Salado.

South of Quebrada de la Cachina, two major fault traces 4-6 km apart are obvious. Northward the entire fault zone describes a gentle arc to the northwest with a western branch -- the Aguada Chépica fault (to be discussed separately) -- completing a stronger

northwestward arc and escaping truncation by the Taltal fault. Multiplication of fault traces north of Quebrada de la Cachina is marked, so that numerous elongate fault-slice ridges and a multiplicity of alluvial fault scarps characterize the fault trough (see Fig. 31). The entire north-northwest-trending fault zone crosses large south- to southwest-trending drainages which, in some cases such as Quebrada de la Cachina, are continuous across the fault zone; in other cases, apparent uplift along the west side of the fault zone has caused a ponding of alluvium within the fault trough. The easternmost branch of the El Salado sector will first be discussed, then the central branches.

The easternmost branch. -- The easternmost branch of the El Salado sector extends southward beyond the map area of Plate 5; northward it is truncated by the Taltal fault (Pl. 4). Along the 55 km segment mapped in Plates 4 and 5, the expression of the fault is varied but, generally, it appears as a narrow band of closely spaced crushed zones -- commonly two parallel bands 100-300 m apart -- that transects silicified and altered crystalline rocks in several interfluve areas, each several kilometers long. The interfluves are separated by large east-west quebradas, where older alluvium is broken along the fault trace. Significantly, along most of its course, this fault bounds the Jurassic-Cretaceous sequence of andesitic volcanic rocks, juxtaposing them against Paleozoic metamorphic and Mesozoic batholithic rocks. From Quebrada de Cifuncho northward, the east side of the fault is higher standing, forming a dissected west-facing fault-line (?) scarp a few hundred meters high that bounds the trough of the Atacama fault

Fig. 31. (following page) Vertical aerial photograph of the Atacama fault zone (El Salado sector) in the vicinity of Taltal airport. A multiplicity of fault branches can be distinguished within a broad zone approximately 6 km wide. Abundant alluvial fault scarps throughout the zone attest to continuing activity, despite truncation of the zone by the Taltal fault to the north. Compare with geologic maps (Pls. 4 and 5).

A. Alluvial fault scarp. Location of profile J (Fig. 9)

B. Alluvial fault scarp along trace of Aguada Chépica fault. Location of profile H (Fig. 9)

C. Fault slice of Neocomian (?) limestones

D. Alluvial fault scarp along trace of Aguada Chépica fault at Aguada La Isla

E. Intensely faulted alluvium

F. Location of profile D (Fig. 9) and Figure 11

G. Faulted fanglomeratic gravels along easternmost branch of Atacama fault zone

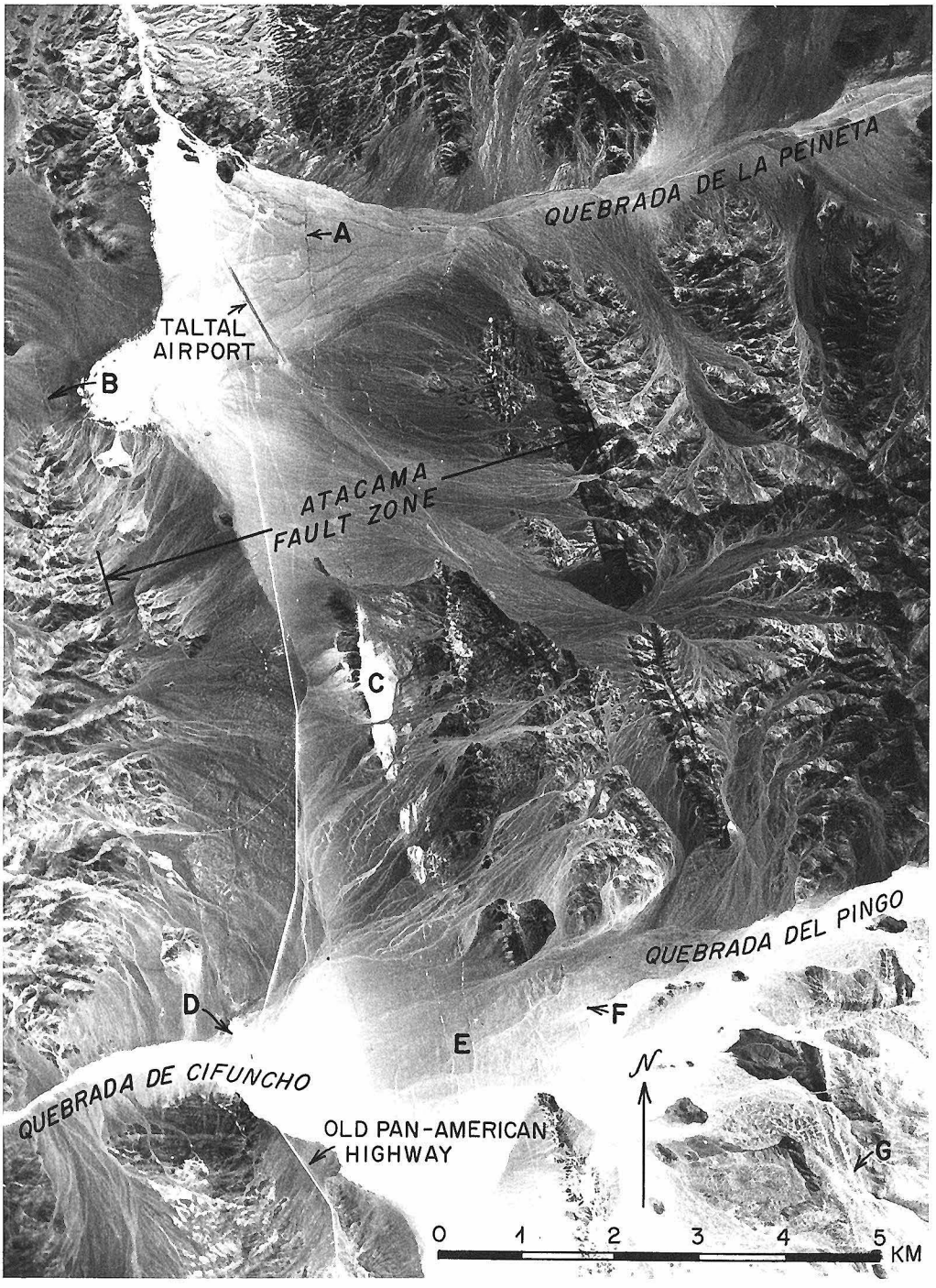
QUEBRADA DE LA PEINETA
A
TALTAL
AIRPORT
B
ATACAMA
FAULT ZONE
C
QUEBRADA DEL PINGO
D
F
E
QUEBRADA DE CIFUNCHO
OLD PAN-AMERICAN
HIGHWAY
N
G
0 1 2 3 4 5 KM

Figure 31

zone. South of Quebrada de Cifuncho, however, high-standing interfluve ridges that parallel the fault on the west reverse the sense of relief.

The larger-scale fault forms along this branch of the El Salado sector may be secondary in origin because no lateral offset of the crossing quebradas is apparent, and no consistent sense of recurrent uplift can explain the topography -- unless pivotal faulting is invoked. Alluvial scarps crossing many of the quebradas are clearly primary, however. In Quebrada de la Cachina, both north and south of the road to Altamira, a linear fault trench is developed in alluvium along the trace of the fault. Crossing the interfluve to the north, the fault trace is marked by aligned ravines, gullies, fault-line saddles and also fault slices that form elongate resistant ridges (because of silicified rocks within the fault slice) that are drainage divides. Erosional irregularities cause an apparent scissoring of relief. South of Cerro 1135 near Quebrada de Cifuncho, a linear east-facing scarplet less than 1 m high breaks the alluvium of a small wash over a distance of about 1 km. Where the fault crosses Quebrada de Cifuncho, an east-facing scarplet in alluvium is also seen.

In the interfluve between Quebrada del Pingo and Quebrada de Cifuncho, two parallel faults about 100 m apart form fault benches as they cross the western slope of Cerro del Pingo. Parts of their traces are covered by colluvial debris which itself is disturbed. A large debris lobe approximately 2 km long that had moved down a steep western slope of the Sierra del Pingo across the fault trace, and which has subsequently been dissected, is cut by both traces. At this locality

the double fault band appears on aerial photos as two light-colored, perfectly parallel lines cutting across fanglomeratic boulder gravels (Fig. 31, point G). On the ground these lines are trench forms along which varnished and lichen-covered bouldery alluvium has been disturbed and, in the western band, eroded along the fault line.

The erosional resistance of silicified rocks along the fault zone is typified in the interfluve north of Quebrada del Pingo. The western branch of a double band of faults lies at the base of an east-facing scarp. At Quebrada de la Peineta there is an anomaly in projection of segments of the fault across the quebrada. A concealed northwest-trending fault is interpreted to displace the fault left-laterally at least 500 m. East of Cerro Breadal (Pl. 4) systematic left-lateral step offsets displace the fault branch 65 m and about 300 m before it is displaced a much larger distance by the Taltal fault (see below).

South of Quebrada de la Cachina (Pl. 5), exposure of the easternmost branch of the Atacama fault zone is mainly limited to a few fault-line saddles where coherent silicified rocks with a cataclastic fabric, rather than incoherent gouge, define the fault separation of different lithologies. Northwest of the Sierra del Carmen, fault trenches break alluvium along the fault trace, but farther south the fault is concealed as it projects beyond the map area. Fault branching in the Sierra del Carmen contrasts with the narrowness of the fault trace to the north.

The easternmost branch of the El Salado sector trends N. 10°-15°W. throughout most of its mapped extent. Its linearity over irregular

topography for a large distance and the measured attitudes of numerous exposed crushed zones indicate that the fault is very steeply dipping and near vertical. Dips between 80° and 90°, both east and west, were consistently measured.

Central branches.-- The most remarkably regular segment of the El Salado sector is the single fault trace south of Pampa Cachina (Pl. 5) that traces a very gentle arc N.5°-10°W. over the 27 km distance to the southern map limit. Its trace is marked by a subdued east-facing fault scarp a few meters high that might best be described along most of its course as an out-facing piedmont scarp. Alluvial-veneered pedimented rocks are uplifted on the west. Because of the maturity of relief, tapering spurs had receded from the fault line so that no faceting resulted. Only the very youngest alluvium is undisturbed along the fault trace. Crossing Quebrada de la Cachina, the fault cuts across a broad alluvial fan-like body along a 2 km distance, uplifting the western side and causing enhanced dissection of that side. The youngest drainage line crossing the fault there is a narrow incised channel floored with silt beds. Neither the channel nor silt beds is disturbed by faulting.

Jurassic-Cretaceous andesitic rocks are inferred to be juxtaposed along this entire segment of the fault. The only exposure of the fault zone was seen in the Anita mine approximately 4.6 km south of the axis of the large east-west drainage between latitudes 25°50' and 25°55'S. Andesite is faulted against andesite. At a depth of approximately 20 m, the fault zone comprises highly sheared, mineralized andesite in a

zone at least 3 m wide that strikes N.06°W. and dips approximately 84° east. The linearity of the fault trace also implies a near vertical dip.

In the Pampa Cachina area at least four faults converge to the single fault described above. With the exception of the Aguada Chépica branch, the converging faults are part of a zone about 4 km wide that is truncated by the Taltal fault to the north. The prominent linear fault that consistently breaks alluvium along its trace south of Quebrada de la Cachina does not have a straight-line projection that is a similar prominent alluvium-breaking trace. Instead, a parallel band about 1 km to the west has more continuous and prominent alluvial scarps.

Elongate subdued ridges within fault slices parallel the north-northwest grain of the fault trough. Most rock exposures are deeply weathered, but there is abundant evidence of brecciation and shearing throughout the zone. In addition, fault-controlled copper mineralization is common and is being actively exploited at the Unión mine a few kilometers south of Taltal airport and at the Anita mine mentioned above. Hydrothermal alteration, particularly silicification, is more pronounced in the eastern half of the fault zone.

Isolated fault slices of Neocomian (?) marine limestones occur in a very narrow band between Taltal airport and Pampa Cachina (Fig. 31, point C). St. Amand and Allen (personal communication) inferred that the distinctiveness of these fault slices, compared to adjacent rocks, was suggestive of significant fault displacement. On the other hand, mapping in that area (Pl. 5) shows that volcanic-clastic rocks

assignable to the Bandurrias formation, whose base is Neocomian, crop out within a wedge bounded by the Aguada Chépica fault and a fault to the east of the limestone blocks. Since the Bandurrias formation is known to include intercalations of similar marine limestones, the above-mentioned fault slices need not necessarily be exotic.

In those areas where alluvium has been broadly distributed over the fault trough by transverse drainage, such as Quebrada de Cifuncho, Quebrada del Pingo, and Quebrada de la Peineta, the alluvium is literally butchered by faulting (Fig. 31, point E). Virtually all the alluvial scarps have an anomalous ridge-trench-ridge morphology that has been discussed; the most continuous occur along projections of the major mapped basement faults that trend N.10°-15°W., although other sets N.40°-50°W. and N.10°-15°E. complicate the structural pattern.

East of Taltal airport, a prominent east-facing alluvial scarplet along the trace of the fault bounding the Neocomian (?) limestones (Fig. 31, point A) indicates uplift of the alluvial surface 1.0-1.3 m on the west, although the scarp displays a modified ridge-trench-ridge form (Fig. 9, profile J). This same fault appears to connect with a co-linear basement fault north of Quebrada de la Peineta; however, the co-linearity may be coincidental because the failure of the easternmost branch of the El Salado sector to project linearly across Quebrada de la Peineta suggests left-lateral offset of the entire fault zone by a partially concealed fault.

As a whole, the north-northwest-trending zone of faults between the Aguada Chépica fault and the easternmost branch of the El Salado sector maintain the linearity and the very gentle northwestward arc of the single fault trace south of Pampa Cachina. Both the linearity of the zone over a distance of nearly 60 km, and the linearity of individual fault segments imply steeply-dipping faults. Attitudes of exposed fault surfaces include dips generally exceeding 80°, both to the east and west; occasionally, dips as shallow as 70° were measured, as along the boundary faults of the limestone slices.

Age and Displacement

Relation of faults to Mesozoic mineralization.-- Two lines of reasoning suggest that branches of the Atacama fault zone in the El Salado sector have had a long history dating back to the Mesozoic: (1) understanding of the relationship between mineralization and faulting in the western part of the Andean geosyncline, and (2) interpretation of the development and paleogeography of the Andean geosyncline. A host of important copper and iron mines are located within the El Salado sector between Taltal and Copiapó, exploiting mineralization that, to a large extent, has been controlled and localized by faulting and which is genetically related to batholithic intrusions of Late Jurassic to Late Cretaceous age (Ruiz and Ericksen, 1962; Ruiz, 1965).

Syngenetic copper mineralization unrelated to faulting accompanied the deposition of andesitic lava flows as early as Jurassic time and accounts for some of the mineralization in the Taltal area (Ruiz,

1965, p. 146, Table 1). Nevertheless, in the El Salado sector, numerous copper deposits of hydrothermal origin occur predominantly as fissure-filling veins or tabular to irregular replacement bodies, either within zones of the major north-northwest to north-northeast striking faults or along divergent fractures that are genetically related to the latter (Ruiz, 1965, p. 210-218). In one of the major copper mines in this sector, the Manto Verde del Salado mine, the ore body is a tabular body of tectonic breccia some tens of meters thick that occurs within the zone of the Manto Verde (Atacama) fault and is impregnated with copper oxides (Ruiz, 1965, p. 218). Ortiz (1968) documents the definite relationship of hydrothermal alteration and mineralization to the Manto Verde (Atacama) fault in the Los Pozos mining area south of El Salado. Mineralization of rocks of the Bandurrias formation (early to mid-Cretaceous) in the El Salado sector, such as south of Taltal airport, implies Late Cretaceous rather than Jurassic ore deposition, but pre-existing faults are also implied.

The relationship of Late Cretaceous iron mineralization to regional faulting is even stronger; both to the south and north of Copiapó important iron mines and magnetic anomalies define a lineament along which pre-mineralization fracturing controlled the development of ore formation (Ruiz, 1965, p. 223-243). Between Copiapó and Taltal the lineament coincides with the Atacama fault zone. There is compelling evidence, then, for assigning a minimum age to the El Salado sector of the Atacama fault zone that would correspond to an origin in mid- to late Cretaceous time. In addition, there is

suggestive evidence of regional faulting as early as Jurassic, in a zone through which the Atacama fault passes.

Relation of faults to the Andean geosyncline.--According to Ruiz (1965, p. 67-74, 144-149), the western margin of the Andean geosyncline was characterized by tectonic instability through most of the history of the geosyncline and was affected by orogenic movements and batholithic intrusion before the end of the Jurassic Period. Differential subsidence of individual blocks and transgressive-regressive relations lead Ruiz to interpret regional faulting within the eugeosynclinal trough; in particular, block faulting at the end of Oxfordian time is postulated for a zone including the area of this study. It is difficult to offer clear proof that either the Atacama fault or its El Salado sector did indeed originate in the Jurassic Period. It seems reasonable, however, to suspect that the major faults that had caused extensive regional fracturing prior to Late Cretaceous time may have been the same that accommodated movement during the earlier history of the geosyncline.

Slickenside information.-- Slickensides and mullions observed in mine workings and crushed zones along faults of the El Salado sector provide clear evidence for horizontal motion during some period of the fault's history. Horizontal slickensides are reported by Segerstrom (1960b, p. 25) and Segerstrom and Ruiz (1962, p. 54) in mines at the southern end of the El Salado sector and were recorded by St. Amand and Allen (1960; also C. R. Allen, personal communication) in various mines throughout the sector. In this study, abundant

near-horizontal slickensides were also observed along various branches of the El Salado sector. Along the easternmost branch, near-horizontal slickensides predominate in the exposed crushed zones. A plunge of 23° is an average of measurements at 15 localities. In and near an abandoned mine 0.8 km north of sample locality CE-346, between the double band of faults, ten measurements averaged 17° plunge. Along the easternmost branch several examples of superposed slickensides were noted. A set plunging 60°-70° appeared to be younger than a low-angle set. Near-horizontal slickensides on east-west fractures were common, as well as along fractures approximately N. 50° W., i.e., parallel to the Taltal fault trend.

Access to other abandoned mine workings within the fault zone was restricted because of their vertical adits. At two mines in operation, the Anita mine and the Unión mine referred to earlier, additional information was gathered. Illustrative slickensides were observed in open trenches and head-workings at the northern end of the limestone fault slice near the Unión mine. Several clear examples of superposed slickensides were seen in which an older set (11 measurements) has an average plunge of 12°, and a younger set (10 measurements), 68°. In the Anita mine only a single good example was found showing striations plunging 18° and 83°.

In another open trench approximately 16 km south-southeast of the Unión mine, along the fault bounding the Neocomian (?) limestone fault slices on the east, reddish brown pebbly to sandy alluvium is seen in fault contact to the west with greenish phacoidal fault breccia

at least 2 m thick. On the smooth fault surface separating the units, four examples of well developed slickensides plunging 79°-81° were observed.

At still other localities within the El Salado sector where slickensides were noted on bedrock fracture surfaces, slickensides were observed to plunge either less than 25° or more than 60°. An additional locality at which slickensides are well displayed is an open pit at the Bandurrias mine, 1.2 km northeast of sample locality CE-343. On an excellently exposed fault surface striking N. 10° W., 83° SW., 11 measured slickensides had an average plunge of 12°.

The observed slickensides are interpreted to support two conclusions: (1) An episode of strike-slip motion occurred along branches of the El Salado sector. (2) At least one episode of dip-slip motion occurred along faults and fractures that had earlier accommodated near-horizontal motion.

Changes in tectonic stresses. -- Even without the information on slickensides, it is obvious that changing tectonic stresses have to be considered because of the great age of the faults and because of the simple fact that they were disrupted by the Taltal fault system. Throughgoing strike-slip displacements are obviously constrained, but the faults are by no means inactive, as attested by the abundant Quaternary and Recent scarps along their traces -- both along the easternmost branch and the central branches. Moreover, most -- if not all -- of these alluvial scarps postdate movement on the Taltal fault (see below). No evidence was seen for either crosscutting of

the Taltal fault north of Taltal airport or for thrusting along the trace of the Taltal fault. The oceanographic data show that the Taltal fault is crossed by the more recently active Aguada Chépica fault offshore (Fig. 30). Onshore studies of the latter fault (see below), however, show that it does not appear to be an active strike-slip fault.

Sense of displacement. -- No mapped contacts define obvious lateral offsets along branches of the El Salado sector. Along the easternmost branch, the juxtaposition of Jurassic-Cretaceous volcanic rocks against Paleozoic basement rocks and Mesozoic batholithic rocks (Pl. 5) requires either a large lateral offset beyond the area of Plate 5 or a substantial vertical displacement. An incomplete knowledge of the age, stratigraphy, and structure of andesites across the El Salado sector make interpretations of their displacement tenuous.

With regard to plutonic rocks, some observations can be made. Similar appearing granodiorites of the JK suite occur on both sides of the eastern branches of the El Salado sector in the Sierra del Carmen area (southeast corner of Pl. 5), and introduce the possibility of constraints on allowable lateral displacement. These rocks are discussed in the section on problems of large lateral offset.

Another observation concerns the map relations of small granitic plugs that are intrusive into andesites west of the Atacama fault zone, south of Pampa Cachina (Pl. 5). These small bodies include lithologies of the JK suite (confirmed by thin-section study of CE-314A and CE-312B). There is no evidence for interpreting them as apophyses of large granitic bodies of the JK suite cropping out east

of the Atacama fault zone, although the variability of rocks of the JK suite does not prohibit doing so.

A small plug within the Atacama fault zone south of Quebrada de Cifuncho (CE-340) consists of a fine-grained, aplitic, altered leucoadamellite with a few per cent of an epidotized ferromagnesian mineral. This outcrop is tentatively assigned to the JK suite. The rock bears no similarity to the biotite-hornblende granodiorite of the large stock cropping out on the opposite side of the fault to the east, so that it cannot be used as an argument for a relation across the fault.

No clear evidence was found anywhere along branches of the El Salado sector to support continuing strike-slip motion in recent geological history. Faults of the sector strike normal to the trend of drainage lines providing the opportunity for physiographic lateral offset. Although the origin of ridge-trench-ridge alluvial fault scarps remains enigmatic (Part IV), it would seem that recent faulting of alluvium in the El Salado sector is more likely related to vertical motion. The occurrence of alluvial scarps along traces of faults that controlled late Mesozoic mineralization bears testimony to a long and probably complicated history of movement. At least two conclusions are firm: the inference of reactivation of the faults, with activity continuing into Quaternary time, and the interpretation of strike-slip motion of unspecified magnitude at some time during the history of the faults. The problem of large lateral displacement is discussed in a later section.

TALTAL FAULT

Nomenclature and Previous Work

St. Amand and Allen (1960) apparently were the first to note the offset of the Atacama fault zone north of Taltal airport by "...a northwest-trending sinistral fault". Bowes et al. (1961) indicate the fault on their map and refer to it as a southeast-trending fault that has deformed the Atacama fault: "The deformity of the Atacama fault coincides with its near intersection with the Salar del Carmen fault, resulting in a drag-induced shear trending southeast". Preliminary mapping was completed by this writer along that fault in 1966 (Arabasz, 1968) prior to the Taltal earthquake ($M \cong 7.5$) of December 28, 1966. Field reports have been published on effects of the earthquake (Alvarez et al., 1967; Lemke et al., 1968). In the Chilean publication (Alvarez et al., 1967), the northwest-trending fault was first called the Taltal fault, a nomenclature which is followed here.

Features of the Fault Trace

The Taltal fault (Pl. 4) can be traced for more than 35 km from the northeast end of the Sierra del Pingo to the town of Taltal, through which it passes into the Bahía Nuestra Señora. Less extensive faults roughly parallel the main break, which splays at its southeast end.

On aerial photographs the most impressive segment of the fault is north of Taltal airport where a sharp line trending N. 50° W. defines the fault trace that abruptly truncates branches of the El Salado sector of the Atacama fault. The fault is clearly etched by erosion resulting

in the alignment of narrow linear segments of fault-line drainage that expose crushed zones 2-5 m wide (Fig. 32). Between upper Quebrada de Taltal and Quebrada de Cortaderas the fault zone follows the base of a dissected southwest-facing fault scarp, probably created by slicing apart of pre-existing relief by the Taltal fault. Undisturbed colluvial debris descending from the high-standing block on the northeast blankets the fault trace, but numerous exposures are seen where gullies cross the zone or where the colluvial material has been otherwise stripped by erosion. Deeply weathered crushed zones up to 7 m wide are visible. Along this same interval, the juxtaposition of dark-colored andesites and light-colored Paleozoic metasedimentary rocks enhances definition of the fault.

Quebrada de Cortaderas is deflected at the fault trace. Northwestward the fault slowly changes strike to N. 40° W. as it crosses aligned fault-line saddles and irregular topography before passing into lower Quebrada de Taltal -- a linear fault-line valley a few hundred meters wide and 7 km long. Dissected gravels, deposited at the mouth of Quebrada de Típias, cross the fault trace. The fault is concealed beneath alluvium in lower Quebrada de Taltal and is inferred to pass beneath the town of Taltal, which is built on alluvial sands and gravels, south of the hill dedicated to the Madonna.

Inland along the Taltal fault a still different expression is displayed. Intermittent crushed zones are exposed in a broad fault-line saddle north of Cerro Breadal, but to the southeast as it crosses Quebrada de la Peineta, the fault is apparently concealed beneath

Fig. 32. Taltal fault. Fault-line drainage along the Taltal fault north of Taltal airport exposing a crush zone that separates Jurassic-Cretaceous andesites (left) from Paleozoic metasedimentary rocks (right). View is to the northwest with Quebrada de Taltal passing from right to left in the middle distance. Man at left for scale.

alluvium. Consequent drainage lines that align with the fault trace appear on aerial photos to indicate faulting of alluvium near Quebrada de la Peineta. Field observations do not support this conclusion inasmuch as the alluvial channels cannot be shown to be fault-controlled; their alignment with the fault trace, in this writer's opinion, is merely coincidental.

Southeast of Quebrada de la Peineta the Taltal fault develops a more gently sinuous trace as diverging branches strike more to the west. Subdued bedrock fault scarps mantled with a veneer of alluvium and aeolian sand define the main trace of the fault, but it is not clear that young alluvium is actually broken along the fault.

Between Quebrada de la Peineta and lower Quebrada de Taltal, the attitude of the Taltal fault is either near vertical or very steeply dipping to the northeast (greater than 75°, generally 80°-90°). The marked linearity of segments over several kilometers such as north of Taltal airport preclude a shallower dip. At its southeast end, however, where no good exposures of fault planes were found, the curving traces may indicate departure from being near vertical.

A few kilometers to the north of the Taltal fault another similar, though less linear, fault can be traced for nearly 17 km. It crosses more irregular topography than the Taltal fault, but is characterized by aligned fault-line saddles where it crosses ridge crests. This fault also dips steeply to the northeast (greater than 75°).

Age and Displacement

Displacement. -- Of all the faults studied, the Taltal fault displays the most convincing evidence for significant lateral offset. Fault and intrusive contacts of rocks, the youngest of which are either Late Cretaceous or early Tertiary, are obliquely cut and consistently offset left-laterally a distance of the order of 10 km (see Pl. 4). Fault surface reconstructions imply that the motion was predominantly strike-slip. The fact that the easternmost strand of the Atacama fault zone is near vertical, as supported by field measurement, virtually precludes large dip-slip motion when the other offset contacts are taken into account. The sense of interpreted slip is further supported by the observance of near-horizontal slickensides along the Taltal fault and parallel branches (an average plunge of 13° for measurements at ten localities), and the step-like offset of the easternmost branch of the Atacama fault zone in a consistent left-lateral fashion.

Bracketing the time of movement. -- Timing the origin of the Taltal fault is not a simple matter, despite the fact that it clearly cuts and offsets branches of the El Salado sector that have alluvial scarps along their traces. It is certain that most of those alluvial scarps postdate lateral movement on the Taltal fault, for reasons discussed below.

At no point along the Taltal fault was evidence found to support continuing lateral motion during the Recent epoch. On the contrary, key field observations suggest that lateral motion on the Taltal fault ceased before Quaternary time. The canyon of Quebrada de Taltal,

infilled with aggradation gravels, crosses the Taltal fault northeast of Estación Breas (Pl. 4) with no indication of offset or deflection. A stream channel that has incised the gravels to a depth of 30 m near the fault also crosses the fault trace undeflected and then turns northwest, just to the north of Aguada Chépica. Mapping and detailed study of the dissected aggradation gravels (Fig. 33) provide important information on the Taltal and Aguada Chépica faults.

The gravel units.-- The gravel units distinguished in Figure 33 are briefly characterized in the figure caption. Unit 1 comprises well stratified, distinctly light-colored (light grayish brown to tan) pebble and cobble gravels with boulders of heterogeneous granitic rocks. The gravels were carefully studied northeast of the Taltal fault, between the Taltal and Aguada Chépica faults, and at a locality 6-7 km west of the Aguada Chépica in Quebrada los Zanjones. Their continuity across the fault zones is confidently asserted. A maximum thickness of 58 m was measured south of Estación Breas. Along the northern feather edge of the unit, fragments of Paleozoic quartzite and andesite are locally abundant and granitic clasts may be absent, but the latter characterize most of the body of the gravels.

Unit 2 consists of brown to dark brown pebble gravels and pebbly sands, with cobbles of andesite and quartzite, to the exclusion of granitic clasts. This unit does not attain the thickness of Unit 1 which infilled the deepest part of the sedimentary trough. Units 1 and 2 were contemporaneously deposited as evidenced by their interfingering, although Unit 1 stands higher because of greater resistance

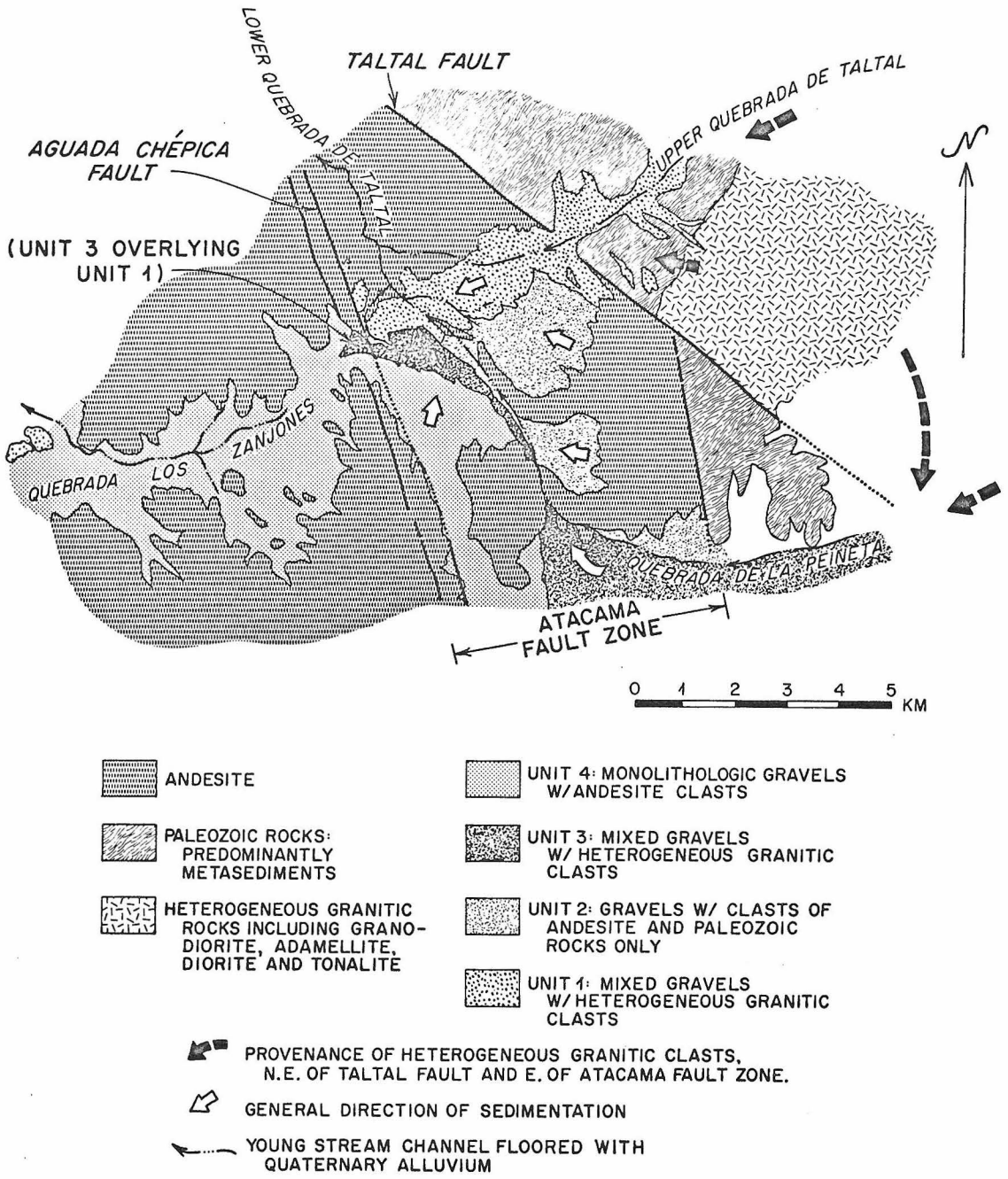

Fig. 33. Generalized map of the Aguada Chépica-Estación Breas area (Pls. 4 and 5) showing gravel units that provide key information on the Taltal and Aguada Chépica faults. (See text for discussion.)

to erosion.

Unit 3 is stratigraphically younger than Units 1 and 2. It is similar to Unit 1 in that it includes pebble and cobble gravels with clasts of granitic rocks derived from east of the Atacama fault zone. The brownish color of the unit, due to sandy material derived from andesites, generally serves to distinguish the unit from Unit 1. Thickness of the unit averages 10-15 m.

Unit 4 is the youngest stratigraphically, consisting of a blanket of small cobbles and pebbles of andesitic detritus derived from flanking hills of andesite.

Sequence of events. -- The sequence of events inferred from the gravels in Figure 33 is the following: (1) At some time following the termination of strike-slip motion along the Taltal fault, a major southwest-trending quebrada was cut across both the Taltal and Aguada Chépica fault zones, and included both Quebrada los Zanjones and upper Quebrada de Taltal. (2) A channel of gravels was deposited in the quebrada reaching a thickness of about 50-60 m with debris derived from rocks northeast of the Taltal fault (Unit 1); contemporaneous gravels (Unit 2) can be distinguished with a different provenance. (3) Gravels with a provenance east of the Atacama fault zone (Unit 3) were deposited by streams flowing from Quebrada de la Peineta. (4) Locally derived andesite debris (Unit 4) surficially blanketed the floor of Quebrada los Zanjones and concealed part of the trace of the Aguada Chépica fault. (5) Dissection of the gravels east of the Aguada Chépica fault resulted from headward erosion of lower Quebrada de

Taltal, which captured and diverted inland drainage northwestward to the sea.

Geologic implications. -- Although basement contacts demand a left-lateral offset of the order of 10 km across the Taltal fault, the relations outlined above imply that subsequent to the termination of that motion, there followed a period of canyon cutting, a period of aggradation during which a maximum of about 60 m of fluvial gravels were deposited, and another period of incision.

Earlier arguments (Part IV) lead to the conclusion that cutting of the canyon including upper Quebrada de Taltal and Quebrada los Zanjones probably commenced in Pliocene time. Referring to the chronologic stages presented in Part IV, this corresponds to stage 5. Infilling of the canyon and a basin-like area between the Taltal and Aguada Chépica faults is correlated with stage 6. Dissection of the aggradation gravels is correlated with stage 8.

The channel of gravels whose continuity is indicated by Unit 1 is undisturbed by the Taltal fault, yet at some time subsequent to its deposition, it was faulted along the Aguada Chépica fault (see below). Unit 3, stratigraphically younger than Unit 1, is correlative with the gravels cut by the prominent alluvial fault scarp northeast of Taltal airport (compare Figs. 33 and 31) -- implying faulting along a branch of the El Salado sector subsequent to its truncation by the Taltal fault.

Age of the fault. -- In summary, to bracket the age of the Taltal fault, we can assert that the fault originated subsequent to crystallization of the granodiorite stock that it offsets (Late Cretaceous to early

Tertiary). In addition, if one examines the relief along the trace of the Taltal fault, a case can be made that presently existing topography was sliced apart by lateral displacement on the fault. (1) Summit levels on the north side of the fault in lower Quebrada de Taltal are concordant with those 10 km to the southeast on the opposite side of the fault. (2) The high eastern border of the offset segment of the Atacama fault zone near Taltal, and the termination of the trough of the Atacama fault zone by low hills at the Taltal fault, suggest that the broad rift of the Atacama fault zone predated lateral motion on the Taltal fault. (3) The narrowness of upper Quebrada de Taltal and its broadening into a basin southwest of the Taltal fault (Fig. 33) adds support to the previous statement. It is proposed that strike-slip movement on the Taltal fault must have taken place during Tertiary time to allow the development of the displaced topographic forms. More detailed geomorphologic study will be necessary to correlate those forms with the chronology worked out by Sillitoe et al. (1968), so that the age can be refined.

If one accepts the arguments for cutting of upper Quebrada de Taltal and Quebrada los Zanjones beginning in Pliocene time, then lateral movement on the Taltal fault ended by that time.

Comment on ground fractures and the 1966 Taltal earthquake.--Lemke et al. (1968), having investigated geologic effects of the 1966 Taltal earthquake, reported the occurrence of small fractures breaking the ground surface along the traces of the Taltal fault and what is termed the Aguada Chépica fault in this paper; no evidence of horizontal or vertical displacements along the fault zones were observed by

them. In view of the conclusion that movement on the Taltal fault has ceased, the ground fractures would seem to suggest contradictory evidence of some continuing activity. The micro-earthquake recording (Part VII) shows no detection of clear activity along the Taltal fault, which might be expected -- even at such a later date -- if there were significant activation of the fault in connection with the earthquake. This writer has observed the fractures reported by Lemke et al. and tends to agree with the suggestion of C. R. Allen (in Lemke et al., 1968, p. 855) that "...the fracturing may have been caused by minor 'jostling' of the fault blocks in response to displacement of unknown character at depth". If the Coast Ranges are within a zone that is subject to gravity faulting because of subcrustal underthrusting (Malahoff, 1970), then virtually all the steeply-dipping major faults may be zones of potential weakness, regardless of trend, and may accommodate varying degrees of minor episodic motion.

QUEBRADA DEL HUESO SEGMENT OF THE ATACAMA FAULT ZONE

The zone of north-northwest-trending faults situated a few kilometers east of Taltal in the Quebrada del Hueso area is referred to in this paper as the Quebrada del Hueso segment of the Atacama fault zone -- solely for convenient reference. The zone is bounded on the south by the Taltal fault and represents the displaced continuation of the El Salado sector. St. Amand and Allen (1960) suggested the continuity and indicate it on their map (Fig. 1). Bowes et al. (1961, p. 13-14)

simply refer to "...subsidiary faults [that]are concentrated near the zone of intersection [of the Atacama and Salar del Carmen faults]". The interpretation of these authors clearly differs from that of St. Amand and Allen. Bowes et al. view the structural complications near Taltal as the result of the intersection of two distinct fault zones having opposing senses of lateral displacement, and argue that the deformity and northwestward curving of their "Atacama fault" (El Salado sector) are caused by drag effects of right-lateral movement along the Salar del Carmen fault. Their interpretation is untenable because of the documentation in an earlier report (Arabasz, 1968), and here, of lateral offset of the Atacama fault zone by the Taltal fault. The Taltal fault is the cause of disruption, not a secondary result. Likewise the Quebrada del Hueso segment is part of the formerly continuous Atacama fault zone, not a group of subsidiary faults.

AGUADA CHÉPICA FAULT

Nomenclature and Previous Work

The name Aguada Chépica fault is applied in this report to the northwestward-curving fault that diverges from the Atacama fault zone in the Pampa Cachina area (Pl. 5) and eventually passes through the town of Taltal (Pl. 4) into the Bahía Nuestra Señora. A separate name is applied to the fault for the sake of reference because it plays a key role in understanding the sequence of faulting in the Taltal area. Clear expression of the fault near Aguada Chépica, where fluvial gravels are in fault contact against andesite, leads to the name.

The fault is indicated on the map of St. Amand and Allen (Fig. 1) as well as that of Bowes et al. (1961), who simply relate it to the Atacama fault zone. Alvarez et al. (1967) and Lemke et al. (1968) briefly mention the fault trace near Taltal, referring to it as the Atacama fault. Separate designation is a matter of preference in this report to avoid confusion in referring to the fault and to promote clear thinking about the relation of the fault to the Atacama fault zone.

Features of the Fault Trace

Aguada Chépica to Taltal.-- The Aguada Chépica fault can be traced for approximately 42 km onshore and at least another 20 km offshore (Part V). Its expression is varied, but along most of its trace the west side of the fault is a higher-standing block. At Aguada Chépica the fault strikes N. 15° W. and dips steeply 84° to the southwest. A parallel fault about 400 m west dips 85° in the opposite direction. Maintaining the steep dip to the southwest, the fault gradually assumes a more northwesterly strike as it approaches Taltal. Throughout this interval its expression reflects the youthful excavation of lower Quebrada de Taltal that contrasts with the mature topography of the Atacama fault trough south of Taltal airport.

Between Aguada Chépica and Taltal the west side of the fault is an irregularly dissected northeast-facing scarp with relief of about 50 m to a few hundred meters, increasing as the opposite side of the fault is progressively more eroded. The fault trace itself is characterized by fault-line saddles, ravines and valleys, as the fault

crosses a markedly irregular topography. Elevated fault-line saddles appear to be erosional remnants that were developed along the fault trace prior to deeper excavation of the major quebrada. Irregular ridge development on both sides of the fault, that locally results in a shutter-ridge-like topography, reflects erosional irregularity in the excavation of both the fault zone and lower Quebrada de Taltal. The irregularity is partly due to the fact that the block between the Aguada Chépica fault, and the Taltal fault was lower than the block to the southwest prior to dissection.

Throughout the entire interval between Aguada Chépica and Taltal, the steep southwest dip of the fault ranges approximately between 75° and 85°. The fault trace is obscured by debris as it crosses a northwest-facing cliff overlooking Taltal; from that point it is concealed beneath the fluvial sands and gravels and fill that underlie Taltal. The fault projects seaward approximately N. 35° W. along Martinez Street, where minor effects were reported to accompany the 1966 Taltal earthquake (Alvarez et al., 1967, p. 8).

Southeast of Aguada Chépica. -- Southeast of Aguada Chépica the fault is roughly a mirror image of the easternmost branch of the El Salado sector; it cuts across large transverse quebradas resulting in fault-bounded interfluves with east-facing scarps and disrupted alluvium along the intervening quebradas. It is significant that modern ephemeral drainage in the transverse quebradas has succeeded in crossing the fault at only one point -- Aguada La Isla (Fig. 31, point D). There, a narrow west-draining channel fed by drainage from Quebrada del Pingo,

and by drainage that is diverted along the Atacama fault trough from eastern Quebrada de Cifuncho, crosses the fault. Elsewhere the large quebradas on the west side of the fault that have gradients to the west are cut off at the fault because of relative uplift. Drainage interior to the Atacama fault trough resulted.

On the south side of the road to Cifuncho, where it crosses the Aguada Chépica fault in Quebrada los Zanjones, a veneer of relatively young alluvium sweeping down from the interfluve to the southwest conceals the fault, but aligned crushed zones and fault-disturbed alluvium delineate the fault trace farther southeast as it follows the base of a dissected east-facing fault scarp about 100 m high. As it approaches and crosses the transverse quebrada southwest of Taltal airport, ridge-trench-ridge scarps are well developed in alluvium along its trace (Fig. 31, point B; Fig. 9, profile H). A closed depression roughly 1 km in diameter lies east of the fault and is floored with light-colored silty alluvium reflecting ponded drainage where Quebrada de la Peineta was disrupted by the fault.

The next interfluve south is similar to that just described. Aligned crushed zones and fault-disturbed alluvium mark the fault trace at the base of a dissected east-facing scarp some 50-100 m high. Bounding both interfluves the fault trends N. 15°-20° W.; exposures of crushed zones reveal a steep dip to the northeast exceeding 80°.

At Aguada La Isla (Fig. 31, point D), water-saturated silty alluvium supports vegetation on the east side of the fault; springs suggest groundwater damming. Although alluvium actually stands

2-3 m higher on the east side of the fault, gravity data (Part VIII) suggest that basement may actually be uplifted on the west. If the sense of displacement at the surface is indeed reversed, perhaps it is related to heaving of the water-saturated, very fine-grained alluvium.

Southeastward the western border of the Atacama fault trough becomes more irregular as the fault ceases to be a major topographic control. It passes through the saddle at P.N. (Bench Mark) 809.3, crosses the low-relief trough of the Atacama fault zone, and projects into the zone of converging faults near Pampa Cachina.

Age and Displacement

Much of the field evidence suggests that vertical motion has predominated along the Aguada Chépica fault during its recent history. This includes the apparent vertical offsets detected offshore, the higher elevation of the west side of the fault along most of its course, the disruption of westward-grading quebradas by the fault, and the faulting of gravels against apparently uplifted basement west of Aguada Chépica. In the latter area a minimum of 12 m of fluvial gravels is in direct fault contact with brecciated andesite; knick points on the east-facing fault scarp and other measurements along this interval suggest a consistent vertical displacement of about 15 m with the east side relatively down. On aerial photos the faulted gravels show an apparent left-lateral separation of 1 km across the fault, but this is due to erosional and pre-faulting irregularity. The gravels on the east side that appear left-laterally displaced are part of the northern feather

edge of the dissected channel of gravels trending transverse to the fault (Fig. 33); field study showed that the axis of the channel of gravels cannot be laterally displaced such a distance. No offset of drainage or any physiographic feature was found at any point along the fault to support such a lateral offset.

Near Aguada La Isla at the northern end of the vegetated silty alluvium, some argument might be made for the left-lateral offset of gullies crossing the fault. One small apparently beheaded gully may be displaced up to 50 m but the relation is not convincing. The reversal of relief at Aguada La Isla is curious but may not be tectonic. On the other hand, one of two plane-table profiles across ridge-trench-ridge alluvial fault scarps southeast of Taltal airport suggests that an alluvial surface has been uplifted up to 1 m on the east side of the Aguada Chépica fault (Table 1, profile I). One might invoke local changes in the sense of vertical motion along the fault. In the absence of clear evidence for Recent lateral offset, the physiographic evidence for recurrent vertical motion, perhaps up to 100 m, must be weighed heavily.

An important result of studies along the Aguada Chépica fault, particularly those synthesized in Figure 33, is that clear restriction is placed on the amount of allowable lateral offset subsequent to canyon cutting and deposition of gravels across the fault. Postulating lateral offset of even a few kilometers presents serious difficulty.

Factors bearing on the age of the Aguada Chépica fault indicating that it did not simply originate as a new break, as an adjustment

response, subsequent to disruption of the Atacama fault zone by the Taltal fault are the following:

(1) The relative elevations of blocks on both sides of the Aguada Chépica fault imply an amount of vertical separation certainly greater than 15 m -- the amount of minimum offset near Aguada Chépica that postdates movement on the Taltal fault.

(2) Crushed zones 3-15 m wide comparable to those seen along the Taltal fault are exposed along the trace of the fault.

(3) Along the interfluve north of Aguada La Isla, remnants of a thick section of sedimentary rocks assignable to the Bandurrias formation -- a thickness that, at a minimum, must be several hundred meters -- are in fault contact with a section of well stratified andesite flows of the La Negra formation. The absence of Bandurrias-like sedimentary rocks on the west side of the fault in that locality demands vertical separation exceeding 100 m.

(4) With regard to mineralization near the trace of the fault, one can follow two lines of reasoning. Prospect pits certainly do indicate mineralization in the vicinity of the fault, but fracture-controlled mineralization and mineralization unrelated to faulting occur over a broad area west of the fault trace. Was the curving trace of the Aguada Chépica fault a control for mineralization, or did it cut across a mineralized terrain, which had been earlier highly fractured, perhaps breaking along older favorably aligned faults? One way to choose between the possibilities is to consider the southern end of the fault. Unfortunately, the final projection of the fault beneath alluvium into the

zone of convergence is a matter of some interpretation (Pl. 5). There is a strong suggestion to connect the Aguada Chépica fault with the mineralized fault exposed in the Bandurrias mine (already discussed in connection with the El Salado sector). If this is done, then the Aguada Chépica fault must be assigned a Mesozoic age. On the other hand, one might simply project the fault into the zone of convergence, not relating its origin to the Mesozoic fractures of the El Salado sector.

This writer can offer no final answer regarding the time of origin of the Aguada Chépica fault. It undoubtedly is an old fault and does not simply postdate the Taltal fault. Either it pre-existed the Taltal fault and perhaps was deformed by lateral motion on that fault, or -- an interesting alternative -- perhaps it developed contemporaneously with the Taltal fault. One fact is certain: the Aguada Chépica fault has been more recently active than the Taltal fault; offshore data (Part V) imply that it presently cuts across the trace of the Taltal fault beneath Bahía Nuestra Señora.

SALAR DEL CARMEN FAULT

Nomenclature and Previous Work

As noted in the introductory remarks to this chapter, the main branch of the Atacama fault north of Bahía Nuestra Señora is synonymously referred to in this report as the Salar del Carmen fault. The fault is briefly discussed by Bowes et al. (1959), Knowles et al. (1959), and Bowes et al. (1961) in their reports on reconnaissance for uranium in northern Chile. St. Amand and Allen (1960) were the first to interpret continuity of the fault with the El Salado sector (Fig. 1). Burnol and Bournat (1966) report observations on the Salar del Carmen fault between Paposo and 24°S., but their reconnaissance was focused in the coastal area west of the fault. No systematic mapping had heretofore been attempted along the fault south of 24°S.

Features of the Fault Trace

Between 24°S. and 25°S. (Pls. 1 and 2), the Salar del Carmen fault lies near the base of a linear east-facing fault scarp 200-400 m high that is continuous for nearly 100 km. The fault itself can be continuously traced for 125 km within the map area from Punta Grande, south of Paposo, to the northern map limit at 24°S.

The steep youthful scarp of the Salar del Carmen fault (Fig. 34) is one of the dominant features of the Coast Ranges (see Figs. 3 and 4). Parallel and diverging faults to the west define numerous fault blocks of varying size that display characteristic features of young block faulting. For example, the block between the Izcuña and Salar del

Fig. 34. Youthful scarp of the Salar del Carmen fault in the Pampa de Remiendos area (Pl. 1) with an old-age topography surmounting the uplifted block. A segment of the fault approximately 7 km long is included. The height of the fault scarp is about 300 m. View is to the southwest.

Carmen faults (Pl. 2), although internally broken, is a classic tilted fault block with a front face along the Salar del Carmen fault, and a back slope bounded by the east-facing scarp of the Izcuña fault (see Davis, 1903). Between the Caleta Coloso and Salar del Carmen faults (Pl. 1), a major wedge-shaped block is itself broken into smaller wedges. North of 25°S., additional blocks are defined by other faults located between the map area and the coastline. For example, the north-northeast-trending Remiendos fault (Burnol and Bournat, 1966), located a few kilometers west of the area of Plate 1, forms the eastern boundary of Jurassic-Cretaceous andesites cropping out in that area.

The fault line along the base of the Salar del Carmen fault scarp can be continuously followed on aerial photographs as a remarkably straight line with an occasional minor kink. A minor en échelon offset is apparent at one locality -- near the intersection of the Paposo-Antofagasta road and the road to Santa Luisa (northern end of Pl. 2). Proceeding north, the fault line there suddenly appears to follow an en échelon trace about 400 m to the west; an alluvial fan conceals the intervening area.

Coalescing alluvial fans blanket rock outcrops on the east side of much of the Salar del Carmen fault, but outcrops trending across the broad trough are sufficient to preclude the existence of through-going breaks parallel to the major fault.

The large linear valley created by the Salar del Carmen fault is primarily a fault-angle valley (Cotton, 1950) rather than an

erosional rift. In a typical profile across the fault zone (see, for example, the topographic profile in Fig. 41), the fault scarp generally has a slope of 20°-25° or steeper with a steepened base. Fan slopes of 7°-8° descend eastward from the fault line and merge with rock-cut slopes of about 2°-4° grading westward.

The broad trough paralleling the fault scarp is divided into a regular series of elongate closed depressions 10-15 km long and about 5 km wide. Rims of crystalline rock define the closure, and the basins are mostly floored with a thin veneer of pediment gravels, except along their western margins. The origin of the closed depressions is suggestively related, in part, to the disruption of pre-existing east-west drainage. Note, for example, the locations of closed depressions east of the head of Quebrada de Remiendos (southern area of Pl. 1), and again east of the head of Quebrada de Izcuña (northern area of Pl. 2). The relation of Quebrada de Remiendos to a negative lineament east of the Salar del Carmen fault was mentioned earlier (see Fig. 4). On the other hand, relief along suitably oriented secondary faults -- northeast- and northwest-trending -- at the eastern margins of the closed depressions suggests a tectonic origin. Differential subsidence of small blocks east of the Salar del Carmen fault has apparently occurred in addition to large uplift along that fault.

To the north of Quebrada Paposo the exceptional linearity of the fault (Fig. 6) and measurements of the attitude of the fault plane indicate that the Salar del Carmen fault is either near-vertical or very steeply dipping to the east. In Quebrada Agua Buena (Pl. 3, 4.5 km S.

of Paposo), however, where the Salar del Carmen fault emerges from being bounded on the west by a high block because of erosion, the fault assumes a dip of about 25° east along a short interval. Orthogneissic granitic rocks form the hanging wall, overlying at least 30 m of phacoidal to phyllonitic sheared andesite. To the southeast the fault is obscured by colluvium, but at three other localities between Quebrada Agua Buena and Punta Grande the fault demonstrably again adopts a moderately steep dip to the east -- 65°-75°. The shallow dip at Quebrada Agua Buena is not proof of active thrusting. The sense of recent motion at almost every other point along the fault indicates uplift of the west side, not the east. An older episode of local thrusting could be invoked, or the fault plane may have simply been deformed at that locality due to the steepness of topography to the east and the "free face" to the west.

To the southwest of Quebrada Agua Buena, the Salar del Carmen fault lies along the east slope of the Sierra El Jote and passes through Quebrada Los Morados (Pl. 3). At the mouth of the quebrada it is concealed beneath fanglomeratic gravels, but it reappears near the beach displacing marine terrace gravels and forming a small east-facing scarp slightly more than 1 m high. The bearing of the fault as it projects into Bahía Nuestra Señora is S.15° W. Mapping of the main fault break through Quebrada Los Morados and the bearing of S.15° W. importantly differs with mapping of Bowes et al. (1961) that shows the Salar del Carmen fault passing through Punta Grande and projecting S.30° W. into the sea. Such a projection creates a bias in terms of

dissociating the Salar del Carmen fault from the El Salado sector.

On the southeast slope of Cerro Carnero, small ravines crossing the Salar del Carmen fault (see Fig. 6, point A) reveal the best exposures that were seen of the zone of cataclasis associated with the main break of the fault, other than the exposure in Quebrada Agua Buena. Exposures in these ravines reveal the following:

(1) Downfaulting of well stratified fluvial gravels on the east against phacoidal to phyllonitic cataclasites: in one gully a thickness of at least 11 m of well bedded gravels -- undeformed near the fault -- are in direct fault contact with such cataclasites.

(2) Intense cataclasis that preceded faulting of the gravels of a zone of variable thickness up to 50 m wide: highly fractured rocks near the fault become increasingly phacoidal closer to the main break. The most intensely sheared rocks are orange, green, and maroon colored phyllonites associated with cataclastic rocks that have small phacoidal pods of coherent material.

Study of exposures in these ravines provides evidence that the cataclastic rocks are themselves irregularly broken by the younger faulting that has displaced the alluvial gravels.

North of these small ravines no other exposures of the fault plane were seen. Alluvial fans are sporadically segmented by small synthetic faults with consistent uplift to the west. The alluvial apron is interpreted to be faulted along the entire length of the Salar del Carmen fault. Faulting or disturbance of young alluvium at the trace

of the main fault is variable, but is generally more marked as one proceeds northward. In the small interfluve areas between fanheads, features of interest are sags and closed depressions in the colluvial detritus forming a bench that aligns with faulted alluvium at the fanheads.

The occurrence of ridge-trench-ridge forms along the fault trace in the Pampa de Remiendos area was noted earlier. At the cited locality (PA-102: Appendix Pl. A), a trench crosses the fanhead and is flanked on the downfan side by a ridge nearly 2 m high.

Alluvium throughout the broad fault trough in the northern Pampa de Remiendos area (Pl. 1) is much more intensely faulted than to the south -- typical of the more recent expression of faulting in the Antofagasta area.

At the latitude of Cerro Cristales (Pl. 1), the relief of the steep scarp of the Salar del Carmen fault rapidly diminishes (Fig. 35), while that along other branch faults such as the Caleta Coloso fault is marked. North of the map area the fault break that can be continuously traced from Punta Grande apparently merges with the branch located a few kilometers to its west at the northern map limit.

Age and Sense of Displacement

Recurrent movement. -- Movement on the Salar del Carmen fault has been recurrent, so that discussion of the age of the fault must refer to initial and other episodes of movement. The idea of recurrent movement is supported by (1) the faulting of older cataclastic rocks revealed in the exposures southeast of Cerro Carnero, (2) the

distribution of rock units across the fault, and (3) the linearity of the fault. The preservation of Paleozoic and Mesozoic stratified rocks in the block to the west of the Salar del Carmen fault, together with the exposure of granitic rocks of the KT suite on the east side, can only be explained by former uplift of the east side. This is exactly opposite the sense of recent motion that has created the prominent fault scarp along the Salar del Carmen fault. If the linearity of the fault scarp is not explained by uplift along an old strike-slip fault, then long-continued vertical motions must certainly be required to create such straightness and continuity. This straightness is particularly marked when the Salar del Carmen fault is compared to other large faults in the area, such as the Izcuña fault, that have accommodated sizeable block motions.

Age of faulting. -- Timing the origin of the fault depends on arguments similar to those put forth for the El Salado sector of the fault zone. The author is not aware of mineralization of the main branch of the Salar del Carmen fault within the map area; nevertheless, mineralization in its immediate vicinity and along secondary faults, particularly in the area east of Paposo (Burnol and Bournat, 1966), implies pre-Late Cretaceous faulting. Synorogenic deformation and mineralization of granitic rocks near the fault that are likely Jurassic in age suggests the possibility of a pre-Cretaceous origin. The parallelism of large andesite feeder dikes with the trend of the fault (see Fig. 6) implies the existence of that structural trend during late Jurassic or early Cretaceous time.

Other general information bears on the timing of episodes of movement. Relief of the Salar del Carmen fault scarp implies vertical uplift of about 200-400 m across the fault of a Tertiary old-age surface. This surface is no younger than late Miocene, but possibly older -- Eocene to Miocene (Part IV). The youthful aspect of the Salar del Carmen fault scarp (Fig. 34) favors an episode of late Tertiary to Quaternary movement. Marine terrace gravels cut by the fault near Punta Grande are assumed to be Pleistocene. Finally, modern alluvium -- considered by this writer to be Recent -- is broken along the fault trace at some of the fanheads in the northern part of the map area (Pl. 1). The most illustrative examples of recent faulting along the Salar del Carmen fault occur north of the map area. Near Salar del Carmen (Fig. 1), for example, east-facing piedmont scarplets that disrupt alluvial fans show little modification (see Brüggen, 1950, p. 311; Rich, 1942, photo. 232).

Episodic faulting in the Coast Ranges undoubtedly accompanied phases of movement in the uplift of the Andes which began in the Miocene, with important later phases in mid-Pliocene and Late Pliocene or Pleistocene time (Hollingworth, 1964; Rutland et al., 1965; Hollingworth and Rutland, 1968). Also, faulting presumably occurred in the Coast Ranges contemporaneous with the formation of the Longitudinal Depression earlier in the Tertiary at some time during the Eocene to Miocene (Sillitoe et al., 1968). If the Salar del Carmen fault originated in the Mesozoic, it would have been, as a "master fault", susceptible to reactivation during episodes of Tertiary

faulting. Without dated Tertiary units, little more can be done to specifically time the age of fault movements within the map area.

Sense of displacement. -- The mapping along the Salar del Carmen fault (Pls. 1, 2, and 3) reveals no clear scheme for matching displaced rock units. Instead, an ambiguity results -- large lateral offset versus large vertical displacement. This problem is discussed later so that the Atacama fault within the entire map area can be considered.

Is the Salar del Carmen fault an active strike-slip fault? The sense of recent displacement along the Salar del Carmen fault within the map area is consistent -- vertical motion with the west side up. Despite continuing activity of the fault, as indicated by alluvial scarps, no evidence was found for any recent lateral offset. Where the fault crosses the beach near Punta Grande, it is difficult to accept any significant lateral offset of the faulted marine terrace gravels. The faulted gravels exposed in the small ravines near Cerro Carnero contain clasts that match the adjacent rock types on the opposite side of the fault. The Pleistocene (?) marine gravels are uplifted about 1 m, a minimum thickness of 11 m of alluvial gravels are in direct fault contact with cataclasites near Cerro Carnero, and a minimum uplift of 200 m is implied by the relief of the Salar del Carmen fault scarp.

The large closed depressions along the Salar del Carmen fault might be attributed to differential subsidence related to strike-slip movement (see, for example: Kingma, 1958; Lensen, 1958). However,

without concrete evidence of any demonstrable lateral motion during Tertiary time, such an explanation is hypothetical.

The Salar del Carmen fault, just as branches of the El Salado sector, appears to have had a long and changing history. Other investigators have noted the necessity to invoke downdropping of the west side of the fault to explain the regional distribution of rock units both within the map area and far to the north (Bowes et al., 1959; Knowles et al., 1959; Burnol and Bournat, 1966). The reversed sense of recent motion is emphasized here -- uplift of the west side.

St. Amand and Allen (1960) acknowledged the predominance of recent vertical displacements along parts of the Salar del Carmen sector, but maintained that the overall history of the Atacama fault was one of dextral strike slip. Numerous horizontal slickensides were recorded by C. R. Allen (personal communication) in mines of the Paposo mining area, and a fair number were also observed by this writer in the Sierra El Jote area. Sparse slickenside information was gathered along the main trace of the Salar del Carmen fault.

There is no indisputable evidence for strike-slip movement in either the fault forms or the mapped geology along the Salar del Carmen fault. In addition to slickenside information, the reasoning that is resorted to for interpreting an episode of strike-slip movement involves the linearity and steep dip of the fault, which is suggestively more compatible with strike-slip rather than dip-slip faulting. (See discussion on problem of total displacement.)

IZCUÑA FAULT

Nomenclature and Previous Work

West of the Salar del Carmen fault, a large north-south fault about 60 km long roughly parallels its trace at a distance of 7-10 km between Rada de Paposo (Pl. 2) and Quebrada de Remiendos (Pl. 1). The fault was mapped in reconnaissance and termed the Iscuna-Punta de Cañas fault by Burnol and Bournat (1966). In this report the fault is simply termed the Izcuña fault (spelling herein follows usage on the 1 : 100, 000 base maps), because it does not curve southwest toward Punta Cañas at its southern end as shown by those workers.

Features of the Fault Trace

The Izcuña fault exerts a topographic control similar to that of the Salar del Carmen fault (see Fig. 4, G). Recent westward tilting of the large block between the two faults is reflected by relative down-dropping on the east side of the Izcuña fault. An irregular east-facing scarp 100-200 m high bounds a narrow fault trough 1-2 km wide in which alluvium from the tilted block on the east is ponded.

A single fault trace characterizes the southern half of the fault zone, while parallel and converging faults complicate the structure west of Cerro Paranal and to the north. Along the southern half of the fault trough, the fault follows the west side and is marked by disturbed colluvium at the base of steep east-facing scarps. Low alluvial scarplets with the west side up occur where the fault scarp has receded.

At its southern end (Pl. 2) the fault trace is concealed beneath the alluvial coverhead of the coastal platform but can be seen at the shoreline, where a zone of gneissoid rocks several meters wide separate highly sheared and fractured dike-injected granodiorite from brecciated andesite and cherty siltstones.

Westward drainage crosses the Izcuña fault at a few localities such as at Quebrada de Izcuña and about 8 km south-southwest of Cerro Paranal (Pl. 2), where an east-west fault cuts across the Izcuña fault trough dropping it down to the north. At other localities east-west drainage lines have been disrupted by uplift on the Izcuña fault.

The Izcuña fault has a sinuous trace, but its trend roughly parallels that of the Salar del Carmen fault. Near Quebrada de Remiendos (Pl. 1) the Izcuña fault apparently dies out. The fault dips 82° east at a locality southwest of Cerro Yumbes (Pl. 2) -- one of the few areas where exposures of the fault can be seen -- and about 70° east at the shoreline. Most of its map trace also requires a steep eastward dip.

Age and Displacement

Origin and episodic activity. -- The parallelism of the Izcuña and Salar del Carmen faults suggests a contemporaneous origin, although movement on the latter fault has undoubtedly been more important because of its greater extent. The Izcuña fault has probably accommodated episodic movements during the Tertiary and Quaternary Periods. Modern alluvium that assuredly is Recent is disturbed along

the trace of the fault where it crosses a small wash 2 km south of Quebrada de Izcuña (Pl. 2). Quaternary scarps are abundant elsewhere along the fault.

The relief along the west side of the Izcuña fault indicates an amount of late Cenozoic uplift of the order of a few hundred meters. This movement postdates formation of a Tertiary old-age topography, and presumably accompanied the uplift or tilting that has formed the Salar del Carmen fault scarp. Quaternary-Tertiary alluvium infilling the Izcuña fault trough was down-dropped against the fault prior to formation of the present coastal escarpment, as can be demonstrated southwest of Cerro Yumbes (Pl. 2) where hanging remnants of the alluvial trough are in fault contact with basement rocks.

Although no evidence was found for recent lateral motion, and the most recent sense of displacement appears to have been vertical, horizontal slickensides were observed within the zone of fractured basement rocks southwest of Cerro Yumbes.

Total displacement. -- The data at hand favor large net uplift of the west side of the Izcuña fault and appear to preclude large lateral offset. More detailed mapping of individual phases of the JK suite along the fault will be required to fix a possible amount of small lateral displacement. The lines of reasoning are:

(1) A stratigraphic section of Paleozoic metasedimentary rocks, Liassic marine rocks, and Jurassic-Cretaceous andesites are bounded by the Izcuña fault southwest of Cerro Yumbes (Pl. 2). The only link

with these stratified rocks that could be found on the west side of the fault is the occurrence of Paleozoic metasedimentary rocks, irregularly intruded by fine- to medium-grained granodiorite, that crop out immediately on the east side of the fault in that same area. About 40 km to the north, andesites of the La Negra formation crop out to the west of the map area (Burnol and Bournat, 1966), but the dying out of the Izcuña fault near Quebrada de Remiendos and other constraints preclude their being a laterally offset continuation of the Cerro Yumbes stratigraphic section. A minimum uplift of 1-2 km is required to explain stripping of the Liassic marine rocks on the west side of the Izcuña fault. Even taking into account consumption of the Paleozoic metasedimentary rocks by intrusive bodies, their limited occurrence on the west side of the fault probably reflects vertical offset exceeding the 1-2 km minimum.

(2) South of Quebrada de Remiendos (Pl. 1), medium-grained equigranular adamellite (KTa_1) crops out in a well defined northeast-trending band that appears to be continuous across the Izcuña fault zone. This continuity and the apparent dying out of the fault in that area are judged to eliminate the possibility of large lateral offset.

(3) Similar fine- to medium-grained granodiorites ($JKgd_3$) crop out on both sides of the fault near the coastal platform (Pl. 2). At numerous other localities granitic rocks on opposite sides of the fault are distinctly different -- mainly different phases of the JK suite. Although the reconnaissance mapping suggests no lateral offset of a

large distinctive body, mapping of the phases of the JK suite is not detailed enough to affirm or reject lateral displacement. On the basis of present mapping, it is this writer's opinion that large vertical uplift of the west block can adequately explain the distribution of different granitic rocks across the fault. A component of lateral displacement may amount to a few kilometers; an amount exceeding several kilometers is doubtful.

CALETA COLOSO FAULT

General Features

A major north-northwest-trending fault zone that diverges from the Salar del Carmen fault in the Pampa de Remiendos (Pl. 1), passes east of Cerro Cristales and continues beyond the map area to Caleta Coloso, where it projects into the Bay of Antofagasta (see Figs. 1 and 29). The continuity of the fault over this distance of approximately 80 km was indicated by St. Amand and Allen (Fig. 1). Studies of the fault north of the map area include mapping by Alarcón and Vergara (1964) and C. Klohn, whose unpublished map of the Antofagasta quadrangle is synthesized in the 1968 geologic map of Chile (Inst. Invest. Geol.). Burnol and Bournat (1966) sketched the main segments of the fault south of 24°S. on their reconnaissance map.

Topographic control exerted by the fault within the map area is strong (see Pl. 1, Figs. 4 and 35). A prominent alluviated fault trough that is bounded on the west by high relief -- amounting to more

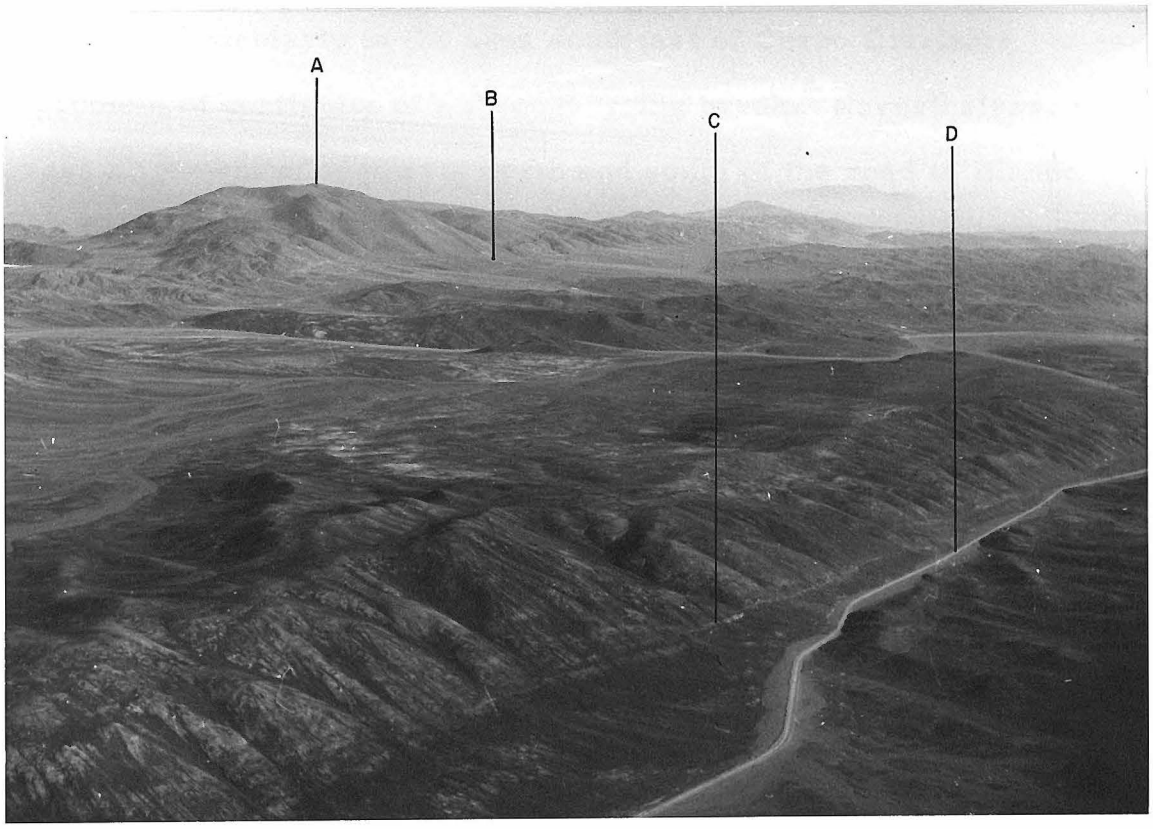

Fig. 35. Salar del Carmen and Caleta Coloso faults. Oblique aerial view looking northwest toward Cerro Cristales (A) showing the traces of the Caleta Coloso fault (B) and the Salar del Carmen fault (C). The Paposo-Antofagasta road (D) is in the foreground. The steep scarp of the Salar del Carmen fault, continuous from north of Paposo, dies out to the right. In contrast, relief across the Caleta Coloso fault is marked. Differential movement of blocks between branches of the Atacama fault system is typical in this area. (See Fig. 4, Pl. 1.)

than 600 m east of Cerro Cristales -- can be traced from the Sierra de Remiendos north-northwest to the northern map limit. Branch faulting, particularly in the area southeast of Cerro Cristales, raises a problem of continuity of a through-going break. Nevertheless, the gross alignment of segments north and south of the road to Blanco Encalada, and the occurrence of rocks of the KT suite primarily on the west side of those aligned segments suggest continuity along the structural line that is labeled the Caleta Coloso fault on Plate 1. The name applied to this break follows the usage of local geologists, although the author is not aware of a published antecedent.

North of the road to Blanco Encalada, a prominent fault trace continuously breaks alluvium raising it a few meters on the west (see Table 1, profile A) and forming excellent examples of ridge-trench-ridge fault scarps. A parallel break several hundred meters to the west follows the east base of Cerro Cristales until the two breaks merge to the north and continue along the west side of the fault trough. Slightly diverging faults transect crystalline rocks both east and west of the trough.

South of the road to Blanco Enclada, a major break follows the base of an east-facing scarp a few hundred meters high, breaking alluvium along the fault trace. As the fault crosses the Sierra de Remiendos, the east block is higher-standing but low scarps along the fault trace are predominantly east-facing. Arcuate splaying characterizes the fault near its intersection with the Salar del Carmen fault, and it is difficult to envision a through-going break along which lateral

motion could have been transferred from the latter fault (see Pl. 1).

As most faults in the area, the Caleta Coloso fault either follows the base of an uplifted block or is marked by subdued relief where it transects crystalline rocks. The attitude of the fault could not be directly measured, but the linearity of the fault on a regional scale indicates a steep dip along most of its course.

Age and Displacement

Horizontal slickensides were observed at one locality north of Cerro Cristales, and they are common in prospect pits south of Caleta Coloso. The fault traces show no indication of recent lateral offset, however, and alluvial scarps consistently indicate recent uplift on the west side. Measurements across a well developed ridge-trench-ridge scarp indicate net uplift across the fault feature (Table 1, profile A).

As one of the main branches of the Atacama fault system, the Caleta Coloso fault has apparently shared the changing history of movement and episodic activity that has characterized the principal fracture zone. Extensive hydrothermal alteration of the fault zone near Caleta Coloso probably reflects the existence of the fault during the late Mesozoic. At any rate, major movement on the fault occurred subsequent to crystallization of the late Cretaceous and/or early Tertiary granitic rocks of which it forms a major boundary.

The distribution of rocks along the 50-km mapped segment of the Caleta Coloso fault (Pl. 1) suggests (1) net uplift of the west block and (2) differential subsidence of blocks between the Caleta Coloso and

Salar del Carmen faults, as indicated by the preservation of stratified andesites and rocks of the Caleta Coloso formation.

A striking aspect of the pattern of rock distributions is the bounding of rocks of the KT suite along nearly 40 km of the fault without an apparent lateral offset of these rocks. North of the Sierra de Remiendos, a long narrow band only 1 to 2 km wide of medium-grained hornblende-biotite granodiorite is bounded by the Caleta Coloso fault and suggestively appears to be the western margin of a much more laterally extensive body -- at least in view of the configuration of typical bodies of the KT suite elsewhere in the map area.

Distinctly different phases of the JK suite crop out on opposite sides of the fault north of Cerro Cristales. Medium-grained hornblende tonalite with minor biotite crops out on the west. The development of stubby euhedral greenish black hornblende prisms (1-3 mm long) in a whitish gray matrix of plagioclase and quartz gives the rock a distinctive appearance (color index = 15-20). Cropping out on the east are light gray, fine- to medium-grained hornblende-biotite granodiorite (color index = 10-15) and medium- to coarse-grained diorite. The granodiorite is tentatively assigned to the JK suite because it is pervasively intruded by swarms of dikes, including dacite (?) porphyry, to an extent not seen in any body of the KT suite. Whatever the age assignment, this granodiorite is distinctly different from the granodiorites on the west of the fault. The most abundant type of the latter granodiorites contains 20% or more of dark minerals, although more leucocratic granodiorite occurs in parts of the Sierra de Remiendos.

The granodiorite bodies on the west of the fault are xenolithic and none exhibits dike swarms as seen in the body on the east.

Outcrops of tonalite to diorite (JKt_3) on the east side of the fault south of the road to Blanco Encalada are grossly similar to the hornblende tonalite north of Cerro Cristales in being hornblendic with prismatic, frequently euhedral, hornblende. Dark mineral abundances of the former rocks tend to be greater and approach 50%, but the differences can be attributed to variability of color index, which typifies most of the rocks of the JKt_3 unit. Despite some similarity, rocks from the two locales are not considered to be laterally displaced equivalents, because similar tonalites and diorites are widespread in both blocks on opposite sides of the Caleta Coloso fault -- a unique association cannot be made.

Although different rocks are juxtaposed along most of the fault, a tenable pattern of lateral offset does not emerge from the mapping. The occurrence of granodiorite plutons of the KT suite along the east side of the Salar del Carmen fault (Pls. 1 and 2) makes it appear that the western part of one of these plutons may have been sliced off and laterally shifted to the Caleta Coloso fault. However, the map configuration at the southern end of the Caleta Coloso fault precludes this possibility. Identical medium- and coarse-grained pyroxene granodiorites crop out on both sides of the fault in the Sierra de Remiendos and toward the southern end of the fault. These rocks crop out in a north-south band that together with a swath of meta-andesites and

andesites parallels the Salar del Carmen fault and crosses the interval through which a main break of the Caleta Coloso fault must pass to intersect the Salar del Carmen fault. Thus, a large right-lateral offset of rocks along the Salar del Carmen fault could not have been transferred to the Caleta Coloso fault.

Another scheme of displacement is suggested by the distribution of rocks of the KT suite within the entire northern area of Plate 1. A large plutonic body may underlie an area extending from east of the Salar del Carmen fault to west of the Caleta Coloso fault. (See "Possible Constraints on Large Lateral Displacement, Cerro Cristales Area".) If this is true, then uplift on the west of the Caleta Coloso fault could have caused the present distribution of rocks along that fault.

Lateral displacement on the Caleta Coloso fault is not precluded by the present mapping. It is plausible that total displacement on the fault may include a horizontal component of several kilometers. A component of strike-slip movement cannot be completely disregarded because of horizontal slickensides along the fault. Also, the overall linearity of the fault resembles that of the Salar del Carmen fault, intimating a possible early history of strike-slip movement. Nevertheless, the writer presently sees no need for hypothesizing lateral displacement of tens of kilometers; indeed, it is difficult to reconcile large lateral displacement with the nature of the intersection of the Caleta Coloso and Salar del Carmen faults. The writer favors large uplift of the west block, of an amount measured in kilometers, to explain the juxtaposition of different rocks along the Caleta Coloso fault.

A few kilometers north of the road to Blanco Encalada, there is an area of local complexity along the Caleta Coloso fault that will require more detailed mapping of the granitic rocks to determine if there is a continuous through-going break. The southern continuity of the prominent break that cuts alluvium east of Cerro Cristales is also not clear.

SIERRA EL JOTE FAULT

At the southern end of the Salar del Carmen fault, another fault 4-5 km to the east roughly parallels its trace for a distance of 20 km and projects southwest into the Bahía Nuestra Señora (see Pl. 3). This fault is herein referred to as the Sierra El Jote fault because the fault trace and defining relationships are best expressed in that area.

Jurassic and/or Cretaceous andesites, including both extrusive flows and sizeable intrusive stocks, are bounded on the east by the fault, which juxtaposes them against granitic rocks of the JK suite. These latter are part of a large complex pluton in the Matancilla area east of Paposo (Pls. 2 and 3) that mainly comprises medium- to coarse-grained pyroxene granodiorite extensively crosscut by veins and dikes of adamellite and andesite.

In the Sierra El Jote, the fault is marked by a zone of gouge and fault breccia about 4 m wide, where purple, deeply weathered andesites are juxtaposed against pyroxene granodiorite. The zone of intense fracturing in the vicinity of the fault generally does not exceed a few

tens of meters in width and is minor in comparison with cataclasis along the Salar del Carmen fault. Northward the fault is defined by a shear zone a few meters wide that cuts medium- to coarse-grained granodiorite along a trace that could not be followed more than 3-4 km north of Quebrada La Araucana. At its southern end the fault is concealed beneath the alluvial coverhead of the coastal platform, but can be defined at the shoreline immediately north of Punta Cachinalito where it separates stratified andesites from an inclusion-rich hybrid phase of the pyroxene granodiorite pluton.

The Sierra El Jote fault trends N. 20°-25° E. along most of its course but curves northward at its northern end. The dip of the fault is consistently steep -- 80°-85° to the northwest.

Near-horizontal slickensides on the fault in the Sierra El Jote indicate strike-slip movement. No evidence was found to indicate either recent activity or reactivation of the fault in late Tertiary time.

Apparent vertical uplift of the east block is indicated along the Sierra El Jote fault. It is doubtful that horizontal displacement indicated by the slickensides can be large if the fault dies out within the complex of pyroxene granodiorite to the north.

THE CONTINUITY OF THE ATACAMA FAULT ZONE

Arguments in Favor of Former Continuity

The ultimate proof of the former continuity of the El Salado and Salar del Carmen sectors of the Atacama fault rests on physically tracing beneath Bahía Nuestra Señora the continuation of the Salar del Carmen fault and that of the Quebrada del Hueso fault zone segment. We have seen that this could not be done by offshore seismic profiling (Part V). Nevertheless, arguments for former continuity can be based on the mapped geology and suggestive evidence. Lines of evidence are:

(1) On a regional scale, the similar trend, extent, and continuity of both the Salar del Carmen and El Salado sectors (see Fig. 1) suggest their continuity with each other prior to disruption by the Taltal fault. It might be argued that the trends of the Salar del Carmen and El Salado sectors of the fault are not really similar inasmuch as north of 26°S., the El Salado sector trends north-northwest (Pl. 5), while the Salar del Carmen sector trends north-northeast within the map area (Pls. 1 and 2). Deformation due to lateral motion on the Taltal fault explains part of the divergence; perhaps there also was a gentle bend in the fault in the Taltal area -- similar to the bend in the Salar del Carmen sector east of Antofagasta (Figs. 1 to 4). The present difference in trend between the El Salado and Salar del Carmen sectors of the fault is no greater than that of segments of the fault involved in the bend near Antofagasta.

(2) The regional distribution of rock units requires net uplift of the east block along the entire mapped segment of the Salar del Carmen

fault. The El Salado sector of the fault is a similar major structural break; net uplift of the block east of the fault zone has controlled the distribution of stratified rocks and basement rocks in the same manner as along the Salar del Carmen fault.

(3) The occurrence of gneissic metasedimentary rocks, orthogneisses, and migmatites on the east side of the Salar del Carmen fault near its southern end (Pl. 3) and along the east side of the Quebrada del Hueso fault zone segment (Pl. 4) suggests the possible continuity of those branches.

(4) No evidence from the offshore work supports the projection of the Quebrada del Hueso zone to the west of Punta Grande. On the contrary, the geology -- particularly the distribution of andesites -- strongly suggests its continuity with either the Salar del Carmen or Sierra El Jote faults.

(5) If the Salar del Carmen and El Salado sectors of the fault had undergone vertical displacements only, there would be no compelling necessity to connect them, and they might well be independent -- but probably not mechanically unrelated. The indication of strike-slip movement along both sectors of the fault, however, favors through-going breaks because of their length. If lateral slip of the same sense occurred on both sectors of the fault, and if those sectors were independent, they probably soon would have been connected by a through-going break because of their configuration -- unless they were en échelon breaks. Given the gross alignment of both sectors prior to

disruption by the Taltal fault, the writer cannot subscribe to the idea of opposing senses of lateral motion on the two sectors as indicated by Bowes et al. (1961).

Correlation of Branches

Inasmuch as three well defined breaks enter the Bahía Nuestra Señora from the north -- the Izcuña fault, the Salar del Carmen fault, and the Sierra El Jote fault (see Fig. 30), the manner in which branches of the El Salado and Salar del Carmen sectors were probably connected requires some comment.

To begin with, some interpretations do considerable violence to the distribution of rock units. These include simply correlating the Quebrada del Hueso zone with the Izcuña fault, or projecting the Salar del Carmen fault west of Taltal and postulating lateral displacement on it. The mapped geology, as earlier noted, strongly suggests continuity of the Quebrada del Hueso zone with either the Salar del Carmen or Sierra El Jote faults.

Thick crushed zones and wide zones of intense shearing are exposed within the Quebrada del Hueso segment of the fault. Likewise a wide zone of shearing (at least 30 m wide), irregularly blanketed by colluvium in Quebrada Los Morados (Pl. 3), indicates that the Salar del Carmen fault is still a major fracture as it projects into the sea. The zone of cataclasis along the Sierra El Jote fault, however, is by no means comparable to that of the Salar del Carmen fault and we have seen that the Sierra El Jote fault apparently dies out after about 20 km.

Cataclasites exposed along the Salar del Carmen fault are more impressive than those viewed anywhere in the map area; they certainly define a much wider zone of shearing than was observed along the Taltal fault, which accommodated 10 km of lateral movement.

The Sierra El Jote fault may connect with the easternmost branch of the Quebrada del Hueso zone or it may converge with the Salar del Carmen fault as suggested by their trends. At any rate, the most likely course for a master break would have been a connection of the Salar del Carmen fault with one of the major shears of the Quebrada del Hueso zone. There is a possibility -- suggested by the convergence of multiple branches to a single trace at Pampa Cachina (Pl. 5) -- that the Quebrada del Hueso zone similarly converged to a single major break northward.

The Salar del Carmen fault might presently be traced to the Quebrada del Hueso zone by bowing or a series of step offsets; or it may have prolonged itself farther southwestward subsequent to its termination by the Taltal fault. The expression of such a prolongation was not detected by offshore profiling.

THE PROBLEM OF TOTAL DISPLACEMENT ON THE ATACAMA FAULT

Introduction

The Atacama fault is a major structural break that juxtaposes different rocks along virtually the entire extent of a 200-km mapped

segment. The pattern of rock exposures (Pls. 1-5) defines no obvious scheme of consistent lateral offset; however, apparent vertical displacements of thousands of meters are indicated across the fault with the east side consistently raised. Certain rocks are thus more extensively exposed on either one or the other side of the fault. Large lateral offset of hundreds of kilometers might be invoked to have displaced rock bodies beyond the map area, or it might be argued that large vertical displacements alone have caused the juxtaposition of different rocks along the fault. There are sufficient indications that total displacement must involve both vertical and horizontal separation. Information bearing on the possible magnitude of lateral displacement is of great interest and is discussed here along with some general problems that make a recognition of lateral offset difficult.

Necessity of a Component of Horizontal Separation

The most compelling evidence adduced by St. Amand and Allen (1960) for lateral displacement on the Atacama fault is the occurrence of widespread horizontal slickensides and mullions in mines and prospect pits, and the remarkable linearity of segments of the fault over hundreds of kilometers. The writer emphatically supports the observation of numerous horizontal slickensides along branches of the Atacama fault and concurs that strike-slip motion occurred at some time during the history of the fault, although recent motion has been predominantly vertical between 24°S. and 26°S.

Problems of Discerning a Scheme of Lateral Displacement

Large vertical uplift. -- It seems safe to conclude that uplift of the east side of the Atacama fault is not only apparent, but that the east side has indeed been raised along the 200-km mapped segment. The regional distribution of rock units is sufficiently well known in northern Chile (see 1968 Geologic Map of Chile) to preclude invoking large horizontal shift beyond the map area simply to explain the exposure of deeper-level basement rocks on the east of the fault or the more extensive occurrence of stratified rocks on the west side.

Vertical motion on the Atacama fault has caused a basic asymmetry of regional outcrop patterns. (1) Outcrops of extrusive andesites are more extensive on the relatively lowered west side; outcrops of andesites on the east are smaller and commonly roof pendants. (2) Exposures of plutonic bodies of the KT suite are more common on the relatively uplifted east side. (3) Liassic marine rocks and the Caleta Coloso formation bound the Salar del Carmen fault only on its lowered western side. (4) Paleozoic basement rocks and batholithic rocks of the JK suite are exposed on both sides of the fault, however, because they are the most widespread basement rocks in the area.

A minimum vertical separation between 0.5 and 1 km can be fixed at numerous localities along the fault on the basis of present relief and the pattern of rock exposures. Along the El Salado sector (Pls. 4 and 5), the termination of a regionally east- to southeast-dipping

sequence of Jurassic-Cretaceous andesitic rocks along the eastern-most branch of the fault, combined with the appearance of Paleozoic rocks on the east side, requires a vertical separation of several kilometers. That the Atacama fault is such a major structural break consistently requiring net vertical uplift of the east side indicates that, along the entire trace of the fault between 24°S. and 26°S., the component of total vertical displacement undoubtedly exceeds a few kilometers and probably amounts to several kilometers.

Nature of the rock units.-- Jurassic-Cretaceous andesites and Jurassic to Tertiary (?) batholithic rocks underlie 95% of the mapped area and have general trends that parallel that of the north-trending Atacama fault. Every major map unit, including the Paleozoic metamorphic and granitic rocks, maintains similarity over extensive areas of northern Chile, so that uniquely associating rocks across the fault is not a simple matter.

The most voluminous granitic rocks are those of the JK suite, which crop out on both sides of the Atacama fault within the map area. They are characterized by great textural and compositional variability, however, so that their usefulness is limited without more detailed mapping of their contacts -- the occurrence of individual phases is generally widespread throughout the map area and few phases are geographically restricted. Granitic rocks of the KT suite, while more homogeneous than the older batholithic rocks, maintain textural and compositional similarity from body to body over distances greater than

a hundred kilometers, which also creates a problem of unique association.

The fact that batholithic rocks are transected by the fault ideally should facilitate the recognition of offset bodies. That a scheme of lateral offset does not emerge from the mapping may be primarily due to the component of vertical displacement. For example, several large discordant stocks of the KT suite are bounded by the major fault branches, but no laterally offset equivalents of these bodies could be found within the map area (recall that transfer onto the Caleta Coloso fault is not allowed). This can be explained by vertical block motions rather than lateral displacements beyond the map area. The possibility must also be considered that stocks of the KT suite were emplaced subsequent to large lateral slip on the Atacama fault. Their bounding by linear branches of the fault indicates that major movement occurred, subsequent to their crystallization, along the presently defined major fault breaks.

Possible Constraints on Large Lateral Displacement

Although the mapping has not revealed a scheme of lateral offset, there are map relations which appear to constrain the amount of allowable lateral displacement. For example, in at least three areas, surprisingly similar granitic rocks of the JK suite -- although not contiguous across the Atacama fault -- occur in proximity on opposite sides of the fault.

Sierra del Carmen area. -- In the Sierra del Carmen area (southeast corner of Pl. 5), mapping indicates the occurrence of highly tectonized, similar appearing, fine- to medium-grained granodiorites on both sides of the main eastern branch of the El Salado sector. The rocks are assigned to the JK suite. Rocks on both sides of the fault are altered and highly fractured, typically appearing greenish brown in color because of saussuritization of calcic plagioclase and alteration of the ferromagnesian minerals to chlorite, epidote and secondary amphibole. In slightly fresher samples, small interstitial grains of flesh-colored K-feldspar can be seen without difficulty. As is typical of the JK suite, a range of textural variations occurs and no basis was found for proving that rocks on both sides of the zone of complicated branch faulting are identical. Thin-section study of rocks across the zone (CE-292, CE-338, CE-321, CE-322) confirms that rocks on both sides are compositionally granodiorite. Altered ferromagnesian minerals, including remnant hornblende and biotite, constitute about 15-20% of all the rocks. No modal pyroxene was found. Complete modes were not calculated because of the degree of alteration and some obvious textural differences in the rocks. Nevertheless, the recurrence of fine to medium grain size, similar alteration and degree of tectonization, and composition in the granodiorite range, combine to make these rocks sufficiently similar, so that the freedom to hypothesize large lateral displacement across this part of the fault zone is constrained -- unless the dissimilarity of these rocks is proved. There remains the possibility that such similar rocks could be juxtaposed

after large lateral shift because of the regional occurrence of such rocks within the JK suite. If restriction is accepted for the sake of argument, it is judged that lateral motion only up to a few tens of kilometers, either right-lateral or left-lateral, combined with vertical separation, would then be allowable across this particular branch of the fault zone.

Paposo area.-- Similar granodiorites assigned to the JK suite crop out on opposite sides of the Salar del Carmen fault near Paposo. On the east side of the fault, south of Quebrada Paposo (Pl. 3), a body of fine- to medium-grained biotite-hornblende granodiorite is in fault contact with the gneissic rocks that immediately bound the Salar del Carmen fault. The granodiorite intrudes medium- to coarse-grained pyroxene granodiorite to the northeast, and in turn is intruded by fine- to medium-grained adamellite on the west. Abundant dark aphanitic dikes irregularly crosscut the body. Similar fine- to medium-grained granodiorite crops out on the west side of the fault near Paposo, and its appearance in Aguada Yumbes (S. W. corner of Pl. 2) is closely similar to that seen in Quebrada El Jote (Pl. 3) on the opposite side of the fault. Mineral abundances of a sample from the latter area (T-363) were compared with those of a sample from Aguada Yumbes (S-177) and found to be similar (see Appendix Table 10). A third sample (T-372) from the west side of the fault in Quebrada Paposo has a coarser grain size than the other two samples, but was studied for comparison of composition. Microscopically, it proved to be quite different from the other two rocks.

Samples T-363 and S-177 display the same brownish gray color, grain size, dark mineral abundance, and texture in hand specimen, but some minor petrographic differences are apparent. Sample T-363 contains a slightly more calcic andesine that shows more pronounced oscillatory and normal zoning than that of S-177; the former rock also has a greater ratio of hornblende to biotite. Their microscopic appearance is otherwise similar.

To determine whether or not these granodiorites on opposite sides of the Salar del Carmen fault are identical would require a more thorough study of the bodies and statistical sampling. The similarity of the rocks is difficult to ignore. Andesites occur on both sides of the Salar del Carmen fault south of Paposo tending to support the idea that perhaps lateral displacement across the Salar del Carmen may not be exceedingly large. The andesites on the east of the Salar del Carmen fault are covered with colluvial debris and poorly exposed on the coastal escarpment. The writer has no basis for either associating or dissociating them from the andesites to the west of the fault.

Cerro Cristales area.-- The third area in which similar granitic rocks occur on opposite sides of the Atacama fault is at the latitude of Cerro Cristales (Pl. 1). There is a tendency for rocks of the JK suite to be more consistently hornblendic over a wider area than seen elsewhere in the map area. Fine- to medium-grained, and medium-grained equigranular hornblende tonalite, hornblende diorite and hornblende granodiorite crop out east of the Salar del Carmen fault, in the block between the Salar del Carmen and Caleta Coloso faults, and

west of the Caleta Coloso fault. The dark mineral abundance of these rocks varies from about 25 to 50%, but stubby prismatic hornblende without biotite is characteristic, giving all these rocks a similar appearance in hand specimen. Again, the variability and regional occurrence of rocks of the JK suite is emphasized, but the writer is impressed with the general resemblance of rocks sampled on opposite sides of the Salar del Carmen fault in that area.

Another argument that might be proposed for limiting the amount of allowable lateral displacement on the Salar del Carmen fault in this same area involves the apparent continuity of a large pluton beneath an area extending from east of the Salar del Carmen fault to west of the Caleta Coloso fault. Granodiorites of the KT suite to the west of the Caleta Coloso fault are similar to those east of the Salar del Carmen fault, although the predominant type in the first area -- biotite-hornblende granodiorite (PA-104B, PA-104C) tends to have a slightly higher dark mineral abundance; rocks in the second area are locally gradational to adamellite. Present data neither prove nor disprove that the rocks across the fault are part of the same pluton. A detailed petrologic study would be required to see if zoning can explain minor differences across the fault. Moreover, the occurrence of other similar granodiorite stocks to the south along the east side of the Salar del Carmen fault demands that a unique relation across the fault be established before lateral displacement of one of the other bodies is precluded.

Conclusion

Geologic evidence for large vertical displacement along the Atacama fault is concrete, and one can reasonably explain the distribution of rocks along the fault by vertical offset alone -- as some Chilean geologists would strongly prefer to do. However, an opponent of strike-slip displacement would have to explain the abundance of horizontal slickensides, the near vertical attitude of most of the faults, and the linearity of the fault traces -- particularly the single trace south of Pampa Cachina (Pl. 5) and the Salar del Carmen fault (Pls. 1 and 2).

In this writer's opinion, the great length of the Atacama fault, the profound shearing observable along its main zones, and the length of linear segments of the fault demand a component of lateral displacement measured at least in tens of kilometers.

An advocate of hundreds of kilometers of horizontal displacement must face the arguments for apparent constraint on such large offset. Even though these arguments for constraint are not conclusive, there is no real need to hypothesize displacement of hundreds of kilometers.

Restricting lateral displacement along the eastern branch of the El Salado sector to a few tens of kilometers is not unreasonable in view of the marked fault branching in the Sierra del Carmen. Additional strike-slip displacement could have been accommodated on parallel breaks to the west.

Along the Salar del Carmen fault, attempts to reconcile a minimum lateral displacement with the constraints along that fault lead to a stipulation of right-lateral horizontal displacement up to a few tens of kilometers. Limited amounts of horizontal strain could have been absorbed on numerous branch faults.

The largest speculative lateral offset suggested by the mapping is an apparent right-lateral separation -- amounting to 80-100 km -- of two northeast-trending bands of Paleozoic basement rocks. One band crops out in the Cerro Yumbes-Cerro Paraña ve area (Pl. 2), and the other in a broad area east of Taltal (Pl. 3, 4, 5). Shifting these bands to alignment would do no violence to juxtaposition of the other rock units because of their great regional extent and the flexibility allowed in reconstructing effects of large vertical motion. Nevertheless, the writer adheres to the constraints that must first be disproved before larger displacement can be advocated.

In summary, a best judgment of total displacement on the Atacama fault includes (1) vertical uplift of the east side of the fault -- probably of several kilometers, and (2) moderate right-lateral displacement, probably of a few tens of kilometers.

VII. MICRO-EARTHQUAKE SURVEY

GENERAL STATEMENT

A packframe-mounted portable seismograph, similar to those in use by workers of the Lamont Geological Observatory (see Ward et al., 1969), was taken to Chile in 1968 for a reconnaissance survey of micro-earthquake activity in the vicinity of the Atacama fault zone. Systematic recording of micro-earthquakes has been completed by Brune and Allen (1967) along the San Andreas fault in California, and similar surveys have subsequently been reported by Ward et al. (1969) for Iceland, Tobin et al. (1969) for the Rift Valley of Kenya, and Boucher and Fitch (1969) for the Denali fault in Alaska. The intention was to leave the single instrument operating unattended for 24-hour periods near areas where geologic mapping was being carried out.

The usefulness of recording in the micro-earthquake range for purposes other than recording aftershock sequences is discussed at length by Oliver et al. (1966). Sampling of micro-earthquakes is a means of monitoring the tectonic activity of an area and can be used in some cases to establish the overall seismicity of a region. In this study the purpose of the micro-earthquake survey was simple -- to determine whether micro-earthquakes were occurring in the immediate vicinity of the Atacama fault zone. The design of the program was to move a single instrument to evenly spaced points along the Atacama fault paying particular attention to events with an S-P time of less than 3 sec; the level of near seismicity would hopefully allow some comment on the degree of activity of the fault.

An earthquake with an approximate magnitude of 7.5 had occurred offshore near Taltal on December 28, 1966 (Pitt and Ellis, 1968; Lemke et al., 1968; Arabasz, 1968), but neither the main event nor its aftershock sequence bore any likely relation to onshore faults. Although it was anticipated that micro-aftershocks of the large 1966 earthquake would be recorded, activity of the onshore faults was of primary concern.

INSTRUMENTATION

The instrument used in this study is one of three packframe-mounted portable seismographs packaged in 1967 at the Caltech Seismological Laboratory under the direction of F. Lehner. A Ranger type seismometer (T_0 = 1 sec, M = 2 kg, R = 50 Ω) was used in connection with a Teledyne EA-310 filteramplifier, a selectable filter (CIT 12025) for band limitation (set at 40 Hz -- narrow band, high frequency), and an output amplifier (CIT 12027) that drives a Brush pen motor. For the pen galvanometer, T_g = .05 sec, R = 1300 Ω. A Sprengnether miniature drum recorder using smoked paper (21.6 × 28 cm) was arranged for spring drive for use in Chile and operated at a paper speed of 25 mm/min, which allowed recording for a period up to 25 hours. The instrument was operated without a radio for time calibration because of the location, the use of a single instrument, and the intention to simply read S-P intervals. Minute marks were imposed on the record by a Sprengnether clock. Two battery packs (12 volts, 18 volts) of standard C and D flashlight cells

provide power for continuous operation of the instrument for a one-week period.

The response curve for the instrument is almost identical to Curve C of Brune and Allen (1967, p. 278), the curve indicated as representative for most of their recording sites. Maximum gain for the backpack instrument at 20 Hz is 3.0×10^6. The recorder box, seismometer, and backpack weigh approximately 27 kg and constitute a highly portable system which can operate at moderately high gains. The ability to operate without benefit of an external power source and the use of readily available flashlight cells were advantageous in the remote areas of Chile. Visible recording on smoked paper has been recognized as an advantageous technique for allowing immediate interpretation of data in reconnaissance field programs.

FIELD PROGRAM

Between late July, 1968 and late February, 1969, a total of 16 stations (Fig. 36, Table 2) were established along branches of the major fault zone between latitudes 24° and 26° S. and were operated for a total of 1286 hours. Instrumental difficulties interrupted recording between November and January. Stations were selected at intervals of roughly 20 km or less so that monitoring would be complete for a hemispherical volume of 24-km radius about the station. In many cases the instrument was operated continuously for a minimum of two to three days while in other cases the site was reoccupied several times. Station 4 located near Taltal was reoccupied several times as

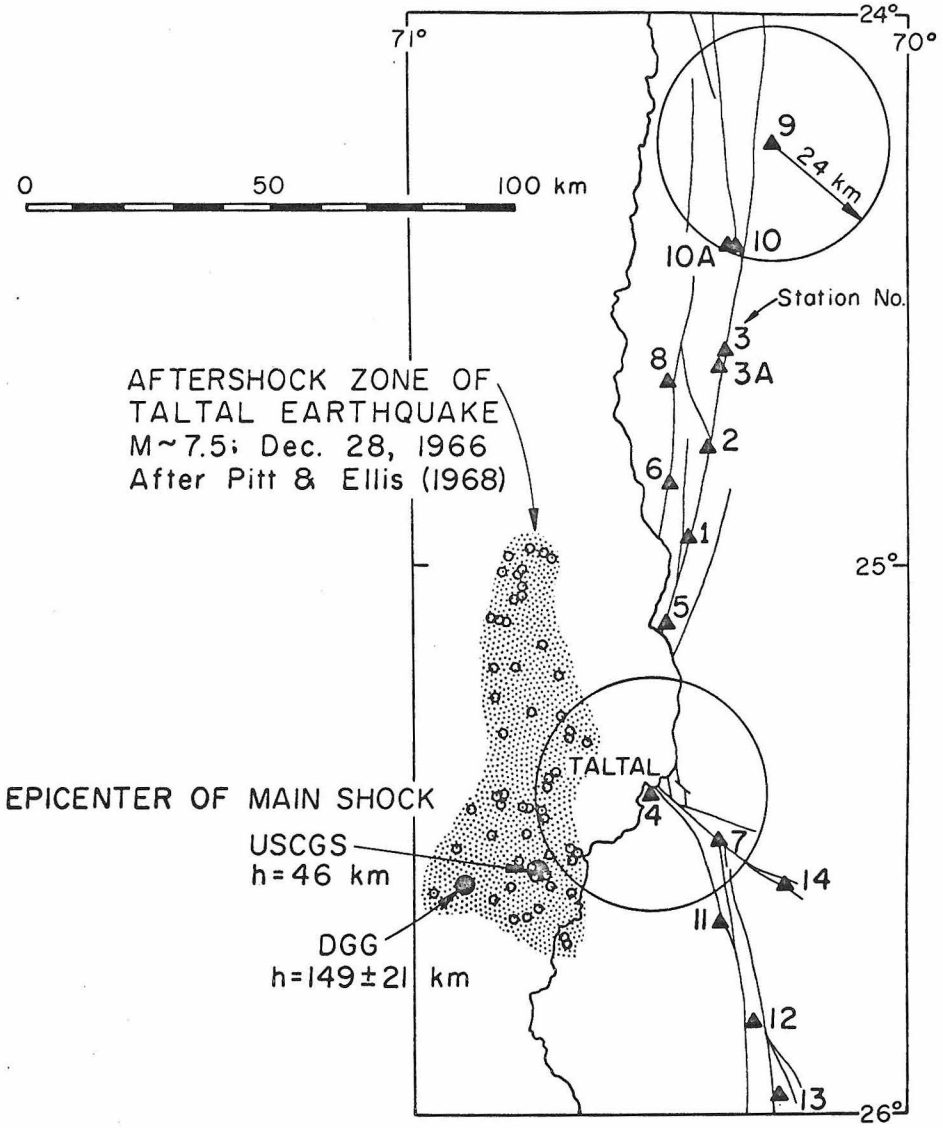

LOCATION OF MICRO-EARTHQUAKE RECORDING STATIONS

Figure 36

a control on temporal changes.

Criteria for site selection included proximity to the major fault zones, accessibility with a four-wheel drive vehicle, exposure of crystalline bedrock, shelter from wind, and distance from cultural noise such as roads. Abandoned prospect pits with horizontal adits were ideal when available. In many locales the subdued topography near the fault traces resulted in exposure to wind, which was a prime source of noise and limited the gain at which the instrument could be operated. Because the seismograph was left unattended for 24-hour periods, the maximum gain was generally attenuated more than would have been necessary if the instrument were constantly monitored.

In addition to stations along the main trace of the Atacama fault, sites were occupied along the Izcuña fault and inland along the Taltal fault while mapping was in progress in those areas. The priority of mapping restricted micro-earthquake recording to a central segment of the Atacama fault zone. Under different circumstances stations would have been picked with a greater spacing and operated for shorter intervals to give a more extensive sampling of the fault.

DATA ANALYSIS

The procedure followed for reducing the micro-earthquake data is straightforward. An S-P time was read for every recorded event, except those off scale, and the events were counted and divided into three groups: (1) $S\text{-}P < 3$ sec, (2) $S\text{-}P \geq 3$ sec but ≤ 10 sec, and (3)

S-P > 10 sec. For each station the number of hours of noise-free or useful recording was noted and used to calculate the number of events per day for each category. A correction term was then applied for different levels of attenuation in order to normalize the data to a standard gain.

A summary of the micro-earthquake data is presented in Table 2 which contains a tabulation of the number of events recorded, together with corresponding statistics in terms of adjusted events per day. The order of listing of attenuations follows the decreasing proportion of time for which a particular setting was used at a station. The standard gain was selected as 24 dB because it was the median level of attenuation at which the instrument was operated in terms of proportion of time. Correction to the standard gain was made by multiplying the number of events per day at a certain attenuation by 2 raised to the (attenuation - 24)/6 power. Boucher and Fitch (1969) use this standardization procedure which assumes a proportionality between the number of earthquakes recorded at a particular site and the gain of the instrument. The multiplication factor is, of course, an amplitude correction, but is commonly judged to be reasonable for correcting data of this type. For 85% of the recording time, the correction term does not exceed a factor of 2. The final normalized statistic for events per day at each station is an average of the corrected numbers for the various gains. There was a close correspondence between the number of observed events per day and the normalized number of events per day, with differences generally less

Table 2. Summary of Micro-Earthquake Data

Station	Lat. S.	Long. W.	Date first Occupied	Useful Recording Hours	Attenuation (dB)	Events Recorded	Events/Day (normalized to std. gain) 0-3sec	3-10sec	>10sec
1	24°56.5'	70°25.9'	7-30-68	58.7	30,18,24	28	0	7	3
2	24°46.5'	70°23.4'	8-1-68	56.5	30,18,12	62	0	10	10
3	24°35.8'	70°21.1'	8-12-68	90.8	30,24,36,18	94	0	8	21
3A	24°37.4'	70°21.9'	8-19-68						
4	25°24.8'	70°30.0'	8-16-68	203.2	18,24,12,30	312	0	16	6
5	25°05.6'	70°28.7'	8-27-68	34.7	24,18	18	0	7	4
6	24°51.1'	70°28.3'	9-9-68	49.9	30,24	19	0	10	8
7	25°30.4'	70°22.1'	9-22-68	93.0	30,36,24	60	0	15	18
8	24°39.8'	70°27.6'	9-26-68	49.2	18,24	58	0	7	12
9	24°14.2'	70°16.0'	10-1-68	66.8	24,18,12	85	0	2	14
10	24°25.5'	70°20.2'	10-11-68	153.4	30	72	0	4	18
10A	24°25.5'	70°21.3'	10-12-68						
11	25°39.3'	70°22.3'	1-30-69	112.7	12,18	200	0	8	7
12	25°50.4'	70°17.7'	2-13-69	66.9	24,30	62	0	10	17
13	25°57.6'	70°14.2'	2-16-69	56.7	18	98	0	6	15
14	25°34.6'	70°14.4'	2-20-69	61.8	18,24	118	0	12	17

than a factor of 2.

S-P intervals were read to an accuracy of 0.5 sec and are plotted (versus number) for each station in Figure 37. Events with an S-P time of an even second are grouped with events having an S-P time a half-second greater. For events with S-P > 20 sec, uncertainty in picking the S-arrival often precluded accuracy of 0.5 sec so that most of these intervals are approximate to within a few seconds.

DISCUSSION

The Problem of Events with S-P < 3 Sec

The basis for interpreting the S-P time intervals is the approximation that 1 sec S-P time is equivalent to 8 km distance. This assumes a compressional velocity of 5.8 km/sec, a straight line path to the source, and an elastic half space with σ (Poisson's ratio) = 1/4. For this reason, it is stated that a hemispherical volume of 24-km radius about the station is monitored when there is control for recording events with S-P < 3 sec.

The data in Table 2 indicating no micro-earthquakes with S-P < 3 sec require some explanation. For small events with S-P < 1 sec, decision as to whether they are true micro-earthquakes can be difficult, especially with data from a single instrument. A small burst of noise can have an appearance similar to a small shock since both can have an abrupt beginning and no distinct S-phase resolvable at a drum speed of 25 mm/min. Five stations (2, 3, 10A, 11, and 12) each had

one small questionable event that was rejected after consultation with J. Brune, who had greater experience with this problem in recording micro-earthquakes in California. Stations 4 and 14 were more problematical inasmuch as 78 questionable events with S-P $<$ 1 sec had been recorded at station 4 during 203 hours, and 17 such events at station 14 during 62 hours. Again, after careful study with J. Brune, all these events were rejected as probably representing either acoustic or cultural noise.

The questionable events at station 4 (located 2 km from the town of Taltal) were mainly recorded at the highest gain settings and many tended to suspiciously cluster between 6 and 8 o'clock in the morning. Moreover, there is a distinct hiatus between these very close events and numerous micro-earthquakes having an S-P time $\geq$ 3.5 sec at station 4; two clear micro-earthquakes had an S-P time exactly equal to 3.0 sec and for this reason, group (2) was set as 3-10 sec where S-P $\geq$ 3 sec. If the rejected events were accepted, the normalized statistics for events per day would be 8/day for station 4, and 2/day at station 14. The numbers for the other five stations mentioned above would still be close to 0/day. The sampling is interpreted to show virtually no activity, or at most, very little, in the immediate vicinity of the major onshore faults.

Events with S-P $\geq$ 3 Sec

General statement. -- Despite the absence of micro-earthquakes close to the stations, abundant seismic activity was recorded for

larger distances. During 1154 hours of useful recording, 1258 earthquakes registered. Of these, 47 were completely off scale (trace amplitude > 15 mm) throughout the P to S interval, which would give an average of 6 large events per week for the total recording period of 54 days. These events even clipped at 30 dB attenuation, and many of them probably represent shocks with magnitudes exceeding 3.0. Several earthquakes per week were large enough to be felt at Taltal during the writer's 1968-69 stay. When compared to such background seismicity, the low level of seismicity along the onshore faults is striking.

Distribution of S-P intervals and sources of seismicity. -- Figure 37 shows the distribution of S-P times for the various stations with the plots arranged according to the latitude of the station; if the left-hand column is placed above the right-hand one, the sequence from top to bottom is the north-to-south sequence of the stations in Figure 36. Plots for individual stations as well as the plot for the total sample (not included) all indicate a bimodal distribution with one peak for a time interval less that 10 sec and another for a time interval greater than 30 sec. The distribution can neither be explained by a single source nor by a simple attenuation factor -- more than 1/3 of the recorded events have an S-P time greater than 30 sec.

Data compiled by Pitt and Ellis (1968) on the aftershock zone of the 1966 Taltal earthquake are of particular importance here and are included in Figure 36. Locations of the epicenter for the main shock, computed by the U. S. Coast and Geodetic Survey (USCGS) and the

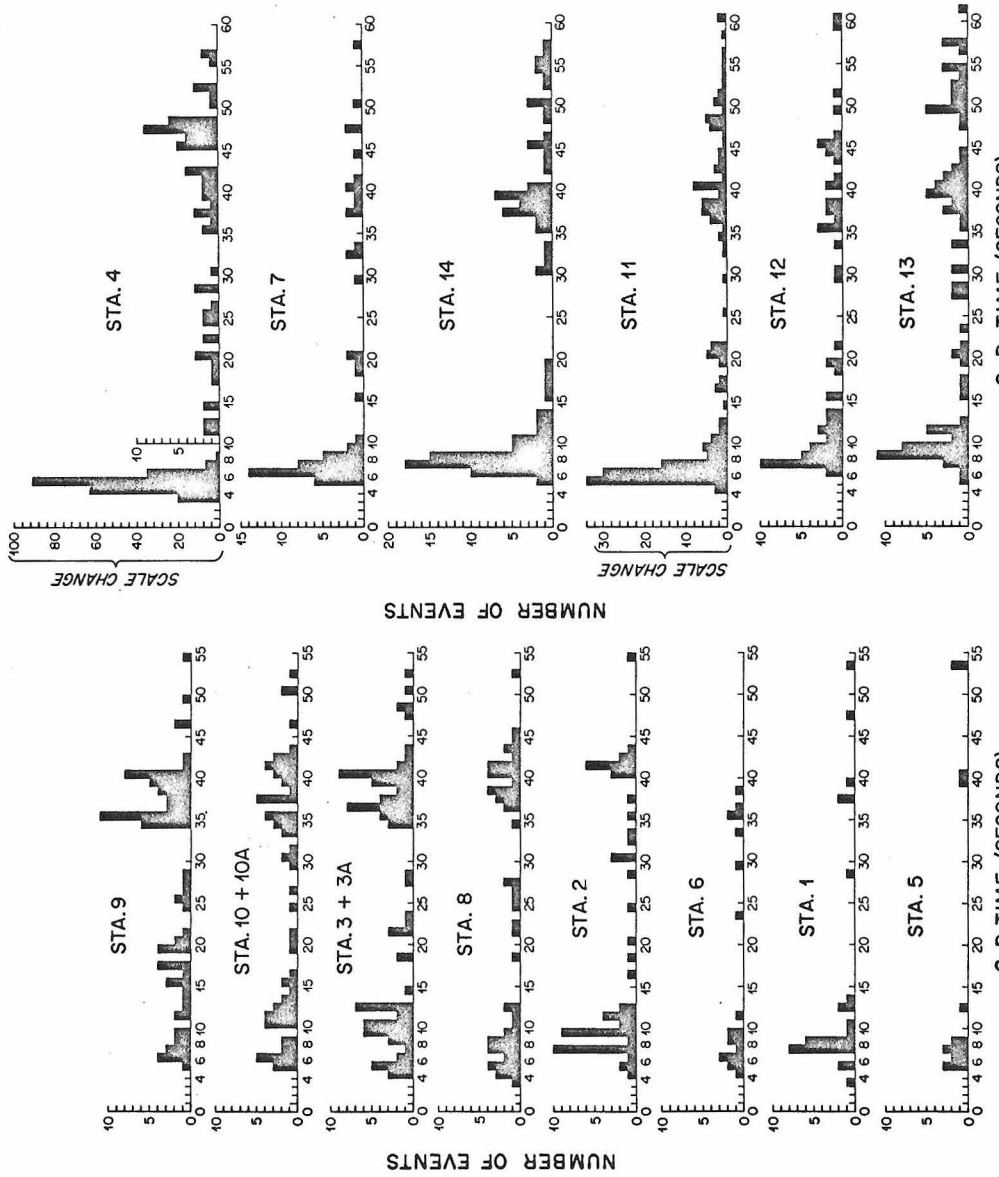

Fig. 37. Distribution of S-P times. (See Fig. 36 for station locations.)

Departamento de Geofísica y Geodesía (DGG) of the University of Chile, are plotted together with 56 aftershocks located by Pitt and Ellis within a 75-km north-trending zone 20 to 30 km off the coastline; most of the aftershocks have an apparent depth of 30 km with a range from 25 to 53 km depth (Pitt and Ellis, 1968).

Inspection of the S-P distributions for S-P < 20 sec in Figure 37 indicates the following:

(1) The station with the highest level of relatively close activity is station 4, with 21 micro-earthquakes having S-P = 3-4 sec.

(2) Inland from station 4 there is a shift from a maximum of 5-6 sec to a maximum of 6-7 sec at station 7; still farther inland the maximum shifts to 7-8 sec at station 14.

(3) Proceeding southward from station 4, the maximum progressively shifts to 5-7 sec at station 11, then to 7-8 sec at station 12, and finally to 8-10 sec at station 14.

These data strongly suggest a source located within the Pitt and Ellis aftershock zone. Examining further:

(4) The data at stations 5, 1, and 6 are not as substantial as those south of Taltal, but taken together with the data for stations 2 through 9, there is an indication of shifts to greater S-P intervals as we proceed northward.

(5) Comparison of station 8 with stations 3 + 3A, and of station 6 with station 2 shows an increase of S-P time away from the coastline.

(6) At stations 10 + 10A and 9, beside the inclusion of greater S-P intervals there is also the persistence of events with small S-P times (5-7 sec). These are not simply compatible with a source within the aftershock zone defined by Pitt and Ellis; the distance is too large. However, extending the offshore zone a few tens of kilometers to the north will explain the smaller S-P intervals at the northern stations.

Taken as a whole, the distributions of S-P intervals suggest that most of the micro-earthquakes with S-P < 20 sec are indeed originating in the offshore aftershock zone of the 1966 Taltal earthquake. Although the 24-km circle of station 4 overlaps the aftershock zone (see Fig. 36), the nearest plotted aftershock (assuming a minimum depth of 20 km) would result in a 4 sec S-P time at station 4. Thus the earlier conclusion that the 24-km hemisphere about station 4 is devoid of activity is reasonable.

Distribution of the maxima for the near micro-earthquakes south of Taltal is compatible with a concentration of activity at the southern end of the Pitt and Ellis aftershock zone -- close to the hypocenter of the main shock (USCGS) at a depth of 30 km. For the northern stations, however, such a concentration would imply a peak for S-P $\cong 17$ sec for stations 10 + 10A and for an interval close to 20 sec for station 9. Attenuation must certainly affect the position of the maxima for the more distant stations. It seems likely that although there is apparently a concentration of activity at the southern end of the aftershock zone, micro-earthquakes continue to occur throughout

the zone and probably occur in a northward extension of the zone. Such activity would explain the range of S-P intervals through 20 sec at the various stations.

Turning our attention to the maxima for intervals greater than 30 sec (Fig. 37), the following observations are important:

(1) Station 9, the northernmost station, appears to be closest to the distant activity with a maximum at 34-41 sec.

(2) There is a shift to greater time intervals for stations south of Taltal, with station 13, the southernmost station, having significant activity with S-P as large as 49-58 sec.

(3) The small variation for S-P maxima between stations 8, 3 + 3A, 10 + 10A, and 9, precludes a major shallow source due north of station 9.

Considering the distance of almost 200 km between stations 9 and 13, and the above observations, it is judged that the S-P maxima for intervals greater than 30 sec imply seismic activity to the northeast or northwest of our array of station sites, or deep activity to the north.

To check the likely source of the more distant seismicity, information was extracted from a computer tape of U. S. Coast and Geodetic Survey hypocenters (including preliminary determinations) for earthquakes with magnitudes greater than 4.0 that occurred during the period of the micro-earthquake survey and within the geographic area bounded by latitudes 21° and 31° S. and longitudes 66° and 74° W.

Epicenters for these events are plotted in Figure 38.

The pattern of seismicity (Fig. 38) consists primarily of a concentration of intermediate-depth earthquakes in the general area of intersection of the borders of Chile, Bolivia, and Argentina, and of earthquakes less than 100 km deep near the coast. The seismicity during a period of several months antecedent to the survey follows the same pattern.

The preliminary nature of some of the hypocenter determinations and common error in an east-west direction for the location of South American shocks in this area lead to reservations about the accuracy of the locations -- for example, the location of a shallow shock as far east as the one plotted near Taltal; nevertheless, the accuracy is sufficient for our present purpose, which is to indicate the probable source of events with the larger S-P times.

The maxima can be reasonably accounted for by attributing most of the activity to the zone of intermediate-depth shocks northeast of our recording sites. Contributions would be expected from zones of shallow shocks near the coast at larger distances, such as near La Serena. Seismicity just beyond the area of Figure 38 would be necessary to explain the largest S-P intervals when higher velocities are assumed, but the S-P distributions imply that such activity would probably be in the northward continuation of the intermediate-depth belt. The recording of high frequency components of such distant activity suggests propagation along a slab of low-attenuation material such as that envisioned in the concept of a lithosphere plunging beneath

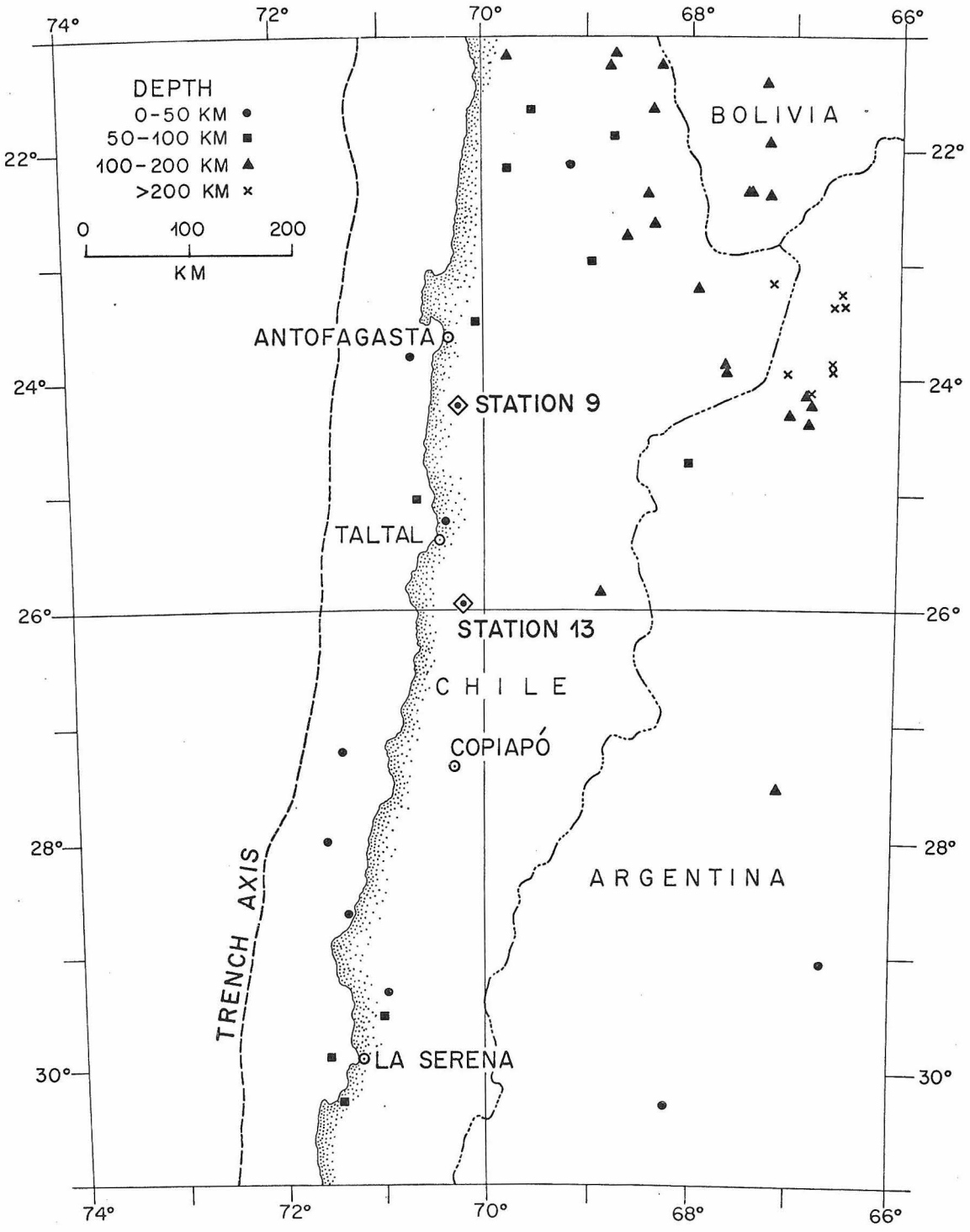

Fig. 38. Epicenters of earthquakes with magnitudes equal to or greater than 4.0 that occurred within the area of the figure during the recording period of the micro-earthquake survey (7-30-68 to 2-24-69). Source of information: U.S.C.G.S.

western South America (Isacks et al., 1968).

With regard to the large shocks that clipped during the actual recording time of the survey, several can be directly related to large events included in Figure 38 -- two in the coastal area near La Serena, one offshore near Taltal, and five in the intermediate-depth zone northeast of station 9. Of the remainder, estimates of the S-P interval and comparison with other events on the same record suggest that they occurred both in the offshore aftershock zone near Taltal and at distances similar to those of earthquakes in the intermediate-depth zone. At least one-third of the 47 off-scale shocks could be assigned to the nearer offshore source.

THE PROBLEM OF MAGNITUDE CALCULATION

It is important to recognize the lower limit of seismicity for which sampling of the hemispheres of 24-km radius is complete. Unfortunately a good deal of uncertainty is involved in computing Richter magnitudes for micro-earthquakes because of the frequency response of the particular instrument used and the various factors entering into an amplitude-versus-distance correction. Isacks and Oliver (1964, p. 1957) discuss this problem and outline a procedure which basically in contained in the following formula:

$$M = \text{Log } A + \text{Log } (G_{WA}/G_X) - \text{Log } A_o$$

where

A = the maximum recorded amplitude in millimeters

G_{WA} = gain of Wood-Anderson torsion seismometer = 2800

G_X = gain of instrument with maximum response for waves of (X) Hz

$-\text{Log } A_0$ = logarithm of the amplitude of a magnitude zero standard earthquake as a function of distance (after Richter, 1958).

It is assumed that the same wave group produces the maximum amplitude on both types of instruments. Isacks and Oliver (1964) further discuss the objections to such a simplified procedure, present a comparison of their magnitude calculations with values calculated from different stations and instruments, and finally judge that their values are good to about ±0.5.

Brune and Allen (1967, p. 284) estimate magnitudes of their recorded micro-earthquakes by the formula:

$$M = \text{Log } A + \text{Log } (G_{WA}/G_{20}) - \text{Log } A_0 + \text{Log } A_{20}$$

where the terms are the same as in the earlier formula and:

G_{20} = gain of instrument with response peaked near 20 Hz

A_{20} = amplitude-versus-distance correction for 20 Hz seismic waves, determined empirically as follows:

$\text{Log } A_{20}$ = 0.55 at 5 km, 1.00 at 8 km, 1.50 at 15 km, 1.70 at 20 km, and 1.80 at 24 km.

Thus in comparing the instrumental recordings of their instruments and standard Wood-Anderson torsion seismometers for the same events, Brune and Allen estimate a correction which is substantial at

a distance of 24 km. A micro-earthquake assigned a magnitude zero by the Isacks-Oliver procedure could have a magnitude 1.8 by the Brune-Allen method.

Such differences in the manner of calculating a micro-earthquake magnitude must be kept in mind when reviewing the literature on micro-earthquakes and comparing rates of occurrence. For example, Brune and Allen (1967, p. 284) state that their sampling of hemispheres of 24-km radius along the San Andreas fault is complete for magnitudes greater than about +0.5, while Ward et al. (1969, p. 667) present data leading to the conclusion that their sampling of roughly similar hemispherical volumes, at lower magnification, would be complete for magnitudes down to -0.7 to -1.0. The latter authors, like Isacks and Oliver, make no correction for 20-30 Hz seismic waves.

Table 3 shows the magnification at different levels of attenuation for the instrument used in this study together with the magnitude of the smallest micro-earthquake which would be detected at a distance of 24 km (assuming a minimum trace amplitude of 1 mm). Magnitudes are calculated both by ignoring the correction term for 20 Hz seismic waves and by incorporating it. The differences between the two magnitudes reflect the basic uncertainty in the calculation.

Amplitude-versus-distance corrections were also calculated for waves of different frequency assuming different attenuation factors, and it is estimated that at 24 km distance, the A_{20} correction of Brune and Allen is probably too large for the Chilean situation. Sampling of

Table 3

Magnitude of events with S-P = 3 sec and having a trace amplitude = 1 mm.

Attenuation	Magnification	Magnitude (after Isacks-Oliver)	Magnitude (after Brune-Allen)
0	3.0×10^6	-1.1	+0.7
6 dB	1.5×10^6	-0.8	+1.0
12 dB	7.5×10^5	-0.5	+1.3
18 dB	3.8×10^5	-0.2	+1.6
24 dB	1.9×10^5	+0.1	+1.9
30 dB	9.4×10^4	+0.4	+2.2
36 dB	4.7×10^4	+0.7	+2.5

the hemispheres of 24-km radius at the standard gain of 24 dB attenuation cannot be complete for magnitudes greater than zero, but quite likely is complete for magnitudes greater than +1.0.

THE PROBLEM OF CORRELATION WITH OTHER AREAS

Differences in instrumentation and difficulties in applying the magnitude scale to micro-earthquakes, as well as other factors such as subjectivity in counting micro-earthquakes and rejecting questionable events (see Stauder and Ryall, 1967), makes comparison of micro-earthquake rates for different regions questionable. Our purpose here is to comment on the possible significance of the low micro-earthquake rate along the Atacama fault.

Levels of magnification for this survey are somewhat lower than those of Brune and Allen (1967) along the San Andreas fault, so comparison between the two areas is difficult. A distance exceeding 200 km was monitored along the Atacama fault without detecting near micro-earthquakes (S-P < 3 sec) with magnitudes greater than about +1.0. Could a similar segment of the San Andreas fault be so quiet? The Cholame-Valyermo sector (Brune and Allen, 1967, p. 286) -- the central section of the San Andreas fault -- is characterized by similar minimal micro-earthquake activity despite the fact that the segment broke during the great 1857 earthquake. Along any other segment, however, if significant activity were occurring just <u>below</u> the level of sensitivity of the Chile survey, several larger events would almost certainly be recorded (J. Brune, personal communication).

The sensitivity of this survey is roughly equal to that of Boucher and Fitch (1969) along the Denali fault in Alaska, yet no 200-km segment of the Denali fault is as quiet as the Atacama fault. Moreover, the useful recording time of this survey exceeds that of the Alaska survey by a factor of 2.

Comparison with the micro-earthquake surveys of Ward et al. (1969) in Iceland, and Tobin et al. (1969) in the Rift Valley of Kenya is confused by conflicting reports of the maximum gain of their instruments. Similar instruments were used in both surveys and are described by Ward et al. (1969, p. 667) as having a maximum gain between 26 and 78 million, while their response curve implies a maximum gain between 3 and 4 million.

INTERPRETATION

The seismic data indicate continuing micro-aftershock activity of the magnitude 7.5 Taltal earthquake, 1 1/2 to 2 years later, in an aftershock zone defined by Pitt and Ellis (1968). Micro-earthquakes of the same size ($M \geqq \sim 1.0$) are virtually absent in the immediate vicinity of the major onshore faults including a 200-km segment of the Atacama fault. One manner of setting a reasonable upper limit on the micro-seismicity near the fault is the following. Suppose that the zone defined exactly by the aftershocks of Pitt and Ellis and no shallower than 20 km were the only allowable source of aftershocks of the Taltal earthquake. What number of recorded events with S-P between 3 sec and 15 sec could not be attributed to that

source? South of station 8 only 6 events during 33 days of useful recording would be marginally excluded from the offshore zone. On the other hand, if a northward extension of the offshore zone were not allowed: 4 events with S-P < 5 sec at station 8, 10 events with S-P < 7 sec at stations 3 + 3A, 13 events with S-P < 9 sec at stations 10 + 10A, and 14 events with S-P < 12 sec at station 9 would be excluded. For these northern stations this would result in an uncorrected rate of 2.7 events/day during 15 days of useful recording. Allowing a northward extension of the offshore zone would resolve the difficulty; if this is rejected for argument, it supposes that micro-earthquake activity near the Atacama fault may be slightly increasing toward the northern end of the survey area -- but only at a rather low level.

The low level of micro-earthquake activity does not lead to the conclusion that the Atacama fault is inactive or dead. To ignore the testimony of Recent alluvial scarps along its branches would be myopic. The limitations of the survey must also be recognized inasmuch as only one segment of the fault was monitored. Also, recording at still higher levels of magnification would lead to detection of activity. The reconnaissance value of this survey should be emphasized and the absence of "hot spots" near the Atacama fault is noteworthy. To advocate continuing accumulation of horizontal strain along the Atacama fault at the latitudes of this study would remain speculative and neither be confirmed nor refuted by the micro-earthquake data.

VIII. GRAVITY-MAGNETIC PROFILES

INTRODUCTION

Four gravity-magnetic profiles, each between 5 and 10 km long, were established across the Atacama fault within the map area of this study -- two across the broad fault zone of the El Salado sector south of Taltal airport, and two across the Salar del Carmen fault scarp north of Paposo. Locations of the profiles are indicated in Appendix Plates B and D. The gravity and magnetic measurements were undertaken for the following reasons: (1) No geophysical examination of the fault had been made in the area, and the offer of collaboration by the Departamento de Geofísica y Geodesía of the University of Chile presented a valuable opportunity to gather preliminary geophysical information. (2) It was of interest to determine whether the fracture zones could be correlated with distinctive gravity or magnetic anomalies. The possibility of encountering a gravity or magnetic "signature" associated with a fault zone is always alluring and, in this case, would bear on the correlation of the El Salado and Salar del Carmen sectors of the Atacama fault. (3) Local problems such as the curious development of elongate closed depressions, 10-15 km long and about 5 km wide, along the Salar del Carmen fault (see Pls. 1 and 2) motivated gravity profiling across one of the basin-like depressions, herein termed "Cuenca 1975". (4) Finally, mineralization along the Atacama fault, particularly the occurrence of iron "pods" as tectonic inclusions within the fault zone north of El Salado, offered potential value to magnetic profiling.

Unfortunately, the results of the gravity and magnetic work (Figs. 39-42) offer no clear help in correlating the Salar del Carmen and El Salado sectors. Because they present little information of great importance to the main problems of this thesis, only a qualitative interpretation of the data is presented herein. Hatherton and Hunt (1968) have called attention to comparison of gravity characteristics of major transcurrent faults, so that while the gravity data along the Atacama fault are supplementary here, their inclusion may be a useful contribution.

GRAVITY AND MAGNETIC MEASUREMENTS

A Worden Prospector gravity meter (#816) was used to make the gravity measurements. Observed gravity values plotted in Figures 39 to 42 are relative to a base station in each profile, not tied from profile to profile. Measurements of vertical magnetic intensity were made with a Jalander fluxgate vertical magnetometer (accuracy: ±10 gammas); plotted values are corrected for drift and likewise are relative to a base station in each profile.

Station elevations were surveyed with a Wild-Heerbrugg T-1 transit allowing sufficient accuracy (±20 cm between successive points) for relative elevations in each profile. Only the Quebrada de la Cachina profile was tied to a bench mark; the other profiles are tied to points whose elevations are photogrammatically determined on the 1 : 100, 000 base maps. The average spacing of stations is about 200 m, becoming greater away from the traces of the major faults.

PRESENTATION OF DATA

For each of the four profiles, values of observed gravity, free air gravity, simple Bouguer gravity, and vertical magnetic intensity are plotted (Figs. 39-42). Values of observed gravity are corrected for both instrumental and diurnal drift. The free air and Bouguer gravity values incorporate a latitude correction for each station (international gravity formula, 1930) and are referred to a datum above sea level in each profile (see figure captions, Figs. 39-42). The plots of simple Bouguer gravity, i.e., uncorrected for terrain effects, assume a density of 2.67 g/cm^3. Terrain corrections were made for four to six stations in each profile (discussed below) to a distance of 22 km using the method of Hammer (1939). The gravity profiles are not corrected for an east-west regional gradient.

The profiles were laid out normal to the fault lines and are essentially linear, except for the western end of the Quebrada de Yumbes profile, which has been projected onto a straight line. The topographic plots and station locations are based on the transit data. Mapping of the surface traces of the faults allows their location; they are arbitrarily plotted as vertical.

Unless otherwise noted, discussion of gravity anomalies in the individual profiles refers to simple Bouguer gravity.

DISCUSSION

Quebrada del Pingo Profile

The Quebrada del Pingo profile (Fig. 39) is 10 km long and trends N. 77°-81° E. along the axis of Quebrada del Pingo (Appendix Pl. D, Pl. 5). Figure 31 includes the area of the profile, which begins at the right edge of the photo in Quebrada del Pingo, crosses the alluviated expanse of the Atacama fault zone, crosses the Aguada Chépica fault a few hundred meters south of point D, and continues 2 km along Quebrada de Cifuncho. Terrain corrections at station 1 (+0.95 mgal), station 5 (+0.88 mgal), station 18 (+0.47 mgal), and station 35 (+0.75 mgal) indicate that the form of the profile of Bouguer gravity would be virtually unaffected by their incorporation.

Superposed on the eastward regional gravity gradient are positive anomalies within the Atacama fault zone and a small step of about 1 milligal across the Aguada Chépica fault. The large anomaly of 9 milligals occurs along the eastern margin of the Atacama fault zone, where silicification and hydrothermal alteration are common. Immediately to the north, andesites form a resistant ridge bounded by two parallel faults (Fig. 31). A negative magnetic anomaly of 180 gammas coincides with the western one of these faults. The gravity anomaly may be related to buried relief -- either a ridge or hill -- along the projected axis of the fault-bounded ridge. The magnitude of the anomaly, though, is somewhat difficult to explain, if it is real. The half-width of the anomaly cannot be more than 150 m -- the distance between stations 6 and 7 is 212 m. Using formulas of Nettleton (1940) for a buried sphere

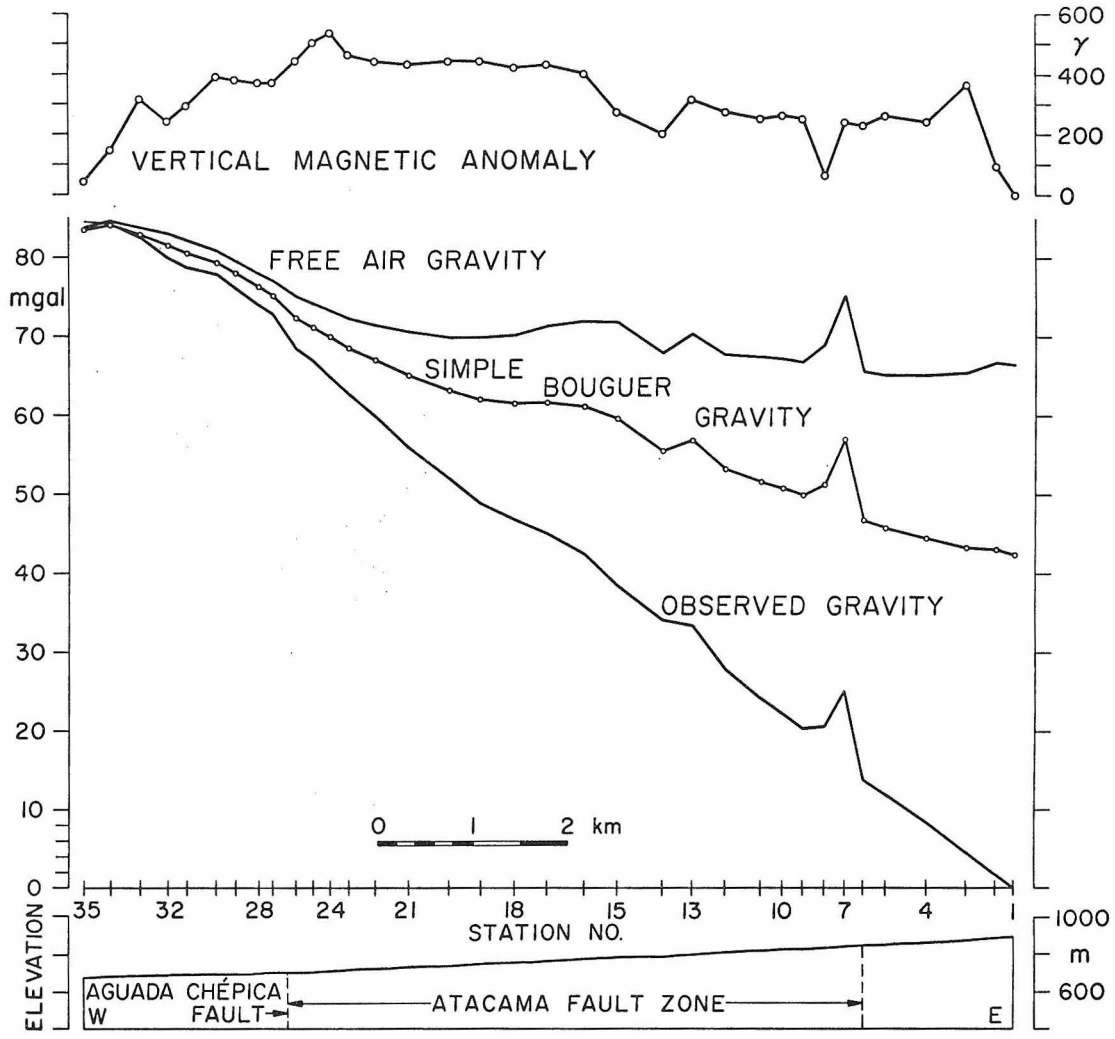

Fig. 39. Reduced gravity and magnetic measurements across the Atacama fault zone at lat. 25°37'S. Values relative to station 1. Free air and Bouguer gravity corrections to datum 680 m above sea level.

and a buried cylinder, calculations indicate that the effect of a very shallow ridge, i.e., a horizontal cylinder, would approach the large anomaly only by allowing the maximum half-width of 150 m and using a density contrast close to 1.5 g/cm^3. The magnetometry rules out invoking the presence of a high-density magnetically susceptible body. The anomaly remains enigmatic.

Broad buried ridges of basement rock paralleling the north-northwest trend of ridges north and south of Quebrada del Pingo (Fig. 31), can account for the smaller positive anomalies within the Atacama fault zone. The step of about 1 milligal across the Aguada Chépica fault may reflect uplift of basement on the west, consistent with the sense of displacement on the fault to the north.

Quebrada de la Cachina Profile

The Quebrada de la Cachina profile (Fig. 40) crosses an alluviated segment of the Atacama fault trough 16 km south of Quebrada del Pingo along the axis of Quebrada de la Cachina (Appendix Pl. D, Pl. 5). The profile is 8.8 km long and trends N.68°-74° E. The narrower dimension of the Atacama fault zone, as compared to that in Figure 39, is due to convergence of several fault strands to the north of the profile (see Pl. 5).

Terrain corrections are again negligible; their only effect would be to systematically raise the profile of simple Bouguer gravity. The following terrain corrections were calculated: +0.31 mgal at station 1, +0.45 mgal at station 12, +0.20 mgal at station 22, and +0.19

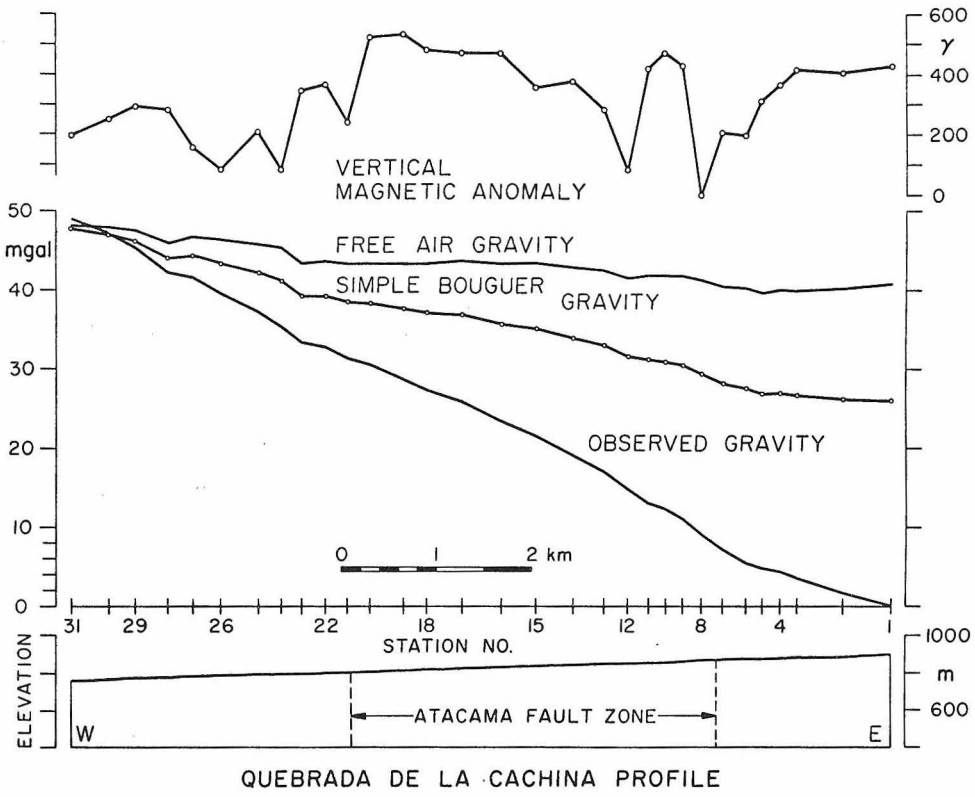

Fig. 40. Reduced gravity and magnetic measurements across the Atacama fault zone at lat. 25°46'S. Gravity values relative to station 1. Magnetic values relative to station 8. Free air and Bouguer gravity corrections to datum 760 m above sea level.

mgal at station 19.

No significant gravity anomaly is noted across the Atacama fault zone. The amplitude of the magnetic anomalies suggests a thin alluvial cover. Negative mangetic anomalies coincide with the traces of the easternmost and westernmost branches of the fault zone, but the association of negative anomalies with fracture zones does not appear to be unique.

"Cuenca 1975" Profile

A linear profile 7.8 km long (Fig. 41) was established across the Salar del Carmen fault by crossing its steep eastward-facing scarp at "Cuenca 1975" (Appendix Pl. B, Pl. 2). The profile is normal to the scarp and trends N.84° W. Cylindrical symmetry of the scarp reduces irregular terrain effects; plotting of terrain corrections (Fig. 41) shows that they would systematically raise, and slightly tilt, the profile of simple Bouguer gravity without destroying its remarkable smoothness across the fault. The terrain corrections are: +1.70 mgal at station 04, +1.73 mgal at station 0, +1.42 mgal at station 6, +1.27 mgal at station 12, +0.80 mgal at station 20, and +0.78 mgal at station 29.

The sharp positive magnetic anomalies in the vicinity of the fault are attributed to andesite dikes (see Fig. 6) that are intrusive into Paleozoic metasedimentary rocks on the western side of the fault here, but not into granodiorite on the eastern side. Plotting of the main fault trace at station 7, coinciding with a line on the aerial photographs similar to that in Figure 6 (point A), is apparently erroneous, as is

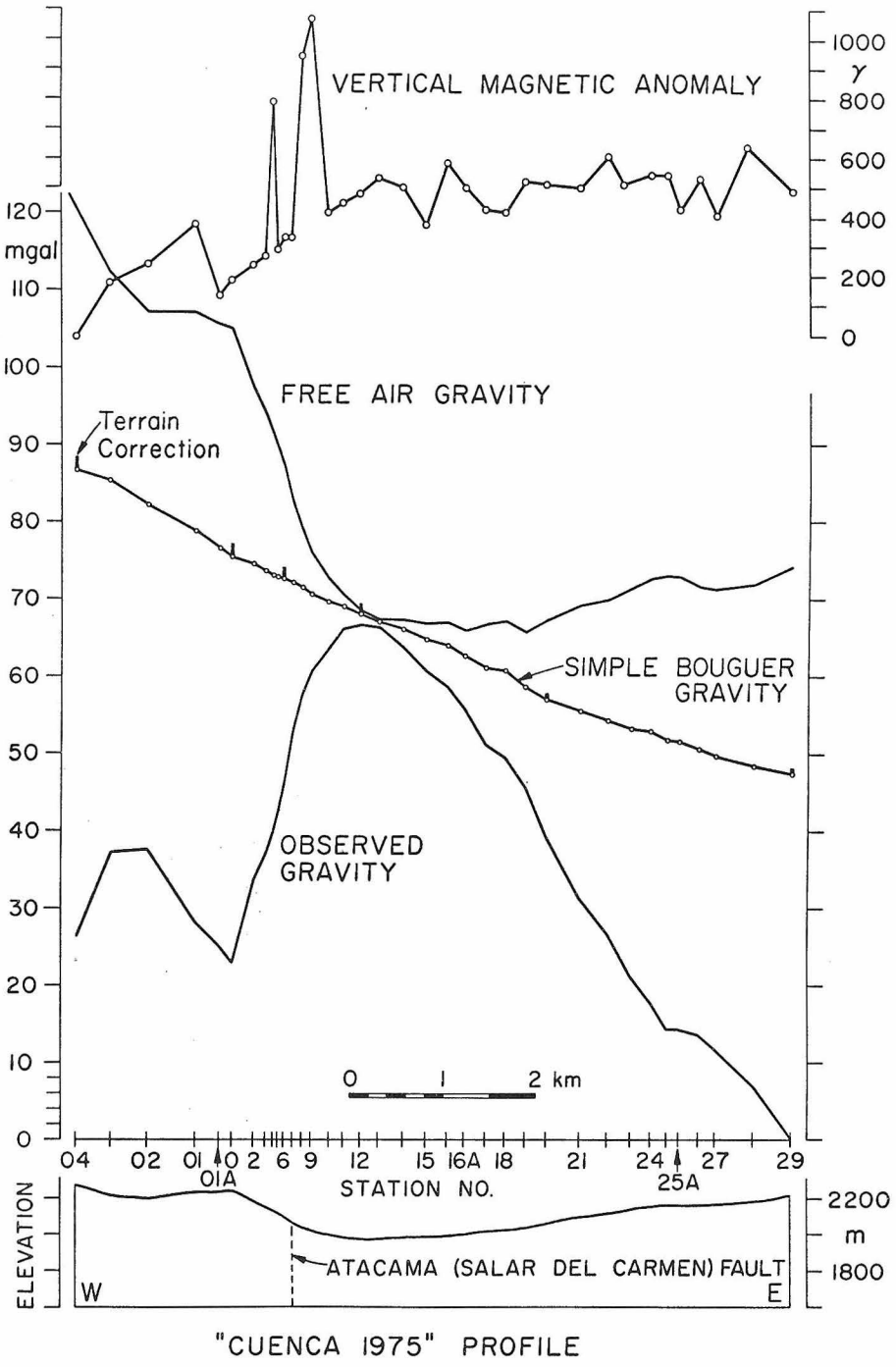

Fig. 41. Reduced gravity and magnetic measurements across the Atacama fault at lat. 24° 42' S. Gravity values relative to station 29; magnetic values relative to station 04. Datum = 1970 m above sea level. Terrain corrections discussed in text.

indicated by the location of the large magnetic spike slightly to the east of station 7. That is, an andesite dike to the east of station 7 must be in the western block. This illustrates the common problem of pin-pointing a fault trace at the base-line of a steep fault scarp where talus or alluvium is not clearly broken at the surface or where synthetic faults occur.

Quebrada de Yumbes Profile

An additional profile 5.4 km long was established across the Salar del Carmen fault at Quebrada de Yumbes (Appendix Pl. B, Fig. 2) in order to afford some comparison with the "Cuenca 1975" profile. Unfortunately, terrain irregularities in the Quebrada de Yumbes area are more severe, as indicated by the terrain corrections in Figure 42, partly because of proximity of the western stations to the steep coastal escarpment. Terrain corrections are: +5.11 mgal at station 1, +4.14 mgal at station 7, +2.12 mgal at station 18, and +2.24 mgal at station 24. The nature of the anomaly at the fault trace is uncertain because of the large terrain corrections, but a step up to the west is suggestive.

SUMMARY STATEMENT

The gravity and magnetic profiles include useful information pertinent to local features, but do not indicate distinctive anomalies that would provide a basis for correlation of the major faults. Some of the fracture zones in the El Salado sector are associated with negative magnetic anomalies of a few hundred gammas. Within the broad zone

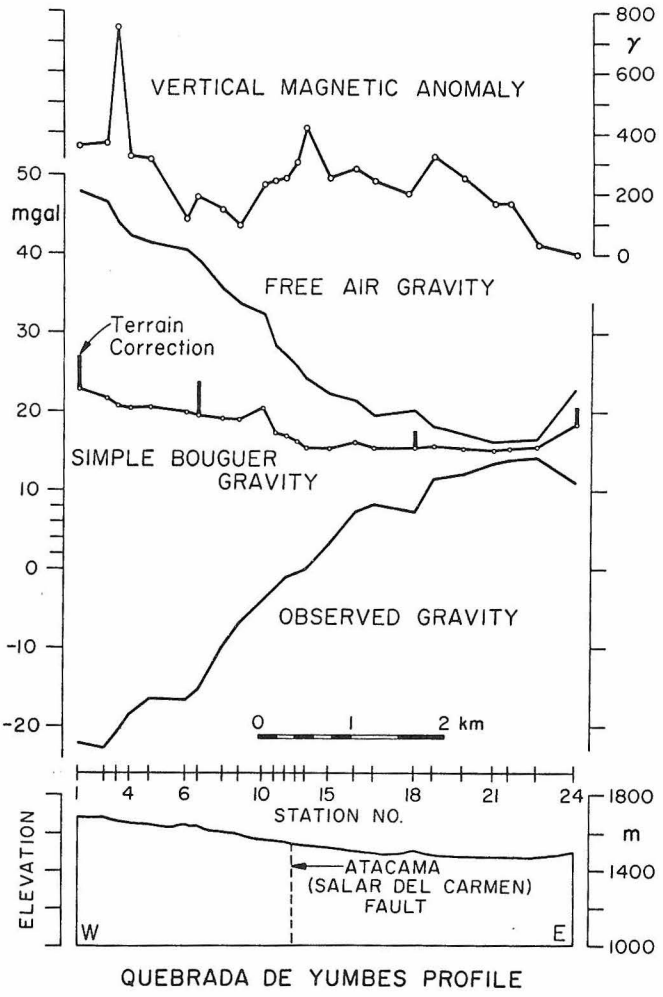

Fig. 42. Reduced gravity and magnetic measurements across the Atacama fault at lat. 24°55'S. Gravity values relative to station 14. Magnetic values relative to station 24. Free air and Bouguer gravity corrections to datum 1460 m above sea level. Terrain corrections discussed in text.

of the El Salado sector, the spacing of stations may not be adequate for recognizing the small gravity effects of individual faults. No large-scale gravity anomalies occur across the fault zones. The smoothness of Bouguer gravity across the Salar del Carmen fault at "Cuenca 1975" is striking. Recognition of the deeper effects of the major fault zones would require more detailed analysis.

IX. SEA FLOOR SPREADING, PLATE TECTONICS, AND THE TECTONIC FRAMEWORK OF NORTHERN CHILE

BACKGROUND

In order to examine the implications of sea floor spreading and plate tectonics to the geology of northern Chile, we need to consider more details of the framework of spreading and plate movement in the southeastern Pacific.

Pattern of Magnetic Anomalies off the Coast of Chile

The general anomaly pattern for the southeastern Pacific Ocean roughly parallels the northeast trend of the Pacific-Antarctic ridge and the East Pacific rise (Pitman et al., 1968, Fig. 10). A branch of the mid-ocean ridge system, the Chile ridge (also called the Chile rise), introduces considerable complexity in the zone between the Chilean coast and the mid-ocean ridge system. The Chile ridge extends from the coast of Chile at about latitude 45° S. northwest toward Easter Island (see inset, Fig. 43).

Magnetic anomalies based on several profiles of airborne magnetometry and the pattern of seismicity in the vicinity of the Chile ridge lead Morgan et al. (1969) to interpret active spreading along north-northeast-trending segments of the Chile ridge at a rate of 2.7 cm/yr (see Fig. 43). An important observation is the occurrence northeast of the Chile ridge of an older block of oceanic crust whose linear anomalies (7 through 21, i.e., 25-55 m.y. BP) have a

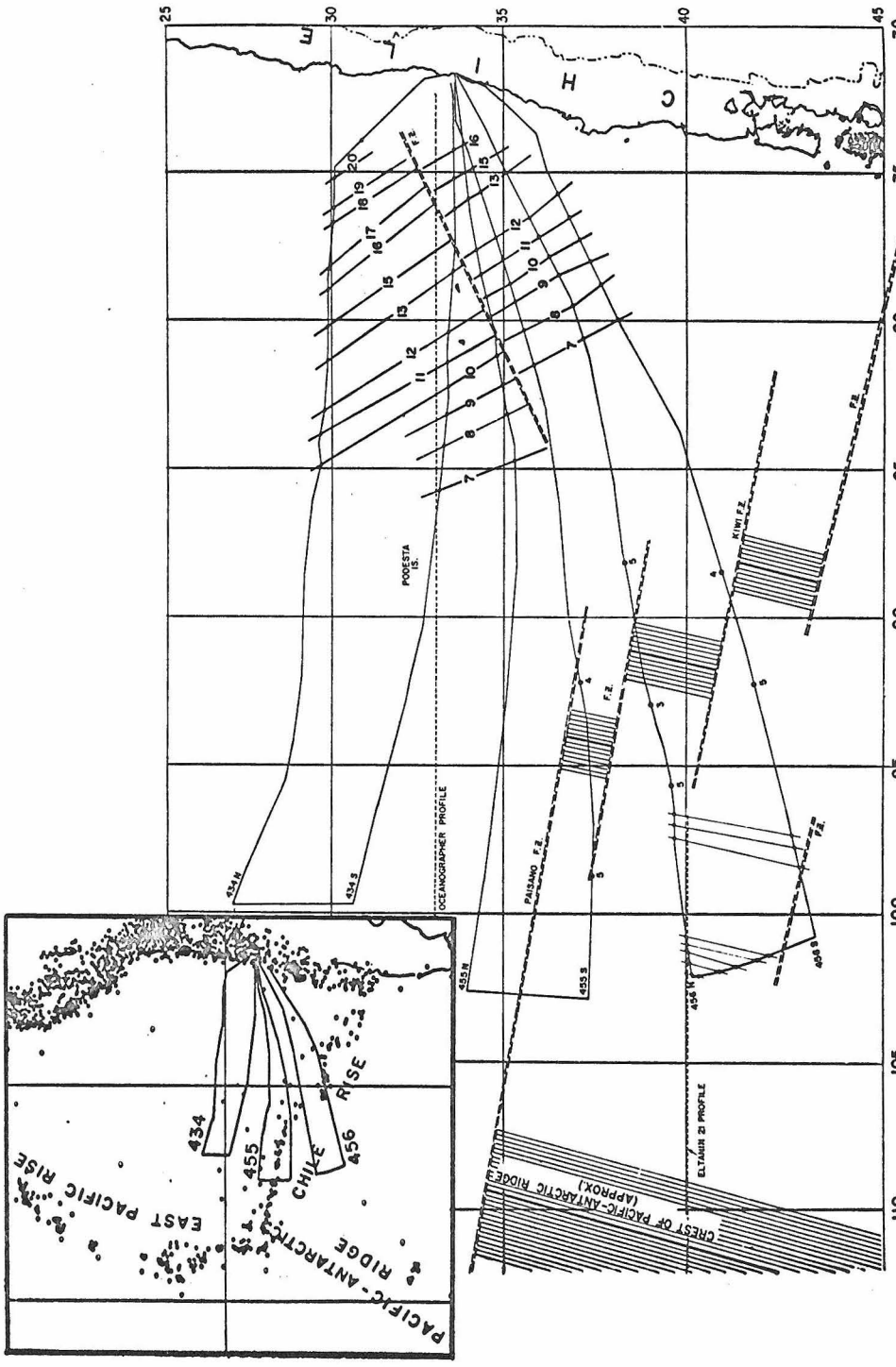

Structural interpretation of the Chile Rise, inferred largely from magnetic anomalies and distribution of earthquake epicentres. Double-dashed lines denote fracture zones, with the schematic linear pattern showing new crust generated by the Chile and Pacific–Antarctic ridges since 3·5 m.y. BP. The numbering of older anomalies (questionable identifications so marked) follows the convention of Heirtzler *et al.*[1]. Dashed lines show tracks of Eltanin 21 (ref. 10) and R.V. Oceanographer[11], whose magnetic data were also considered in present interpretation. Inset map in upper left shows position of tracks with respect to seismic epicentres[9].

Fig. 43. Structural interpretation of the Chile rise. Figure and caption reproduced from Morgan et al. (1969).

north-northwest orientation; the older crust implies a spreading rate of about 4.6 cm/yr and a spreading direction that is inconsistent with either the Chile ridge or the present mid-ocean ridge system (Morgan et al., 1969).

Herron and Hayes (1969), with more substantial control on the young axial anomalies of the Chile ridge (anomalies 1 through 5), show that they trend 320°, not northeast as inferred by Morgan et al. (compare Figs. 43 and 44). Herron and Hayes (Fig. 44) also show that:

(1) Older anomalies trending 335° occur on both flanks of the Chile ridge -- numbers 7 through 12 on the southwest flank, and 7 through 18 on the northeast flank. (The latter correspond to those shown near the coast of central Chile in Fig. 43; Morgan et al. (1969) identify anomalies 7 through 21.)

(2) Axial anomalies of the Pacific-Antarctic ridge parallel its north-northeast trend, but flank anomalies (numbers 7 and older) on the west side of the Pacific-Antarctic ridge north of 45°S. trend north-northwest indicating an ancient spreading pattern that is distinctly different from the present.

Morgan et al. (1969) conclude from their data that either a rotation of the block north of the Chile ridge has occurred or that the spreading pattern has recently changed. Herron and Hayes (1969) conclude the latter and suggest that the latest period of spreading began about 10 m.y. ago; since that time the axis of the Chile ridge and the axis of the Pacific-Antarctic ridge have migrated away from one another.

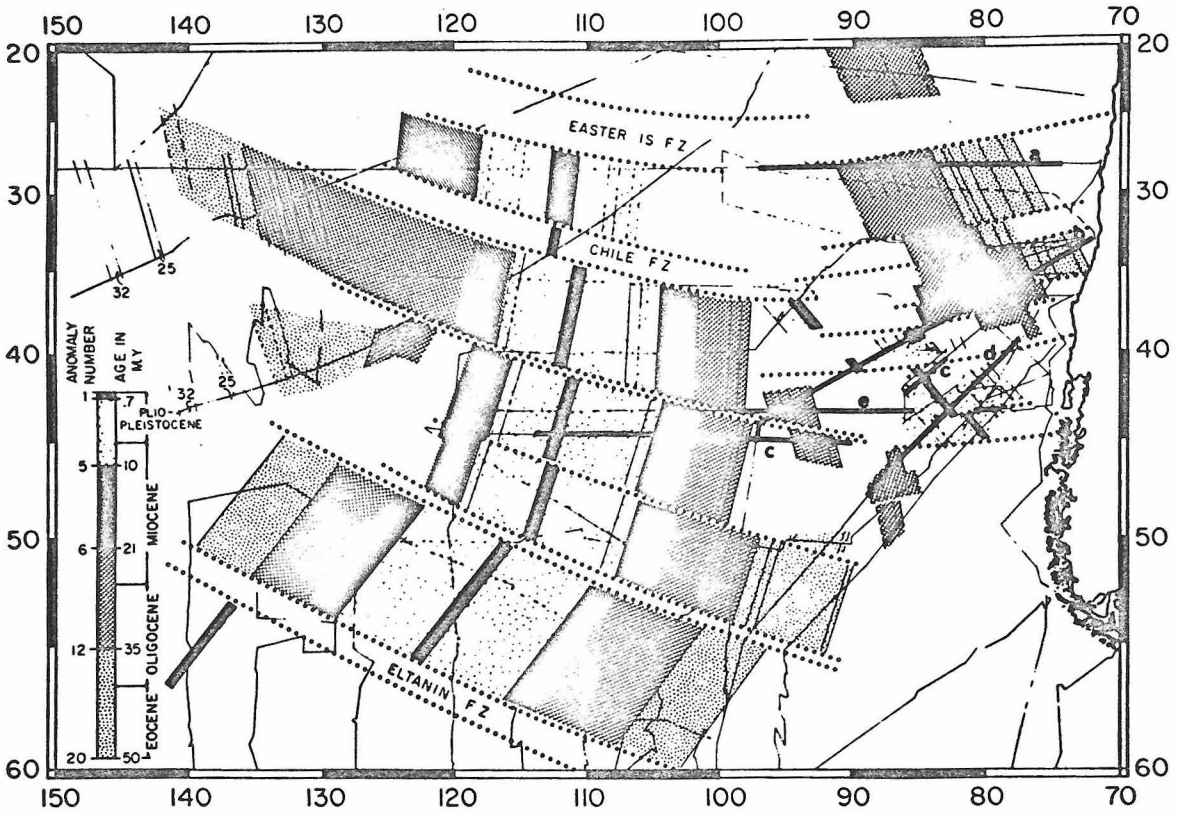

Magnetic anomaly patterns associated with the Pacific-Antarctic and Chile Ridges. Dotted lines represent large fracture zones as inferred from seismicity, topography and discontinuities in the magnetic patters. *Eltanin* and *Conrad* track lines are shown by the thin continuous lines. Magnetic lineations are identified by the thin lines connecting adjacent tracks. Note the three trends outlined north of 50°S; the north-northeast trend of the Pacific-Antarctic Ridge; the north-northwest trend of the flank anomalies (numbers 7 and older), on the west flank of the Pacific-Antarctic Ridge north of 45°S, on the west flank of the Chile Ridge near 45°S and on the east flank of the Chile Ridge north of 40°S, and the northwest trend associated with the axial zone of the Chile Ridge. Identification of the anomalies between 5 and 6 in the basis northeast of the Chile Ridge is tentative.

Fig. 44. Magnetic anomaly patterns off the Chilean margin. Figure and caption reproduced from Herron and Hayes (1969).

During the older episode of spreading (25-50 m.y. BP), the mid-ocean ridge system trended north-northwest instead of northeast as it presently does.

The Plates

Plate boundaries.-- The motion and interaction of rigid aseismic plates is considered in plate tectonics (McKenzie and Parker, 1967; Morgan, 1968; Le Pichon, 1968; Isacks et al., 1968). Along the plate boundaries, new crustal material may be formed (rise type of boundary), crustal surface may be destroyed (trench type), or crustal surface may neither be destroyed nor created (transform fault type).

Rigid plates with different boundaries have been defined by various workers. Generally, North and South America are included in the same plate together with the western Altantic (Morgan, 1968; Le Pichon, 1968; Isacks et al., 1968). Molnar and Sykes (1969) call this the Americas plate. Between the Peru-Chile trench, which forms a western boundary of the Americas plate, and the East Pacific rise, which forms an eastern boundary of the Pacific plate, an intermediate plate occurs whose boundaries are not consistently demarcated in schemes of defining plates. A plate boundary clearly exists along the Chile ridge (Figs. 43 and 44). To the north the seismically active Galapagos rift zone forms another east-west plate boundary (Molnar and Sykes, 1969, Fig. 1). A plate, then, is defined by the Galapagos rift zone on the north, the Peru-Chile trench on the east, the Chile ridge on the south, and the East Pacific rise on the west. Although aseismicity

suggests that it presently defines a single rigid-body plate (see inset, Fig. 43), the Nazca ridge and the Easter Island fracture zone complicate its internal structure (see Menard et al., 1964, Fig. 1).

Spreading rates and directions. -- The South American portion of the Americas plate is spreading westward from the mid-Atlantic ridge at a rate of approximately 2 cm/yr between 25°S. and 50°S. (Heirtzler et al., 1968, p. 2131). North of the Chile ridge, the plate immediately west of the Peru-Chile trench has been spreading eastward from the East Pacific rise at a rate of about 6 cm/yr during the last 10 m.y. (Heirtzler et al., 1968, p. 2131). Axial ridge anomalies along the Chile ridge indicate a spreading rate of 2-3 cm/yr (Herron and Hayes, 1969, p. 79).

Slip vectors derived from earthquake mechanism studies show that the plate east of the East Pacific rise and northeast of the Chile ridge has a horizontal component of motion east to northeast toward the Peru-Chile trench (Isacks et al., 1968, p. 5861).

The Peru-Chile Trench

Some aspects of the Peru-Chile trench have already been discussed in Parts II and V. Off the coast of northern Chile (north of 32°S.) its characteristic features include its linearity and continuity, maximum depths greater than 6000 m (about 8050 m west of Antofagasta), paucity of sediment in the trench bottom, average slopes of about 3°-6° on the nearshore flank and about 2°-3° on the offshore flank, absence of a well developed outer ridge, gravity anomaly minima along the trench axis,

and crustal thinning beneath the outer flank of the trench (Fisher and Raitt, 1962; Hayes, 1966; Zeigler et al., 1957).

Despite considerable study of the trench, its age and origin are not well known, and controversy persists with regard to its tectonic role in sea floor spreading (Scholl et al., 1968; Scholl and von Huene, 1970; Scholl et al., in press). The trench is of particular interest because it is supposed to mark the line of convergence of two plates of lithosphere (Isacks et al., 1968). Le Pichon (1968, p. 3677) indicates differential movement of the plates, i.e., plate consumption at the trench at the rate of 5.2-6.0 cm/yr. The paleomagnetic data of Herron and Hayes (1969) and Morgan et al. (1969) likewise imply roughly similar rates of convergence; the latter workers suggest a rate as high as 10 cm/yr.

The assumption that oceanic crust has been actively underthrusting western South America along the line of the Peru-Chile trench has been challenged (Scholl et al., 1968), because no evidence has been found for the expected deformation of sediments in the trench. Moreover, the volume of undeformed terrigenous sediment in the trench is close to the amount which is estimated to have been supplied by late Cenozoic erosion -- no sediment of this age is obviously missing (Scholl et al., in press). The weight of magnetic and seismological evidence implying that ocean floor has indeed been descending beneath western South America in late Cenozoic time is difficult to refute, but the mechanics involved at the trench axis are not established.

With regard to the age and origin of the trench, Scholl et al. (in press) believe that (1) the structural framework of the trench may have been laid out as long ago as the Jurassic, (2) the present form of the trench has probably existed for the past 20 m.y., and (3) formation of the trench occurred at about the same time as uplift of the Andes and Coast Ranges, which was accompanied by the subsidence of structures such as the Central Valley.

The main structure of the trench appears to be related to extension, as noted earlier in Part V. Scholl et al. (in press) concur with the idea that it is a graben-like structure. (See also Worzel, 1966.) In earlier papers (Scholl, 1968; Scholl et al., 1968; Scholl and von Huene, 1969; von Huene et al., 1968), these authors advance the idea that the continental slope represents downwarped or foundered continental basement rocks, and they explore the implications. Hayes (1966) suggests high-angle normal faulting at the base of the continental slope citing similarities with other trenches. Isacks et al. (1968, p. 5868-5870) discuss extension at trenches, which is predicted to accompany the bending of a down-going slab of lithosphere. (See also Elsasser, 1968.) The reader is referred to Scholl et al. (in press), Isacks et al. (1968), and Malahoff (1970) for further discussion.

TECTONIC IMPLICATIONS IN NORTHERN CHILE

General Statement

Ultimately, the orogenic phenomena of northern Chile must be explainable in terms of crust-mantle interaction and episodes of sea floor spreading. These include: the development of extensive geosynclines in the Paleozoic and the Mesozoic Eras; orogeny and batholithic intrusion in late Paleozoic, Late Jurassic, and Late Cretaceous to early Tertiary time; voluminous andesitic volcanism in the Jurassic and Cretaceous Periods; uplift of the Andes and development of the Peru-Chile trench in Cenozoic time; active volcanism in the Andes; abundant shallow, intermediate, and deep-focus seismicity; and, of course, continuing active faulting. These items constitute too large a problem to discuss here, but some observations might be made that are pertinent to the structural history of the Coast Ranges.

Plate Motions and Strike-Slip Faulting

We have seen that sea floor spreading and plate tectonics imply continuing motion of a lithospheric plate toward the trench, more or less normal to the continental margin of northern Chile. Horizontal motions along large strike-slip faults, however, are difficult to explain when they parallel a boundary of plate convergence, as does the Atacama fault. Large horizontal motion can occur along some plate boundaries by transform faulting (Wilson, 1965), and suitable spreading configurations explain the strike-slip motion along the San Andreas and Alpine faults.

Limited strike-slip motion can be explained by the oblique convergence of two plates. Another possibility is one discussed by McKenzie (1970) for strike-slip motion on the North Anatolian fault. There the horizontal motion is along the boundary of a small rapidly moving plate whose motion is unrelated to that of major plates in the Mediterranean region.

It appears impossible to make the Atacama fault a transform fault (with presently known plate configurations), and relating hypothetical strike-slip motion along the fault at the present time to sea floor spreading poses a serious problem. Extensional faulting, on the other hand, poses no such difficulty and is in accord with the stress distributions generally expected near the trench.

Can strike-slip motion be related to an older episode of spreading? We have already seen that the geometry of smaller plates east of the East Pacific rise is somewhat complicated and could allow motion during an older pattern of spreading that was more oblique to the continental margin (Figs. 43 and 44). It remains to be determined whether the plate between the Galapagos rift zone and the Chile ridge has always consisted of a single rigid-body plate.

If ancient continental movements in the southern hemisphere are considered, motion parallel to the margin of western South America can be postulated. Summaries of the movements of South America and Africa (Heirtzler et al., 1968; Vilas and Valencio, 1970), based on paleomagnetic data and magnetic anomaly patterns in the South Atlantic and Indian Oceans, include the following key points. (1) South America

and Africa moved northward as a single block in Permian to early Mesozoic time. (2) Splitting of South America and Africa occurred between the upper Triassic and middle Cretaceous, during which South America was rotated clockwise and displaced northward. (3) Subsequent to a change in spreading in the South Atlantic about 80 m.y. ago in the Late Cretaceous, South America and Africa have separated by nearly east-west spreading.

Although the nature of plate boundaries along the western margin of South America during the early Mesozoic is unknown, the northward movement of South America during an old episode of spreading offers an attractive rationale for explaining strike-slip motion during the early history of the Atacama fault. This study shows that the continuity of the Atacama fault was disrupted by the Taltal fault in the Tertiary, and that strike-slip movements apparently have not occurred along the Atacama fault between 24°S. and 26°S. subsequent to disruption by the Taltal fault. Because lateral motion on the Taltal fault antedates a period of canyon cutting in the Pliocene, an interesting and logical possibility is that the Taltal fault formed in the Miocene during the interval between 25 m.y. and 10 m.y. BP, during which a change in sea floor spreading caused major readjustment in the oceanic plate between the Peru-Chile trench and the East Pacific rise. The location of the Taltal fault at approximately the same latitude as the Easter Island fracture zone (Menard et al., 1964, p. 239) -- a major fracture zone of the East Pacific rise -- may not be entirely coincidental.

Subsequent to disruption by the Taltal fault, individual segments of the Atacama fault system have been independently reactivated and display block motions that are similar to those displayed on the upper continental slope. Such vertical tectonics can be explained by extension in the area of the Peru-Chile trench. Origin of the faults under a stress system associated with strike-slip faulting and later accommodation of dip-slip motion would perhaps explain the near-vertical attitude of most of the faults.

A more precise dating of both onshore and offshore faulting is needed. The history of sea floor spreading cannot be used to demonstrate the sequence and timing of onshore faulting, but this writer feels that the latter can be fitted within a reasonable scheme that is compatible with the ocean floor history.

X. CONCLUSIONS

(1) Regional geological mapping shows that the Atacama fault is a major structural break that juxtaposes different rocks along nearly the entire extent of a 200-km mapped segment between 24°S. and 26°S. Large vertical separation along the fault is a chief control of the regional distribution of rocks.

(2) The Atacama fault system originated in pre-Late Cretaceous time, possibly syntectonic with the Andean geosyncline in the Jurassic Period. Alluvial scarps along traces of faults that controlled late Mesozoic mineralization bear testimony to a long and probably complicated history of movement. Widespread horizontal slickensides, the linearity of segments of the fault over distances exceeding 100 km, and the near vertical attitude of most of its branches imply strike-slip motion during the early history of the fault.

(3) The El Salado and Salar del Carmen sectors of the Atacama fault are parts of a formerly continuous break through the Taltal area that was disrupted and left-laterally offset 10 km by the Taltal fault during mid- to late Tertiary time. This disruption may have occurred in the Miocene epoch during an interval in which a change in sea floor spreading caused major readjustment in the oceanic plate between the Peru-Chile trench and the East Pacific rise.

(4) Subsequent to segmentation of the Atacama fault, individual sectors have been reactivated independently and display a sense of most recent motion that is predominantly, if not exclusively vertical.

Abundant Quaternary and Recent alluvial scarps displayed along all segments of the Atacama fault -- including branches of the El Salado sector that are truncated by the Taltal fault -- attest to continuing activity.

(5) Alluvial scarps displaying an anomalous ridge-trench-ridge morphology are not necessarily indicative of strike-slip movement; they may be developed by non-tectonic processes combined with vertical faulting.

(6) Lateral motion on the Taltal fault had ceased by Pliocene time, resulting in a structural "knot" that presently would constrain lateral motion along truncated branches of the El Salado sector of the Atacama fault. The northwest-curving branch of that sector that escapes truncation by the Taltal fault, namely the Aguada Chépica fault, either predates the Taltal fault or developed contemporaneously with it. Both onshore and offshore data prove that the Aguada Chépica fault has been more recently active.

(7) Offshore data demonstrate that Cenozoic faulting in the coastal area is not restricted to a narrow localized zone along the Atacama fault system. Major faulting of the upper continental slope begins within 10 to 20 km of the coastline. A very narrow shelf, faulting of sediment aprons on the shelf and upper slope, entrapment basins, and irregular block faulting resulting in the tilting and down-dropping of blocks toward the trench axis all reflect great tectonic instability within the extensional zone of the Peru-Chile trench.

(8) No convincing evidence has been found along any branch of the Atacama fault system between 24°S. and 26°S. for recent lateral offset. On the contrary, the truncation of central branches of the El Salado sector by the Taltal fault without evidence of subsequent thrusting or breaking, and the predominance of recent vertical motion on the Aguada Chépica and Salar del Carmen faults make it difficult to postulate continuing strike-slip motion.

(9) In the sector between 24°S. and 26°S., the Atacama fault is not presently an active strike-slip fault. Vertical block motions characterize recent activity along branches of the fault, particularly north of 25°S. where tilted and uplifted blocks display classic features of young block faulting. A linear fault scarp continuous for at least 100 km along the Salar del Carmen fault reflects recent vertical motion that exactly reverses the sense of large vertical separation implied by the distribution of rocks along the fault.

(10) Late Cenozoic tectonics in the Coast Ranges appear to relate to the formation of the Peru-Chile trench. That segments of the fault have accommodated vertical motion in their recent history is compatible with stress distributions generally expected near the trench and eliminates difficulties that are presented by advocating continuing strike-slip motion along the Atacama fault. Strike-slip displacement may have occurred during an older episode of sea floor spreading, perhaps prior to a change in spreading about 80 m.y. ago.

(11) Although a scheme of consistent lateral offset does not emerge from the present mapping along the Atacama fault, suggestive evidence such as the great length of the fault, the profound shearing observable along its main zones, and the length of linear segments of the fault seem to demand a component of lateral displacement measured at least in tens of kilometers. No need is seen to hypothesize displacements of hundreds of kilometers. Taking into account apparent constraints on lateral offset, the total displacement on the Atacama fault is judged to include several kilometers of vertical uplift of the east side of the fault, and moderate right-lateral displacement, probably of a few tens of kilometers.

(12) A reconnaissance micro-earthquake survey along a 200-km segment of the Atacama fault and along other onshore faults shows virtually no activity, or at most very little, in the immediate vicinity of the major onshore faults. Recording of abundant micro-earthquake seismicity at larger distances implies continuing micro-aftershock activity of the magnitude 7.5 Taltal earthquake (Dec. 28, 1966), 1 1/2 to 2 years later in an offshore aftershock zone defined by Pitt and Ellis (1968).

REFERENCES

Alarcón F., B., and Vergara M., M., 1964, Nuevos antecedentes sobre la geología de la quebrada El Way: Santiago, Univ. de Chile, Inst. Geología, Pub. 26, 28 p.

Allen, C. R., 1962, Circum-Pacific faulting in the Philippines-Taiwan region: Jour. Geophys. Research, v. 67, p. 4795-4812.

_____, 1965, Transcurrent faults in continental areas, in A symposium on continental drift: Royal Soc. London Philos. Trans., v. 258, p. 82-89.

Alvarez S., L., Ortiz O., F., Dobrovolny, E., and Lemke, R., 1967, Efectos geológicos del sismo de Taltal del 28 de Diciembre de 1966: Santiago, Inst. Invest. Geol., Pub. Especial No. 3.

Arabasz, W. J., 1968, Geologic structure of the Taltal area, northern Chile, in relation to the earthquake of December 28, 1966: Seismol. Soc. America Bull., v. 58, p. 835-842.

Barazangi, M., and Dorman, J., 1969, World seismicity maps compiled from ESSA, Coast and Geodetic Survey, epicenter data, 1961-1967: Seismol. Soc. America Bull., v. 59, p. 369-380.

Benioff, H., 1949, Seismic evidence for the fault origin of oceanic deeps: Geol. Soc. America Bull., v. 60, p. 1837-1856.

_____, 1954, Orogenesis and deep crustal structure -- additional evidence from seismology: Geol. Soc. America Bull., v. 65, p. 385-400.

Boucher, G., and Fitch, T. J., 1969, Microearthquake seismicity of the Denali fault: Jour. Geophys. Research, v. 74, p. 6638-6648.

Bowes, W. A., Knowles, P. H., Serrano C., M., and Gruenwald S., R., 1959, Reconnaissance for uranium in the Tocopilla area, Province of Antofagasta, Chile: U. S. Atomic Energy Comm. RME-4534 (rev.).

Bowes, W. A., Knowles, P. H., Moraga B., A., and Serrano C., M., 1961, Reconnaissance for uranium in the Chañaral-Taltal area, Provinces of Antofagasta and Atacama, Chile: U. S. Atomic Energy Comm. RME-4565 (rev.).

Bowman, I., 1924, Desert trails of Atacama: Am. Geog. Soc. Spec. Pub. No. 5, 362 p.

Brüggen M., J., 1950, Fundamentos de la geología de Chile: Santiago, Inst. Geog. Militar, 374 p.

Brune, J. N., and Allen, C. R., 1967, A micro-earthquake survey of the San Andreas fault system in southern California: Seismol. Soc. America Bull., v. 57, p. 277-296.

Burnol, L., and Bournat, G., 1966, Reconnaissance sur les possibilités de mineralisation en cuivre de la cordillere de la côte entre Antofagasta et Paposo -- Province d'Antofagasta (Chile): Santiago, Mission de Coopération Technique Française in cooperation with Inst. Invest. Geol., unpub. rept.

Casertano, L., 1963, General characteristics of active Andean volcanoes and a summary of their activities during recent centuries:

Seismol. Soc. America Bull., v. 53, p. 1415-1433.

Clark, A. H., Cooke, R. U., Mortimer, C., and Sillitoe, R. H., 1967a, Relationships between supergene mineral alteration and geomorphology, southern Atacama Desert, Chile -- an interim report: Inst. Mining and Metallurgy Trans., sec. B, v. 76, p. B89-B96.

Clark, A. H., Mayer, A. E. S., Mortimer, C., Sillitoe, R. H., Cooke, R. U., and Snelling, N. J., 1967b, Implications of the ignimbrite flows, southern Atacama Desert, Chile: Nature, v. 215, p. 723-724.

Cotton, C. A., 1950, Tectonic scarps and fault valleys: Geol. Soc. America Bull., v. 61, p. 717-758.

Davis, W. M., 1903, The mountain ranges of the Great Basin, in Johnson, D. W., Editor, Geographical essays: Boston, Ginn, p. 725-772 [1909].

_____, 1933, Glacial epochs of the Santa Monica Mountains, California: Geol. Soc. America Bull., v. 44, p. 1041-1133.

Denny, C. S., 1965, Alluvial fans in the Death Valley region, California and Nevada: U. S. Geol. Survey Prof. Paper 466, 62 p.

Dragicević, M., 1962, Interpretación de los perfiles de gravedad; Arica, Antofagasta y Valparaíso-Mar del Plata: Santiago, Univ. de Chile, Inst. Geofísica y Sismología, Pub. 28, 10 p.

Dżułyński, S., and Walton, E. K., 1965, Sedimentary features of flysch and greywackes, no. 7 of Developments in sedimentology:

Amsterdam, Elsevier Publishing Co., 274 p.

Elsasser, W. M., 1968, Submarine trenches and deformation: Science, v. 160, p. 1024.

Fisher, R. L., Editor, 1958, Preliminary report on Expedition Downwind: Washington, IGY World Data Center A, IGY General Rept. Ser. No. 2, 58 p.

Fisher, R. L., and Raitt, R. W., 1962, Topography and structure of the Peru-Chile trench: Deep-Sea Research, v. 9, p. 423-443.

Fuenzalida V., H., Cooke, R., Paskoff, R., Segerstrom, K., and Weischet, W., 1965, High stands of Quaternary sea level along the Chilean coast, in Wright, H. E., Jr., and Frey, D. G., Editors, International Studies on the Quaternary: Geol. Soc. America Spec. Paper 84, p. 473-496.

Galli-Olivier, C., 1967, Pediplain in northern Chile and the Andean uplift: Science, v. 158, p. 653-655.

García A., F., 1964, Geología del norte grande de Chile: Santiago, Univ. de Chile, Dept. Geología, 172 p. [1967].

Gutenberg, B., and Richter, C. F., 1954, Seismicity of the earth and associated phenomena (2nd edition): Princeton, Princeton Univ. Press, 310 p.

Hamblin, W. K., 1965, Origin of "reverse drag" on the downthrown side of normal faults: Geol. Soc. America Bull., v. 76, p. 1145-1164.

Hammer, S., 1939, Terrain corrections for gravimeter stations: Geophysics, v. 4, p. 184-194.

Harrington, H. J., 1961, Geology of parts of Antofagasta and Atacama Provinces, northern Chile: Am. Assoc. Petroleum Geologists Bull., v. 45, p. 169-197.

Hatherton, T., and Hunt, T. M., 1968, Gravity profiles across the Alpine Fault, New Zealand: Jour. Geophys. Research, v. 73, p. 5343-5352.

Hayes, D. E., 1966, A geophysical investigation of the Peru-Chile trench: Marine Geology, v. 4, p. 309-351.

Heirtzler, J. R., Dickson, G. O., Herron, E. M., Pitman, W. C., III, and Le Pichon, X., 1968, Marine magnetic anomalies, geomagnetic field reversals, and motions of the ocean floor and continents: Jour. Geophys. Research, v. 73, p. 2119-2136.

Herron, E. M., and Hayes, D. E., 1969, A geophysical study of the Chile ridge: Earth and Planetary Sci. Letters, v. 6, p. 77-83.

Hersey, J. B., 1963, Continuous reflection profiling, in The earth beneath the sea, v. 3 of Hill, M. N., Editor, The sea: New York, Interscience Publishers, p. 47-72.

Hollingworth, S. E., 1964, Dating the uplift of the Andes of northern Chile: Nature, v. 201, p. 17.

Hollingworth, S. E., and Rutland, R. W. R., 1968, Studies of Andean uplift. Part I: Post-Cretaceous evolution of the San Bartolo area, north Chile: Geol. Jour., v. 6, pt. 1, p. 49-62.

Isacks, B., and Oliver, J., 1964, Seismic waves with frequencies from 1 to 100 cycles per second recorded in a deep mine in northern New Jersey: Seismol. Soc. America Bull., v. 54, p. 1941-1979.

Isacks, B., Oliver, J., and Sykes, L. R., 1968, Seismology and the new global tectonics: Jour. Geophys. Research, v. 73, p. 5855-5899.

Kingma, J. T., 1958, Possible origin of piercement structures, local unconformities, and secondary basins in the Eastern Geosyncline, New Zealand: New Zealand Jour. Geology and Geophysics, v. 1, p. 269-274.

Knowles, P. H., Bowes, W. S., Serrano C., M., and Gruenwald S., R., 1959, Reconnaissance for uranium in the Antofagasta area, Province of Antofagasta, Chile: U. S. Atomic Energy Comm. RME-4535 (rev.).

Lachenbruch, A. H., 1962, Mechanics of thermal contraction cracks and ice-wedge polygons in permafrost: Geol. Soc. America Spec. Paper 70, 69 p.

Lambe, T. W., and Whitman, R. V., 1969, Soil mechanics: New York, John Wiley and Sons, 553 p.

Lemke, R. W., Dobrovolny, E., Alvarez S., L., and Ortiz O., F., 1968, Geologic and related effects of the Taltal earthquake, Chile, of December 28, 1966: Seismol. Soc. America Bull., v. 58, p. 851-859.

Lensen, G. J., 1958, A method of graben and horst formation: Jour. Geology, v. 66, p. 579-587.

Leonards, G. A., Editor, 1962, Foundation engineering: New York, McGraw-Hill, 1136 p.

Le Pichon, X., 1968, Sea-floor spreading and continental drift: Jour. Geophys. Research, v. 73, p. 3661-3697.

Levi, B., 1969, Burial metamorphism of a Cretaceous volcanic sequence west from Santiago, Chile: Beitr. Mineralogie u. Petrologie, v. 24, p. 30-49.

Levi, B., and Corvalán, J., 1964, Metamorfismo regional en las rocas volcánicas del Geosinclinal Andino: Santiago, Rev. Minerales, no. 86, p. 6-15.

Levi, B., Mehech, S., and Munizaga, R., 1963 Edades radiométricas y petrografía de granitos chilenos: Santiago, Inst. Invest. Geol., Bol. 14, 42 p.

Light, M., and Light, R., 1946, Atacama revisited -- "Desert trails" seen from the air: Geog. Rev., v. 36, p. 525-545.

Lomnitz, C., 1962, On Andean structure: Jour. Geophys. Research, v. 67, p. 351-363.

_____, 1964, On Andean structure, Part II: Earthquake risk in Chile: Seismol. Soc. America Bull., v. 54, p. 1271-1281.

McKenzie, D. P., 1970, Plate tectonics of the Mediterranean region: Nature, v. 226, p. 239-243.

McKenzie, D. P., and Parker, R. L., 1967, The North Pacific: an example of tectonics on a sphere: Nature, v. 216, p. 1276-1279.

Malahoff, A., 1970, Some possible mechanisms for gravity and thrust faults under oceanic trenches: Jour. Geophys. Research, v. 75, p. 1992-2001.

Meigs, P., 1966, Geography of coastal deserts, v. 28 of Arid zone research: Paris, UNESCO, 140 p.

Menard, H. W., Chase, T. E., and Smith, S. M., 1964, Galapagos Rise in the southeastern Pacific: Deep-Sea Research, v. 11, p. 233-242.

Molnar, P., and Sykes, L. R., 1969, Tectonics of the Caribbean and Middle America regions from focal mechanisms and seismicity: Geol. Soc. America Bull., v. 80, p. 1639-1684.

Morgan, W. J., 1968, Rises, trenches, great faults, and crustal blocks: Jour. Geophys. Research, v. 73, p. 1959-1982.

Morgan, W. J., Vogt, P. R., and Falls, D. F., 1969, Magnetic anomalies and sea floor spreading on the Chile Rise: Nature, v. 222, p. 137-142.

Muñoz Cristi, J., 1956, Chile, in Jenks, W. F., Editor, Handbook of South American geology: Geol. Soc. America Mem. 65, p. 191-214.

Nettleton, L. L., 1940, Geophysical prospecting for oil: New York, McGraw-Hill, 427 p.

Olea M., R., 1967, Determinación de hipocentros y su aplicación al estudio del norte de Chile: Santiago, Univ. de Chile, Dept. Geofísica y Geodesía, Pub. 43, 109 p.

Oliver, J., Ryall, A., Brune, J. N., and Slemmons, D. B., 1966, Microearthquake activity recorded by portable seismographs of high sensitivity: Seismol. Soc. America Bull., v. 56, p. 899-924.

Ortiz O., F., 1968, Reconocimiento geológico del distrito minero los Pozos, Departamento de Chañaral, Provincia de Atacama: Chile, Empresa Nacional de Minería, Unpub. rept.

Ortiz O., F., Corvalán, J., Segerstrom, K., and García, F., 1960, Geología y estratigrafía del área Chañaral-Taltal: Santiago, Inst. Invest. Geol., Unpub. rept.

Pitman, W. C., III, Herron, E. M., and Heirtzler, J. R., 1968, Magnetic anomalies in the Pacific and sea floor spreading: Jour. Geophys. Research, v. 73, p. 2069-2085.

Pitt, A. M., and Ellis, J. O., 1968, Preliminary report on some aftershocks of the December 28, 1966 earthquake in northern Chile: Seismol. Soc. America Bull., v. 58, p. 843-850.

Plafker, G., and Savage, J. C., 1970, Mechanism of the Chilean earthquakes of May 21 and 22, 1960: Geol. Soc. America Bull., v. 81, p. 1001-1030.

Putnam, W. C., 1937, The marine cycle of erosion for a steeply sloping shoreline of emergence: Jour. Geology, v. 45, p. 844-850.

Rich, J. L., 1941, The nitrate district of Tarapacá, Chile -- an aerial traverse: Geog. Rev., v. 31, p. 1-22.

_____, 1942, The face of South America -- an aerial traverse: Am. Geog. Soc. Spec. Pub. 26, 299 p.

Rudolph, W. E., 1953, Weather cycles on the South American west coast: Geog. Rev., v. 43, p. 565-566.

Ruiz F., C., 1943, Los yacimientos de hierro de la región noroccidental de Copiapó, un tipo no descrito de yacimientos de contracto metamórfico: Santiago, Soc. Nac. Min., Bol. Minero, v. 55, p. 820-827, 906-915.

_____, 1965, Geología y yacimientos metalíferos de Chile: Santiago, Inst. Invest. Geol., 305 p.

Ruiz F., C., Aguirre, L., Corvalán, J., Rose, Jr., H. J., Segerstrom, K., and Stern, T. W., 1961, Age of batholithic intrusions of northern and central Chile: Geol. Soc. America Bull., v. 72, p. 1551-1560.

Ruiz F., C., and Ericksen, G. E., 1962, Metallogenetic provinces of Chile, S. A.: Econ. Geology, v. 57, p. 91-106.

Rutland, R. W. R., Guest, J. E., and Grasty, R. L., 1965, Isotopic ages and Andean uplift: Nature, v. 208, p. 677-678.

St. Amand, P., and Allen, C. R., 1960, Strike-slip faulting in northern Chile (abs.): Geol. Soc. America Bull., v. 71, p. 1965.

Scholl, D. W., 1968, Geologic significance of continental slope basement rock, Pacific margin (abs.): Geol. Soc. America Ann. Mtg. Prog., Mexico City, p. 266.

Scholl, D. W., Buffington, E. C., and Hopkins, D. M., 1966, Exposure of basement rock on the continental slope of the Bering Sea: Science, v. 153, p. 992-994.

Scholl, D. W., Christensen, M. N., von Huene, R., and Marlow, M.S., in press, Peru-Chile trench sediments and sea-floor spreading: Geol. Soc. America Bull., v. 81.

Scholl, D. W., and von Huene, R., 1969, Geologic implications of Cenozoic subsidence and fragmentation of continental margins (abs.): Am. Assoc. Petroleum Geologists Bull., v. 53, p. 740-741.

Scholl, D. W., and von Huene, R., 1970, Comments on paper by R. L. Chase and E. T. Bunce -- underthrusting of the eastern margin of the Antilles by the floor of the western north Atlantic Ocean and origin of the Barbados Ridge: Jour. Geophys. Research, v. 75, p. 488-490.

Scholl, D. W., von Huene, R., and Ridlon, J. B., 1968, Spreading of the ocean floor-undeformed sediments in the Peru-Chile Trench: Science, v. 159, p. 869-871.

Segerstrom, K., 1960a, Cuadrángulo Quebrada Paipote, Provincia de Atacama: Santiago, Inst. Invest. Geol., Carta Geol. Chile, v. 2, no. 1, 35 p.

_____, 1960b, Cuadrángulo Llampos, Provincia de Atacama: Santiago, Inst. Invest. Geol., Carta Geol. Chile, v. 2, no. 2, 40 p.

_____, 1963, Matureland of northern Chile and its relationship to ore deposits: Geol. Soc. America Bull., v. 74, p. 513-518.

Segerstrom, K., and Ruiz F., C., 1962, Cuadrángulo Copiapó: Santiago, Inst. Invest. Geol., Carta Geol. Chile, v. 3, no. 1, 115 p.

Segerstrom, K., Valenzuela, B. L. de, and Mehech, S., 1960, Cuadrángulo Chamonate: Santiago, Inst. Invest. Geol., Carta

Geol. Chile, v. 2, no. 3, 42 p.

Seyfert, C. K., 1969, Undeformed sediments in oceanic trenches with sea-floor spreading: Nature, v. 222, p. 70.

Sharp, R. P., 1954, Physiographic features of faulting in southern California, in Jahns, R. H., Editor, Geology of southern California: California Div. Mines Bull. 170, chap. 5, p. 21-28.

Sillitoe, R. H., Mortimer, C., and Clark, A. H., 1968, A chronology of landform evolution and supergene mineral alteration, southern Atacama Desert, Chile: Inst. Mining and Metallurgy Trans., sec. B, v. 77, p. B166-B169.

Stauder, W., and Ryall, A., 1967, Spatial distribution and source mechanism of microearthquakes in central Nevada: Seismol. Soc. America Bull., v. 57, p. 1317-1345.

Tilling, R. I., 1962, Batholith emplacement and contact metamorphism in the Paipote-Tierra Amarilla area, Atacama Province, Chile: Ph.D. thesis, Yale Univ.

Tobar B., A., 1966, Estratigrafía del Área Baquedano-Rencoret, Provincia de Antofagasta: Thesis, Escuela de Geología, Univ. de Chile.

Tobin, D. G., Ward, P. L., and Drake, C. L., 1969, Microearthquakes in the Rift Valley of Kenya: Geol. Soc. America Bull., v. 80, p. 2043-2046.

Trewartha, G. T., 1961, The earth's problem climates: Madison, Univ. of Wisconsin Press, 334 p.

Vilas, J. F., and Valencio, D. A., 1970, The recurrent Mesozoic drift of South America and Africa: Earth and Planetary Sci. Letters, v. 7, p. 441-444.

von Huene, R., Scholl, D. W., and Ridlon, J. B., 1968, Submarine trenches and deformation: Science, v. 160, p. 1024.

Ward, P. L., Pálmason, G., and Drake, 1969, Microearthquake survey and the mid-Atlantic ridge in Iceland: Jour. Geophys. Research, v. 74, p. 665-684.

Washburn, A. L., 1956, Classification of patterned ground and review of suggested origins: Geol. Soc. America Bull., v. 67, p. 823-866.

Wetzel, W., 1927, Beiträge zur Erdgeschichte der mittleren Atacama: Neues Jahrb. Mineralogie, Geologie u. Paläontologie, sec. B, v. 57, p. 507-578.

Willis, B., 1929, Earthquake conditions in Chile: Carnegie Inst. Washington Pub. 382, 178 p.

Wilson, J. T., 1965, A new class of faults and their bearing on continental drift: Nature, v. 207, p. 343-347.

Woolard, G. P., 1960, Seismic crustal studies during the IGY, Part I: Marine program: Am. Geophys. Union Trans., v. 41, p. 107-113.

Worzel, J. L., 1966, Structure of continental margins and development of ocean trenches, in Continental margins and island arcs -- a symposium: Canada Geol. Survey Paper 66-15, p. 357-375.

Zeigler, J. M., Athearn, W. D., and Small, H., 1957, Profiles across the Peru-Chile trench: Deep-Sea Research, v. 4, p. 238-249.

Zeil, W., 1960, Zur Geologie der nordchilenischen Kordilleren: Geol. Rundschau, v. 50, p. 639-673.

_____, 1964, Geologie von Chile: Berlin, Gerbrüder Borntraeger, 233 p.

APPENDIX

APPROXIMATE MINERAL ABUNDANCES OF REPRESENTATIVE SAMPLES OF GRANITIC ROCKS

Explanatory Note

Unless otherwise noted, the reader is referred to Appendix Plates A, B, C, and D for the location of the rock samples. Sample numbers prefixed by "PA" correspond to Plate A, by "S" to Plate B, by "T" to Plate C, and by "CE" to Plate D.

The modes in Appendix Tables 1 through 9 are based on counting of approximately 500 points and include a rough estimate of error. Plagioclase compositions were determined by standard petrographic techniques. Ranges in An% exceeding a few per cent indicate compositional zoning. The modes in Appendix Table 10 were determined by Mr. J. D. Murray of the California Institute of Technology and are based on counting of approximately 1000 points.

Appendix Table 1

Approximate modes of typical Paleozoic granitic rocks

Sample No.	T-51	T-52A	T-57	S-115	S-123
plagioclase (An %)	27-33 An_{23-29}	20-25 An_{29-32}	5-10 An_{23-25}	5-10 $An_{?}$	10-15 An_{6-8}
K-feldspar	17-22	30-40	60-65	40-45	45-50
quartz	35-40	35-40	25-30	45-50	33-38
biotite	5-9	3-5	1-2	---	1-2
hornblende	---	Tr	---	---	---
opaques	Tr	Tr	1	Tr	Tr
non-opaques*	1-2**	1	1-2**	1-2	1
	100%	100%	100%	100%	100%

* Zircon, apatite, chlorite, sericite, white mica, apatite, tourmaline, sphene

**Mainly white mica

T-51: Med.- to coarse-grained equigranular biotite adamellite

T-52A: Fine- to coarse-grained, seriate-porphyritic biotite adamellite

T-57: Coarse-grained inequigranular altered leucogranite

S-115: Med.-grained anhedral altered leucogranite

S-123: Fine- to med.-grained granophyric leucogranite

Appendix Table 2

Approximate modes of typical melanodiorites and gabbros

Sample No.	T-53	PA-103(2)	PA-111	S-116	S-132
plagioclase (An %)	50-60 An_{41-55}	65-70 An_{58-64}	58-63 An_{35-54}	50-55 An_{50-53}	55-60 An_{35-68}
K-feldspar	1-2	---	---	---	---
quartz	3-7	Tr	---	---	2-4
pyroxene	---	1-2	---	[45-50]	---
amphibole	20-25	22-25	35-40		35-40
biotite	10-15	5-7	---	---	---
opaques	1	1	Tr	1-2	2-3
non-opaques*	1-2	1-2	2-3	1-2	2-3
	100%	100%	100%	100%	100%

*Apatite, sphene, zircon, epidote, carbonate, chlorite, sericite, actinolite

T-53: Fine- to med.-grained equigranular biotite-hornblende melanodiorite

PA-103(2): Med.-grained equigranular pyroxene-biotite-hornblende gabbro

PA-111: Med.-grained equigranular hornblende melanodiorite

S-116: Med.- to coarse-grained equigranular altered pyroxene gabbro

S-132: Fine- to med.-grained inequigranular altered melanodiorites

Appendix Table 3

Approximate modes of typical diorites

Sample No.	S-75B	S-94D	S-95	S-99A	PA-102(1)
plagioclase (An %)	65-70 An_{43-48}	55-60 An_{50-54}	50-55 An_{45-48}	55-65 An_{44-48}	55-60 An_{41-44}
K-feldspar	---	---	---	17-20	2-4
quartz	3-5	5-8	---	6-9	3-5
pyroxene	[23-27]	Tr	[40-45]	5-7	---
amphibole		27-33		2-3	20-25
biotite	---	---	---	3-5	---
opaques	1	2-3	2-3	1	1-2
non-opaques*	2	2-4	2-3	Tr	10-13**
	100%	100%	100%	100%	100%

* Apatite, sphene, sericite, chlorite, zircon, epidote, carbonate, actinolite

** Mainly chlorite

S-75B: Med.- to coarse-grained equigranular altered diorite

S-94D: Med.- to coarse-grained equigranular quartz-bearing hornblende diorite

S-95: Med.- to coarse-grained equigranular altered pyroxene diorite

S-99A: Med.-grained equigranular quartz-bearing pyroxene diorite (monzodiorite)

PA-102(1): Med.- to coarse-grained equigranular altered hornblende diorite

Appendix Table 3 (continued)

Approximate modes of typical diorites

Sample No.	BL-108A**	S-120	S-121A	S-121B
plagioclase (An %)	62-70 An_{38-41}	60-65 An_{47-60}	48-53 An_{46-63}	60-65 $An_{?}$
K-feldspar	---	---	---	---
quartz	Tr	5-8	11-14	1-2
pyroxene	[30-38]	Tr	[35-40]	[35-40]
amphibole		25-28		
opaques	1	1	1	1-2
non-opaques*	1-2	3-5***	1	1
	100%	100%	100%	100%

* Apatite, sericite, chlorite, actinolite, sphene, zircon, epidote, carbonate

** Sample locality: lower Queb. de Remiendos, 3.3 km E. of shoreline

*** Mainly chlorite

BL-108A: Med.-grained equigranular altered pyroxene diorite

S-120: Med.-grained equigranular altered quartz-bearing hornblende diorite

S-121A: Fine- to med.-grained inequigranular altered quartz-bearing diorite to tonalite

S-121B: Fine- to med.-grained equigranular altered diorite.

Appendix Table 4

Approximate modes of typical medium-grained equigranular hornblende-biotite granodiorites assigned to Cretaceous-Tertiary suite

Sample No.	CE-8	CE-31	S-86	PA-104B	PA-104C	BL-108**
plagioclase (An %)	45-50 An_{24-33}	45-55 An_{25-29}	50-60 An_{32-40}	45-55 An_{25-39}	45-55 An_{27-44}	45-50 An_{24-30}
K-feldspar	10-15	12-16	10-15	14-16	8-10	9-11
quartz	25-30	20-25	14-16	10-15	10-15	25-30
biotite	6-8	[10-15]	7-8	10-12	10-13	6-8
hornblende	3-4		8-9	7-10	9-12	3-5
opaques	1-2	1	Tr	1	1-2	1
non-opaques*	Tr	Tr	2	1	1-2	2
	100%	100%	100%	100%	100%	100%

* Sphene, zircon, apatite, chlorite, sericite, epidote

** Sample locality: mouth of Queb. de Remiendos, 0.8 km E. of shoreline

Appendix Table 5

Approximate modes of typical pyroxene granodiorites

Sample No.	T-3	T-62	T-119	S-130B
plagioclase (An %)	45-55 An_{28-32}	40-45 An_{27-42}	40-45 An_{38-53}	48-53 An_{40-65}
K-feldspar	10-15	20-25	16-19	10-14
quartz	15-20	15-20	11-14	11-14
pyroxene	[15-20]	[20-25]	16-19	[22-27]
amphibole			1-2	
biotite	---	1	4-6	1
opaques	1	1	1-2	2-3
non-opaques*	2-4	Tr	2-3	2-4
	100%	100%	100%	100%

*Apatite, sphene, sericite, chlorite, epidote, rutile, zircon, actinolite, carbonate

T-3: Fine- to med.-grained inequigranular altered pyroxene granodiorite

T-62: Med.- to coarse-grained porphyritic pyroxene granodiorite to adamellite

T-119: Med.-grained equigranular biotite-pyroxene granodiorite

S-130B: Med.- to coarse-grained porphyritic altered pyroxene granodiorite

Appendix Table 6

Approximate modes of typical medium-grained inequigranular granodiorites

Sample No.	T-47	S-84A	S-84B	S-88	S-90
plagioclase (An %)	45-50 An_{30-34}	50-55 An_{38-43}	50-55 An_{30-42}	45-50 An_{27-33}	50-55 An_{27-38}
K-feldspar	10-17	13-18	14-19	15-20	13-17
quartz	25-30	15-20	12-17	15-20	18-23
biotite	---	7-9	6-8	3-4	8-10
hornblende	1-2	7-9	8-10	9-11	4-5
pyroxene	---	2-3	---	---	---
opaques	Tr	1	Tr	1-2	Tr
non-opaques*	5-7**	2-3	2-3	1-2	Tr
	100%	100%	100%	100%	100%

* Apatite, zircon, sphene, epidote, carbonate, chlorite, sericite

** Mainly chlorite, epidote, carbonate, and sphene

T-47: Altered pyroxene (?) granodiorite

S-84A: Pyroxene-biotite-hornblende granodiorite

S-84B: Biotite-hornblende granodiorite

S-88: Cataclastic biotite-hornblende granodiorite

S-90: Hornblende-biotite granodiorite

Appendix Table 7

Approximate modes of miscellaneous granodiorites

Sample No.	X-5**	CE-26	T-93	S-94E	PA-112A
plagioclase (An %)	55-65 An_{24-31}	45-55 An_{37-40}	50-55 An_{26-38}	55-60 An_{40-42}	40-45 An_{23-28}
K-feldspar	5-10	10-13	8-12	6-9	12-16
quartz	20-25	10-12	15-18	16-19	30-35
biotite	3-6	5-8	2	9-11	8-10
hornblende	---	18-20	7-9	4-6	1-2
pyroxene	---	2-3	---	2-3	---
opaques	1	1-2	Tr	1	Tr
non-opaques*	1-2	2-3	10-12***	Tr	Tr
	100%	100%	100%	100%	100%

* Apatite, sphene, epidote, sericite, chlorite, zircon, actinolite, epidote, carbonate

** Sample locality: 0.2 km N. of lat. 24°; long. 70°18.5'.

*** Mainly chlorite

X-5: Med.-grained equigranular biotite leucogranodiorite

CE-26: Med.-grained equigranular pyroxene-biotite-hornblende granodiorite

T-93: Fine- to med.-grained equigranular altered hornblende-biotite granodiorite

S-94E: Med.-grained equigranular pyroxene-hornblende-biotite granodiorite

PA-112A: Fine- to med.-grained equigranular hornblende-biotite granodiorite

Appendix Table 8

Approximate modes of typical adamellites

Sample No.	CE-7	T-23	S-92	PA-109	S-131
plagioclase (An %)	35-40 An_{23-28}	20-25 An_{24-29}	32-38 An_{28-35}	35-40 An_{28-43}	40-50 An_{24-35}
K-feldspar	30-35	35-45	21-27	25-29	25-30
quartz	25-30	30-35	25-30	20-25	20-25
biotite	3-5	[2-3]	6-7	5-7	2-4
hornblende	1		1-2	6-8	1-2
opaques	Tr	Tr	1	1	1
non-opaques*	Tr	2-3**	6-8**	1-2	1
	100%	100%	100%	100%	100%

* Sphene, apatite, zircon, sericite, chlorite, epidote, carbonate, tourmaline

** Mainly chlorite

CE-7: Fine- to med.-grained anhedral-inequigranular biotite adamellite

T-23: Med.-grained equigranular biotite adamellite

S-92: Fine- to med.-grained equigranular altered hornblende-biotite adamellite

PA-109: Fine- to med.-grained inequigranular biotite-hornblende adamellite

S-131: Med.-grained equigranular micrographic hornblende-biotite adamellite

Appendix Table 9

Approximate modes of typical tonalites

Sample No.	S-72	S-80A	S-82	PA-101	PA-110B
plagioclase (An %)	55-65 An_{28-32}	60-65 An_{33-41}	60-65 An_{26-32}	55-60 An_{36-48}	65-70 An_{26-32}
K-feldspar	Tr	Tr	1-3	1	2-4
quartz	20-25	10-15	10-15	10-13	10-15
biotite	---	10-13	6-8	5-8	3-5
hornblende	9-12	7-10	10-15	15-18	13-16
opaques	Tr	1	1	Tr	1
non-opaques*	4-5**	1	1-2	Tr	1-2
	100%	100%	100%	100%	100%

* Apatite, sphene, zircon, chlorite, sericite, epidote, actinolite

** Mainly chlorite

S-72: Med.-grained equigranular hornblende tonalite

S-80A: Fine- to med.-grained equigranular hornblende-biotite tonalite

S-82: Fine- to med.-grained equigranular biotite-hornblende tonalite

PA-101: Fine- to med.-grained equigranular biotite-hornblende tonalite

PA-110B: Med.-grained equigranular biotite-hornblende tonalite

Appendix Table 10

Modes of selected granodiorites on opposite sides of the Salar del Carmen fault*

Sample No.	S-177	T-363	T-372
plagioclase (An %)	56.63 An_{35}	56.27 An_{45}	50.18 An_{42}
K-feldspar	7.28	10.43	13.81
quartz	20.87	20.06	19.29
biotite	7.48	3.81	---
hornblende	4.95	5.62	---
opaques	1.17	1.81	1.68
alteration of unidentified mafic mineral	2.33	1.81	15.04
other	0.29	0.20	0.00
	100.00	100.00	100.00

* See Part VI, The problem of total displacement on the Atacama fault.

S-177: Fine- to med.-grained equigranular hornblende-biotite granodiorite

T-363: Fine- to med.-grained equigranular biotite-hornblende granodiorite

T-372: Med.-grained equigranular altered granodiorite